INFRARED LASERS BASED ON HO3+:KRE(WO4)2 CRYSTALS WITH TM3+OR YB3+ AS SENSITIZERS

Venkatesan Jambunathan

ISBN:
Dipòsit Legal: T-1243-2011

UNIVERSITAT ROVIRA I VIRGILI
INFRARED LASERS BASED ON HO3+:KRE(WO4)2 CRYSTALS WITH TM3+OR YB3+ AS SENSITIZERS
Venkatesan Jambunathan
ISBN:/DL: T.1243-2011

Infrared lasers based on Ho^{3+}:$KRE(WO_4)_2$ crystals with Tm^{3+} or Yb^{3+} as sensitizers

Venkatesan Jambunathan

Doctoral Thesis

Supervised by:

Dr. Xavier Mateos Ferré

Prof. Dr. Magdalena Aguiló Díaz

Departament de Química Física i Inorgànica

Física i Cristal·lografia de Materials i Nanomaterials (FiCMA - FiCNA)

UNIVERSITAT ROVIRA I VIRGILI

Tarragona

2011

UNIVERSITAT ROVIRA I VIRGILI
INFRARED LASERS BASED ON HO3+:KRE(WO4)2 CRYSTALS WITH TM3+OR YB3+ AS SENSITIZERS
Venkatesan Jambunathan
ISBN:/DL: T.1243-2011

Infrared lasers based on Ho^{3+}:$KRE(WO_4)_2$ crystals with Tm^{3+} or Yb^{3+} as sensitizers

Venkatesan Jambunathan

Física i Cristal·lografia de Materials i Nanomaterials (FiCMA - FiCNA)
Departament de Química Física i Inorgànica
Universitat Rovira i Virgili
C/ Marcellí Domingo, s/n
E-43007, Tarragona, Spain

UNIVERSITAT ROVIRA I VIRGILI
INFRARED LASERS BASED ON HO3+:KRE(WO4)2 CRYSTALS WITH TM3+OR YB3+ AS SENSITIZERS
Venkatesan Jambunathan
ISBN:/DL: T.1243-2011

UNIVERSITAT ROVIRA I VIRGILI
DEPARTAMENT DE QUÍMICA FÍSICA I INORGÀNICA
Campus Sescelades
Marcel·lí Domingo, s/n
43007 Tarragona
Tel. +34 977 55 81 37
Fax +34 977 55 95 63
www.quimica.urv.es

Prof. Dra. Magdalena Aguiló Díaz, Catedrática de Cristal·lografia i Mineralogia, i Dr.Xavier Mateos Ferré, Professor Agregat, del Departament de Química Física i Inorgànica de la Universitat Rovira i Virgili,

CERTIFIQUEM:

Que aquest treball, titulat "Infrared lasers based on Ho^{3+}:$KRE(WO_4)_2$ crystals with Tm^{3+} or Yb^{3+} as sensitizers", que presenta Venkatesan Jambunathan per l'obtenció del títol de Doctor, ha estat realitzat sota la nostra direcció al Departament de Química Física i Inorgànica d'aquesta universitat i que acompleix els requeriments per poder optar a Menció Europea.

Tarragona, 25 de febrer de 2010

UNIVERSITAT ROVIRA I VIRGILI
INFRARED LASERS BASED ON HO3+:KRE(WO4)2 CRYSTALS WITH TM3+OR YB3+ AS SENSITIZERS
Venkatesan Jambunathan
ISBN:/DL: T.1243-2011

UNIVERSITAT ROVIRA I VIRGILI
INFRARED LASERS BASED ON HO3+:KRE(WO4)2 CRYSTALS WITH TM3+OR YB3+ AS SENSITIZERS
Venkatesan Jambunathan
ISBN:/DL: T.1243-2011

Infrared lasers based on Ho^{3+}:$KRE(WO_4)_2$ crystals with Tm^{3+} or Yb^{3+} as sensitizers

Venkatesan Jambunathan

Abstract

This thesis focuses on the development of compact solid-state infrared laser based on Ho-doped monoclinic potassium rare earth double tungstates (Ho:$KRE(WO_4)_2$, RE=Y, Gd, Lu) for the generation of 2.1 μm laser radiation by using either Tm or Yb as sensitizers and by using in-band pump sources emitting around 1.9 μm.

It is necessary and important to understand the structure, composition and spectroscopy of this material because these factors give us a clear idea about the material to understand its behaviour as a laser material. Here we present the growth of single-doped Ho:KREW, co-doped (Ho,Tm) and (Ho,Yb):KLuW crystals at several doping concentrations, and their structural, compositional and spectroscopic characterization. Finally we use these materials to generate laser at around 2.1 μm.

The manuscript is divided into four chapters. Chapter 1 gives an overview of infrared solid-state lasers around 2 μm and a brief summary of the host and active ions studied. Chapter 2 describes the experimental techniques used for obtaining and characterizing these materials. Chapter 3 describes the results achieved in this work on growth of the crystals, and their structural, compositional and spectroscopic characterization which shows that these materials are potential candidates for efficient 2.1 μm laser emission. The final chapter describes the laser generation obtained, which was highly successful.

Keywords: Crystal growth, Rare earth ions, Potassium rare earth double tungstates, Photoluminescence, Solid state laser materials, Infrared solid state laser.

UNIVERSITAT ROVIRA I VIRGILI
INFRARED LASERS BASED ON HO3+:KRE(WO4)2 CRYSTALS WITH TM3+OR YB3+ AS SENSITIZERS
Venkatesan Jambunathan
ISBN:/DL: T.1243-2011

UNIVERSITAT ROVIRA I VIRGILI
INFRARED LASERS BASED ON HO3+:KRE(WO4)2 CRYSTALS WITH TM3+OR YB3+ AS SENSITIZERS
Venkatesan Jambunathan
ISBN:/DL: T.1243-2011

Preface

The Ph.D investigation reported in this thesis was carried out at the group of *Física i Cristal.lografia de Materials i Nanomaterials (FiCMA-FiCNA)* in the *Departament de Química Física i Inorgànica* of the *Universitat Rovira i Virgili, Tarragona, Spain* and was supervised by Dr. Xavier Mateos Ferré and Prof. Dr. Magdalena Aguiló Díaz.

As part of the thesis, we actively collaborated with the following groups: *Short pulse laser system* group led by Dr. Valentin Petrov and Dr. Uwe Griebner at the *Max-Born-Institut for Nonlinear Optics and Short Pulse Spectroscopy, Berlin, Germany* and the *Departamento de Materiales Ferroeléctricos* led by Prof. Carlos Zaldo at the *Instituto de Ciencia de Materiales, Madrid, Spain.*

This work was made possible thanks to the Spanish Government for the grants under projects MAT2008-06729-C02-02/NAN, PI09/90527, DE2009-0002 and the Catalan Authority under project 2009SGR235. I would like to thank the personal support provided by the Universitat Rovira i Virgili under the grant 2007BRDI-06-24 and the Spanish Ministry of Education through the student mobility program grant TME2009-00417.

Venkatesan Jambunathan
Tarragona, 2011

UNIVERSITAT ROVIRA I VIRGILI
INFRARED LASERS BASED ON HO3+:KRE(WO4)2 CRYSTALS WITH TM3+OR YB3+ AS SENSITIZERS
Venkatesan Jambunathan
ISBN:/DL: T.1243-2011

UNIVERSITAT ROVIRA I VIRGILI
INFRARED LASERS BASED ON HO3+:KRE(WO4)2 CRYSTALS WITH TM3+OR YB3+ AS SENSITIZERS
Venkatesan Jambunathan
ISBN:/DL: T.1243-2011

Acknowledgements

This thesis would not have been possible without the guidance and support of several individuals who in one way or another contributed and extended their valuable assistance. It's my great pleasure to acknowledge each of them.

First and foremost, my sincere gratitude to my group head Prof. Dr. Francesc Díaz for giving me the opportunity to join the FiCMA-FICNA group. I always admire him for dedication and enthusiasm towards his work and for his great sense of humor.

Secondly, I am grateful to my thesis directors, Prof. Dr. Magdalena Aguiló and Dr. Xavier Mateos for their support, guidance and encouragement throughout my doctoral thesis. My sincere thanks to Dr. Xavier Mateos for his extraordinary patience, friendly approach and personal advices to me. It is also an honor for me to be his first Ph.D student.

This thesis would also not have been possible without the help of the technicians of this group. I would like to thank Agustí Montero for cutting and polishing my crystals, and for making me laugh everyday with his mimicry and friendly conversations. I am grateful to Nicolette Bakker for cutting and polishing the samples for my experiments. I would like to thank Laura Escorihuela for taking care of my furnaces during my absence and for all her help.

I also want to thank the other senior members of the FiCMA-FiCNA group Dr. Jaume Massons, Dra. Josefina Gavaldà, Dra. Ma Rosa Solé, Dr. Xavier Rius, Dra. Cinta Pujol and Dr. Joan Josep Carvajal for their support during my stay in this research group. My sincere thanks to Cinta pujol for all her help and friendly conversations.

I would like to thank all of my colleagues Montserrat Galceran, Western Bolaños, Martha Segura, Jaume Cugat, Raj kumar, William Barrera, Muhammad Usman Qadri and Oleksandr Bilousov for making FiCMA-FiCNA a home away from home. It has been a pleasure working with all of you and I am grateful for your kindness towards me.

I am grateful to Dr Valentin Petrov, MBI, Berlin, for giving me an opportunity for my three months and several stays to carry out the laser experiments and without him this work would not have been complete. My sincere thanks to Dr. Uwe Gribner, MBI, Berlin for his motivation and

ISBN:/DL: T.1243-2011

help during my stay in Berlin. I extend my sincere thanks to Prof Carlos Zaldo, CSIC, Madrid for helping me in measuring life time in my crystals. I am grateful to Andreas Schmidt, MBI, Berlin for teaching me how to align laser cavity and thanks for his patience and fun loving talks. I am also grateful to John Bates, URV for correcting the language of the entire thesis expect this part.

I am grateful to the past and the present Indian Tarragona friends for their kindness and for their fun loving talks during get together. My sincere thanks to Shruti, Suprio, Sarathi and Chandan for their constant support.

Last but not the least I would like to thank my family member's Amma, Appa, Purush, Sudha, Jai, Athai, Athimber, Baba, Vivek and my family friends Vijay, Dhana, Prakash, Sriram, Kamesh, Sudha akka and Bhava for their support and kindness throughout these years.

UNIVERSITAT ROVIRA I VIRGILI
INFRARED LASERS BASED ON HO3+:KRE(WO4)2 CRYSTALS WITH TM3+OR YB3+ AS SENSITIZERS
Venkatesan Jambunathan
ISBN:/DL: T.1243-2011

To my family with great love……..

UNIVERSITAT ROVIRA I VIRGILI
INFRARED LASERS BASED ON HO3+:KRE(WO4)2 CRYSTALS WITH TM3+OR YB3+ AS SENSITIZERS
Venkatesan Jambunathan
ISBN:/DL: T.1243-2011

List of publications

The results of this doctoral thesis are based on the work reported in the following publications, referred to by roman numerals in the text.

Paper I: V. Jambunathan, X. Mateos, M. C. Pujol, J. J. Carvajal, J. Massons, M. Aguiló and F. Díaz, "Near-infrared photoluminescence from Ho^{3+}–doped monoclinic $KLu(WO_4)_2$ crystal codoped with Tm^{3+}", J. Lumin. **129** (12), 1882-1885 (2009).

Paper II: V. Jambunathan, A. Schmidt, X. Mateos, M. C. Pujol, J. J. Carvajal, U. Griebner, V. Petrov, C. Zaldo, M. Aguiló and F. Díaz, "Crystal growth, optical spectroscopy and continuous-wave laser operation of co-doped (Ho,Tm):$KLu(WO_4)_2$ monoclinic crystals", submitted to J. Opt. Soc. Am. B.

Paper III: V. Jambunathan, X. Mateos, M. C. Pujol, J. J. Carvajal, C. Zaldo, M. Aguiló, F. Díaz, U. Griebner and V. Petrov, "Crystal growth, optical spectroscopy and continuous-wave laser operation of Ho:$KLu(WO_4)_2$ crystals", submitted to Appl. Phys. B.

Paper IV: V. Jambunathan, X. Mateos, M. C. Pujol, J. J. Carvajal, M. Aguiló and F. Díaz "Growth and spectroscopy of (Ho,Yb):$KLu(WO_4)_2$ crystals", Physics Procedia **8** ,162–167 (2010).

Paper V: V. Jambunathan, X. Mateos, M. C. Pujol, J. J. Carvajal, M. Aguiló and F. Díaz, "Control of the cool/warm white light generation from lanthanide ions in monoclinic double tungstate crystals", J. Lumin., Accepted (2011).

Paper VI: V. Jambunathan, A. Schmidt, X. Mateos, M. C. Pujol, J. J. Carvajal, M. Aguiló, F. Díaz, U. Griebner and V. Petrov, "Continuous-wave co-lasing in a monoclinic co-doped (Ho,Tm):$KLu(WO_4)_2$ crystal", submitted to Laser Phys. Lett.

Paper VII: X. Mateos, V. Jambunathan, M. C. Pujol, J. J. Carvajal, F. Díaz, M. Aguiló, U. Griebner and V. Petrov, "CW lasing of Ho in $KLu(WO_4)_2$ in-band pumped by a diode-pumped Tm:$KLu(WO_4)_2$ laser", Opt. Express 18 (20), 20793 -20798 (2010).

ISBN:/DL: T.1243-2011

Paper VIII: V. Jambunathan, X. Mateos, M. C. Pujol, J. J. Carvajal, M. Aguiló, F. Díaz, U. Griebner and V. Petrov, "Diode –Pumped Ho:$KLu(WO_4)_2$ laser at 2.08 μm", submitted to Appl. Phys. Express.

Paper IX: V. Jambunathan, X. Mateos, M. C. Pujol, J. J. Carvajal, F. Díaz, M. Aguiló, U. Griebner and V. Petrov, "Continuous-wave laser generation at ~2.1 μm in Ho:$KRE(WO_4)_2$ (RE= Y, Gd, Lu) crystals: a comparative study ", submitted to Opt. Express.

UNIVERSITAT ROVIRA I VIRGILI
INFRARED LASERS BASED ON HO3+:KRE(WO4)2 CRYSTALS WITH TM3+OR YB3+ AS SENSITIZERS
Venkatesan Jambunathan
ISBN:/DL: T.1243-2011

Table of Contents

UNIVERSITAT ROVIRA I VIRGILI
INFRARED LASERS BASED ON HO3+:KRE(WO4)2 CRYSTALS WITH TM3+OR YB3+ AS SENSITIZERS
Venkatesan Jambunathan
ISBN:/DL: T.1243-2011

UNIVERSITAT ROVIRA I VIRGILI
INFRARED LASERS BASED ON HO3+:KRE(WO4)2 CRYSTALS WITH TM3+OR YB3+ AS SENSITIZERS
Venkatesan Jambunathan
ISBN:/DL: T.1243-2011

UNIVERSITAT ROVIRA I VIRGILI
INFRARED LASERS BASED ON HO3+:KRE(WO4)2 CRYSTALS WITH TM3+OR YB3+ AS SENSITIZERS
Venkatesan Jambunathan
ISBN:/DL: T.1243-2011

Chapter 1
Introduction

This chapter gives an overview of the infrared solid-state lasers that operate in the 2μm range. The role of active media in solid state lasers is discussed. The properties of the monoclinic potassium rare earth double tungstates ($KRE(WO_4)_2$) as hosts for solid-state lasers, which were studied previously at the FiCMA laboratories, are briefly described. The active ions Ho^{3+}, Tm^{3+} and Yb^{3+} are also described. The motivation and objectives of the present work are presented below.

UNIVERSITAT ROVIRA I VIRGILI
INFRARED LASERS BASED ON HO3+:KRE(WO4)2 CRYSTALS WITH TM3+OR YB3+ AS SENSITIZERS
Venkatesan Jambunathan
ISBN:/DL: T.1243-2011

1.1 Overview of infrared solid-state lasers in the 2 μm region

Infrared photons with wavelengths ranging from 800 nm to 12 μm are very important and necessary because of the features of this spectral region. Firstly, this is where the atmospheric transparency windows are located. Most of the infrared light from the universe is absorbed by water vapour and carbon dioxide in the earth's atmosphere and the chance of it reaching the earth is minimal. Secondly, various molecules in this region have strong rotational and vibrational absorption lines. Understanding this situation, various scientific and engineering communities around the world worked towards producing these infrared emissions using a coherent light source: the so called LASER. Now, 50 years on, lasers have evolved from a rather exotic device to a scientific and technological tool for day-to-day life. In the early years the systems were very difficult to operate and inefficient, but they have now improved tremendously in quality, efficiency and ease of use. These improvements have been attained not only because of the better quality components and more efficient excitation techniques but also because the processes that occur in these laser materials are now thoroughly understood.

Solid-state lasers are formed by one or several active ions embedded in a solid-state host and are different from gas lasers, dye lasers, semiconductor lasers and fibre lasers. The present study focuses on infrared solid-state lasers emitting in the 2 μm range. Let us discuss them briefly.

The wavelength range around 2 μm is covered by the laser system operating in the so called “eye safe” wavelength region, which begins at about 1.4 μm. This region has exceptional advantages over systems that operate at shorter wavelengths for certain applications in space, which gives them great market potential for use in LIDAR [1] and gas sensing systems. In addition, because of the favorable absorption in water, these lasers can be used for medical applications such as general surgery, urology, dentistry etc [2]. The 2 μm lasers can also be used to directly measure wind velocity and detect water vapor and carbon dioxide concentration in the atmosphere for forecasting the weather.

This 2 μm laser transition exists in the trivalent rare earth lanthanide ions Tm^{3+} (hereafter Tm) (slightly below 2 μm) and Ho^{3+} (hereafter Ho) (slightly above 2 μm). Using these ions, laser emission was achieved in many different host crystals, glasses and fibres. For continuous wave operation, the Tm laser ($^3F_4 \rightarrow {}^3H_6$) transitions are more interesting, but for pulsed and Q-switched operation the Ho laser ($^5I_7 \rightarrow {}^5I_8$) transition is more attractive because of its longer life time and higher gain in Ho-doped materials. Both the laser ions end their transition in the upper Stark levels of the ground state and can be described as quasi three level lasers with a thermally populated ground state. Tm lasers have the great advantage that Tm ions can be

directly excited with commercially available laser diodes around 800 nm. For efficient Ho-laser operation, however, ions have to be excited directly around 1.9 μm or an energy transfer mechanism process from Tm or Yb has to be used.

The first 2 μm Tm:YAG laser was realized in 1965. It was a flashlamp pumped laser which operated at 77K [3]. Some years later, in 1975, the first pulsed laser was operated at room temperature using Cr,Tm:YAG [4]. The development of AlGaAS laser diodes emitting in the 800 nm region was a real breakthrough because they showed a good match between the absorption bands of Tm-doped materials which made continuous wave laser operation possible at room temperature. To date, Tm-based laser systems have been demonstrated in many different host materials [5, 6, 7]. Nowadays, the main research activity in this field focuses on optimizing the Tm concentration, and the shape of the active medium such as slabs, thin-disks etc., in various crystalline hosts [8, 9,10].

Since the Ho ion does not have an absorption band that is well suited to the available pump sources, researchers first used co-doped systems to realize the Ho laser action. The first Ho-laser action was achieved using Tm co-doping with YAG as the host material. It was a flashlamp pumped pulsed laser working with liquid nitrogen cooling [11]. Some years later room temperature-pulsed Ho-laser operation was achieved using Er and Tm as sensitizers for optimized pump absorption using flashlaremp pumped YAG [12]. The first room temperature CW laser operation of Ho was demonstrated using a krypton lamp as pump source in Cr:Tm:Ho:YSAG and Cr:Tm:Ho:YSGG [13]. Later in the early 1980s many researchers used the 800 nm diode lasers to pump Tm: Ho co-doped lasers. The first CW Ho lasers in the co-doped system utilizing laser diode pumping were demonstrated in YAG [14]. Considerable developments took place in the 1990s in the field of co-doping and, in particular, Ho,Tm:YLF was tested in several pump configuration schemes [15,16,17]. Although much experimental work has been carried out, many approaches have also focused on theoretical modeling in an attempt to understand energy transfer dynamics and optimize the Ho,Tm laser systems [18,19]. In the last few years lasers have been demonstrated with Ho,Tm co-doped systems and different solid state laser hosts [20,21,22] but YAG and YLF are still considered to be the most promising hosts for co-doped Ho,Tm lasers. As well as Ho, Tm systems, some researchers have used Yb as a sensitizer ion to demonstrate 2 μm laser operation from Ho but very few have succeeded [23].

The biggest drawback of these co-doped systems is up-conversion phenomena, which lead to poor efficiency. In order to overcome this problem and attain higher efficiency, in the last decade, several researchers have found an alternative route to pump Ho using resonant or in-band pumping of the $^5I_7$ excited level of Ho at ~1.9 μm. This offers the advantages of high

quantum efficiency for the ~2.1 μm laser transition and minimal heat load for the active element. Resonant pumping of Ho lasers by separate Tm lasers in continuous-wave (CW), Q-switched regimes has been studied extensively, including several Tm crystal lasers and Tm fibre lasers [24, 25, 26, 27, 28, 29]. Some researchers have also demonstrated Ho laser action by intra cavity pump schemes, in which the Ho crystal is placed inside the Tm resonator [30, 31,32]. Since the Tm lasers are diode-pumped near 800 nm, overall efficiency is low and power scaling is limited. Some researchers in recent years have found that direct in-band pumping by 1.9 μm laser diodes will be the ultimate solution for high power scaling of Ho lasers. The first in-band diode pumped Ho laser was achieved in 1995 which made the new researchers confident that direct in-band diode pumping can generally be used to produce laser action in Ho, although the emission bandwidth and laser beam quality of laser diodes are inferior to those of Tm laser systems. They used a mix of GaInAsSb and InGaAsP diode lasers, which were available at that time and each delivers 0.7W of output power [33]. Nowadays diode lasers based on (AlGaIn)(AsSb) shortly as GaSb material systems was significantly improved and using this, direct in-band pumping of Ho:YAG was demonstrated in the CW regime [34]. Table 1.1 gives an overview of some studies that have been made in the 2 micron region.

Table 1.1 Overview of some of the CW regime studies in the 2 μm range.

Laser material	Pump source	λ_{pump} [nm]	λ_{laser} [nm]	Output power [W]	Slope efficiency [%]	Reference
Tm:YAG	Diode	805	2013	115	52	[35]
Tm:YLF	Diode	792	1910	55	49	[36]
$Tm:Lu_2O_3$	Diode	796	2070	40	42	[37]
$Tm:GdVO_4$	Diode	805	1912	2.8	-	[38]
Tm: Lu_2SiO_5	Diode	790	2058	0.67	21	[39]
Tm :$KLu(WO_4)_2$	Diode	800	1950	4	69	[40]
(Ho,Tm):YLF	Diode	792	2067	0.084	60	[41]
$(Ho,Tm):GdVO_4$	Diode	803	2050	10.5	50	[42]
$(Ho,Tm):NaY(WO_4)_2$	Diode	795	2070	2.7	26	[43]
Ho:YAG	Tm:YLF	1908	2090	9.4	40	[31]
Ho:YLF	Tm:fibre	1905	2097	6.4	80	[27]
Ho:YAG	Diode	1910	2120	40	57	[34]

1.2 Fundamental physics of solid state lasers

The word LASER is an acronym of "Light Amplification by Stimulated Emission of Radiation". In order to understand the basic operating principles of a laser we first have to understand the underlying fundamental physics. The term *light* is accepted as being the electromagnetic radiation ranging from 1nm to 1000 μm in wavelength. Generally, the ultraviolet region ranges from 200 to 400 nm, the visible region ranges from 400 to 780 nm, the near-infrared (NIR) region from 780 nm to 10 μm and beyond that is the far infrared region. When the electromagnetic waves interact with the material, several processes occur: absorption, reflection,

ISBN:/DL: T.1243-2011

transmission, scattering etc. Of these, absorption, spontaneous emission and stimulated emission are of interest, because they exploit the fundamental phenomena of a laser.

In general, all the atoms of any material are in the ground energy state. When external energy is imparted to the material, the atoms absorb energy and pass to a higher energy state or excited energy state (i.e., an incoming photon is absorbed by an atom, leaving the atom in an excited state and annihilating the photon). This process is called absorption.

After excitation, the atoms are in the higher energy state, which is inherently unstable because of the tendency of atoms to relax back to the lowest level. Therefore, the atoms remain in the excited state for a short period of time and then relax back to the ground state. During this transition the difference in energy corresponding to these states is emitted in the form of a photon. If the energy difference in these levels is ΔE, the frequency v of the photon emitted is given by the equation $\Delta E = E_2 - E_1 = hv$, where h is Planck´s constant. This emission of photons is called spontaneous emission. It is irregular and takes place at different instants from different atoms, so the light obtained from these atoms is incoherent.

An alternative mechanism in which an atom in the excited state emits photons with very low probability is called stimulated emission. This process is similar to absorption but operates in the opposite direction. In stimulated emission, an incoming photon resonantly stimulates an excited atom to give up its stored energy in the form of a photon that is identical in wavelength, direction, polarization, and phase to that of the stimulus photon.

If the number of atoms in the ground state is N_1 and the number of atoms in the excited state is N_2 and they are in thermal equilibrium, there are more atoms in the ground state than in the excited state (i.e., $N_1 >> N_2$). The necessary condition for achieving stimulated emission is that there are more excited state atoms than ground-state atoms (ie., $N_2 >> N_1$). This is known as population inversion, which can be achieved by using appropriate external pump sources to push the system into the non-equilibrated state.

The basic solid-state laser device mainly consists of three components: (1) an active medium, or gain (lasing) medium that can amplify light by means of stimulated emission; (2) a pump source, or an energizing source, which creates the population inversion in the active medium; and (3) a resonator that traps the light travelling back and forth between the mirrors to increase the probability of stimulated emission. When the active medium is pumped with sufficient energy, some of the emitted photons stimulate the emission of radiation from other excited atoms. As other photons collide with excited atoms, energy within the resonator builds and is amplified by reflections between the mirrors that stimulate more and more atoms to emit laser photons. At the front output mirror, a portion of the energy is permitted to escape and is

collected. This energy is an intense beam of monochromatic, collimated and coherent light which is called LASER. A schematic of the laser cavity is shown in figure 1.1.

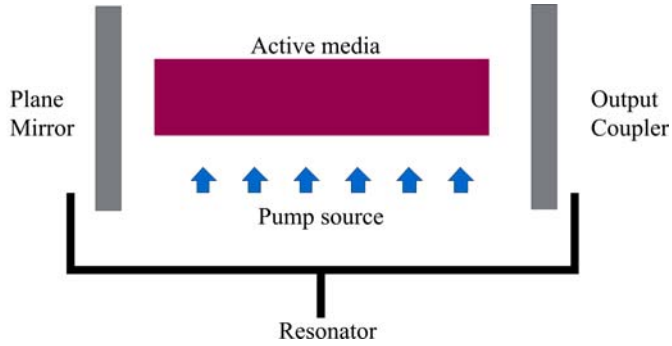

Figure 1.1 Schematic of simple laser cavity

Solid-state lasers have quite different characteristics from other types of laser: for example, reliability, robustness, high level of safety, low cost because of high volume production, compact size, wide range of wavelengths and maintenance free.

1.3 Solid state lasers

1.3.1 Active medium

The active medium is a solid-state material of either glass or crystal with an active ion (either transition metal or rare-earth) and may be broadly classified into three- or four-level systems.

In a three-level system (see figure 1.2 a), the laser transition ends on the ground state with only three levels: the ground level (E_0), the excited level (E_2) and the intermediate level (E_1), which is the emitting level. After excitation of the pump to the excited level E_2, it becomes populated and after a short period of time the excited ion relaxes non-radiatively to E_1. During the relaxation process the lost energy is transferred as heat to the lattice and the main laser transition (electronic transition) occurs from the intermediate level to the ground level. Since the final laser level is directly to the ground state and because of the thermal population at room temperature at this level, the laser threshold is rather high. An example of a three-level laser medium is ruby (Cr^{3+}:Al_2O_3), as used by Maiman, who discovered the laser [44].

The levels in four-level systems (see figure 1.2b) are the ground level (E_0), the first excited level (E_1), the second excited level (E_2) and the third excited level. After pump excitation at the E_3 level, this level gets populated and non-radiatively relaxes to the next intermediate level E_2, where it has a longer life time than level E_3 and E_1. Here, the laser transitions occur mainly between two intermediate levels ($E_2 – E_1$). Again from E_1, the atoms relax non-radiatively. Since

the terminal level is far above the ground level, the thermal population is small and the threshold in the system is lower. The most popular four-level solid-state gain medium is Nd:YAG.

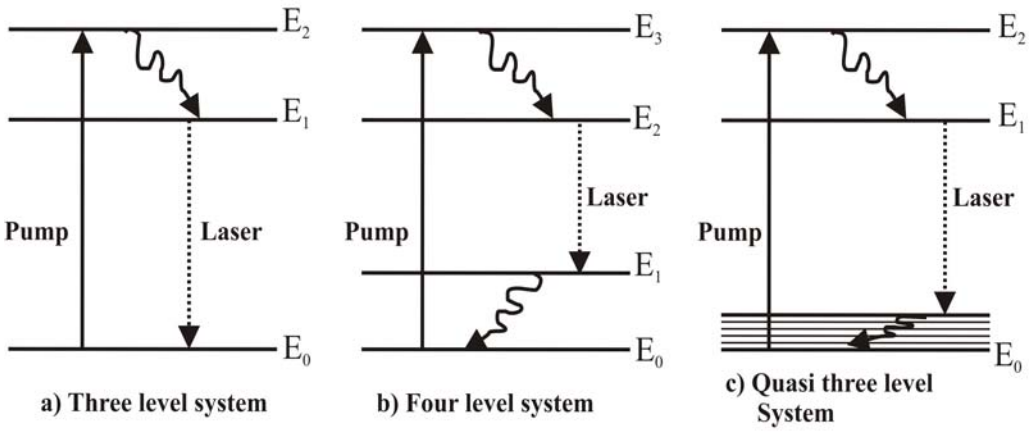

Figure 1.2 Simplified energy diagrams of three-level, four-level and Quasi three-level laser systems

Another important system is the quasi-three-level laser system. It is a kind of intermediate situation (see figure 1.2 c) in which the lower laser level is split into several stark levels with energies of the order of 500 to 1000 cm^{-1}, so that at room temperature the upper Stark levels are weakly populated, thus allowing the laser transition from E_1. In consequence, it suffers some re-absorption loss at the laser wavelength and transparency is reached at a finite pump intensity. Examples of quasi-three-level media are all Yb-doped gain media (e.g.,Yb:YAG) for 2 μm emission, Tm-doped and Ho-doped gain media for 1.8 - 2.1μm emission, and Er-doped gain media for 1.5 - 1.6 μm emission.

1.3.2 Laser matrix (host material)

Solid-state active media are mainly composed of host and active ions, which are the integral part. In this section we shall briefly discuss the solid-state laser host.

Solid-state laser host materials have their own unique microscopic and macroscopic properties and are broadly classified into two categories: glasses and crystals. For laser operation it is desirable that they have optimal optical, chemical, mechanical and thermal properties.

The optical properties include transmission, scattering, absorption, variation of refractive index, and polarisation properties of the host as a result of birefringence. The chemical properties include chemical inertness, crystallographic matching between the size of the host unit cell and the ionic radius of the dopant, and charge compensation to maintain the electrical neutrality of the host. The mechanical properties of the host include hardness, strain and elastic

modulus. The mechanical properties are extremely important for two essential reasons: 1) good mechanical properties will enable the crystal to sustain the extreme pumping and laser energy flux conditions; and 2) they simplify fabrication because cutting and polishing are easier. The thermal properties include thermal conductivity, thermal shock, and the thermal expansion coefficient, which are important because the temperature gradient in the crystal will lead to gradients in the refractive index and hence to poor beam quality.

Glasses are isotropic and the dopant ions are homogenously distributed. This means that the absorption bands have high fluorescent life-times and are easier to fabricate. The main drawbacks of these glasses are their broad emission band, which leads to higher pump thresholds, and their lower thermal conductivity, which leads to thermal load and distortions when the energies inside the cavity are high. Crystalline matrices, on the other hand, are highly ordered structures in which the ions are in fixed positions and are either isotropic or anisotropic. The thermal conductivity of crystals is higher than that of glasses and in general crystals are harder.

The most common host materials are glasses, sapphire, garnets, aluminates, phosphates, silicates, tungstates, molybdates, vanadates, fluorides and ceramics. Table 1.2, presents some of the structural, thermal and optical properties of these host materials.

Table 1.2 List of common hosts with their important structural, optical, thermal and mechanical properties

Host material	Crystal system	Space group	Mohs hardness	Thermal conductivity [W/ m K]	Transparency range [nm]	Reference
YAG ($Y_3A1_5O_{12}$)	Cubic	Ia3d	8.2-8.5	14	200–6000	
Sapphire (Al_2O_3)	Trigonal	R-3c	9	33	190–5200	
$REVO_4$	Tetragonal	$I4_1/amd$	5	5.1	400–5000	[45]
YAP ($YAlO_3$)	Orthorhombic	Pbmn	8.5	11	200–7000	
BaY_2F_8	Monoclinic	C2/m	4 - 5	6	200–9500	
YLF ($LiYF_4$)	Tetragonal	$I4_1/a$	4 - 5	6.3	120–8000	

In the present work, we studied the potassium rare earth double tungstates (KRE $(WO_4)_2$, RE= Y, Gd, Lu) , the main characteristics of which are presented in the next section.

1.3.2.1 Crystalline structure and morphology of $KRE(WO_4)_2$

Potassium rare earth double tungstates ($KRE(WO_4)_2$), (RE = Y, Gd, Lu)—KREW in short—crystallize in the monoclinic system ($a \neq b \neq c$; $\alpha = \gamma = 90°$, $\beta > 90°$) , with space group C2/c [46, 47] and point group 2/m. The crystalline structure of KREW has been studied in depth by

the FiCMA laboratories [48, 49]. The structural, optical and thermal properties of this host are summarized below.

The rare earth is eight-fold coordinated by oxygen atoms to form a distorted square antiprism. The local site symmetry of the RE^{3+} cation is C2 (4e Wyckoff position), and substitution by dopant ions takes place in this unique site. The REO_8 polyhedra form a single zig-zag chain in the [1 0 1] direction and share O – O edges. The length of these edges increases along the KSmW – KLuW series due to the increasing positive charge of the nucleus of the lanthanide (Ln) element. The distances between RE–RE pairs are also important because they affect the energy transfer between the dopant ions. Each rare earth polyhedra chain is surrounded by four equivalent chains. Figure 1a) in reference [49] shows the REO_8 zig-zag chains in the [101] direction and the W_2O_8 double chains in the [0 0 1] direction.

The coordination figure of the tungstate anion is a distorted octahedron which can be seen in figure 1b) of reference [49]. The W_2O_8 units, which consist of two distorted octahedrons sharing O – O edges, form a characteristic double chain in the crystallographic *c* direction by sharing vertex O. The average W–O distance gets shorter along the KSmW–KLuW series which means that the distortion of the WO_6 octahedra decreases and the covalent WO_6 groups are more compact. The K^+ is twelve-coordinated by O ions, and distorted icosahedrons are formed. The atomic coordinates and equivalent isotropic displacement parameters and the interatomic distances can be seen in the references [50] for KYW, [48] for KGdW and for [49] for KLuW.

The morphology of a crystal can be explained by the Hartman – Perdok theory [51]. This theory states that morphology is governed by the presence of periodic bond chains (PCBs). When the crystals grow they show the (010), (110), (310), (111) faces as natural faces, indicating that a larger surface is related to the faster growth rate of the face. For KREW, the dimension along the *c* crystallographic axis is generally about two times larger than the other two dimensions but not for all the crystals grown. The KGdW will mostly appear as a square. Also, the *c* axis and the [1 0 1] direction of the crystals grown appear as natural edges. The detailed morphology of these hosts can be found in reference [48] for KGdW and for [55] for KLuW.

1.3.2.2 Optical and thermal features of $KRE(WO_4)_2$

The physical behaviour of many crystalline substances depends on the direction in which external agents vary. This is called physical anisotropy. In the case of optical properties, optical anisotropy involves a change in the refractive index that depends on the direction of the vibration of the electric field of light inside the material. It is helpful to visualize the values of

the refractive index for all directions of vibrations and relate them to the directions of propagation, which are perpendicular. The resulting geometric figure is called the optic indicatrix. Since the monoclinic phase of KREW belongs to the 2/m point group and is a biaxial crystal with inversion centre. The three orthogonal principal optical axes x, y, z are labelled as N_p, N_m and N_g for monoclinic crystals. They are defined by the ratio of corresponding refractive indices $n_p<n_m<n_g$. In monoclinic crystals one of the principal optical axes coincides with the crystallographic *b* axis, which is N_p. The other two principal optical axes lie in the a-c plane. N_g is located clockwise to the crystallographic axis when the positive *b* axis is pointing towards the observer and N_m is located clockwise to the *a* crystallographic axis. The principal optical angle with respect to the crystallographic axis for each host is reported in table 1.3.

Table 1.3 Angle $\kappa°$ between *c* and N_g and angle $(\beta -90°)+ \kappa°$ between *a* and N_m

Host	κ °	$((\beta -90°)+ \kappa°)$°	Reference
KYW	18.5	59.0	[52]
KGdW	21.5	62.3	[53]
KLuW	18.5	59.2	[49]

The refractive index of KREW depends on the wavelength, the so called dispersive chromatic curves. These curves along each principal optical direction can be found in [52] for KYW, [53] for KGdW and [49] for KLuW. It is inferred that the refractive index is smallest for the N_p principal optical direction, intermediate for the N_m principal optical direction and highest for the N_g principal optical direction.

It is also important to know the optical transparency of the hosts because the host should be transparent at both the pump and the lasing wavelength. The transparency window of KREW (RE =Y, Gd, Lu) was roughly between 300 – 5400 nm and can be found in references [52] for KYW, [54] for KGdW and [55] for KLuW.

Thermal effects are crucial in power scaling with high-power diode pump laser sources. The non-uniform temperature distribution inside the laser crystals produces thermal lensing and thermal stress-induced birefringence which is related to the thermo-optic coefficient, dn/dt and the thermal conductivity of the material. In addition, the thermal expansion stress produces some distortion on the flatness of the crystal faces by generating a thick lens that perturbs the propagation of laser beam. If the temperature distribution is known the thermally induced optical distortions during laser experiments can be reduced. The thermal properties namely thermal conductivity, thermo-optic coefficient, linear thermal expansion and specific heat for KREW were studied in depth by FiCMA and can be found in references [56, 57, 58, 59]. As a summary, the important physical properties of the three hosts are reported in Table 1.4.

Table 1.4 Some important physical properties of KREW hosts

Properties	KYW	KGdW	KLuW	Reference
Crystal system	Monoclinic	Monoclinic	Monoclinic	[50, 48, 49]
Space group – point group	C2/c – 2/m	C2/c – 2/m	C2/c - 2/m	[50, 48, 49]
Symmetry	Centro symmetric	Centro symmetric	Centro symmetric	
Lattice constants	a=10.64Å, b=10.35 Å, c= 7.54Å, β= 130.30 °	a = 10.652Å, b= 10.374Å, c= 7.582Å, β= 130.80 °	a = 10.576Å, b= 10.214Å, c= 7.487Å, β= 130.68 °	[50, 48, 49]
Unit cell volume	633.3	634.2	613.3	[50, 48, 49]
Z - Number of formula units/molecules per unit cell	4	4	4	[50, 48, 49]
Minimum RE-RE separation	-	4.070 Å	4.045 Å	[48, 49]
Ionic radius of RE with coordination number 8	1.019 Å	1.053Å	0.977Å	[62]
Transparency range	350 – 5400 nm	300 – 5320 nm	365 – 5110 nm	[52, 54, 55]
Refractive index @ 2 μ m	N_g - 1.97, N_m -1.93, N_p - 1.90	N_g - 2.02, N_m -1.97, N_p - 1.96	N_g – 2.05, N_m -1.99, N_p - 1.94	[52, 53, 49]
Optical ellipsoid orientation	18.5°	21.5°	18.5°	[52, 53, 55]
Strongest phonon modes [cm^{-1}]	905	901	908	[60, 55]
Specific heat @ 300 K C_p[J/gK]	0.311	0.355	0.324	[59]
Thermal conductivity k [$WK^{-1}m^{-1}$]	κ'_{11}=2.47 κ'_{22}=1.86 κ'_{33}=3.31	κ'_{11}=2.45 κ'_{22}=2.01 κ'_{33}=3.49	κ'_{11}=2.95 κ'_{22}=2.36 κ'_{33}=4.06	[57], Unpublished results for KYW and KGdW
Thermal expansion coefficients α [10^{-6} K]	α'_{11}=8.3 α'_{22}=1.9 α'_{33}=18.0	α'_{11}=10.6 α'_{22}=2.8 α'_{33}=23.4	α'_{11}=8.98 α'_{22}=3.35 α'_{33}=16.72	[56, 57]
Hardness (Mohs scale)	4.5 - 5	4.5 – 5	4 – 5.5	[61, 49]

The KREW hosts stand out because they exhibit high absorption and emission cross-sections when doped with active lanthanide ions, partly due to the strong anisotropy of these biaxial crystals. They can also be doped with high concentrations of the active ions without substantial fluorescence quenching [63]. These hosts proved to be more attractive for intermediate power levels and laser action has been demonstrated in various active ions and interesting results with 11 W of output power in Yb: KLuW [64] and 4 W of output power in Tm: KLuW [40] was reported using a commercially available diode laser.

1.3.3 Active ions

1.3.3.1 Rare earth and transition metal ions

Active ions are either rare earth or transition metals. Generally, the ground-state electronic configuration of rare earth atoms consists of a core which is identical to xenon, plus additional electrons in higher orbits. In xenon, the shells with quantum numbers n = 1, 2, 3 are completely filled. The shell n = 4 has its *s, p,* and *d* sub shells filled, whereas the *4f* sub shell capable of accommodating 14 electrons is completely empty. However, the n = 5 shell has acquired its first 8 electrons, which fill the *5s* and *5p* orbits. The electronic configuration for xenon is [xe] = $1s^2 2s^2 2p^6 3s^2 3p^6 3d^{10} 4s^2 4p^6 4d^{10} 5s^2 5p^6$.

The elements beyond xenon (atomic number 54) have not only this electronic structure but also electrons in the *4f, 5d, 6s* sub shells etc. The rare earths begin when the inner vacant 4*f* orbits are filled. For example, the first rare earth element cerium has only one electron in the f orbit and has the electronic configuration Ce: [Xe] $4f^1 5d^1 6s^2$. And neodymium has four electrons in the *f* orbit and the electronic configuration Nd: [Xe] $4f^4 6s^2$. In crystals, rare earth ions are normally trivalent and when a trivalent ion is formed the atom gives up its outermost 6s electrons and loses its *5d* electron if it has one: if it has not, it loses one of the 4f electrons. For example, the electronic configuration Ce^{3+}: [Xe] 4f and the configuration of Nd^{3+}: [Xe] $4f^3$.

Rare earth ions are the natural candidates to serve as active ions in solid-state laser materials because their sharp optical transitions in the visible and infrared spectral regions occur within the *4f* sub shell. This sub shell is shielded by the outer *5s* and *5p* shells. As a result, emission lines are relatively narrow and the energy level structure varies only slightly from one host to another, so the well known and very useful Dieke diagram [65] can be used to estimate the relative position of the multiplets and the widths of the Stark splitting in the crystals. The electronic structure of trivalent rare earth ions derives from the perturbation of the *4f* energy level in the central field approximation by non-centro symmetric electron - electron interaction, the spin orbit interaction (manifolds) and the crystal field splitting (Stark components). An

example of one of the lanthanide ions – Ho is shown in figure 1.3. The exact energy positions of the manifolds and especially the positions of the Stark levels within each manifold depend on the crystal field and thus on the composition of the host as well as on its site symmetry. Figure 1.4 shows the Dieke energy - level diagram of trivalent rare earth ions in $LaCl_3$, including the main infrared transitions form various rare earth ions.

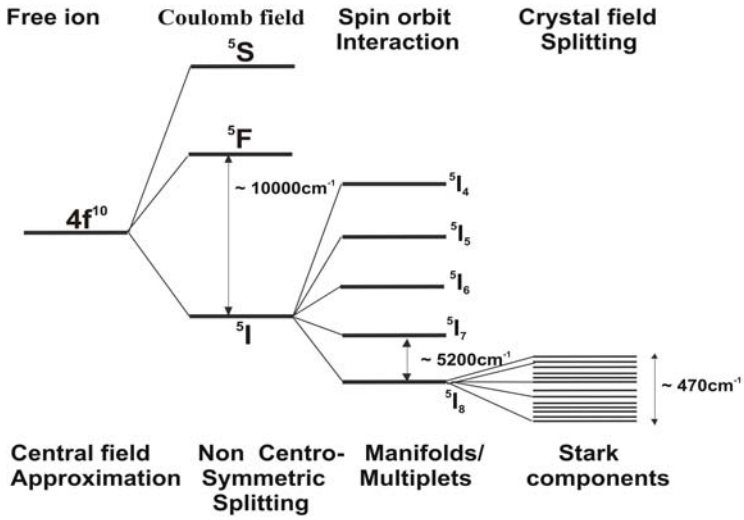

Figure 1.3 The effect of crystal field on the energy level splitting in the lanthanide ion Ho

Transition metals also play an important role as active ions in solid-state laser materials. In transition-metal atoms, the ground-state electronic configuration consists of a core which is identical to argon, plus additional electrons in higher orbits. The electronic configuration for argon is [Ar] = $1s^2\ 2s^2\ 2p^6\ 3s^2\ 3p^6$. The transition metal group includes mainly chromium and titanium. The most valuable characteristic of the transition metal ions is the broadness of the emission band, which extends from more than 300 nm and generates extremely short laser pulses. For example, the Ti: Sapphire laser delivers <10fs pulses [66].

UNIVERSITAT ROVIRA I VIRGILI
INFRARED LASERS BASED ON HO3+:KRE(WO4)2 CRYSTALS WITH TM3+OR YB3+ AS SENSITIZERS
Venkatesan Jambunathan
ISBN:/DL: T.1243-2011

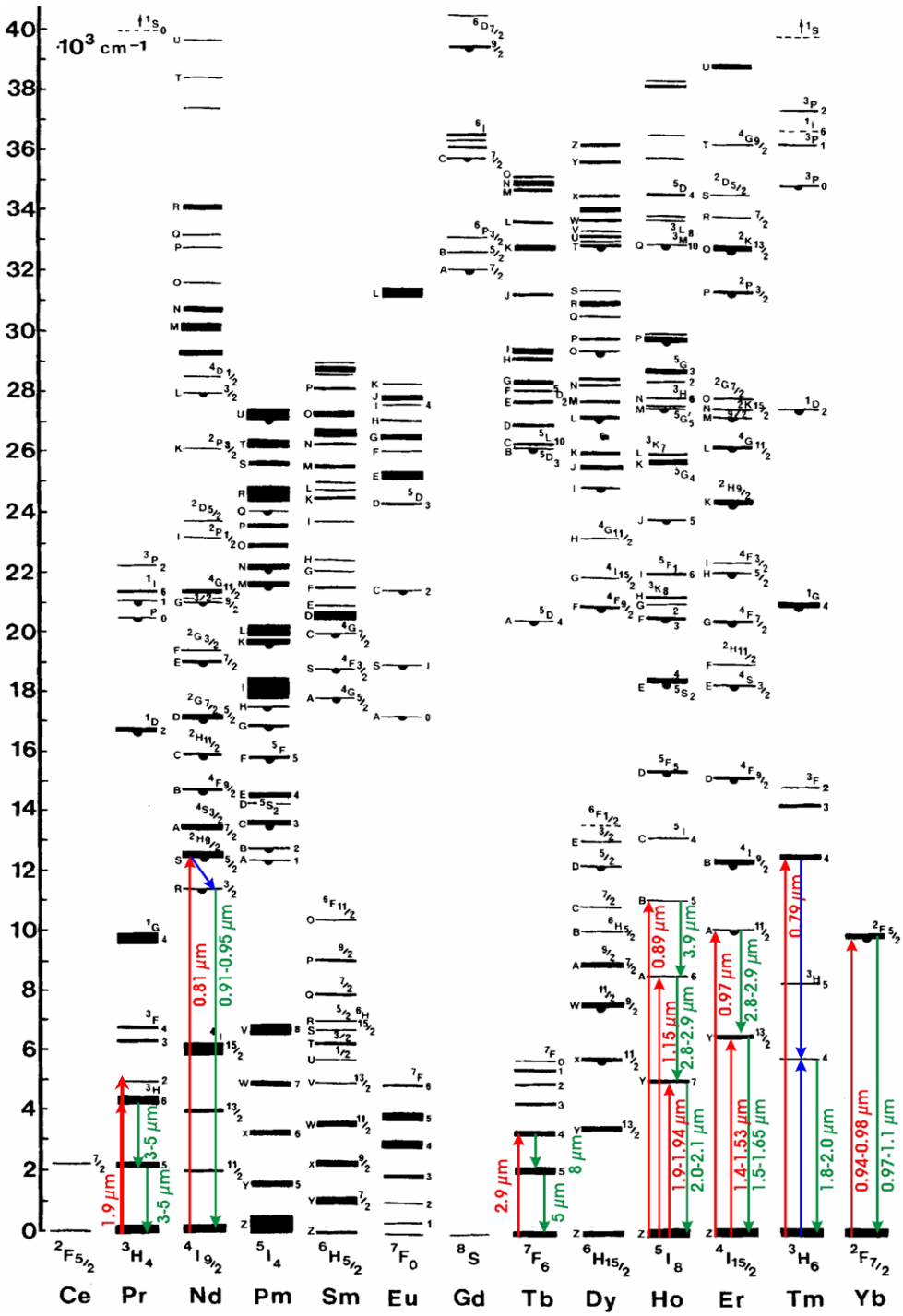

Figure 1.4 Energy-level diagram (Dieke diagram) of trivalent rare earth ions in $LaCl_3$, including the main infrared transitions from various rare earth ions

1.3.3.2 Holmium (Ho^{3+}), thulium (Tm^{3+}) and ytterbium (Yb^{3+}) as active ions

This study focuses on rare earth ions and, in particular, on Ho^{3+} as an activator and Tm^{3+} and Yb^{3+} as sensitizers, which are the active ions used to dope the host. This section briefly discusses these active ions.

The electronic configuration of Ho is [Xe] $4f^{10,}$ when it is in the +3 oxidation state. The energy levels of Ho, in increasing order are $^5I_{8,}$ $^5I_{7,}$ $^5I_{6,}$ $^5I_{5,}$ $^5I_{4,}$ $^5F_{5,}$ $^5S_{2,}$ $^5F_{4,}$ $^5F_{3,}$ $^5F_{2,}$ $^3K_{8,}$ $^5G_{6,}$ $^5G_{5,}$ $^5G_{4,}$ $^3H_{5,}$ $^3H_{6,}$ $^5G_{3,}$ $^3F_4$ and so on (see figure 1.4). Numerous studies have been made of the absorption and emission properties of Ho in various hosts. It shows considerable potential as an active ion for laser generation and nearly fourteen stimulated emission channels have been discovered for the Ho ion as activators from different hosts in the 0.55 to 3.9 μm range [67]. Laser transition, arising from the $^5I_7$ to $^5I_8$ (2.1 μm) level of Ho, has been widely reported [26, 27, 28]. Other transitions like $^5S_2$ + $^5F_4$ to the $^5I_8$ (540 nm) level are also interesting for generating visible solid-state lasers. In the field of sensitizing, the Ho ion is sensitized by such different ions as Cr, Fe, Tm, Yb and Er [68, 69, 70]. Sensitisation can increase the absorption or the lifetime of the emitting level.

In the +3 oxidation state, Tm has the electronic configuration [Xe] $4f^{12}$. In increasing order, the energy levels of Tm, are $^3H_{6,}$ $^3F_{4,}$ $^3H_{5,}$ $^3H_{4,}$ $^3F_{3,}$ $^3F_{2,}$ $^1G_{4,}$ $^1D_2$ and so on (see figure 1.4). The $^3H_4$ level (800 nm) of Tm is particularly interesting because absorption is maximum and it matches the emission bands of the commercially available AlGaAs laser diodes. Using this Tm ion, laser operation has been demonstrated in many hosts with higher output and efficiency [35, 36, 37]. In recent years, Tm-doped lasers are also used as a pump source because of the excellent beam quality and higher output. As a sensitizer ion, it is mainly used for Ho, because Tm can transfer some energy almost resonantly to the neighboring Ho ion [16,20]. It can also be used as a sensitizer ion for Pr [71] and to generate blue and white light fluorescence for solid-state lighting [72].

Ytterbium has the electronic configuration as [Xe] $4f^{13}$ when it is in the +3 oxidation state. The main advantage of Yb^{3+} is that it has only one excited state and makes the system very simple. The energy levels of Yb, in increasing order, are $^2F_{7/2}$ and $^2F_{5/2}$ (see figure 1.4). It is mainly used for the generation of 1.0 μm with a very low quantum defect in many solid-state laser hosts. It is also widely used as the sensitizer ion for lanthanide ions such as Er, Ho, Tm and Pr because it exhibits very high absorption and transfers some energy to the active ions [73].

1.4 Motivation and objectives of the present work

Compact, tunable, continuous-wave or pulsed solid-state laser sources operating in the 2 μm wavelength range are very useful for a variety of scientific and technical applications (see section 1.1). The simplest sources are diode pumped Tm or Ho crystalline lasers. Since there are many, well-developed compact diode pumped Tm crystalline lasers, and bearing in mind the advantages and disadvantages of Ho and the properties of KREW, we decided to take on the challenging task of developing a compact solid-state laser system based on Ho: KREW crystals operating around 2.1 μm, primarily using Tm or Yb as sensitizer ions and subsequently in-band/resonant pumping with a Tm laser and a laser diode stack. Stimulated emission of Ho: KREW had only been achieved previously by flash –lamp pumping at low temperature [74, 75].

The general objective of the present work, then, was to develop a compact and efficient infrared laser that operates at ~2.1 μm and is based on the Ho ion. In order to attain this general objective, several specific objectives also need to be attained.

The first objective was to demonstrate laser generation around ~2.1 μm from Ho by using the sensitizer ion Tm and pumping at 802 nm.

The second objective was to demonstrate laser generation by in-band/resonant pumping using two pump sources and then to compare the laser properties of each host.

The final objective was to demonstrate laser generation from Ho by using the sensitizer ion Yb and pumping at 980 nm.

To accomplish the first objective, crystals were grown with several co-doping ratios of (Ho, Tm): KLuW. The structural, compositional and spectroscopic properties of the grown crystals were then characterized and finally laser was generated from Ho by pumping the sensitizer ion Tm at 802nm with the Ti: Sapphire laser as a pump source.

To accomplish the second objective, we grew several concentrations of single doped Ho: KREW crystals. Then we characterized their structural, compositional and spectroscopic properties and finally laser was generated from Ho by pumping from two sources: 1) a Tm: KLuW laser emitting at 1946 nm, and 2) a GaSb laser diode stack emitting at 1941 nm.

Work on the final objective is still ongoing. We have grown several co-doping ratios of (Ho,Yb):KLuW crystals, and characterized their compositional and spectroscopic properties. We are now working on generating laser from Ho by pumping the sensitizer ion Yb at 980 nm by using the Ti: Sapphire laser as a pump source.

UNIVERSITAT ROVIRA I VIRGILI
INFRARED LASERS BASED ON HO3+:KRE(WO4)2 CRYSTALS WITH TM3+OR YB3+ AS SENSITIZERS
Venkatesan Jambunathan
ISBN:/DL: T.1243-2011

Chapter 2
Experimental techniques

This chapter gives a summary of the experimental techniques used in this work. The principle and procedure involved in each technique are presented. The facilities described in this chapter are those of the FiCMA-FiCNA group laboratories, the Servei de Recursos Cientifics of the Rovira i Virgili University, Tarragona, Spain, the Servei de Recursos Cientifico-Tècnic of the University of Barcelona, Spain, the Instituto de Ciencia de Materiales (ICMM) of the Consejo Superior de Investigaciones Cientificas (CSIC), Madrid, Spain, and the Max-Born Institute for Non linear Optics and Short pulse Spectorscopy, Berlin, Germany.

2.1 Crystal Growth - Top Seeded Solution Growth – Slow Cooling method (TSSG – SC)

The Top-Seeded Solution Growth Slow Cooling (TSSG - SC) method is one of the High Temperature Solution (HTS) growth methods [76] and enables single crystals to be grown in the phase of interest before the melting temperature. It is based on the concepts of solubility and supersaturation. The components of the final materials are dissolved in a solvent. At a particular temperature a certain amount of a substance can dissolve in a particular solvent, and the amount dissolved defines the solubility at that temperature. If a saturated solution is prepared at a particular temperature and then cooled to a lower temperature, it contains more salt than is permitted by the solubility at that temperature. The same occurs if the solution temperature is lowered; the solution will be in the supersaturated state, which is a metastable state, and the extra salt precipitates when a seed crystal is introduced into the solution. The substance precipitating from the solution grows around the seed crystal to form a larger single crystal. In the absence of a seed, even dust particles can provide a nucleus for crystal growth. Crystallisation can be performed in air or any other suitable atmosphere.

The difference between TSSG and other flux techniques is that crystals grow in a crystallographically oriented seed crystal that is in contact with the surface of the solution so that the crystal grows with the seed correctly oriented. The composition of the crucible depends on the temperature of the solution used. Usually, when crystallisation takes place in air, crucibles made of pure Pt should be used. In the presence of O_2, pure Pt melts at 2045 K. We used a pure Pt crucible because of the extremely low reactivity with the oxides used as precursors for growing the crystals. We used a 50 mm high and 50 mm diameter crucible as shown in figure 2.1 a) to obtain larger single crystals. The crucible was supported inside the furnace by a mobile alumina column that could be displaced in order to accurately locate the crucible in the right thermal zone. The crystal seed grows in the supersaturated solution and continues to grow while the temperature decreases at a steady rate. Optionally, the crystal seed can be pulled while it grows to obtain larger crystals. To avoid secondary nucleation, the crystal seed should be at the coldest point in the flux. In this case, the crystal seed is placed on the surface of the solution, just in the centre of the platinum crucible and is rotated in order to enhance the mass and heat transfer in the solution and to avoid inclusions during the growth process. The crystal seed is attached to an alumina bar/rod tied by means of a platinum sheet/ wire as shown in figure 2.1 b).

Figure 2.1 a) Platinum crucible used to grow the crystals

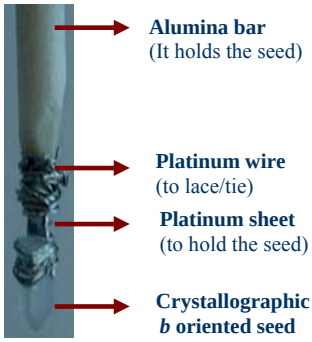

Figure 2.1 b) Alumina bar with seed crystal

A vertical tubular furnace with kanthal heating elements was used and the furnace was equipped with a temperature controller-programmer and thermocouples. The furnace was thermally isolated with firebricks and had a thermal zone of 10 cm in diameter and around 50 cm in length (see figure 2.1 c)). Two thermocouples were used to monitor the crystal growth process. The one in the furnace was connected to the temperature controller, while the other monitoring thermocouple measured the temperature in various places in the heating chamber. We used an s-type thermocouple Pt/Pt-Rh 10% located in the centre of the furnace near the heating resistances to ensure stable and reliable measurement of the temperature. The monitoring thermocouple was used to determine the difference in temperature between the control thermocouple and the surface of the solution where the crystal seed was placed. The monitoring thermocouple was also used to check the thermal axial and radial profile of the solution. The temperature gradient inside the solution is crucial to guarantee the quality of the crystals. The temperature controller was connected to a thyristor to control the power supplied to the furnace. The furnace was controlled by a Eurotherm 903P (minimum cooling ramp of 0.01 Kh^{-1}).

Figure 2.1d) shows the furnace that was used to obtain single crystals. It comprises a vertical metal rigid structure that enables the crystal seed to be vertically displaced and rotated using the mechanical part of the system. We used a Mitutoyo micrometer to measure the changes in the length of the crystal seed to an accuracy of 0.01 mm and to accurately determine the saturation temperature. These furnaces are available at the FiCMA - FiCNA group laboratories.

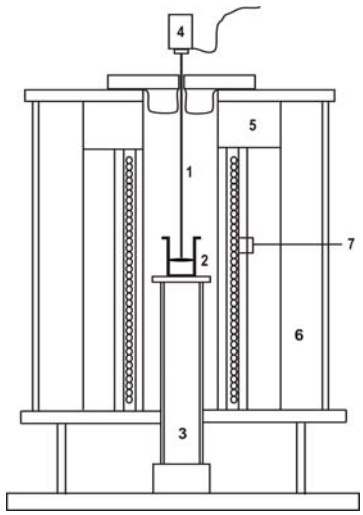

1 – Alumina bar
2 – Platinum crucible
3 – Movable crucible support
4 – Seed rotor system
5 – Alumina brick insulator
6 – Thermal wool insulator
7 – Thermocouple

Figure 2.1 c) Schematic of the cross section of the furnace

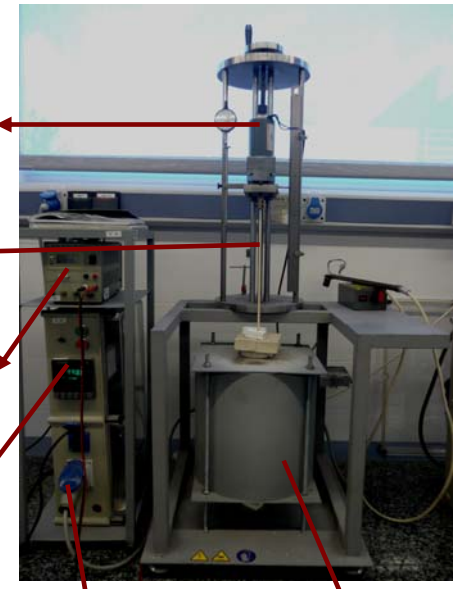

Figure 2.1 d) The furnace used in the present work

2.2 Sample preparation

2.2.1 Cutting

To prepare the samples for optical measurements and laser experiments, the crystals were cut and polished so that they were free of scratches and of very high optical quality. Since the crystals belong to the monoclinic family and are biaxial, the samples were first oriented for the principal optical directions N_g , N_m *and* N_p (which are defined by $n_p<n_m<n_g$ and are related to the principal refractive indices described in chapter 1) using a goniometer (see figure 2.2 a)). They were cut using a diamond saw disk 0.12 mm thick (see figure 2.2 b)).

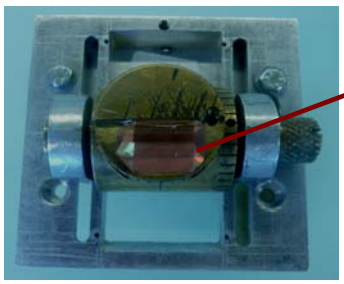

Figure 2.2 a) Sample fixed for cutting in a goniometer

Figure 2.2 b) Diamond saw for cutting the sample

2.2.2 Polishing

Once they had been cut, the samples were mounted in a circular disc (see figure 2.2 c)) and then polished in a Logytech PM5 polisher which has an oscillatory arm (figure 2.2 d)). This makes it possible to accurately rotate and pressurise the samples, depending on the hardness of the material to be polished. Alumina powders (hardness = 7 mohs) of 9, 3, 1 and 0.3 µm were used as abrasive substances depending on the quality of the polishing required. The quality of the polishing was measured with parameters such as roughness, flatness (measured by a self-collimator) and parallelism between opposite faces of the sample (measured by the same self-collimator using the two reflections on the opposite faces of the sample). These systems were available at the FiCMA-FiCNA group laboratories and there are technicians for this purpose.

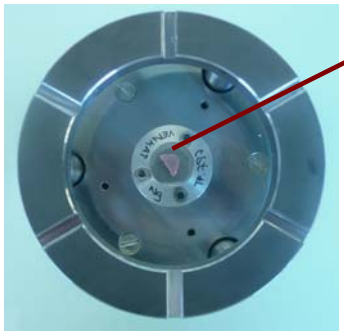

Figure 2.2 c) Cut sample fixed for polishing

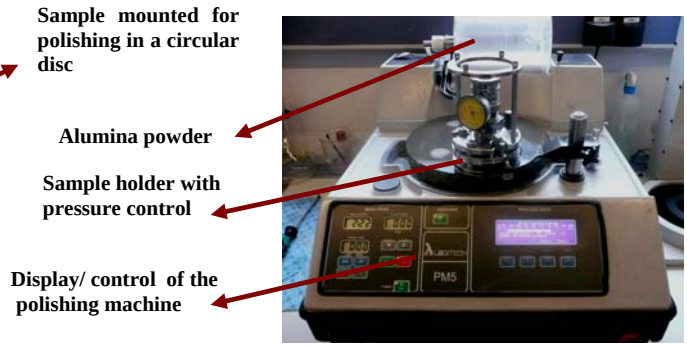

Figure 2.2 d) Logytech PM5 polisher

2.3 Structural characterization - X-ray powder diffraction

X-ray powder diffraction is an analytical technique used to identify the phase of a crystalline material and it can also provide information on unit cell parameters. As the name suggests, the sample is usually in powder form, and consists of fine grains of the single crystalline material which is to be studied. X-ray diffractometers have three basic elements: an X-ray tube, a sample holder and an X-ray detector. The X-rays are generated in a cathode ray tube by heating a filament to produce electrons. After accelerating these electrons towards a target material by applying a voltage, the electrons are bombarded. When the electrons have sufficient energy to dislodge the inner shell electrons of the target material, characteristic X-ray spectra are produced. The specific wavelengths are characteristic of the target material such as copper, iron, molybdenum and chromium. Copper is the most common target material for powder diffraction, with CuK_{α} radiation = 1.5418Å. The X-rays are collimated and directed at the sample. As the sample and detector are rotated, the intensity of the reflected X-rays is recorded. When the geometry of the incident X-rays impinging on the sample satisfies the Bragg equation $2d_{hkl}\sin\theta$

ISBN:/DL: T.1243-2011

= $n\lambda$, constructive interference occurs and results in peak intensity (λ is the wavelength of the incident x-ray beam, d_{hkl} is the interplanar spacing distance in the crystal lattice, θ is the angle between the incident ray and the diffracted beam). A detector records and processes this X-ray signal and converts the signal to a count rate, which is then output to a computer. The geometry of an X-ray diffractometer is such that the sample rotates in the path of the collimated X-ray beam at an angle θ while the X-ray detector is mounted on an arm to collect the diffracted X-rays and rotates at an angle of 2θ. The angle is maintained and the sample rotated with a goniometer. For typical powder patterns, data are collected at 2θ and between 5° and 70°.

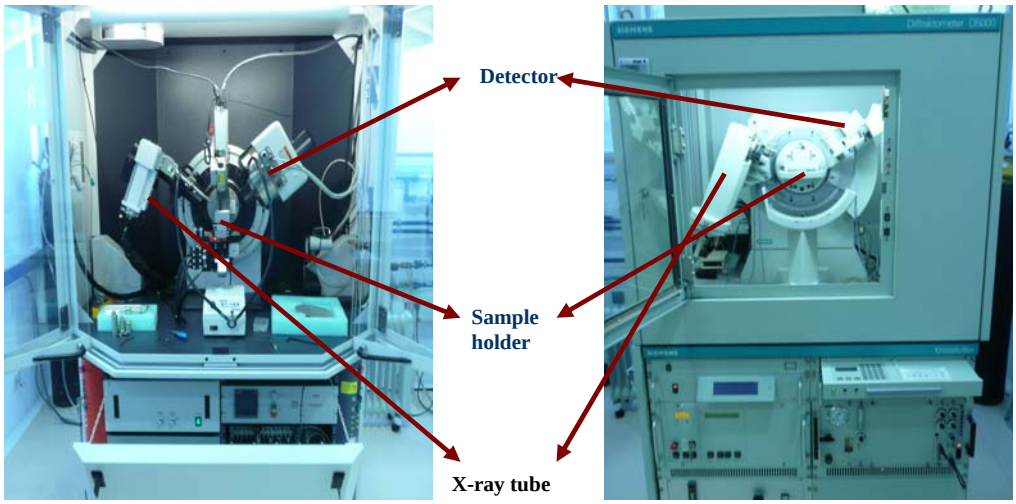

Figure 2.3 a) Bruker - AXS D8- discover diffractometer

Figure 2.3 b) Siemens D-5000 diffractometer

To measure diffraction patterns we used a Bruker-AXSD8-discover diffractometer (see figure 2.3 a)) in step scanning mode and with a diffraction angle (2θ) between 5° and 70°. To measure diffraction patterns with temperature, we used a Siemens D-5000 diffractometer (see figure 2.3 b)) in step scanning mode and with a diffraction angle (2θ) between 10° and 70°. Once the diffraction patterns had been obtained the unit cells were refined using the Fullprof program [77] based on the Rietveld method [78]. This equipment was provided by the Servei de Recursos Científics i Tècnics of the Rovira i Virgili University, Tarragona, Spain and there is a technician for this purpose. Analysis of the results was carried out in the FiCMA-FiCNA group.

2.4 Compositional characterization - Electron Probe Micro Analysis (EPMA)

Electron Probe Micro Analysis (EPMA) is one of the non-destructive quantitative methods used to determine the composition of small areas on specimens. It operates under the principle that if

a solid material is bombarded by an accelerated and focused electron beam, the incident electron beam has sufficient energy to release both matter and energy from the sample. These electron-sample interactions release mainly heat, but also derivative electrons and X-rays. Of most common interest in the analysis of materials are secondary and back scattered electrons, which are useful for imaging a surface or obtaining an average composition of the material. X-rays are produced by inelastic collisions of the incident electrons with electrons in the inner shells of atoms in the sample. When an inner-shell electron is ejected from its orbit, leaving a vacancy, a higher-shell electron falls into this vacancy and energy as X-rays are released. These quantized X-rays are characteristic of the element. EPMA analysis is considered to be "non-destructive" because the X-rays generated by electron interactions do not reduce sample volume, so the same materials can be re-analyzed.

EPMA consists of the following major components: firstly an electron source, commonly a W-filament cathode; secondly, a series of electromagnetic lenses located in the column of the instrument, used to condense and focus the electron beam emanating from the source and consisting of electron optics and operates in an analogous way to light optics; thirdly, a sample chamber with a movable sample stage (X-Y-Z) under a vacuum to prevent gas and vapour molecules from interfering with the electron beam on its way to the sample and with a light microscope that makes it possible to observe the sample directly; and finally, wavelength dispersive spectrometer (WDS) detectors in the sample chamber, which collect the X-rays and electrons emitted from the sample. The cross section of the system is shown in figure 2.4 a). Quantitative analysis is essentially a comparative method. It involves measuring the characteristic X-rays from a sample and a set of standards analyzed under similar conditions. The accuracy depends largely on the similarity of the standards and the sample. For the measurement we used the Cameca SX 50 microprobe analyser available at the Servei de Recursos Cientifico-Tècnics of the University of Barcelona operating in wavelength dispersive mode. The electron beam is generated with an accelerating voltage of 20K and a current of 30-100 nA depending on the concentration of the element to be determined. The dispersive spectrometer crystals used were lithium fluoride 200 (LIF), pentaerythritol 002 (PET), thallium acide phthalate 1011 (TAP) and pseudo crystal (PC1). The wavelength range covered by these crystals was 1-24 Å means that K- lines for elements with an atomic number 9 to 35 and L-lines for elements with atomic number less than 83 and M lines for all elements. Table 2.1 summarizes the measurement conditions and lists the standards used to calculate the chemical composition of the samples by comparing the X-ray intensity of the sample and the standard.

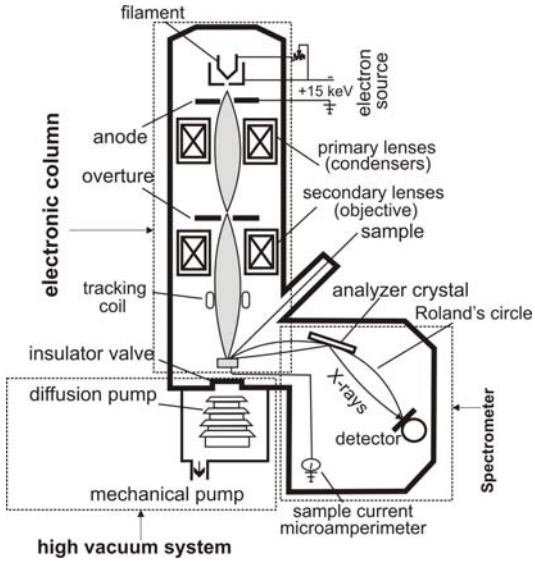

Figure 2.4 a) Schematic of the cross-section of the EPMA equipment

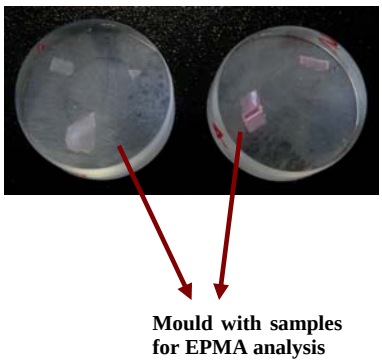

Figure 2.4 b) Samples for EPMA analysis

The samples to be measured were prepared by placing a small piece of the grown sample in a cylindrical polymer container which is used to make a mould using a polyester resin (styrene and phthalic anhydride) with its corresponding catalyst (methyl ethyl ketone peroxide). The mould mixture is solidified for 12 to 15 hrs and then polished to optical quality in a Struers DAP 7-polisher using a velvet polishing cloth with a diamond spray of 3 and 1 µm. The samples were prepared in the FiCMA-FiCNA lab (see figure 2.4 b) and then coated with a fine layer of metal conductor (gold) for better conduction of the sample. For measurement there is a technician for this purpose and the interpretation of the result was carried out in FiCMA-FiCNA group.

Table 2.1 Measurement conditions and standards used in EPMA analysis

Element	Line	Spectrometer crystal	Standard
K	K_α	PET	KLuW
W	M_α	TAP	KLuW
Lu	L_α	LiF	KLuW
Gd	L_α	LiF	KGdW
Y	L_α	LiF	KYW
O	K_α	PC1	KREW (RE=Y, Gd, Lu)
Ho	L_α	LIF	REE2
Tm	L_α	LIF	REE2
Yb	L_α	LIF	REE3

2.5 Spectroscopic characterization

Spectroscopy is the study of properties of matter through its interaction with different frequency components of the electromagnetic spectrum. It is a general methodology that can be adapted in many ways to extract information such as electronic, vibrational and rotational state energies, and the structure and symmetry of molecules. In the following section the fundamentals of the spectroscopic technique used here are discussed.

2.5.1 Optical absorption

The theory which relates the absorption coefficient (α) and the incident light intensity is given by the Beer–Lambert law in the equation

$$I = I_0 e^{-\alpha d} \tag{2.1}$$

where *d* is the thickness of the sample.

The absorbance (A) or Optical Density (*OD*) is given by

$$OD = -\log\left(\frac{I}{I_o}\right) \tag{2.2}$$

This can be measured using atomic absorption spectrometers.

Combining equation (2.3) and (2.4), the absorption coefficient (α) is given by

$$\alpha = OD\left(\frac{1}{d \log e}\right) \tag{2.3}$$

Since α depends on the concentration of the absorbent centres, a more convenient parameter for describing the absorption process is the absorption cross-section (σ), which is defined as the absorption coefficient α over the density of the absorber centres (N).

$$\sigma_{abs} = \left(\frac{\alpha}{N}\right) \tag{2.4}$$

α is given in cm^{-1} and the concentration in $atoms.cm^{-3}$. Therefore, σ is in cm^2.

To measure the optical density we used a Varian Cary 500 scan spectrophotometer. The advantage of this instrument is that it is a double beam spectrophotometer with an effective spectral range of 0.175 to 3.3 μm that can measure optical densities in the range from 0 to 10. It uses a deuterium lamp for UV range and a halogen lamp for the visible IR range. It uses a photomultiplier to detect up to 850 nm and a lead sulphide detector to detect the IR region. The monochromator system has an entrance slit, a collimating lens, a set of diffraction grating elements (namely 1200 lines/mm for the UV-visible region and 300 lines/mm for IR region), a focusing lens and an exit slit. Due to the strong physical anisotropy of our tungstate crystals, we

used a Glan – Thompson polariser in front of the sample to analyze the optical absorption with the electric field parallel to each principal optical direction. To study the optical absorption at low temperature (6K) and determine the Stark levels of the active ions, we used a Leybold helium closed cycle cryostat which has a temperature controller that stabilises the temperature in the 6 -100 K range with a precision of ±3K and in the 200-300K to a precision of ± 5K. The whole spectrophotometer equipment setup is available at the FiCMA-FiCNA laboratories (see figure 2.5).

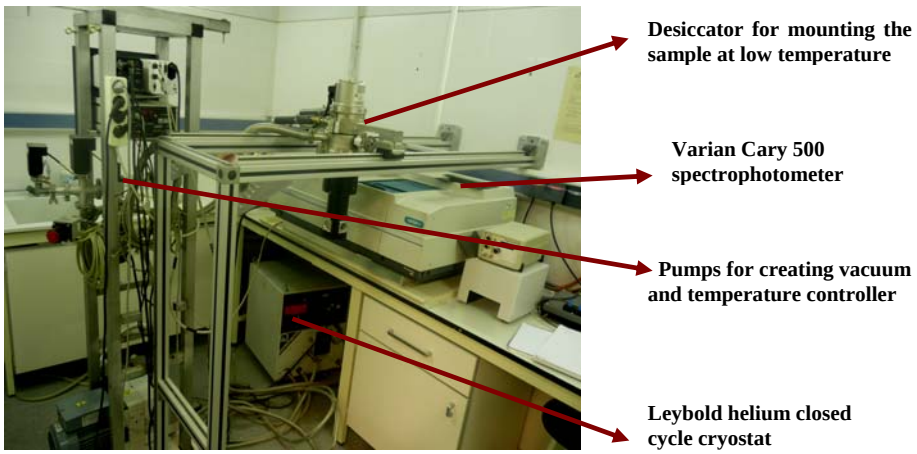

Figure 2.5 Spectrophotometer equipment used for room and low temperature measurement

2.5.2 Photoluminescence (emission and life-time measurements)

Photoluminescence is the process by which a substance absorbs photons at high energy levels and emits photons at lower energy levels or ground state radiatively and non-radiatively. Photoluminescence helps us to determine the possible emission channels between electronic states and their lifetimes in these states.

2.5.2.1 Emission

Emission is the process of exciting the photons from a higher energy state to a lower energy state radiatively or non-radiatively. For emission measurement we excite the crystals with a Ti:Sapphire laser from Coherent (model – Mira 900-P) and an Optical parametric oscillator (OPO) from Opotek (Model-Vibrant HE 355 II+UV) for a particular wavelength depending on the absorption properties of the active ion. The beam from the laser source is then focused on the sample and the emission is collected at 90° geometry in order to minimize the influence of the laser pump. The emission from the sample is collected using a set of collecting lenses, which are dispersed by a Jobin Yvon HR 460 monochromator with a focal length of 460mm, a spectral

resolution of 0.05 nm and different grating elements (1800 g/mm, 600 g/mm and 300 g/mm) depending on the wavelength range to be dispersed. For detection we used different kinds of detector: for example, for visible emission channels we used a Hamamatsu PMTR928 photomultiplier tube. For detecting emission channels between 800 nm and 1700 nm we used a cooled Hamamatsu R5509-72 NIR photomultiplier tube and for emission channels between 1700 and 3000 nm we used a cooled Hemamatsu P7163 – InAs photovoltaic detector. The detectors are connected to a Perkin Elmer DSP-7265 lock in amplifier to detect and amplify the signal and a computer was used to process the data. Figure 2.6 shows a scheme of the setup. To measure the low temperature and determine the ground state splitting we used an Oxford cryostat (CCC1104) which uses a closed cycle helium circuit for cooling and a temperature controller to stabilise the system at 10 K. Figure 2.7 shows the scheme of the photoluminescence equipment at the FiCMA-FiCNA laboratories.

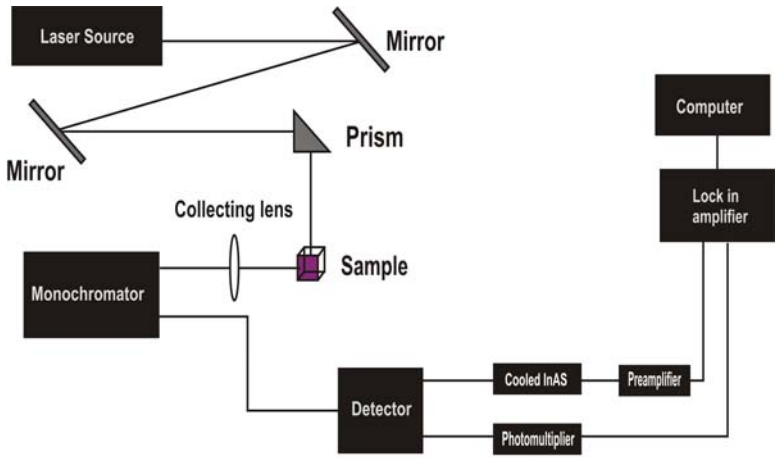

Figure 2.6 Scheme of setup for emission measurement

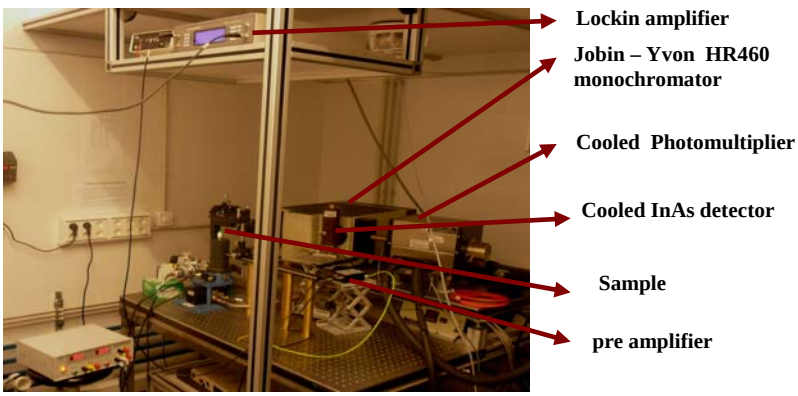

Figure 2.7 Photoluminescence equipment used for emission measurements

2.5.2.2 Lifetime

Measuring the lifetime of a substance helps to identify whether the emission channels are radiative or non-radiative. After pulsed excitation the intensity of emission declines exponentially with time. The radiative lifetime (τ) is the time between the start of emission and the point at which its intensity decreases a factor (1/e) from its initial value. To measure lifetime we excited the samples with a Quanta –Ray –HF OPO system, which provides laser pulses shorter than 10 ns between 440 -680 nm and 730-1750 nm. The fluorescence from the sample was collected and dispersed by a 340 mm single grating SPEX spectrometer, the visible emission was detected with a Hamamatsu PMTR928 photomultiplier tube and emission channels between 1700-3000 nm were detected with a cooled InSb photovoltaic detector. The signals from the detectors were recorded using a TDS-520 Tektronix oscilloscope. A computer was used to process the data. The scheme of the lifetime measurement system is shown in figure 2.8, and the equipment is available at the Instituto de Ciencia de Materiales (ICMM) of the Consejo Superior de Investigaciones Cientificas (CSIC), Madrid, Spain. The measurement was carried out during a week stay of the candidate in the CSIC lab.

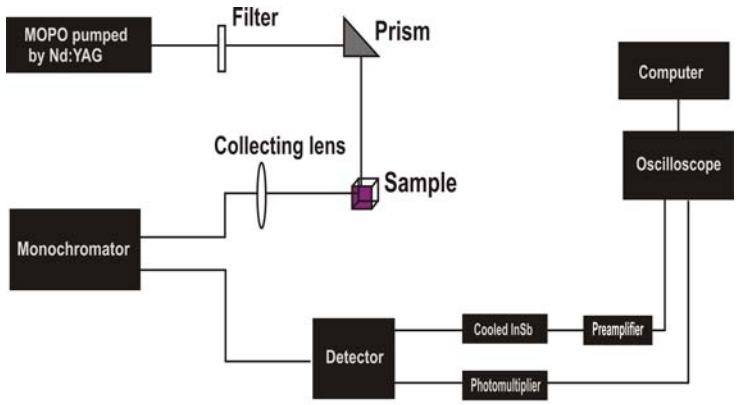

Figure 2.8 Scheme of lifetime measurement system

2.6 Laser generation

2.6.1 Pump sources

The pump source provides energy to the laser system. Generally the pump source of a solid-state laser emits radiation in the spectral range that falls within the absorption bands of the lasing medium. Either continuous or pulsed electrical energy is supplied to the pump source and converted into optical radiation. With the help of the optical systems (lens, mirrors etc) the radiation from the pump source is coupled to the laser material. For our laser generation

experiments we used three different types of pump source depending on the cavity for the generation of 2 μm emission.

2.6.1.1 Ti:Sapphire laser

Ti: sapphire lasers are tunable lasers which emit red and near-infrared light in the range from 650 nm to 1100 nm. They are mainly used in scientific research because of their tunability and their ability to generate ultra short pulses. For our laser experiments we used a commercially available Ti:Sapphire laser from Coherent (model – Mira 900-P) which delivers a maximum of 1.6W of output at 802nm. The pump source for this Ti:Sapphire is a Coherent Verdi V-10 laser which is a diode-pumped frequency doubled Nd:YVO_4 laser system that is capable of generating 10 W CW optical power at 532 nm.

2.6.1.2 Diode-pumped Tm:KLuW laser

The diode-pumped Tm:KLuW laser is a homemade laser which has been described elsewhere [40]. The pump source of the Tm laser was a fibre-coupled diode from Lumics whose emission at high current was centered at 806 nm. The output from this Tm:KLuW has a maximum of 5.1W centered at 1946 nm. The output radiation was linearly polarized along its N_m principal optical axis.

2.6.1.3 Diode laser (~ 1941 nm)

The diode pump source was a fibre-coupled GaSb laser diode module (from DILAS) which has a maximum output of 16 W and a wavelength between 1932 and 1941 nm depending on the current level. The core diameter of the fibre was 400 μm (NA=0.22).

2.6.2 Optical resonators

2.6.2.1 V-type cavity for the co-doped (Ho,Tm):$KLu(WO_4)_2$ laser

Laser assessment for the co-doped (Ho,Tm):KLuW crystals were performed by constructing a V-type astigmatically compensated resonator as shown in figure 2.9. It was formed by two curved mirrors (M1 and M2), with a radius of curvature (R_{oc}= -100mm), with transmission > 98% at pump wavelength and high reflection in the 1800-2100 nm range. One curved mirror serves as a pump mirror for the sample and a folding mirror for the output coupler. The other serves as a pump end mirror and pump power that leaks from the sample can be collected behind it. So, these experiments consisted of single pass pumping. High optical quality un-coated active medium (Ho,Tm):KLuW samples were mounted in a copper holder and positioned at Brewster's

angle in between the two curved mirrors and the samples were oriented so that light propagated along the N_g axis and polarized parallel to the N_m axis. The active element was 3 mm thick and the aperture was 3x3 mm^2. The cavity terminal was formed with one of the plane output couplers (OC) with the transmissions (T_{oc}) = 1.5 (±0.5), 3.0 (±0.5), 5.0 (±0.5), and 9.0 (±1.0) % in the 1820-2050 nm range. The pump source was a Ti:Sapphire laser centered at 802 nm as mentioned, where Tm absorbance is maximum. To focus the pump beam into the crystal, we used a lens L1 with a focal length of 75 mm, anti reflection coated for the 650-1100 nm range. The active elements were wrapped using indium foil on the top and bottom surfaces so that contact was better with the copper holder, the bottom of which was actively water cooled to 16°C and the top of which was passively cooled so that the heat dissipated. All these equipments were available at the FiCMA-FiCNA laboratories.

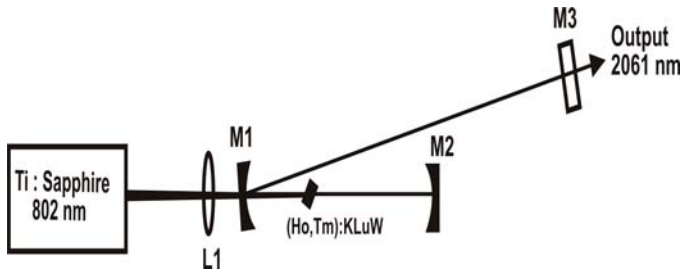

Figure 2.9 Laser Setup for the CW experiments on (Ho,Tm):KLuW crystals

2.6.2.2 Hemispherical two mirror cavity for Ho:KRE(WO_4)$_2$ lasers

Two kinds of pump sources were used for the Ho:KREW lasers. One was the diode- pumped Tm:KLuW laser and the other was the laser diode described above. For the laser experiments for a single-doped Ho:KREW, we used a hemispherical two mirror cavity. It consisted of a plane mirror (M5), which served as a pump mirror, antireflection (AR) coated for the pump wavelength (1940 nm) and high-reflection (HR) coated for the laser wavelength (2060 nm). The output coupler series (M6) consisted of several curved mirrors with 25, 50 and 75 mm radii of curvature (R_{OC}). The transmissions of the output couplers used (T_{OC}) were 0.5(±0.2)%, 1.5%(±0.3)%, 3.0(±0.5)%, 5.0(±1.0)%, 10.0(±2.0)% and 20.0(±4.0)% in the range 1820 to 2050 nm. When the pump source was the Tm: KLuW laser, two lenses (L2) was used to pump the Ho crystals with focal lengths of 50 and 150 mm. The active element (Ho:KLuW) was mounted in a Cu holder that served as a heat sink but no cooling was applied. The schematic of this cavity setup is shown in figure 2.10. After the attenuator we placed an optical isolator (I) to avoid any back coupling from the Ho-laser set-up. A quarter-wave plate was used to make the pump beam to the Ho-laser circularly polarized.

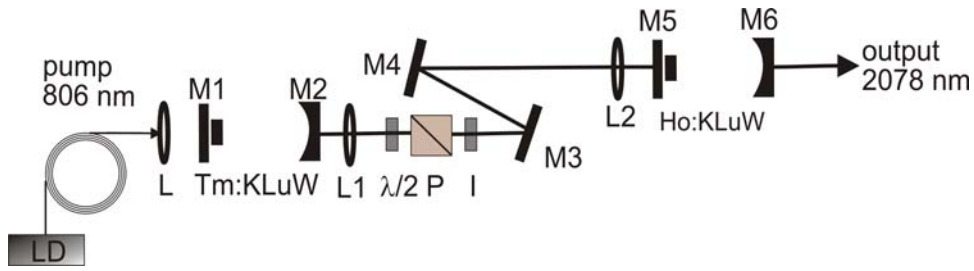

Figure 2.10 Laser setup for the CW experiments on Ho: KREW resonantly pumped by diode pumped Tm: KLuW laser

For diode pumping, we used a special lens (L1) assembly which comprised a collimator and an aspherical lens with a working distance of 3 mm resulting in a pump spot size of about 220µm. The active element (Ho:KREW) was mounted in a Cu holder that served as a heat sink and which was cooled to 16°C and the crystals were anti reflection coated in a broad range (1800 – 2200 nm). The schematic of this cavity setup is shown in figure 2.11. All these equipments were available at the Max Born Institute for Nonlinear Optics and Short Pulse Spectroscopy, Berlin, Germany. The results achieved with these setups are carried out by the candidate during his three months stay and several 15 days stay.

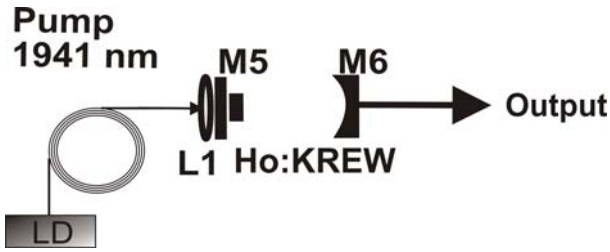

Figure 2.11 Laser setup for the CW experiments on Ho: KREW crystals in-band pumped by diode laser

UNIVERSITAT ROVIRA I VIRGILI
INFRARED LASERS BASED ON HO3+:KRE(WO4)2 CRYSTALS WITH TM3+OR YB3+ AS SENSITIZERS
Venkatesan Jambunathan
ISBN:/DL: T.1243-2011

Chapter 3

Growth and characterization of Ho-doped $KRE(WO_4)_2$ crystals

3.1 Crystal growth of Ho, (Ho,Tm), (Ho,Yb), (Ho,Tm,Yb) -doped $KRE(WO_4)_2$ crystals

3.2 Structural characterization. Study on the variation of unit cell parameters as a function of doping level and temperature

3.3 Compositional characterization

3.4 Spectroscopic characterization of Ho:$KRE(WO_4)_2$, (Ho, Tm):$KLu(WO_4)_2$, (Ho,Yb): $KLu(WO_4)_2$ and (Ho,Tm,Yb):$KLu(WO_4)_2$ crystals

3.4.1 Optical absorption

3.4.2 Photoluminescence

3.4.2.1 Optical emission

3.4.2.2 Lifetime measurements

3.4.2.3 Calculation of emission and gain cross-sections

This chapter summarizes the main experimental results obtained in relation to the crystal growth, structure, composition and spectroscopy of the single-doped, co-doped and triply doped systems. Firstly, the crystal growth is presented and discussed. Secondly the structural characterization related to the variation of unit cell parameters as a function of doping concentration and temperature is presented, taking into account that the structure of KREW has already been determined by the FiCMA group. Thirdly, the composition was characterized to determine the real ion density in the crystals. Finally the spectroscopy is studied in terms of room- and low-temperature optical absorption, and photoluminescence which consists of the emission and lifetime measurement of single-doped, co-doped and triply doped systems.

The following papers describe some of the results included in this chapter.

Paper I: V. Jambunathan, X. Mateos, M. C. Pujol, J. J. Carvajal, J. Massons, M. Aguiló and F. Díaz, "Near-infrared photoluminescence from Ho^{3+}–doped monoclinic $KLu(WO_4)_2$ crystal codoped with Tm^{3+}", J. Lumin. **129** (12), 1882-1885 (2009).

Paper II: V. Jambunathan, A. Schmidt, X. Mateos, M. C. Pujol, J. J. Carvajal, U. Griebner, V. Petrov, C. Zaldo, M. Aguiló and F. Díaz, "Crystal growth, optical spectroscopy and continuous-wave laser operation of co-doped (Ho,Tm):$KLu(WO_4)_2$ monoclinic crystals", submitted to J. Opt. Soc. Am. B.

Paper III: V. Jambunathan, X. Mateos, M. C. Pujol, J. J. Carvajal, C. Zaldo, M. Aguiló, F. Díaz, U. Griebner and V. Petrov, "Crystal growth, optical spectroscopy and continuous-wave laser operation of Ho:$KLu(WO_4)_2$ crystals", submitted to Appl. Phys. B.

Paper IV: V. Jambunathan, X. Mateos, M. C. Pujol, J. J. Carvajal, M. Aguiló and F. Díaz "Growth and spectroscopy of (Ho,Yb):$KLu(WO_4)_2$ crystals ", Physics Procedia **8**, 162–167 (2010).

Paper V: V. Jambunathan, X. Mateos, M. C. Pujol, J. J. Carvajal, M. Aguiló and F. Díaz, "Control of the cool/warm white light generation from lanthanide ions in monoclinic double tungstate crystals", J. Lumin., Accepted (2011).

3.1 Crystal growth of Ho, (Ho,Tm), (Ho,Yb), (Ho,Tm,Yb) - doped $KRE(WO_4)_2$ crystals

Five series of crystal growth experiments were planned. They were Ho:KLuW, Ho:KGdW, Ho:KYW, (Ho,Tm):KLuW and (Ho,Yb):KLuW. The first three series studied and compared the spectroscopic and laser properties of Ho in KREW (RE=Y, Gd, Lu) under similar experimental conditions. The fourth series studied the spectroscopic and laser properties of Ho after sensitization by Tm and the fifth series of crystals studied the spectroscopic and laser properties of Ho after sensitization by Yb. In addition to this, a separate series of (Ho,Tm,Yb):KLuW crystals was grown in order to study and understand the energy transfer process and upconversion phenomena for the generation of white light fluorescence in crystals.

Macro defect free crystals of singly doped Ho:KREW with different doping concentrations, co-doped (Ho,Tm) and (Ho,Yb):KLuW crystals and triply doped (Ho,Tm,Yb):KLuW crystals at different doping ratios were grown by the TSSG- SC method (see chapter 2). To obtain the single crystals and depending on the series to be grown, in a platinum crucible 50 mm in diameter and 50 mm high, 200 g of the solution mixture (12 mol.% KREW as solute and 88.0 mol.% $K_2W_2O_7$ as solvent) using K_2CO_3, Ho_2O_3, Tm_2O_3, Yb_2O_3, WO_3, Y_2O_3, Gd_2O_3 , Lu_2O_3 reagents from Aldrich, Fluka and Metall rare earth limited with analytical grade of purity were taken. We chose a solution mixture with a 12/88 ratio because previous studies at the FiCMA laboratories showed it to be optimum for growing crack- and inclusion-free crystals with relatively fast growth rates [79]. The thermal axial gradient in the solution was maintained around ~1.5 K/cm for all the crystal growth experiments. The mixtures were homogenised above the saturation temperature at about 50 K for 7 to 8 hours. To grow the single crystal a crystallographic *b* oriented KREW seed was used at the centre of the surface of the homogeneous solution (for example, a KYW seed for Ho:KYW). The reason a *b* oriented seed was used is that previous studies carried out at the FiCMA laboratories confirmed that the crystals are better quality and the growth rate higher than other oriented seeds [48]. The saturation temperature was determined by accurately determining the growth and dissolution of the seed at the surface. The solution temperature was decreased by about 20K at a rate of 0.05 - 0.15 Kh^{-1}. The crystal rotation was maintained at 40 rpm for KLuW and KYW hosts and 60 rpm for the KGdW host and it ensures the volumic growth in the presence of a forced convective flow near the crystal. After 8 – 10 days of crystal growth, the crystals were slowly removed from the solution at rate of 1mm/10min and, once the grown crystals had lost contact with the solution, the furnace was cooled to room temperature at a rate of $25Kh^{-1}$ to avoid thermal shock.

Tables 3.1, 3.2, 3.3 summarize the crystal growth parameters of the grown crystals and figure 3.1 shows a photograph of the 5at.%Ho:KREW, RE = (Y, Gd, Lu) crystals as examples.

UNIVERSITAT ROVIRA I VIRGILI
INFRARED LASERS BASED ON HO3+:KRE(WO4)2 CRYSTALS WITH TM3+OR YB3+ AS SENSITIZERS
Venkatesan Jambunathan
ISBN:/DL: T.1243-2011

Table 3.1 Experimental results for single-doped Ho:KYW crystals

at. % Ho	Saturation temp. [K]	Cooling rate [K/h]	Cooling interval [K]	Crystal weight [g]	Growth rate x 10^{-4} [g/h]	Crystal dimensions [mm] along crystallographic directions		
						c	***a****	***b***
0.5	1164.6	0.1	17.1	3.1	183	15.70	7.49	7.78
1	1166.0	0.1	21.5	4.2	196	17.47	8.58	8.26
3	1168.2	0.1	21.4	4.1	193	15.86	8.42	8.70
5	1166.6	0.1	23.8	5.4	228	16.81	11.17	8.90
7.5	1168.0	0.1	23.5	5.1	219	13.59	10.66	10.29

Table 3.2 Experimental results for single-doped Ho:KGdW crystals

at. % Ho	Saturation temp. [K]	Cooling rate [K/h]	Cooling interval [K]	Crystal weight [g]	Growth rate x 10^{-4} [g/h]	Crystal dimensions [mm] along crystallographic directions		
						c	***a****	***b***
0.5	1186.9	0.05	22.4	3.8	169	12.04	11.92	5.23
1	1180.7	0.05	22.0	3.0	136	12.15	7.57	8.48
3	1179.5	0.05	22.0	3.5	158	12.80	9.60	5.86
5	1180.0	0.05	24.4	3.8	156	15.11	9.11	5.08
7.5	1180.2	0.05	22.0	3.3	148	11.91	9.81	5.70

Table 3.3 Experimental results for single-doped Ho:KLuW crystals

at. % Ho	Saturation temp. [K]	Cooling rate [K/h]	Cooling interval [K]	Crystal weight [g]	Growth rate x 10^{-4} [g/h]	Crystal dimensions [mm] along crystallographic directions		
						c	***a****	***b***
0.5	1158.3	0.1	24	5.5	231	18.43	9.85	7.71
1	1157.9	0.1	20	4.8	242	19.13	10.16	6.87
3	1166.5	0.1	21.2	4.9	230	20.84	10.07	6.90
5	1167.8	0.1/0.15	17/3	4.5	238	17.13	10.03	7.30
7.5	1164.9	0.1/0.15	16.5/3.5	4.6	243	17.64	9.96	7.26

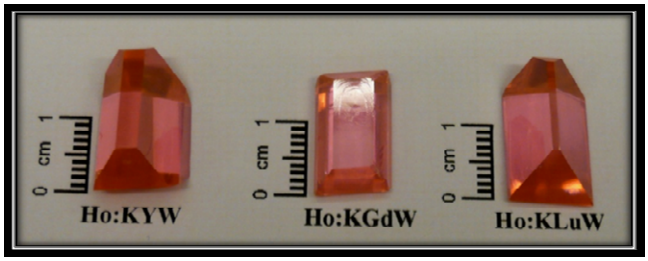

Figure 3.1 Photograph of Ho-doped crystal with three different host of the same family

Tables 3.1, 3.2 and 3.3 indicate that the crystal weight was in the range 3.0 - 5.5 g and depended on the cooling interval for each host. The crystal dimensions were between 12.04 - 20.84 mm in the *c* crystallographic direction, between 5.08-10.29 mm in the *b* crystallographic direction, and between 7.57-11.17 mm in the *a** crystallographic direction, which is independent of the host. In general in our growth experiments we observed that the dimension in the *c* crystallographic direction is approximately twice as long as the other two dimensions but not for all grown crystals, except for the Ho: KGW series which appears as a square. The growth rate of the crystals follows the tendency Ho:KLuW > Ho:KYW > Ho:KGdW, which is mainly related to the cooling rate of the crystal. We also observed that adding a doping element to the KYW - $K_2W_2O_7$ solution decreased its saturation temperature with respect to the un-doped KYW (1183 K). On the other hand, adding a doping element to the KGdW - $K_2W_2O_7$ solution showed no significant change in the saturation temperature with respect to the un-doped KGdW (1186 K) and adding a doping element to the KLuW - $K_2W_2O_7$ solution increased its saturation temperature with respect to the un-doped KLuW (1155 K). The saturation temperature followed the solubility curves of each of the hosts and can be found in [56] for KYW and for KGdW and in [78] for KLuW. Detailed information about the crystal growth experiments of single-doped Ho:KLuW can be found in paper III.

Table 3.4 Experimental results for co-doped (Ho,Tm):KLuW crystals

at.% Ho	at.% Tm	Saturation temp. [K]	Cooling rate [K/h]	Cooling interval [K]	Crystal weight [g]	Growth rate x10-4 [g/h]	Crystal dimensions [mm] along crystallographic directions		
							c	a*	b
0.5	2.5	1164.8	0.1	11.7	3.2	273	11.06	11.33	8.92
0.5	5.0	1155.9	0.1	21.2	6.5	311	15.22	15.62	9.89
1.5	5.0	1157.0	0.1	21.0	6.5	310	16.97	12.94	8.16
2.5	5.0	1152.8	0.1	20.0	7.3	363	15.73	14.31	10.61
2.5	7.5	1161.6	0.1	20.0	8.2	408	20.90	12.98	7.64
2.5	10.0	1163.6	0.1	20.0	6.7	336	19.92	12.30	7.33

Table 3.5 Experimental results for co-doped (Ho,Yb):KLuW crystals

at.% Ho	at.% Yb	Saturation temp. [K]	Cooling rate [K/h]	Cooling interval [K]	Crystal weight [g]	Growth rate x10-4 [g/h]	Crystal dimensions [mm] along crystallographic directions		
							c	a*	b
0.5	0.5	1168.0	0.1	23.6	5.8	248	17.87	10.18	7.80
0.5	2.5	1164.5	0.1	19.5	4.4	226	18.21	9.75	6.77
1.5	2.5	1182.6	0.1	23.8	5.6	236	17.34	9.55	6.89
2.5	2.5	1177.2	0.1	17.0	5.3	310	18.61	10.90	5.10
3.5	2.5	1173.3	0.1	19.5	6.6	338	15.77	13.51	6.62
3.5	3.5	1174.1	0.1	21.0	7.5	355	19.08	12.03	6.09
3.5	5.0	1178.7	0.1	23.7	8.4	356	17.21	14.84	7.08

Table 3.6 Experimental results for the triply doped (Ho,Tm,Yb):KLuW crystals

at. % Ho	at. % Tm	at. % Yb	Saturation temp. [K]	Cooling rate [K/h]	Cooling interval [K]	Crystal weight [g]	Growth rate x 10^{-4} [g/h]	Crystal dimensions [mm] along crystallographic directions		
								c	*a**	*b*
0.2	0.2	1.0	1160.9	0.1	23.8	7.5	317	15.07	14.72	9.62
0.5	0.5	1.0	1168.3	0.1	19.6	6.4	327	16.03	12.77	10.65
1.0	0.5	1.0	1171.4	0.1	19.6	6.3	322	15.00	11.96	10.09
1.0	0.8	1.0	1167.7	0.1	19.7	6.9	348	19.08	11.40	5.00
1.2	0.8	1.0	1171.8	0.1	19.6	6.1	310	17.90	11.20	6.11
1.5	0.8	1.0	1167.4	0.1	19.6	5.9	301	18.50	11.40	6.33
1.5	1.0	1.0	1167.9	0.1	19.0	5.7	301	17.22	12.50	6.77

The co-doped and triply doped crystals were grown using the same methodology and conditions as for the single-doped crystals. Tables 3.4 and 3.5 summarize the growth parameters of the grown co-doped crystals. Detailed information about the crystal growth experiments for co-doped (Ho,Tm):KLuW and co-doped (Ho,Yb): KLuW can be found in paper II and paper IV, respectively. Table 3.6 shows that the weight of the triply doped (Ho,Tm,Yb):KLuW crystals was in the range 5.7 – 7.5 g. The crystal dimensions were between 15.00 – 18.55 mm in the *c* crystallographic direction, between 5.00 - 10.65 mm in the *b* crystallographic direction, and between 11.40 – 14.72 mm in the *a** crystallographic direction. The saturation temperature was in the range 1160.9 – 1171.8 K and was higher than that of the un-doped crystal. The growth rate was in the range 301 – 348 x 10^{-4} g/h.

3.2 Structural characterization. Study on the variation of unit cell parameters as a function of doping level and temperature

The study of cell parameters (*a, b* and *c)* as a function of the doping level is of great interest because it shows how the structure distorted with the dopant concentration. To this end we made X-ray powder diffraction studies of the grown crystals. To prepare the powder, we took a small portion of the samples from the bulk crystal. At concentrations higher than 7.5 at.% Ho, we used a platinum wire to nucleate small crystals. These were then crushed to powder using a ceramic mortar and pestle. The diffraction patters were obtained using the powder X-ray diffraction technique with $2\theta = 5 - 70°$, step size = 0.02 and step time = 16s (see chapter 2). The diffraction patterns obtained were refined and fitted using the FULLPROF software program as was mentioned above. Two types of iteration were applied: firstly without fractional atomic coordinates and secondly with fractional atomic coordinates [50, 48, 49] for all the diffraction patterns obtained. We also obtained diffraction patterns of the un-doped powder crystals in order to determine the unit cell parameters under the same experimental conditions.

Here four sets of crystals were examined and the evolution of the unit cell parameters was studied as a function of the doping content of each of the crystal sets. Tables 3.7, 3.8 and 3.9 show the refined and fitted unit cell parameters of the Ho:KYW, Ho:KGdW and Ho:KLuW, respectively. Table 3.10 shows the refined and fitted unit cell parameters of the co-doped (Ho,Tm):KLuW host. Careful examination of the data shows that the *chi* (best fit) is high (see tables 3.7, 3.8, 3.9, 3.10), for parameters that are refined and fitted using the fractional atomic coordinates of the single crystal of the corresponding host. So we decided to study the evolution of unit cell parameters as a function of the doping level with the refined and fitted parameters without considering the fractional atomic coordinates of the single crystal in order to minimize

the error. Figure 3.2 shows the evolution of the unit cell parameters as a function of the Ho^{3+} content in the three hosts. Figure 3.3 shows the evolution of the unit cell parameters as a function of Ho^{3+} and Tm^{3+} contents in KLuW. Figure 3.2 a) shows that there is not much change in the unit cell parameter because the ionic radii of (1.015 Å) Ho^{3+} and (1.019 Å) Y^{3+} are close to one other. Figure 3.2 b) shows a small decrease in the unit cell parameters when the doping concentration increases. This is due to the fact that the ionic radius of (1.053 Å) Gd^{3+} is greater than that of (1.015 Å) Ho^{3+}. Figure 3.2 c) shows a small increase in the unit cell parameters when the doping concentration increases. This is due to the fact that the ionic radius of (0.977 Å) Lu^{3+} is smaller than that of (1.015 Å) Ho^{3+}. A similar effect was seen in the co-doped crystal, which is shown in figure 3.3. The ionic radius values were taken from Shannon [62] for a coordination number of 8 as is the case in the monoclinic rare earth double tungstates.

Table 3.7 Refined and fitted unit cell parameters of Ho:KYW crystals

Fit	Compound	*a*	*b*	*c*	*β*	*V*	*Chi*	status
1	KYW	10.6254(3)	10.3394(3)	7.5496(2)	130.745(1)	628.37(3)	8.95	without atomic coordinates
2	KYW	10.6249(5)	10.3391(5)	7.5491(3)	130.744(2)	628.29(5)	24.6	with atomic coordinates
	KYW	10.6313(4)	10.3452(6)	7.5547(3)	130.752(2)	629.44(5)		[56]
3	1% Ho: KYW	10.6257(4)	10.3386(4)	7.5497(2)	130.744(2)	628.36(4)	13.3	without atomic coordinates
4	1% Ho: KYW	10.6233(2)	10.3354(2)	7.5479(2)	130.734(1)	627.92(2)	29.0	with atomic coordinates
5	5% Ho: KYW	10.6253(4)	10.3387(4)	7.5494(2)	130.744(2)	628.31(4)	11.4	without atomic coordinates
6	5% Ho: KYW	10.6217(2)	10.3362(2)	7.5466(2)	130.743(1)	627.73(2)	25.5	with atomic coordinates
7	10%Ho : KYW	10.6255(4)	10.3386(4)	7.5495(2)	130.744(2)	628.33(4)	17.9	without atomic coordinates
8	10%Ho : KYW	10.6230(2)	10.3361(2)	7.5474(1)	130.738(1)	627.91(2)	38.3	with atomic coordinates
9	15%Ho : KYW	10.6245(4)	10.3410(5)	7.5488(3)	130.750(2)	628.30(4)	26.4	without atomic coordinates
10	15%Ho : KYW	10.6225(2)	10.3383(2)	7.5470(1	130.742(1)	627.95(2)	42.1	with atomic coordinates
11	25%Ho : KYW	10.6248(3)	10.3401(4)	7.5491(2)	130.746(2)	628.33(3)	12.5	without atomic coordinates
12	25%Ho : KYW	10.6223(2)	10.3370(2)	7.5468(1)	130.739(1)	627.87(2)	28.2	with atomic coordinates
13	35%Ho : KYW	10.6251(3)	10.3399(3)	7.5490(2)	130.743(1)	628.35(3)	9.01	without atomic coordinates
14	35%Ho : KYW	10.6232(2)	10.3373(2)	7.5468(1)	130.735(1)	627.99(2)	33.0	with atomic coordinates
15	50%Ho : KYW	10.6250(3)	10.3404(3)	7.5485(2)	130.741(2)	628.36(3)	10.5	without atomic coordinates
16	50%Ho : KYW	10.6233(2)	10.3387(2)	7.5469(2)	130.738(1)	628.05(2)	29.4	with atomic coordinates
17	KHoW	10.6260(4)	10.3424(4)	7.5483(2)	130.735(2)	628.58(4)	15.6	without atomic coordinates
18	KHoW	10.6265(5)	10.3442(5)	7.5479(3)	130.734(2)	628.69(5)	27.5	with atomic coordinates of KYW
	KHoW	10.6403(2)	10.3445(2)	7.5515(9)	130.736(7)	629.80(0)		[80]

Table 3.8 Refined and fitted unit cell parameters of Ho:KGdW crystals

Fit	Compound	*a*	*b*	*c*	*β*	*V*	*Chi*	status
1	KGdW	10.6820(3)	10.4406(3)	7.5985(2)	130.767(1)	641.83(3)	4.92	without atomic coordinates
2	KGdW	10.6834(5)	10.4396(5)	7.5995(3)	130.769(2)	641.91(5)	13.1	with atomic coordinates
	KGW	10.6890(6)	10.4438(5)	7.6036(4)	130.771(3)	642.83(5)		[56]
3	1% Ho: KGdW	10.6812(3)	10.4376(4)	7.5981(2)	130.774(2)	641.48(4)	3.74	without atomic coordinates
4	1% Ho: KGdW	10.6816(5)	10.4380(6)	7.5978(3)	130.768(2)	641.57(6)	8.09	with atomic coordinates
5	5% Ho: KGdW	10.6789(4)	10.4339(4)	7.5954(2)	130.770(2)	640.94(4)	3.19	without atomic coordinates
6	5% Ho: KGdW	10.6780(6)	10.4327(6)	7.5951(4)	130.770(3)	640.78(6)	6.39	with atomic coordinates
7	10%Ho : KGdW	10.6755(4)	10.4297(4)	7.5923(2)	130.764(2)	640.27(4)	4.29	without atomic coordinates
8	10%Ho : KGdW	10.6763(6)	10.4286(7)	7.5930(4)	130.768(3)	640.27(7)	10.8	with atomic coordinates
9	15%Ho : KGdW	10.6732(4)	10.4271(4)	7.5899(2)	130.791(2)	639.79(4)	3.9	without atomic coordinates
10	15%Ho : KGdW	10.6729(6)	10.4241(6)	7.5906(4)	130.766(2)	639.60(6)	8.23	with atomic coordinates
11	25%Ho : KGdW	10.6666(5)	10.4165(6)	7.5850(3)	130.755(2)	638.39(5)	6.17	without atomic coordinates
12	25%Ho : KGdW	10.6656(6)	10.4132(6)	7.5847(4)	130.758(3)	638.08(6)	8.82	with atomic coordinates
13	35%Ho : KGdW	10.6618(4)	10.4062(5)	7.5801(2)	130.758(2)	637.05(4)	5.58	without atomic coordinates
14	35%Ho : KGdW	10.6615(5)	10.4027(5)	7.5797(3)	130.761(2)	636.74(5)	11.6	with atomic coordinates
15	50%Ho : KGdW	10.6513(7)	10.3928(7)	7.5711(4)	130.741(3)	635.00(7)	23.0	without atomic coordinates
16	50%Ho : KGdW	10.6524(7)	10.3884(7)	7.5718(5)	130.746(3)	634.81(7)	28.1	with atomic coordinates
17	KHoW	10.6260(4)	10.3424(4)	7.5483(2)	130.735(2)	628.58(4)	15.6	without atomic coordinates
18	KHoW	10.6265(5)	10.3442(5)	7.5478(3)	130.734(2)	628.70(5)	27.4	with atomic coordinates of KGdW
	KHoW	10.6403(2)	10.3445(2)	7.5515(9)	130.736(7)	629.80(0)		[80]

Table 3.9 Refined and fitted unit cell parameters of Ho:KLuW crystals

Fit	Compound	*a*	*b*	*c*	*β*	*V*	*Chi*	status
1	KLuW	10.5894(3)	10.2353(3)	7.4956(2)	130.742(1)	615.53(3)	10.2	without atomic coordinates
2	KLuW	10.5889(4)	10.2347(4)	7.4951(3)	130.742(2)	615.42(4)	18.1	with atomic coordinates
	KLuW	10.5898(5)	10.2362(5)	7.4962(3)	130.745(2)	615.64(5)		[49]
3	1% Ho: KLuW	10.5915(3)	10.2392(2)	7.4975(2)	130.737(2)	616.10(3)	10.8	without atomic coordinates
4	1% Ho: KLuW	10.5930(4)	10.2401(4)	7.4986(3)	130.739(2)	616.31(4)	18.1	with atomic coordinates
5	5% Ho: KLuW	10.5942(2)	10.2441(3)	7.5003(2)	130.747(2)	616.69(3)	11.7	without atomic coordinates
6	5% Ho: KLuW	10.5953(5)	10.2450(4)	7.5011(3)	130.749(2)	616.86(5)	17.2	with atomic coordinates
7	10%Ho : KLuW	10.5948(4)	10.2493(4)	7.5028(2)	130.739(2)	617.30(4)	12.3	without atomic coordinates
8	10%Ho : KLuW	10.5956(5)	10.2503(5)	7.5038(3)	130.740(2)	617.49(5)	19.0	with atomic coordinates
9	15%Ho : KLuW	10.5960(4)	10.2525(4)	7.5043(3)	130.739(2)	617.70(4)	17.3	without atomic coordinates
10	15%Ho : KLuW	10.5979(5)	10.2554(5)	7.5060(3)	130.737(2)	618.13(5)	24.3	with atomic coordinates
11	25%Ho : KLuW	10.6012(4)	10.2675(4)	7.5112(3)	130.740(2)	619.47(4)	17.5	without atomic coordinates
12	25%Ho : KLuW	10.6022(5)	10.2686(5)	7.5126(3)	130.743(2)	619.68(5)	23.9	with atomic coordinates
13	35%Ho : KLuW	10.6067(4)	10.2805(4)	7.5185(3)	130.740(2)	621.16(4)	16.5	without atomic coordinates
14	35%Ho : KLuW	10.6068(5)	10.2811(5)	7.5190(3)	130.739(2)	621.27(5)	22.7	with atomic coordinates
15	50%Ho : KLuW	10.6116(4)	10.2987(5)	7.5272(3)	130.737(2)	623.30(5)	28.5	without atomic coordinates
16	50%Ho : KLuW	10.6112(5)	10.3001(5)	7.5272(3)	130.731(3)	623.43(5)	35.5	with atomic coordinates
17	KHoW	10.6260(4)	10.3424(4)	7.5483(2)	130.735(2)	628.58(4)	15.6	without atomic coordinates
18	KHoW	10.6266(5)	10.3444(5)	7.5478(3)	130.732(2)	628.71(5)	27.8	with atomic coordinates of KLuW
	KHoW	10.6403(2)	10.3445(2)	7.5515(9)	130.736(7)	629.80(0)		[80]

Table 3.10 Refined and fitted unit cell parameters of (Ho,Tm):KLuW crystals

Fit	Compound	*a*	*b*	*c*	*β*	*V*	*Chi*	status
1	KLuW	10.5894(3)	10.2353(3)	7.4956(2)	130.742(1)	615.53(3)	10.2	without atomic coordinates
2	KLuW	10.5889(4)	10.2347(4)	7.4951(3)	130.742(2)	615.42(4)	18.1	with atomic coordinates
	KLuW	10.5898(5)	10.2362(5)	7.4962(3)	130.745(2)	615.64(5)		[49]
3	0.5%Ho2.5%Tm:KLuW	10.5935(3)	10.2408(4)	7.4998(2)	130.741(2)	616.45(3)	19.6	without atomic coordinates
4	0.5%Ho2.5%Tm:KLuW	10.5940(5)	10.2409(5)	7.5000(3)	130.741(2)	616.51(5)	26.1	with atomic coordinates
5	0.5%Ho5.0% Tm:KLuW	10.5942(4)	10.2404(3)	7.4999(2)	130.741(2)	616.48(3)	13.1	without atomic coordinates
6	0.5%Ho5.0% Tm:KLuW	10.5951(5)	10.2404(5)	7.5008(3)	130.745(2)	616.58(5)	19.3	with atomic coordinates
7	1.5%Ho5.0% Tm:KLuW	10.5931(4)	10.2420(3)	7.5000(2)	130.740(2)	616.53(3)	14.1	without atomic coordinates
8	1.5%Ho5.0% Tm:KLuW	10.5940(5)	10.2439(5)	7.5009(3)	130.743(2)	616.75(5)	21.8	with atomic coordinates
9	2.5%Ho5.0% Tm:KLuW	10.5936(3)	10.2434(3)	7.5006(2)	130.742(2)	616.68(3)	11.9	without atomic coordinates
10	2.5%Ho5.0% Tm:KLuW	10.5951(5)	10.2455(5)	7.5017(3)	130.745(2)	616.95(5)	21.7	with atomic coordinates
11	2.5%Ho7.5% Tm:KLuW	10.5944(3)	10.2448(3)	7.5015(2)	130.746(2)	616.84(3)	10.2	without atomic coordinates
12	2.5%Ho7.5% Tm:KLuW	10.5956(5)	10.2456(5)	7.5022(3)	130.748(2)	616.99(5)	19.1	with atomic coordinates
13	2.5%Ho10.0% Tm:KLuW	10.5947(3)	10.2457(4)	7.5020(2)	130.747(2)	616.94(3)	9.32	without atomic coordinates
14	2.5%Ho10.0% Tm:KLuW	10.5961(5)	10.2471(5)	7.5030(3)	130.748(2)	617.18(5)	16.8	with atomic coordinates

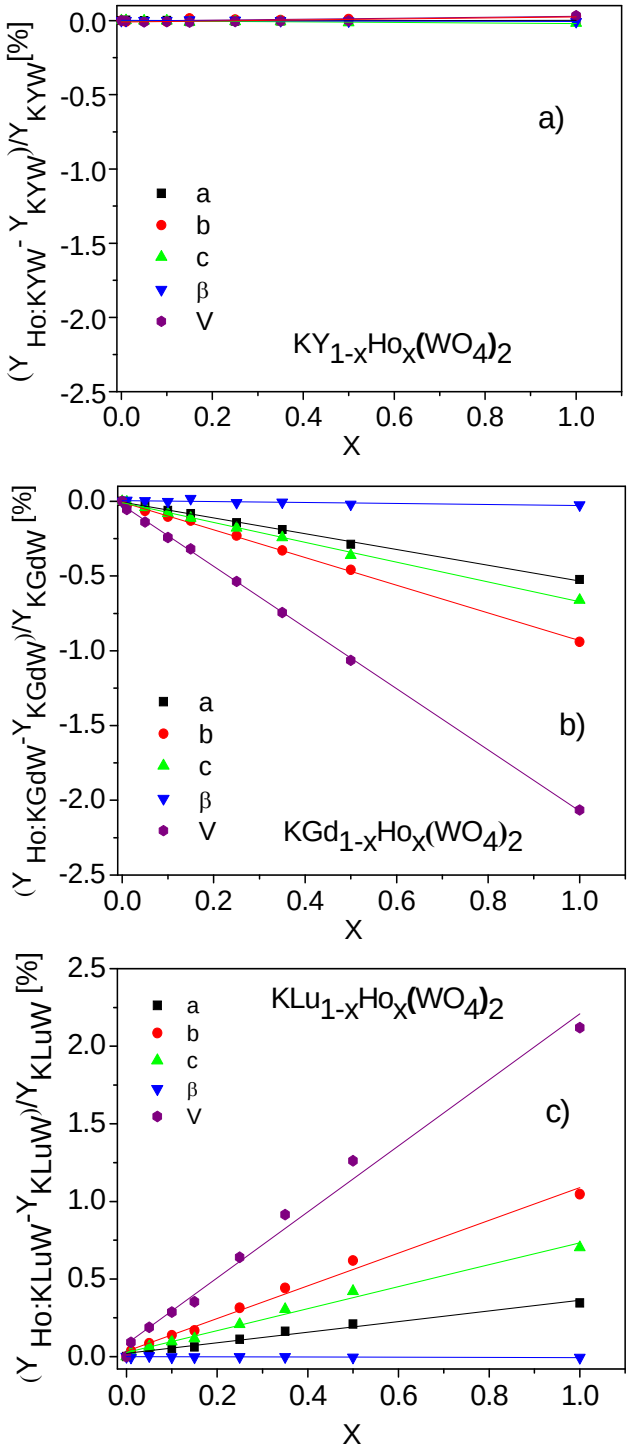

Figure 3.2 Evolution of the unit cell parameters as a function of Ho in KREW, RE=(Y, Gd, Lu)

UNIVERSITAT ROVIRA I VIRGILI
INFRARED LASERS BASED ON HO3+:KRE(WO4)2 CRYSTALS WITH TM3+OR YB3+ AS SENSITIZERS
Venkatesan Jambunathan
ISBN:/DL: T.1243-2011

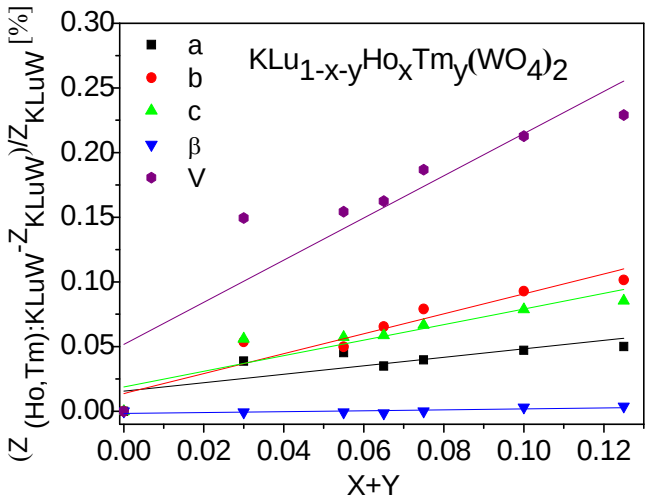

Figure 3.3 Evolution of the unit cell parameters as a function of Ho and Tm in KLuW

Thermal expansion is the tendency of matter to change in volume in response to a change in temperature. Unit cell parameters *(a, b, c)* need to be studied if we are to understand how structure distorts as a result of temperature because during laser experiments some energy is dissipated as heat inside the crystal even though the sample is cooled. The thermal stability of the geometry of crystals in the laser system can be predicted if the anisotropic linear thermal expansion of the laser material is known. A good laser cavity design should take into account the anisotropy at temperatures higher than room temperature. The samples considered were 3at.%Ho:KREW, RE= (Y, Gd, Lu). Here as well a small portion of the bulk sample was powdered using the same ceramic mortar and pestle. The diffraction patterns were obtained from the powder X-ray diffraction technique with 2θ = 10 - 70°, step size = 0.03 and step time = 5 s as discussed in chapter 2. The diffraction patterns of the 3at.% Ho:KREW crystals at different temperature (303, 323, 373, 473, 573, 673, 773, 873 K) were obtained and the unit cell parameters were calculated by fitting the X-ray patterns obtained using the same software program as before. Here we haven't considered the fractional atomic coordinates for iterating of the data. The refined and fitted unit cell parameters of the 3at.% Ho:KREW are reported in table 3.11. Figure 3.4 shows the evolution of the unit cell parameters with respect to temperature and it can be seen that they increase as temperature increases and β (angle between *a* and *c*) remains basically constant. This means that increasing temperature makes the crystal expand.

As a consequence of measuring the effect of temperature on unit cell parameters we found the linear thermal expansion coefficient in the crystallographic directions. It is given by $\alpha = (\Delta L / \Delta T) / L_{RT}$, where L_{RT}, is the initial parameter at room temperature. The values of

the linear thermal expansion coefficients are the slopes of the linear relationship between the change in the $(\Delta L / L_{RT})$ and the temperature ΔT with respect to the different crystallographic directions.

Since the linear thermal expansion of a crystal is represented by a symmetrical second – rank tensor and for the monoclinic system it has four non-zero components in the crystallo - physical frame $X_{1\alpha}$ //a, $X_{2\alpha}$ //b and $X_{3\alpha}$ //c*, where c* is a vector from the reciprocal crystallographic system. The values of the diagonal elements are $\alpha_{11}= \alpha_{110}$, $\alpha_{22}= \alpha_{010}$ and $\alpha_{33}= \alpha_{c^*}$ and they form the equation $\alpha_{001} = n_i n_j \alpha_{ij}$, where n_i and n_j are the direction cosines, so one can deduce $\alpha_{13,}$ which is the unknown quantity if α_{001} is measured. On the basis of the deduced values, the linear thermal expansion tensor in the crystallographic system $X_{1\alpha}$//a, $X_{2\alpha}$ //b and $X_{3\alpha}$ //c* is given in table 3.12. The linear thermal expansion in the principal system $X'_{1\alpha}$ //a, $X'_{2\alpha}$//b and $X'_{3\alpha}$ //c can be obtained by diagonalising the above tensor, which is also reported in table 3.12, and the principal axis with minimal thermal expansion, which is tabulated in table 3.13, can also be determined. Figure 3.5 shows the thermal expansion ellipsoid in the principal system and the crystallographic system. Since the orientation of the $X'_{1\alpha}$ and $X'_{3\alpha}$ lies in the N_g –N_m principal optical plane the linear thermal expansion coefficient can be determined for each of the principal optical axes with the known linear thermal expansion tensor in the principal system and the orientation of the optical ellipsoid. Table 3.14 shows the linear thermal expansion coefficients of KREW and 3%Ho: KREW. The procedure used to calculate the thermal expansion tensor and liner thermal expansion coefficient is described elsewhere [56, 57].

Table 3.11 Refined and fitted unit cell parameters of 3at.% Ho:KREW, RE=Y,Lu, Gd crystals

Fit	Compound	Temp [K]	*a*	*b*	*c*	*β*	*V*	*Chi*	status
1	3% Ho: KYW	303	10.6107(7)	10.3287(8)	7.5413(1)	130.780(6)	625.83(7)	14.7	without atomic coordinates
2		323	10.6121(6)	10.3283(6)	7.5415(1)	130.779(6)	625.92(6)	13.4	without atomic coordinates
3		373	10.6129(6)	10.3284(6)	7.5423(0)	130.780(6)	626.03(6)	11.6	without atomic coordinates
4		473	10.6287(7)	10.3300(5)	7.5610(0)	130.801(7)	628.40(7)	13.6	without atomic coordinates
5		573	10.6390(7)	10.3321(5)	7.5710(3)	130.807(7)	629.93(8)	13.6	without atomic coordinates
6		673	10.6492(9)	10.3365(7)	7.5825(5)	130.813(8)	631.70(9)	13.6	without atomic coordinates
7		773	10.6610(0)	10.3400(1)	7.5974(6)	130.821(9)	633.78(2)	15.8	without atomic coordinates
8		873	10.6784(6)	10.3455(3)	7.6215(1)	130.856(7)	636.83(7)	28.6	without atomic coordinates
1	3% Ho: KGdW	303	10.6760(6)	10.4305(6)	7.5957(3)	130.752(3)	640.58(6)	4.1	without atomic coordinates
2		323	10.6762(6)	10.4304(6)	7.5943(4)	130.753(3)	640.63(6)	4.4	without atomic coordinates
3		373	10.6780(7)	10.4310(6)	7.5995(4)	130.770(3)	641.04(7)	4.5	without atomic coordinates
4		473	10.6903(7)	10.4320(9)	7.6165(5)	130.803(3)	642.96(8)	4.5	without atomic coordinates
5		573	10.7021(7)	10.4287(9)	7.6311(6)	130.819(3)	644.54(9)	4.0	without atomic coordinates
6		673	10.7152(7)	10.4320(9)	7.6481(6)	130.835(3)	646.82(8)	4.0	without atomic coordinates
7		773	10.7307(8)	10.4352(9)	7.6636(7)	130.862(4)	649.01(10)	4.6	without atomic coordinates
8		873	10.7513(9)	10.4411(0)	7.6895(8)	130.912(3)	652.32(11)	5.1	without atomic coordinates
1	3% Ho: KLuW	303	10.5906(5)	10.2367(4)	7.4966(3)	130.746(2)	615.73(4)	4.1	without atomic coordinates
2		323	10.5912(5)	10.2372(4)	7.4974(4)	130.747(2)	615.86(4)	3.8	without atomic coordinates
3		373	10.5965(6)	10.2406(5)	7.5029(4)	130.742((2)	616.87(6)	4.2	without atomic coordinates
4		473	10.6083(5)	10.2438(6)	7.5152(4)	130.750(2)	618.68(6)	4.1	without atomic coordinates
5		573	10.6209(6)	10.2489(6)	7.5270(4)	130.751(2)	620.69(6)	5.5	without atomic coordinates
6		673	10.6332(5)	10.2523(5)	7.5414(3)	130.764(2)	622.67(5)	4.5	without atomic coordinates
7		773	10.6468(5)	10.2569(5)	7.5574(3)	130.777(2)	624.96(5)	4.0	without atomic coordinates
8		873	10.6588(5)	10.2593(5)	7.5726(3)	130.795(2)	626.90(5)	4.4	without atomic coordinates

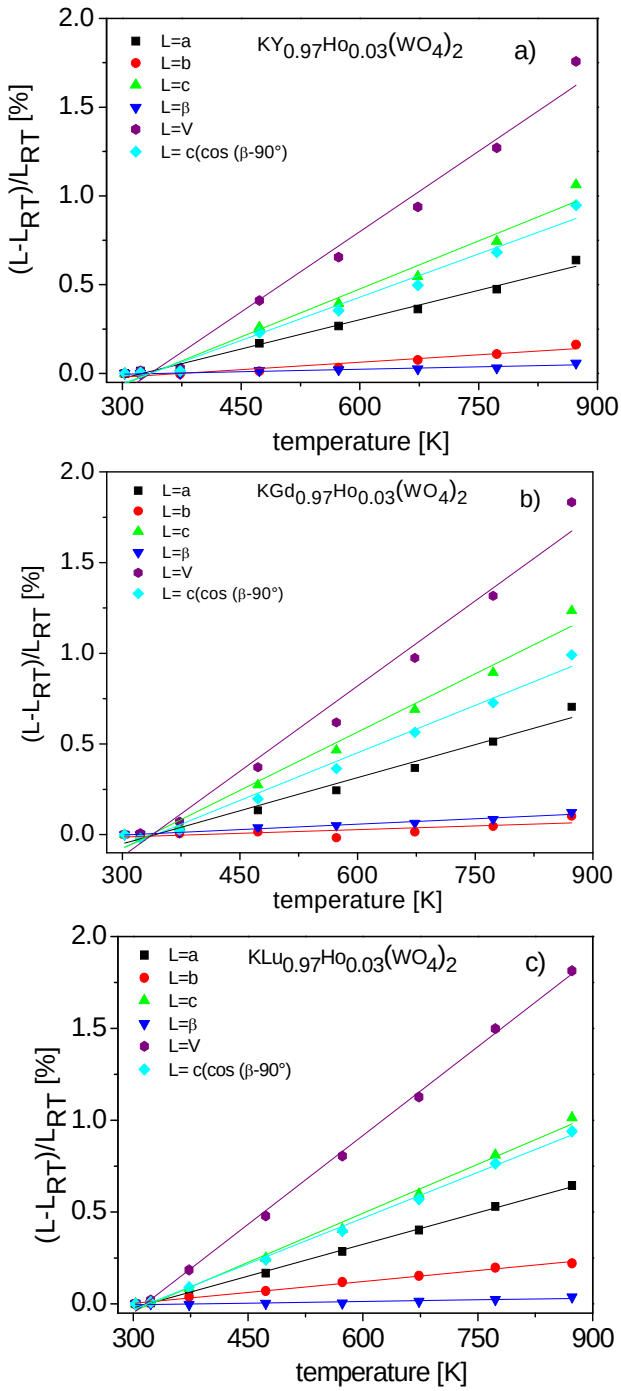

Figure 3.4 Evolution of the unit cell parameters as a function of temperature in 3at.%Ho: KREW

Table 3.12 Linear thermal expansion tensor in the crystallographic system X_1//a, X_2//b and X_3//c* and the principal system X'_1//a, X_2'//b and X_3'//c*

Linear thermal expansion tensor in the crystallographic system X_1//a, X_2//b and X_3//c*	Linear thermal expansion tensor in the principal system after diagonalising X'_1//a, X_2'//b and X_3'//c
$\alpha_{ij} = \begin{pmatrix} 11.01 & 0 & -4.08 \\ 0 & 2.79 & 0 \\ -4.08 & 0 & 16.24 \end{pmatrix} \times 10^{-6} K^{-1}$ $(3at.\%Ho:KYW)$	$\alpha'_{ij} = \begin{pmatrix} 8.78 & 0 & 0 \\ 0 & 2.79 & 0 \\ 0 & 0 & 18.47 \end{pmatrix} \times 10^{-6} K^{-1}$ $(3at.\%Ho:KYW)$
$\alpha_{ij} = \begin{pmatrix} 12.14 & 0 & -6.27 \\ 0 & 1.35 & 0 \\ -6.27 & 0 & 17.47 \end{pmatrix} \times 10^{-6} K^{-1}$ $(3at.\%Ho:KGdW1)$	$\alpha_{ij} = \begin{pmatrix} 7.99 & 0 & 0 \\ 0 & 1.35 & 0 \\ 0 & 0 & 21.62 \end{pmatrix} \times 10^{-6} K^{-1}$ $(3at.\%Ho:KGdW1)$
$\alpha_{ij} = \begin{pmatrix} 11.50 & 0 & -3.41 \\ 0 & 3.98 & 0 \\ -3.41 & 0 & 16.60 \end{pmatrix} \times 10^{-6} K^{-1}$ $(3at.\%Ho:KLuW)$	$\alpha'_{ij} = \begin{pmatrix} 9.79 & 0 & 0 \\ 0 & 3.98 & 0 \\ 0 & 0 & 18.31 \end{pmatrix} \times 10^{-6} K^{-1}$ $(3at.\%Ho:KLuW)$

Table 3.13 Angle ρ between a and $X'_1$and δ between c and X'_3

Host	$\delta = (\beta - 90°) - \rho$	ρ	$\Phi = \delta + \kappa$
3at.%Ho:KYW	12.12	28.66	30.62
3at.%Ho:KGdW	7.26	33.48	28.76
3at.%Ho:KLuW	14.14	26.60	32.64

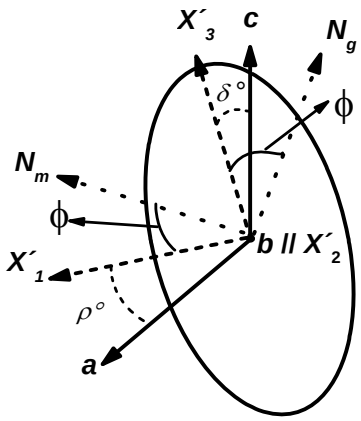

Figure 3.5 Thermal expansion ellipsoid of Ho:KREW

Table 3.14 Linear thermal expansion coefficients of 3%Ho:KREW

x 10^{-6} [K^{-1}]	3at.% Ho:KYW	3at.% Ho:KGdW	3at.% Ho:KLuW
α_{100}	11.01	12.14	11.50
α_{010}	2.79	1.35	3.98
α_{001}	18.04	21.40	17.80
α_{c^*}	16.24	17.47	16.60
α_V	30.18	31.30	32.20
α'_{11}	8.78	7.99	9.79
α'_{22}	2.79	1.35	3.98
α'_{33}	18.47	21.62	18.42
α'_g	15.96	18.47	15.83
α'_m	11.29	11.14	12.27
α'_p	2.79	1.35	3.98
α'_g/α'_m	1.41	1.66	1.29
α'_g/α'_p	5.72	13.68	3.98
α'_m/α'_p	4.05	8.26	3.08

3.3 Compositional characterization.

The composition of the grown crystal was measured by using electron probe micro analysis (EPMA) (see chapter 2). On the basis of the EPMA results and the solution composition, we determined the distribution coefficients of lanthanides in the crystals (see tables 3.15, 3.16, 3.17, 3.18, 3.19 and 3.20). A distribution coefficient of the dopant ions around unity means that the stoichiometry of the solute is conserved. Here the distribution coefficient was a little lower than one for Ho in KGdW, a little higher than one for Ho in KYW and considerably higher than one for singly doped, co-doped and triply doped crystals with KLuW. The substitution of RE_2O_3 for Ln_2O_3 is easier when the ionic radius of Ln^{3+}(Ho^{3+}, Tm^{3+}, Yb^{3+}) is similar to that of RE^{3+} (Y^{3+},Gd^{3+}, Lu^{3+}) and the distribution coefficient decreases from growth to growth when it is greater than one. The distribution coefficient was calculated by using the following formula [48].

$$K_{Ln^{3+}} = \frac{(\text{moles}_{Ln^{3+}}/(\text{moles}_{Re^{3+}} + \text{moles}_{Ln^{3+}})_{\text{crystal}}}{(\text{moles}_{Ln^{3+}}/(\text{moles}_{Re^{3+}} + \text{moles}_{Ln^{3+}})_{\text{solution}}} \quad (3.1)$$

Table 3.15 Distribution coefficient, real ion density and stoichiometric formula of Ho in KYW

at.% of Y	at.% of Ho	K_Y	K_{Ho}	Ho in KYW at./cm^3	Stoichiometric formula
99.5	0.5	1.00	1.22	$3.87x10^{19}$	$KY_{0.994}Ho_{0.006}(WO_4)_2$
99.0	1.0	1.00	1.15	$7.31x10^{19}$	$KY_{0.988}Ho_{0.012}(WO_4)_2$
97.0	3.0	1.00	1.13	$2.16x10^{20}$	$KY_{0.966}Ho_{0.034}(WO_4)_2$
95.0	5.0	0.99	1.12	$3.53x10^{20}$	$KY_{0.944}Ho_{0.056}(WO_4)_2$
92.5	7.5	1.00	1.02	$4.84x10^{20}$	$KY_{0.924}Ho_{0.076}(WO_4)_2$

Table 3.16 Distribution coefficient, real ion density and stoichiometric formula of Ho in KGdW

at.% of Gd	at.% of Ho	K_{Gd}	K_{Ho}	Ho in KGdW at./cm^3	Stoichiometric formula
99.5	0.5	1.00	1.05	$3.30x10^{19}$	$KGd_{0.995}Ho_{0.005}(WO_4)_2$
99.0	1.0	1.00	0.86	$5.42x10^{19}$	$KGd_{0.991}Ho_{0.009}(WO_4)_2$
97.0	3.0	1.00	0.90	$1.71x10^{20}$	$KGd_{0.973}Ho_{0.027}(WO_4)_2$
95.0	5.0	1.01	0.85	$2.68x10^{20}$	$KGd_{0.958}Ho_{0.042}(WO_4)_2$
92.5	7.5	1.01	0.87	$4.14x10^{20}$	$KGd_{0.934}Ho_{0.066}(WO_4)_2$

Table 3.17 Distribution coefficient, real ion density and stoichiometric formula of Ho in KLuW

at.% of Lu	at.% of Ho	K_{Lu}	K_{Ho}	Ho in KLuW at./cm^3	Stoichiometric formula
99.5	0.5	1.00	1.67	$5.45\ x10^{19}$	$KLu_{0.992}Ho_{0.008}(WO_4)_2$
99.0	1.0	1.00	1.43	$9.30\ x10^{19}$	$KLu_{0.986}Ho_{0.014}(WO_4)_2$
97.0	3.0	0.99	1.30	$2.54\ x10^{20}$	$KLu_{0.961}Ho_{0.039}(WO_4)_2$
95.0	5.0	0.99	1.26	$4.12\ x10^{20}$	$KLu_{0.937}Ho_{0.063}(WO_4)_2$
92.5	7.5	0.99	1.07	$5.25\ x10^{20}$	$KLu_{0.920}Ho_{0.080}\ (WO_4)_2$

UNIVERSITAT ROVIRA I VIRGILI
INFRARED LASERS BASED ON HO3+:KRE(WO4)2 CRYSTALS WITH TM3+OR YB3+ AS SENSITIZERS
Venkatesan Jambunathan
ISBN:/DL: T.1243-2011

Table 3.18 Distribution coefficient, real ion density and stoichiometric formula of Ho and Tm in KLuW

Sample no	at.% of Lu	at.% of Ho	at.% of Tm	K_{Lu}	K_{Ho}	K_{Tm}	Ho in KLuW at./cm^3	Tm in KLuW at./cm^3	Stoichiometric formula
1	97.0	0.5	2.5	0.99	1.70	1.26	5.53×10^{19}	2.06×10^{20}	$KLu_{0.960}Ho_{0.008}Tm_{0.032}(WO_4)_2$
2	94.5	0.5	5.0	1.01	1.62	0.71	5.29×10^{19}	2.30×10^{20}	$KLu_{0.957}Ho_{0.008}Tm_{0.035}(WO_4)_2$
3	93.5	1.5	5.0	1.00	1.41	0.97	1.38×10^{20}	3.15×10^{20}	$KLu_{0.931}Ho_{0.021}Tm_{0.048}(WO_4)_2$
4	92.5	2.5	5.0	0.99	1.34	0.94	2.18×10^{20}	3.06×10^{20}	$KLu_{0.920}Ho_{0.033}Tm_{0.047}(WO_4)_2$
5	90.0	2.5	7.5	0.99	1.17	1.08	1.90×10^{20}	5.28×10^{20}	$KLu_{0.890}Ho_{0.029}Tm_{0.081}(WO_4)_2$
6	87.5	2.5	10.0	0.99	1.13	1.06	1.85×10^{20}	6.89×10^{20}	$KLu_{0.866}Ho_{0.028}Tm_{0.106}(WO_4)_2$

Table 3.19 Distribution coefficient, real ion density and stoichiometric formula of Ho and Yb in KLuW

Sample no	at.% of Lu	at.% of Ho	at.% of Yb	K_{Lu}	K_{Ho}	K_{Yb}	Ho in KLuW at./cm^3	Yb in KLuW at./cm^3	Stoichiometric formula
1	99.0	0.5	0.5	0.99	1.66	1.52	5.40×10^{19}	4.97×10^{19}	$KLu_{0.984}Ho_{0.008}Yb_{0.008}(WO_4)_2$
2	97.0	0.5	2.5	0.99	1.38	1.21	4.49×10^{19}	1.98×10^{20}	$KLu_{0.963}Ho_{0.007}Yb_{0.030}(WO_4)_2$
3	96.0	1.5	2.5	0.99	1.15	1.19	1.13×10^{20}	1.96×10^{20}	$KLu_{0.953}Ho_{0.017}Yb_{0.030}(WO_4)_2$
4	95.0	2.5	2.5	0.99	1.09	1.17	1.77×10^{20}	1.90×10^{20}	$KLu_{0.944}Ho_{0.027}Yb_{0.029}(WO_4)_2$
5	94.0	3.5	2.5	0.99	1.11	1.20	2.53×10^{20}	1.95×10^{20}	$KLu_{0.931}Ho_{0.039}Yb_{0.030}(WO_4)_2$
6	93.0	3.5	3.5	0.99	1.10	1.15	2.50×10^{20}	2.62×10^{20}	$KLu_{0.921}Ho_{0.038}Yb_{0.040}(WO_4)_2$
7	91.5	3.5	5.0	0.99	1.10	1.12	2.52×10^{20}	3.65×10^{20}	$KLu_{0.905}Ho_{0.039}Yb_{0.056}(WO_4)_2$

Table 3.20 Distribution coefficient, real ion density and stoichiometric formula of Ho, Tm and Yb in KLuW

Sample no	at.% of Lu	at.% of Ho	at.% of Tm	at.% of Yb	K_{Lu}	K_{Ho}	K_{Tm}	K_{Yb}	Ho in KLuW at./cm^3	Tm in KLuW at./cm^3	Yb in KLuW at./cm^3	Stoichiometric formula
1	98.60	0.2	0.2	1.0	0.99	2.34	1.78	1.51	$3.05x10^{19}$	$2.32 x10^{19}$	$9.87 x10^{19}$	$KLu_{0.9766}Ho_{0.0047}Tm_{0.0036}Yb_{0.0151}(WO_4)_2$
2	98.00	0.5	0.5	1.0	0.99	1.68	1.28	1.34	$5.47 x10^{19}$	$4.17 x10^{19}$	$8.77 x10^{19}$	$KLu_{0.9718}Ho_{0.0084}Tm_{0.0064}Yb_{0.0134}(WO_4)_2$
3	97.50	1.0	0.5	1.0	0.99	1.27	1.24	1.36	$8.25 x10^{19}$	$4.05 x10^{19}$	$8.90 x10^{19}$	$KLu_{0.9675}Ho_{0.0127}Tm_{0.0062}Yb_{0.0136}(WO_4)_2$
4	97.20	1.0	0.8	1.0	0.99	1.21	1.13	1.23	$7.88x10^{19}$	$5.87 x10^{19}$	$8.02 x10^{19}$	$KLu_{0.9660}Ho_{0.0121}Tm_{0.0090}Yb_{0.0123}(WO_4)_2$
5	97.00	1.2	0.8	1.0	0.99	1.24	1.12	1.24	$9.67 x10^{19}$	$5.86 x10^{19}$	$8.06 x10^{19}$	$KLu_{0.9638}Ho_{0.0148}Tm_{0.0090}Yb_{0.0124}(WO_4)_2$
6	96.70	1.5	0.8	1.0	0.99	1.49	1.32	1.19	$1.45 x10^{20}$	$6.90 x10^{19}$	$7.77 x10^{19}$	$KLu_{0.9552}Ho_{0.0223}Tm_{0.0106}Yb_{0.0119}(WO_4)_2$
7	96.50	1.5	1.0	1.0	0.99	1.24	1.21	1.16	$1.21 x10^{20}$	$7.86 x10^{19}$	$7.58 x10^{19}$	$KLu_{0.9577}Ho_{0.0186}Tm_{0.0121}Yb_{0.0116}(WO_4)_2$

3.4 Spectroscopic characterization of Ho:$KRE(WO_4)_2$, (Ho,Tm):$KLu(WO_4)_2$, (Ho,Yb):$KLu(WO_4)_2$ and (Ho,Tm,Yb):$KLu(WO_4)_2$

Because of the strong anisotropy of the crystal (see chapter 1) we oriented and cut the samples so that the faces were perpendicular to the principal optical directions N_g, N_m *and* N_p (see chapter 2) and then polished them for optical quality. The N_g cut sample propagates the light in the N_g direction and makes the polarized light parallel to either the N_m or the N_p directions. The N_p cut sample propagates the light in the N_p direction and makes the polarized light parallel to either the N_m or the N_g. Figure 3.6 shows a sample of 1.5%Ho2.5%Yb:KLuW cut and polished for absorption measurements. The samples and their dimensions are listed in table 3.21.

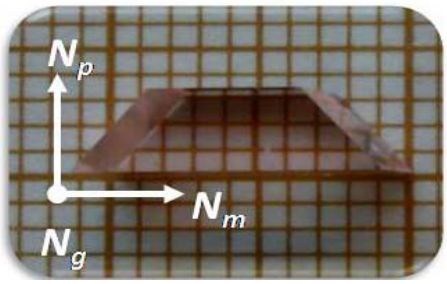

Figure 3.6 Photograph of cut and polished sample for absorption measurements

Table 3.21 Dimensions of the samples for absorption measurements

Sample	Thickness along N_g	Thickness along N_p
1% Ho:KYW	2.99mm	2.82mm
5% Ho:KYW	3.06mm	2.96mm
0.5% Ho:KYW	0.73 mm	-
1% Ho:KGdW	3.07mm	3.06mm
5% Ho:KGdW	2.99mm	3.05mm
0.5% Ho:KGdW	0.84 mm	-
1% Ho:KLuW	2.71 mm	2.91mm
3% Ho:KLuW	2.98 mm	3.32 mm
5% Ho:KLuW	3.00mm	2.96mm
0.5%Ho:KLuW	0.89mm	-
0.5%Ho2.5%Tm:KLuW	2.90mm	4.39 mm
1.5%Ho2.5%Yb:KLuW	3.14mm	3.10 mm
1.0%Ho0.5Tm1.0%Yb:KLuW	2.93 mm	2.85 mm

3.4.1 Optical absorption

Our study of optical absorption made it possible to determine the transitions between the ground energy level and the excited energy levels. We performed the polarized optical absorption of single doped, co-doped and triply doped crystals at room and low temperature. The experiments were carried out with polarized light perpendicular to the principal optical directions and the samples were oriented as described in figure 3.6. We used the conventional notation wavelength in nanometres (nm) or energy in wave numbers (cm^{-1}) to denote the manifolds and Stark levels. For single-doped and co-doped crystals the spectral range measured was between 300 and 2200 nm because the double tungstate family of crystals are not transparent below 300 nm and the active ions (Yb, Tm and Ho) do not absorb at wavelengths longer than 2200 nm (see figure 1.4 of chapter 1). For triply doped crystals we measured between 300 -1050 nm because we were interested in the visible range and the infrared range to pump Yb ions.

The single-doped crystals of the three hosts were measured under similar experimental conditions. Figure 3.7 shows the absorption cross-sections of 1at.%Ho:KREW (RE=Y, Gd, Lu). There are several transitions which are labelled with their corresponding manifolds and are associated with the transition from the ground state to the higher excited states of Ho^{3+}. The figures show that the absorption strongly depends on the light polarization and is maximal for E//N_m, medium for E//N_p and minimal for E//N_g. The anisotropy is remarkable in these materials. The figures also show that the absorption maximum cross section follows the tendency Ho: KGdW(43.04 x 10^{-20} cm^2) >Ho: KYW (37.72 x 10^{-20} cm^2) >Ho: KLuW(27.11 x 10^{-20} cm^2) at 454 nm.

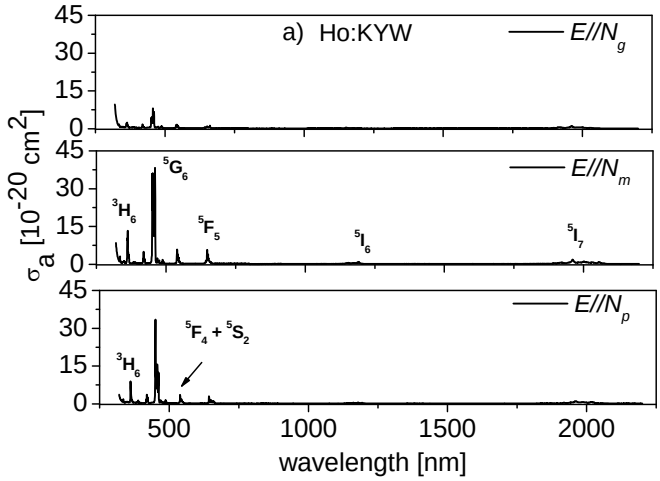

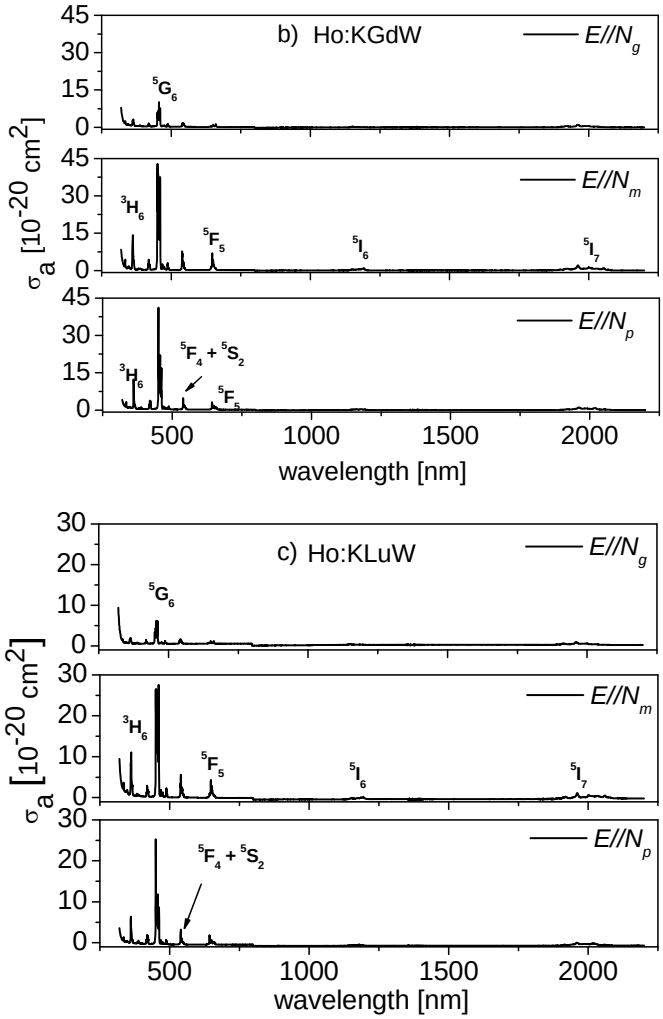

Figure 3.7 Room temperature polarized optical absorption cross-section spectra of Ho: KREW, RE= (Y, Gd, Lu)

The co-doped (Ho,Tm):KLuW and (Ho,Yb):KLuW crystals were measured in the same range as that of the single-doped crystals. The absorption results for the (Ho,Tm) system can be found in paper I and paper II and the results of the (Ho,Yb) system can be found in paper IV. It is worth discussing the absorption range of the sensitizer ions because this is the region where some of the energy is absorbed and transferred to the activator ion by the process of energy transfer, which is necessary for the photoluminescence and laser experiments.

Figure 2 in paper I shows that Tm has an absorption for E//N_p principal optical axis centred at 793.4 nm with a maximum absorption cross-section of 9.7 x 10^{-20} cm^2 and for E//N_m

principal optical axis centred at 801.8 nm with a maximum absorption cross-section of 5.2 x 10^{-20} cm^2. This means that either Ti:Sapphire or AlGaAs diode lasers can be perfectly used as a pump source for the laser action. More detail can be found in the discussion section in paper I.

Figure 3 of paper IV shows that Yb has a maximum absorption coefficient for E//N_m centred at 981nm, which is rather broad, and the other polarizations are less intense. This makes the requirement for the pump source less strict in terms of line-width, so here too the diode pump or Ti: Sapphire laser could be perfectly used for laser action. Figure 3.8 shows the polarized absorption cross-section between 900 and 1050 nm for (Ho,Yb):KLuW. It can be seen that Yb has a maximum absorption cross-section of 8.45 X 10^{-20} cm^2 for E//N_m centered at 981nm with a FWHM of ~4 nm.

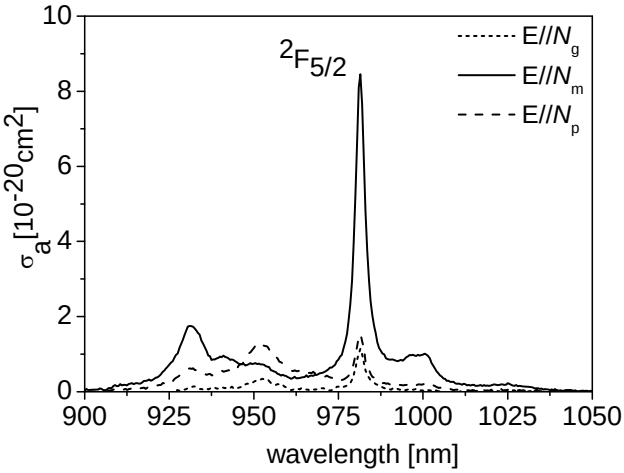

Figure 3.8 Room temperature polarised optical absorption cross section in the 900 – 1050 nm range of (Ho,Yb):KLuW

As mentioned above, the absorption for triply doped (Ho, Tm, Yb): KLuW crystal is measured in the 350 – 1050 nm range (see figure 3.9) and the absorption cross-section of Yb around 980 nm in the triply doped crystal is of the same order as that of the co-doped (Ho,Yb):KLuW crystal.

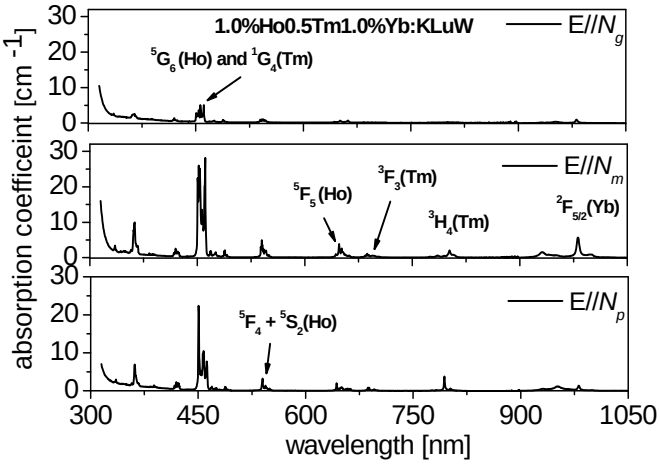

Figure 3.9 Room temperature polarized optical absorption spectra of (Ho,Tm,Yb):KLuW

To determine the Stark energy levels of Ho in the single doped crystals, we measured the low temperature absorption at 6K with polarized light parallel to the three principal optical axes. When the temperature decreases, extra peaks caused by the thermal population of the various sublevels of the ground state and possible vibronic (electron–phonon interaction) peaks are eliminated. Since Ho has an even number of active electrons in the 4f shell, $4f^{10}$ (see chapter 1), and is located in the C_2 symmetry site, the polarization-dependent selection rules for the electronic transitions are expected as can be seen in table 3.22. According to the selection rules [81] of induced electric dipole (ED), for a monoclinic system with C_2 symmetry, the allowed transitions with the corresponding irreducible representation are given in table 3.23. The table shows that the number of absorption peaks and transitions are dependent on polarization although the intensity of the peaks associated with the three polarizations can vary. As an example, the $^5I_7$ manifold should have 15 Stark levels and the allowed transitions are $7\Gamma_1+8\Gamma_2$, the $^5I_6$ manifold should have 13 stark levels and the allowed transitions are $7\Gamma_1+6\Gamma_2$, and so on.

Table 3.22 Polarization dependent selection rules

C_2	Γ_1	Γ_2
Γ_1	$E//N_p$	$E//N_g$, $E//N_m$
Γ_2	$E//N_g$, $E//N_m$	$E//N_p$

Table 3.23 Allowed transitions with the corresponding irreducible representation

J =	0	1	2	3	4	5	6	7	8
Γ =	Γ_1	$\Gamma_1 + 2\Gamma_2$	$3\Gamma_{1+} 2\Gamma_2$	$3\Gamma_{1+} 4\Gamma_2$	$5\Gamma_{1+} 4\Gamma_2$	$5\Gamma_{1+} 6\Gamma_2$	$7\Gamma_{1+} 6\Gamma_2$	$7\Gamma_{1+} 8\Gamma_2$	$9\Gamma_{1+} 8\Gamma_2$

To measure the optical density (OD) we used 1at%Ho: KREW. To measure OD for the $^5I_5$ and $^5I_4$ levels, however, we used 5at.% Ho: KREW since the concentration of 1at.%Ho:KREW was not sufficient to give good resolution. To measure the OD for $^5G_6$ and $^3F_1$ we used 0.5at.% Ho:KREW since the detector in the spectrophotometer saturated due to the high absorption of these energy levels. The Stark energy levels at 6K of each of the manifolds corresponding to Ho:KYW are shown in table 3.24 and the whole collection of spectra is shown in figure 3.10. The Stark energy level splitting for Ho:KGdW has already been reported in a previous study [82, 83]. The Stark energy levels at 6K of each manifold for Ho:KLuW can be found in table 2 of paper III and the whole collection of spectra is shown in figure 7 of paper III. The table indicates that some follow irreducible representation and some doesn't follow (for example $^5I_7$ manifold follow and $^5I_6$ manifold doesn't follow) and in some cases we observed an intense N_g peak. From figure 7 in paper III, we also inferred some extra peaks in all the higher excited sublevels, which occur mainly due to the thermal population in the ground state although the crystal is cooled to 6K. It should also be mentioned that in table 2 of paper III, the labels that are not in parenthesis indicate the polarization character of every peak and the ones which are in brackets indicate the contribution of the other polarizations.

The low temperature measurement for the (Ho,Tm):KLuW co-doped system was carried out and it was found that the energy levels exactly match those of the single-doped Ho:KLuW system (paper III) and the single-doped Tm:KLuW [84] system after the acquired low temperature absorption spectra were merged. No deviation in the energy levels was observed. To avoid repetition, the table and figures have not been reported here. For the same reason, the low temperature measurement of the co-doped (Ho,Yb):KLuW and triply doped (Ho,Tm,Yb):KLuW have not been reported.

Table 3.24 Energy level splitting of Ho: KYW

$^{2S+1}L_J$	E// $N_{g,m,p}$	Energy (cm^{-1})
$^5I_7$	m	5100
	p(g)	5101
	p(g)	5106
	m(p)	5109
	mg(p)	5145
	p(g)	5179
	m	5193
	mg	5204
	p	5206
	mg	5209
	p	5213
	p	5223
	g(m)	5226
	p	5245
	mg(p)	5281
$^5I_6$	p(mg)	8609
	m(p)	8617
	p	8624
	p(g)	8649
	m(g)	8661
	g	8676
	p	8684
	mg	8688
	g(m)	8695
	p	8722
	mg	8726
	p	8756
	mg	8771
$^5I_5$	p	11174
	mg	11182
	p	11192
	mg	11196
	g	11221
	m	11232
	p(g)	11235
		(11237)
	p	11263
	m	11270
	p(mg)	11313
	mg	11315
$^5I_4$	m	13187
	g	13192
	m	13217
	mg(p)	13255
	mg	13307
	p	13313
	p(mg)	13388
	p(mg)	13405
$^5F_5$	g(p)	15357
	mg	15373
	p	15375
	p	15407
	mg	15410
	m	15438
	m	15445
	p	15448
	p(g)	15554
	m	15558
$^5S_2$	p	18369
	g	18372
	mg	18387
	p	18395
	mg	18399
$^5F_4$	mg	18452
	p	18455
	p	18480
	mg	18493
	m	18509
	p	18526
	m	18536
	p	18548
	m	18576
$^5F_3$	mg	20483
	p	20503
	g(m)	20529
	p(g)	20597
	m	20602
	m	20626
	g(p)	20638
		(20639)
$^5F_2$	m	21011
	p	21032
	mg(p)	21055
	p(g)	21084
	m	21088
$^3K_8$	p	21301
	mg(p)	21037
	mg	21331
	p	21336
	mg	21342
	m	21376
	m	21384
$^5G_6$ and $^5F_1$	p(m)	21914
	p	22011
	m	22013
	m	22037
	m	22041
	p	22049
	m	22124
	p(m)	22185
	m(p)	22203
	p(m)	22225
$^5G_5$	p	23801
	p(g)	23823
		(23821)
	mg	23826
	mg	23838
	p(mg)	23849
	mg(p)	23909
	p(m)	23924
	p(mg)	23976
	p	23990
	m(p)	23998
$^5G_4$	p(mg)	25743
	p(mg)	25760
	p(gm)	25779
	m	25791
	g	25803
$^3H_5$	p(m)	27401
	mg	27446
	p(mg)	27454
	mg(p)	27466
	mg(p)	27484
	mg(p)	27528
	p(g)	27547
	mg	27557
	mg(p)	27578
$^3H_6$	m	27640
	p(g)	27643
	p	27690
	mg	27705
	mg(p)	27755
	p	27790
$^5G_3$ and $^3L_9$	mg	28620
	m	28709
	p(m)	28739
	m(p)	28761
	g	28764
	p	28826
	g	28834
	m	28840
	p(g)	28883
	m(p)	28942
	p(mg)	29129
$^3F_4$ and $^3K_6$	p	29821
	mg	29824
	mg	29836
	p	29837
	mg(p)	29861
	m	29886
	g	29892
	p	29896
	mg(p)	29913
	mg(p)	29952
	mg(p)	29967
	g(m)	29981
	mg(p)	29998
	m	30026
$^5I_8$		0
		43
		78
		94
		123
		136
		176
		187
		205
		239
		281

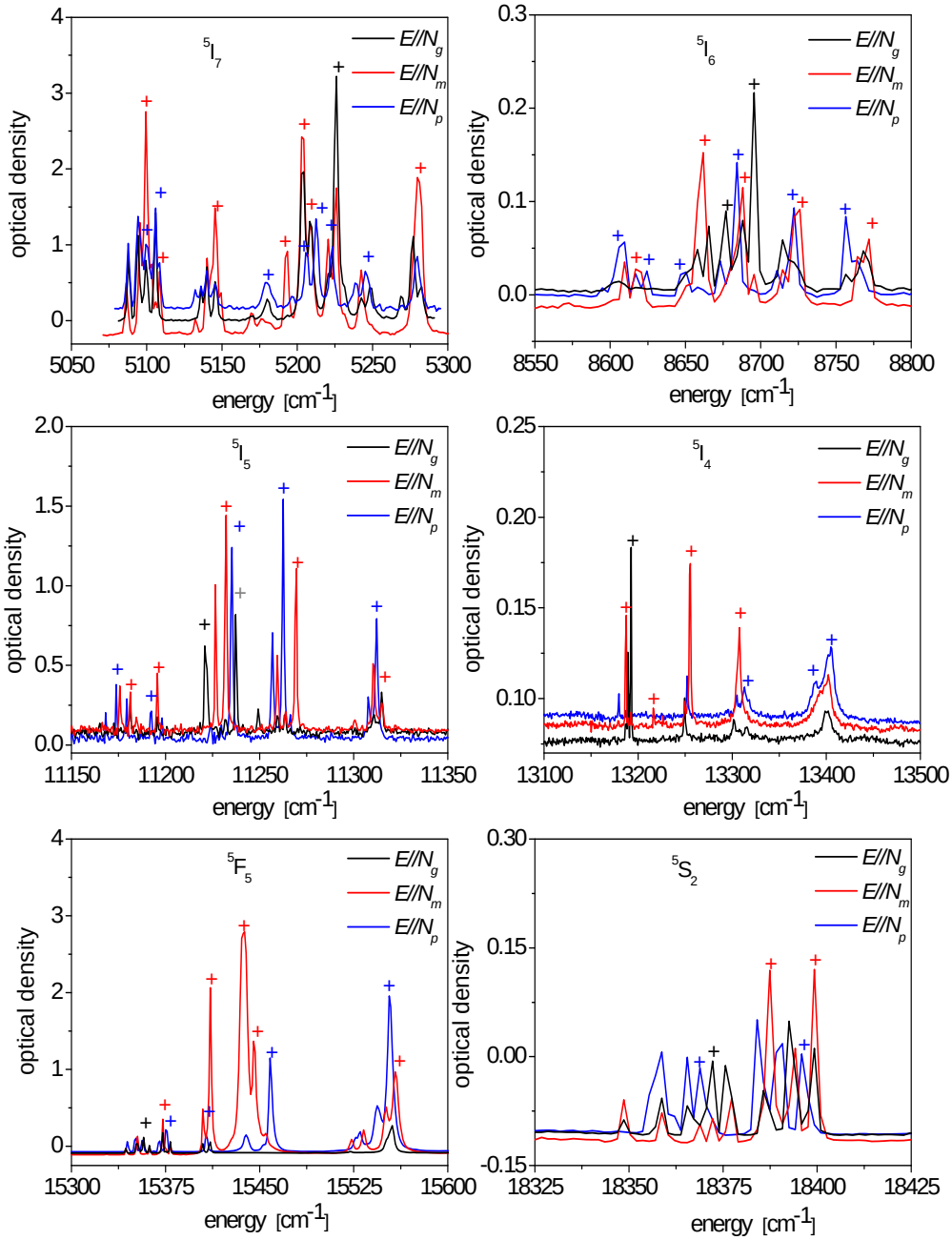

to be continued…....

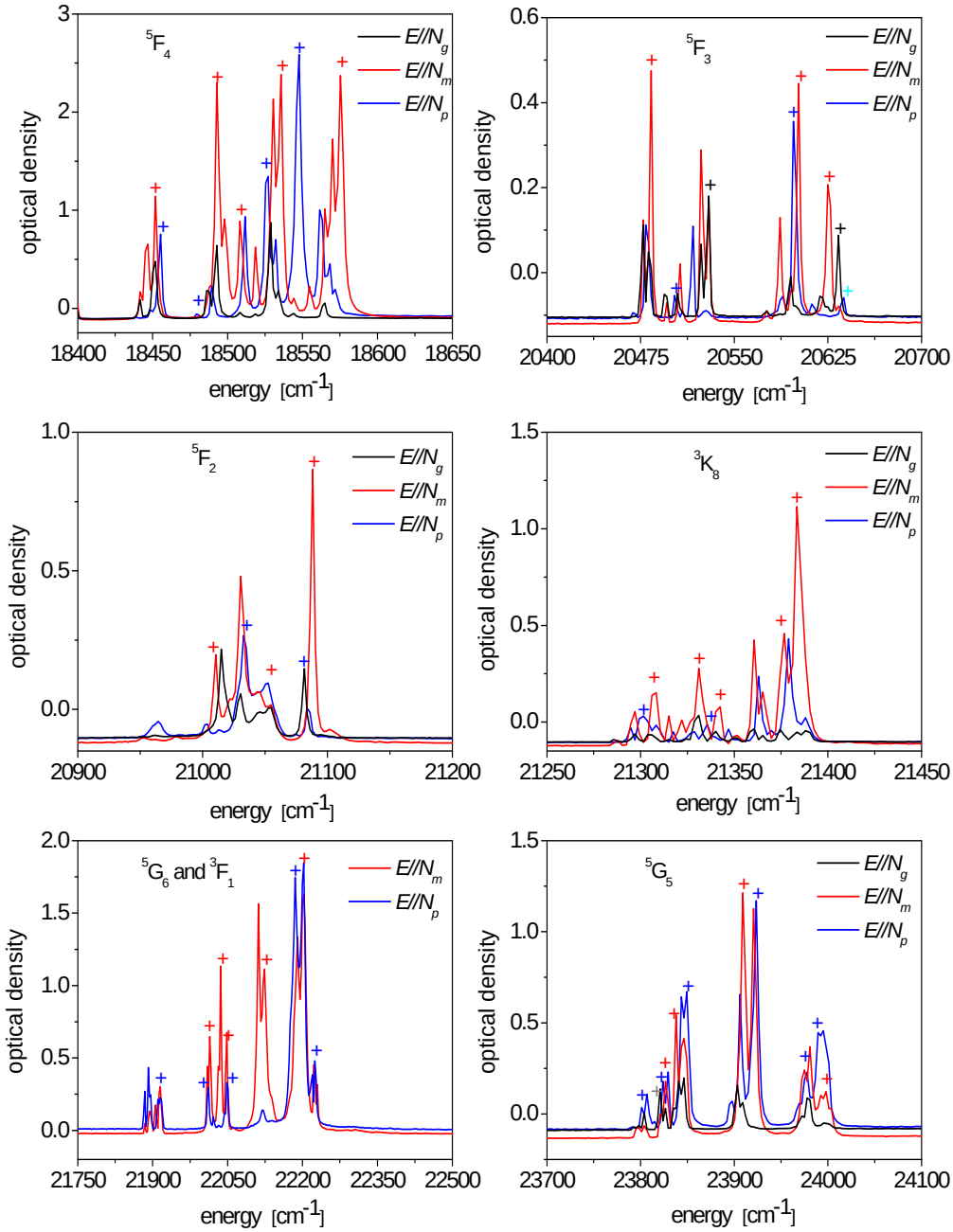

to be continued…....

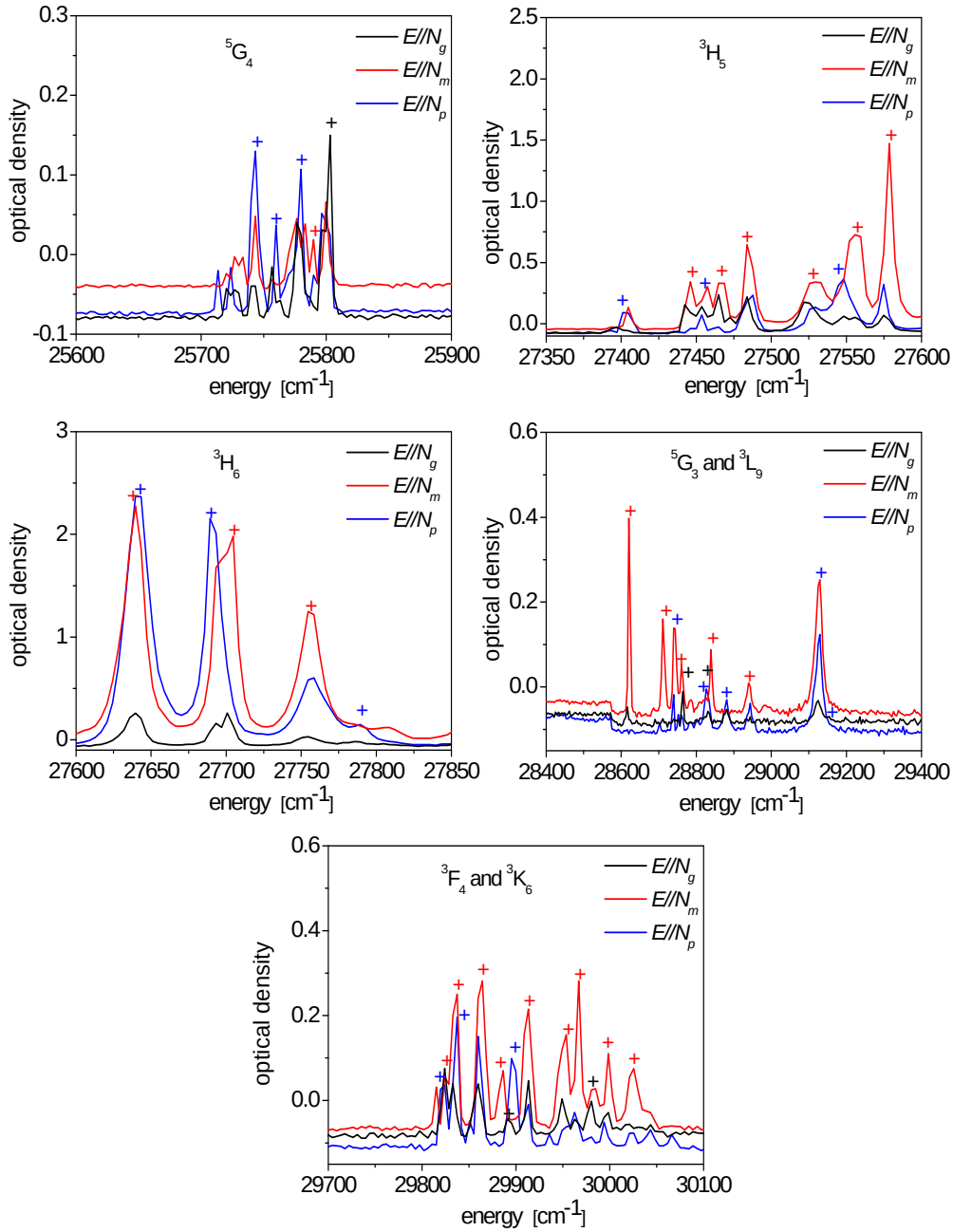

Figure 3.10 Low temperature (6K) optical absorption of KYW single crystal doped with Ho and recorded with polarized light parallel to the three principal optical directions N_g, N_m and N_p

3.4.2 Photoluminescence (emission and life times)

3.4.2.1 Optical emission

The objective of the photoluminescence experiments was to determine the emission channels of the Ho ion and the Stark energy levels in the ground state ($^5I_8$ manifold) by low temperature emission measurement.

For single-doped crystals the photoluminescence was carried out in the 5at.% Ho: KREW crystals and was excited around 454 nm (22000 cm^{-1}), where the absorption cross-section is maximum. The sample was placed behind the focusing lens and the signal was collected from the monochromator situated at an angle of 90° to the incident beam (see chapter 2). After excitation, several de-excitation processes take place radiatively and non-radiatively (see energy level diagram in figure 8, paper III). We observed several emission channels like blue, green, red and infrared 2 μm emissions, respectively. Here we focused mainly on the 2 μm emission which is the main objective of this work. Figure 3.11 shows the room temperature 2 μm emission from the Ho:KREW crystals.

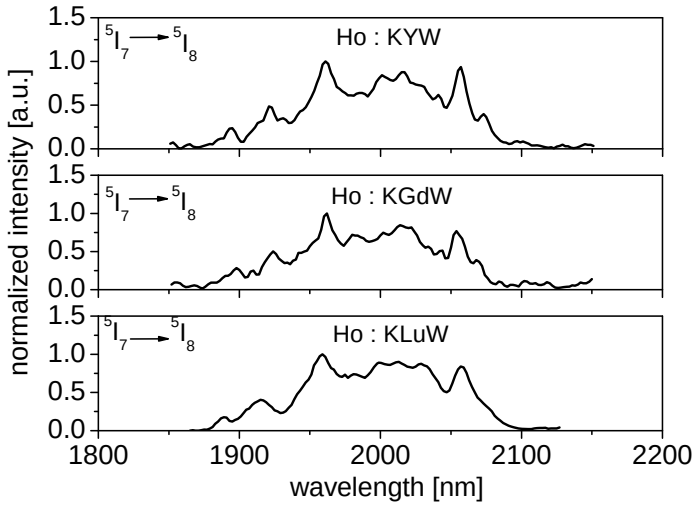

Figure 3.11 Room temperature 2 μm emission from Ho:KREW crystals

In order to determine the energy of the ground Stark levels ($^5I_8$ level) from the Ho ion, we measured the low temperature photoluminescence spectra of the first exited level ($^5I_7$ level) and the green emission which goes directly from the $^5S_2$ level to the ground state. After subtracting the first excited sublevel of each of the sublevels we determined the ground state. Figure 3.12 shows the low temperature emission spectra around 2 μm emission and green

emission from the Ho:KYW and Ho:KLuW crystals. The ground state values of Ho: KYW and Ho:KLuW can be seen in table 3.24 and table 2 of paper III, respectively.

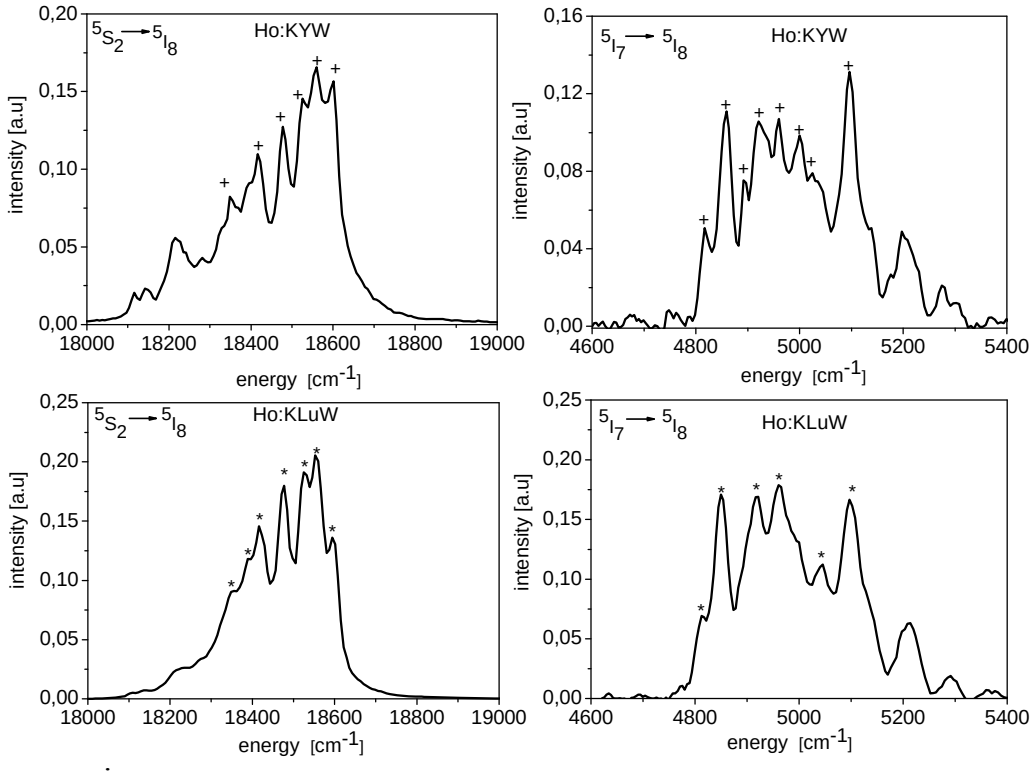

Figure 3.12 Low temperature emission spectra of Ho: KYW and Ho: KLuW

For co-doped (Ho,Tm):KLuW crystals the photoluminescence was carried out for all six samples after the crystal had been excited at 802 nm, the wavelength at which the sensitizer ion Tm absorbs most and transfers some energy to Ho by the process of energy transfer. A detailed explanation of the energy transfer mechanism and the up-conversion phenomena that occur in this (Ho,Tm):KLuW system can be found in paper II. Figure 5 in paper II shows the photoluminescence spectra around 2 μm for all the co-doped (Ho,Tm):KLuW crystals. To discuss the influence of the Tm and Ho doping ratio and to understand the relative ratio of energy transfer from Tm-Ho, we considered the maximum intensity of thulium and normalized it to unity (see figure 5 in paper II). Table 4 of paper II shows the normalized relative ratio data and calculated energy transfer. Using the information in table 4 and figure 5 of paper II the following points are inferred.

1) For samples 1 and 2 (case 1), we set the Ho concentration to 0.5 at% and increased the thulium concentration from 2.5% in sample 1 to 5% in sample 2. From the spectra, we conclude that the relative intensity of the Ho emission decreases as the Tm doping increases. This could be explained by greater interaction among the Tm ions. The decrease is not very pronounced because the real ion density (see table 3.18) in the crystals is not very different between the samples .

2) For samples 2, 3 and 4 (case 2), we set the Tm concentration to 5% and increased the holmium concentration to 0.5% (sample 2), 1.5% (sample 3) and 2.5% (sample 4), respectively. From the relative ratio of the two emissions we conclude that an increase in the Ho doping increases the Ho emission at 2 µm. This may be because the higher Ho doping improves energy transfer.

3) For samples 4, 5 and 6 (case 3), the Ho doping was the same as in case 1 and the Tm doping increased. The trend observed is the same as in case 1. The difference here is the doping level: Ho is set to 2.5 % and the Tm doping ranges from 5 to 10%. What is clear is that higher (Ho+Tm) doping levels (case 3) show higher emission intensity from Ho than lower doping levels (case 1), which proves that re-absorption effects are not detrimental at the 2.5at.% doping level of Ho.

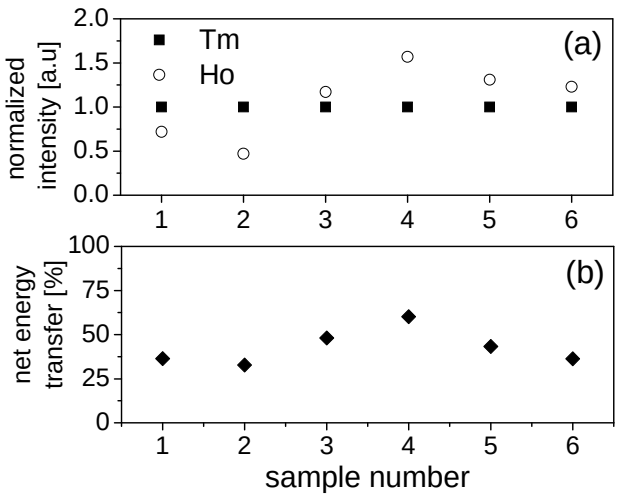

Figure 3.13 a) Evolution of the normalized relative intensity of the 2 µm emission from experimental values and b) evolution of net energy transfer from calculated values

We also calculated the net energy transfer for each crystal (see table 4 of paper II). Figure 3.13 shows the plot obtained using table 4 of paper II, which shows a) the evolution of normalized relative intensity of the 2 µm emission from experimental values, and b) the

evolution of net energy transfer from calculated values. The figure shows that the net energy transfer from the calculated values follows the same tendency as that of normalized experimental photoluminescence.

For co-doped (Ho,Yb):KLuW crystals, we also measured photoluminescence after exciting the crystal at 980 nm, the wavelength at which Yb absorbs most and transfers some energy to Ho. A discussion of the energy transfer mechanism of this (Ho,Yb).KLuW can be found in paper IV. The visible, 1.2 μm and 2 μm emission channels were observed from the photoluminescence experiments (see paper IV). As an example, figure 3.14 shows the measured room temperature photoluminescence spectra around 2 μm from the (1.5%Ho2.5%Yb):KLuW crystal after excitation at 980 nm using the Ti: Sapphire laser as the pump.

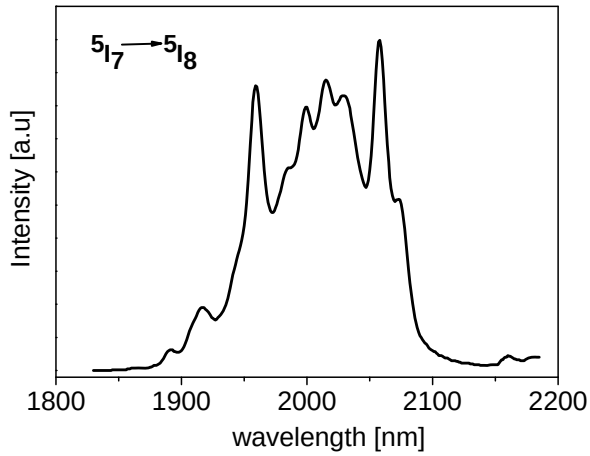

Figure 3.14 Room temperature 2 μm emission from Ho after excitation of Yb at 980nm

For the triply doped crystals, we were mainly interested in generating white light fluorescence. We used the Ti:Sapphire laser as pump source to excite the crystal at 980 nm, the wavelength at which it absorbs most and transfers part of its energy to Ho and Tm. After this energy transfer the Ho and Tm experience exited stated absorption (ESA) or energy transfer up-conversion (ETU) [85], which in turn populates the higher exited levels of Ho and Tm, and produces green, red and blue emission. A detailed explanation of the energy transfer mechanism of these triply doped crystals is given in paper V with the help of the energy level diagram (see figure 3 of paper V). A proper combination of red, green and blue generates cool and warm white light fluorescence from the triply doped crystals when exited at 980 nm using the Ti: Sapphire laser. In order to confirm white light fluorescence in the crystals, we made a photoluminescence study of all the triply doped crystals grown. With the help of the CIE 1931

UNIVERSITAT ROVIRA I VIRGILI
INFRARED LASERS BASED ON HO3+:KRE(WO4)2 CRYSTALS WITH TM3+OR YB3+ AS SENSITIZERS
Venkatesan Jambunathan
ISBN:/DL: T.1243-2011

XYZ colour space, chromaticity colour coordinates x, y and z, were calculated by integrating the area of the photoluminescence spectra of each colour at different wavelengths.

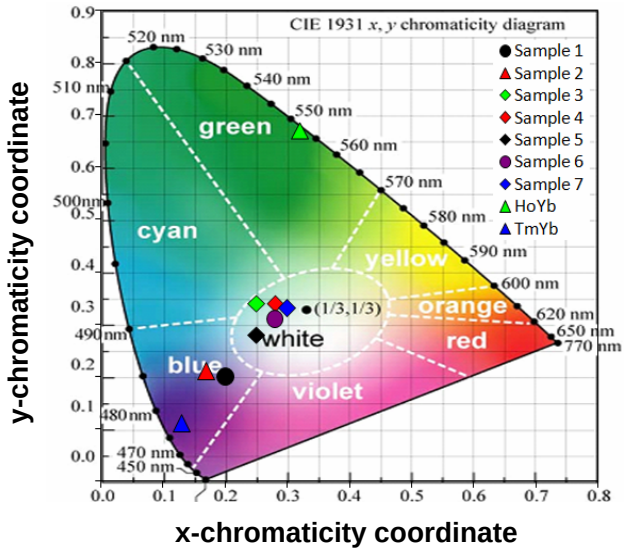

Figure 3.15 CIE (x,y) chromaticity diagram indicating the colour coordinates

A plot was made using the calculated colour coordinates (see figure 3.15) for each of the triply doped crystals (for sample numbers, see table 3.20 or paper V). The figure shows that the triply doped crystals with a doping level of Ho greater than 1at.% were in the white colour region, while the coordinates of sample 7 gave the warmest white colour fluorescence.

3.4.2.2 Life time measurement

Life time was measured firstly for the Ho:KREW sets and then for the (Ho,Tm):KLuW set. In the case of Ho:KREW, the life time of $^5I_7$ around 2µm was measured by exciting the $^5I_6$ level (1174 nm) for Ho:KYW and Ho:KGdW, and $^5I_6$ (1175 nm) and $^5I_5$ (914 nm) for Ho:KLuW. The decay curves were found to be a good single exponential curve. Figure 3.16 shows the light intensity decays of the $^5I_7$ level emission of Ho: KREW with different holmium concentrations. From the experimental decay curves, the radiative lifetimes were computed (see table 3.25).

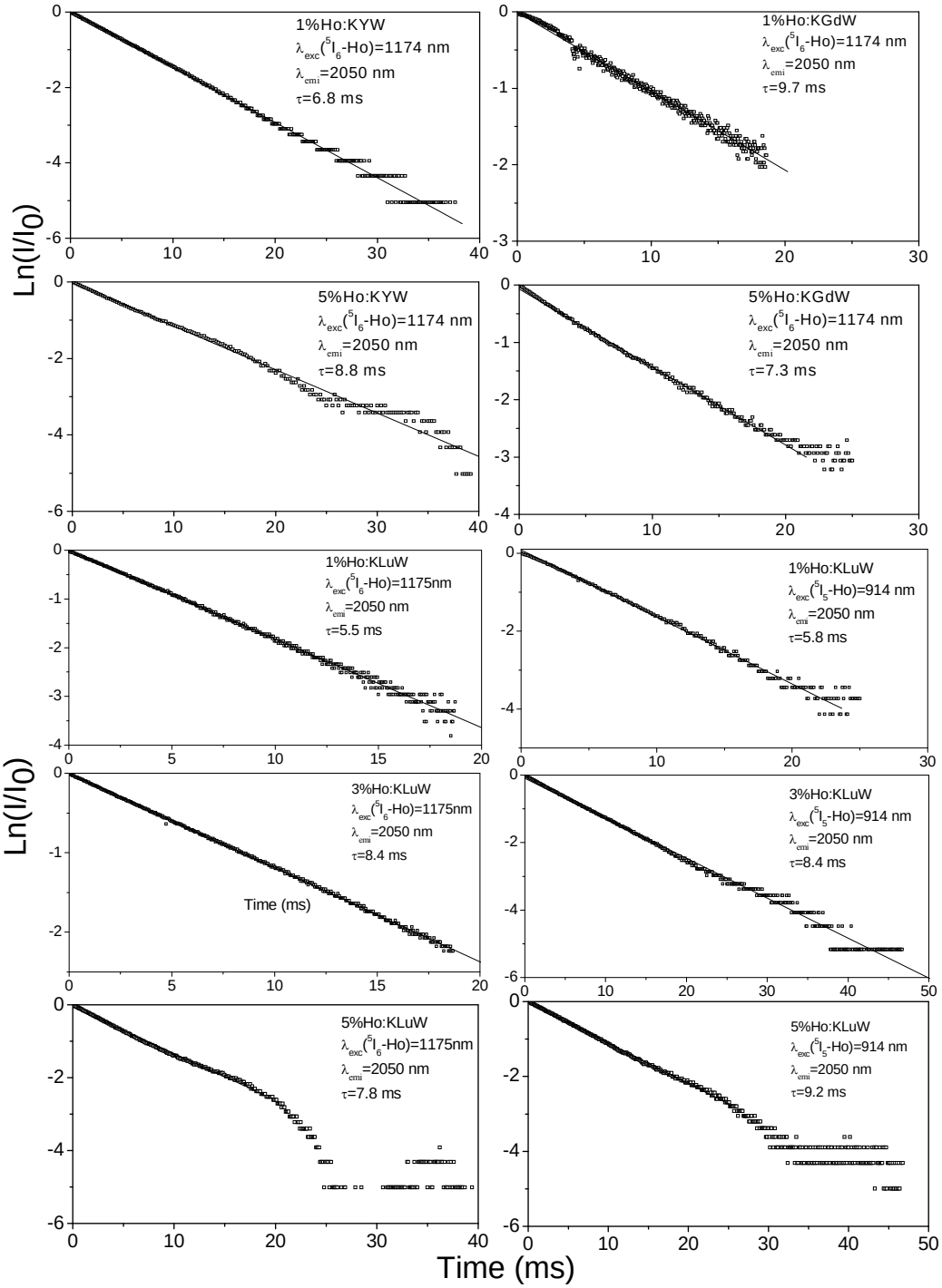

Figure 3.16 Light intensity decays of the $^5I_7$ level emission of Ho: KREW for different Ho concentrations

Table 3.25 Computed radiative life times for $^5I_7$ level emission of Ho:KREW for different Ho concentrations

Sample	λ_{exc} [nm]	τ [ms] for λ_{emi} = 2.05 µm
1%Ho:KYW	1174	6.8
5%Ho:KYW	1174	8.8
1%Ho:KGdW	1174	9.7
5%Ho:KGdW	1174	7.3
1%Ho:KLuW	1175	5.5
	914	5.8
3%Ho:KLuW	1175	8.4
	914	8.4
5%Ho:KLuW	1175	7.8
	914	9.2

Table 3.25 shows that life time gets longer as concentration increases even though it normally gets shorter because of the interaction between ions, which leads to fast decay. From the results, we conclude that all the measurements are affected by re-absorption as the measured values are larger than the radiative values calculated using the Judd-Ofelt approach (5.863 ms for the $^5I_7$ level of Ho:KGdW) [83].

For co-doped (Ho,Tm):KLuW, we measured the lifetimes of the $^5S_2$ level at around 540 nm (dominant green emission) and the $^5I_7$ level at around 2µm by exciting the $^5I_5$ level of Ho at 915 nm and the $^3H_4$ level of Tm at around 802 nm, respectively. These measurements were made for each combination of dopant ions. Figure 3.17 shows the light intensity decays of $^5S_2$ level emission of the (Ho,Tm):KLuW for each combination of dopant ions by exciting at 915 nm and figure 3.18 shows the light intensity decays of $^5I_7$ level emission by exciting at 802 nm. In both cases the curves are single exponential. From the experimental decay curves radiative lifetimes were computed (see table 3.26).

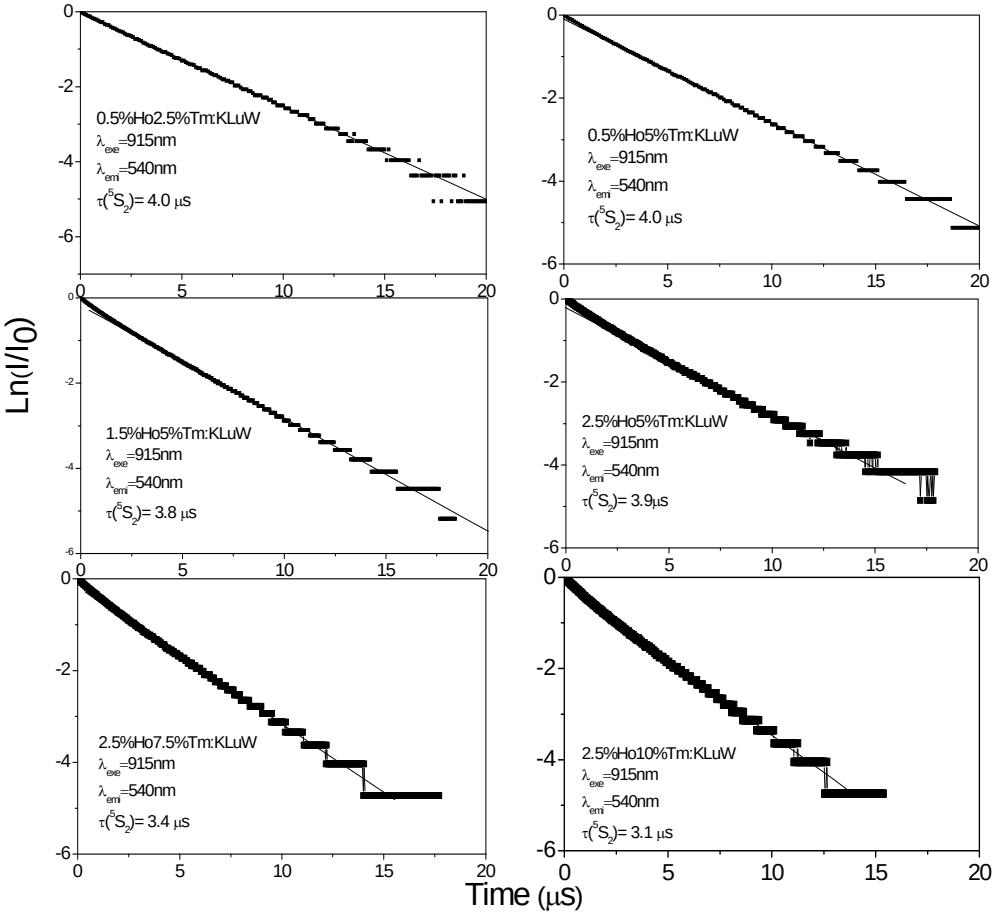

Figure 3.17 Light intensity decays of (Ho,Tm):KLuW for each combination of dopant ions of $^5S_2$ level emission by exciting at 915 nm

Table 3.26 Computed radiative life times of $^5S_2$ level and $^5I_7$ level emission of (Ho,Tm):KLuW for each combination of dopant ions

Sample no	Sample name	τ [μs] for λ_{emi} = 540 nm	τ [ms] for λ_{emi} = 2.05 μm
1	0.5%Ho2.5%Tm:KLuW	4.0	3.7-4.1
2	0.5%Ho2.5%Tm:KLuW	4.0	3.8-4.0
3	0.5%Ho2.5%Tm:KLuW	3.8	5.3-5.6
4	0.5%Ho2.5%Tm:KLuW	3.9	5.1-5.6
5	0.5%Ho2.5%Tm:KLuW	3.4	4.1-4.3
6	0.5%Ho2.5%Tm:KLuW	3.1	3.0-3.3

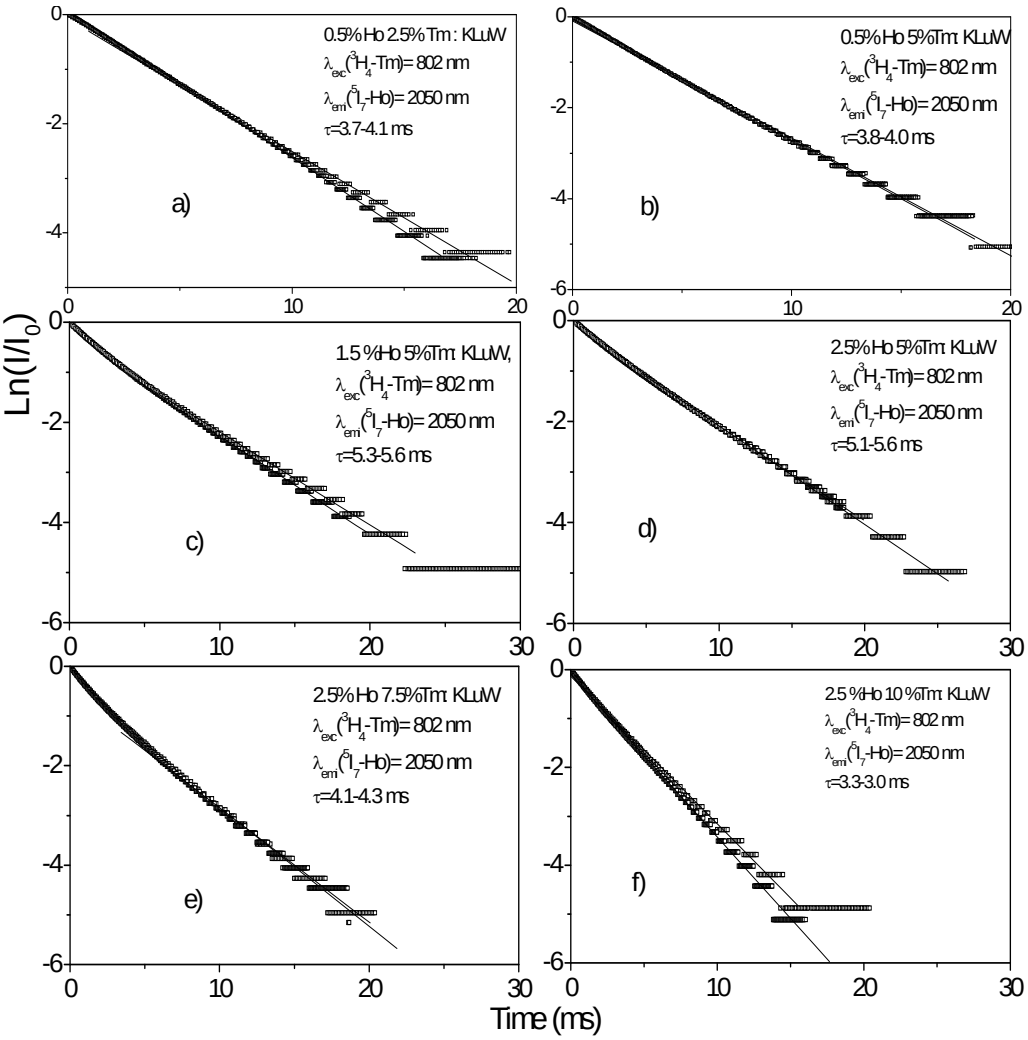

Figure 3.18 Light intensity decays of (Ho,Tm):KLuW for each combination of dopant ions of $^5I_7$ level emission by exciting at 802 nm

Table 3.26 shows that the lifetime for green emission is essentially the same as the lifetime for the single-doped Ho:KREW crystal reported previously [82]. Parallel to this, the lifetime of green emission after excitation at 802 nm shows a rise time which corresponds to the energy transfer. However, it does not give any information about the realistic values since it is affected by the longer lifetime of the $^3H_4$ level (the values ranged from 69 to 6μs). From the measured values for 2 μm emission we deduced that at low Ho doping levels (0.5%, samples 1 and 2) the values are realistic, but the increase in Ho doping levels (samples 2, 3 and 4, keeping fixed the Tm doping level) shows that re-absorption phenomena considerably lengthen the

lifetime. In samples 4, 5 and 6, the Ho doping level was kept constant and the Tm doping level was increased. There was evidence of a strong interaction among the Tm ions, which shortened the lifetime of the $^5I_7$ level of Ho.

The re-absorption effects observed in the lifetime measurements can be avoided by using crystal powder or the pinhole method.

3.4.2.3 Calculation of emission and gain cross-sections

The parameters that define the laser performance of a material are the emission and gain cross-sections. They can be calculated using the reciprocity method [86] and the Füchtbauer-Ladenburg (FL) method [86]. The reciprocity method is normally used to calculate the emission cross section of an optical transition from the optical absorption cross-section line shape at room temperature of a particular energy level. Absorption and emission processes are characterized by their absorption (σ_a) and emission cross sections (σ_e), respectively. From the energies and degeneracies of the upper and lower energy levels, we can find a mathematical expression that contains a direct relationship between these two cross-sections so that the emission cross section can be calculated. The reciprocity calculation is based on

$$\sigma_e(\upsilon)=\sigma_a(\upsilon)\frac{Z_l}{Z_u}\exp\left[\frac{(E_{zl}-h\upsilon)}{kT}\right] \tag{3.2}$$

where σ_e is the emission cross-section to be calculated as a function of the frequency (or wavelength) and σ_a is the absorption cross section obtained from the room temperature optical absorption, which in our case is the optical absorption of Ho ($^5I_8$ to $^5I_7$ transition). The E_{zl} is the 'zero-line,' or the energy separation, derived from the crystal field component. This is the difference between the lowest energy sublevel of the excited energy level (upper) and the lowest energy sublevel of the ground level (lower). K is Boltzmann's constant and h is Planck's constant.

Z_u and Z_l are the partition functions of the upper and lower energy levels, respectively, which are calculated from

$$Z_{u,l}=\sum_k d_k \exp\left(-\frac{E_k}{(kT)}\right) \tag{3.3}$$

where d_k and E_k are the degeneracies and the energy of each sublevel of the upper and the lower energy levels involved in the system.

The other way to compare the emission cross section is to use the Füchtbauer-Ladenburg (FL) method, which uses the mathematical expression

$$\sigma_e(\lambda) = \frac{\lambda^4 I(\lambda)}{8\pi n^2 c \tau_f \int I(\lambda) d\lambda} \tag{3.4}$$

where $I(\lambda)/\int I(\lambda)\, d\lambda$ is the normalized emission line shape function, which in our case, corresponds to the $^5I_7$ to $^5I_8$ transition of Ho, n is the refractive index, c is the speed of light, and τ_f is the fluorescence time. The FL method requires only the room temperature emission spectrum and fluorescent life. The reciprocity method requires room and low temperature optical absorption spectra to determine excited energy Stark levels and low temperature emission spectra to determine the ground Stark levels.

Light amplification is expected when the emitted light is higher than the absorption at the same wavelength for a given inversion ratio β. The expression which relates the gain cross section with the absorption and emission cross section is given by

$$\sigma_g = \beta\sigma_e - (1-\beta)\sigma_a \tag{3.5}$$

where σ_g is the effective gain cross section, σ_e is the calculated emission cross section, σ_a is the absorption cross section and β is the population inversion rate.

Using the above mentioned formulas we quantified the emission cross-section from the absorption cross-section using the reciprocity method. To measure absorption we used the 5at.% Ho:KREW crystals. From the emission cross sections in figures 3.21, 3.22 and 3.23, a maximum emission cross-section of ~2.65×10^{-20} cm^2 at 2056 nm for Ho:KYW, ~2.70×10^{-20} cm^2 at 2054 nm for Ho:KGdW and ~2.45×10^{-20} cm^2 at 2059 nm for Ho:KLuW are calculated for E//N_m. But for the other two polarizations, N_g and N_p, the emission cross-sections were less intense with maximums at different wavelengths for all three hosts. To quantify and compare the shape of the experimental photoluminescence obtained around 2 μm from Ho with all three hosts, we averaged the three polarizations and used this average to make comparisons with the un-polarized experimental photoluminescence. Figures 3.19, 3.20 and 3.21 show the average of three polarised absorption cross-sections and the emission cross- sections calculated using the reciprocity method and the Fücht-Ladenburg method. They show that the shape of the spectra is quite similar when calculated by the reciprocity method and the FL method, but the intensity is higher for the reciprocity method because it does not take re-absorption into account.

We computed the gain cross section using equation 3.5 and from the gain curves in figures 3.19, 3.20 and 3.21, we found that gain is maximum at 2056 nm for Ho: KYW, 2054 nm for Ho: KGdW, and 2059 nm for Ho: KLuW. These, then, are the expected laser wavelengths for N_m polarization at higher inversion levels and the expected gain at low inversion levels could be around 2073 nm for Ho:KYW, 2071 nm for Ho:KGdW, and 2078 nm for Ho: KLuW. The

reason we recalculated the absorption, emission and gain cross sections of Ho: KGdW is that they had not been calculated for each of the principal optical directions but for E//b and E⊥b [83]. Table 3.27 summarizes the absorption cross sections, the maximum emission cross-sections and the expected laser wavelengths of Ho:KREW.

Table 3.27 Summary of absorption cross-sections, maximum emission cross- sections and expected laser wavelengths of Ho:KREW

Crystal	Absorption cross section (σ_a) [10^{-20} cm^2]			Emission cross section (σ_e) [10^{-20} cm^2]			Expected laser wavelength [nm] for *E// N_m*	
	E// $N_{m,p}$	**λ [nm]**	**σ_a**	***E// $N_{m,p}$***	**λ [nm]**	**σ_e**	**For high β rates**	**For low β rates**
Ho:KYW	N_m	1941	0.38	N_m	2056	2.65	2056	2073
	N_p	1941	0.32					
	N_m	1946	0.52					
	N_p	1946	0.44					
	N_m	1961	1.60					
	N_p	1961	0.83					
Ho:KGdW	N_m	1941	0.47	N_m	2054	2.70	2054	2071
	N_p	1941	0.34					
	N_m	1946	0.65					
	N_p	1946	0.40					
	N_m	1961	2.00					
	N_p	1961	0.74					
Ho:KLuW	N_m	1941	0.40	N_m	2059	2.45	2059	2078
	N_p	1941	0.32					
	N_m	1946	0.49					
	N_p	1946	0.42					
	N_m	1961	1.43					
	N_p	1961	0.75					

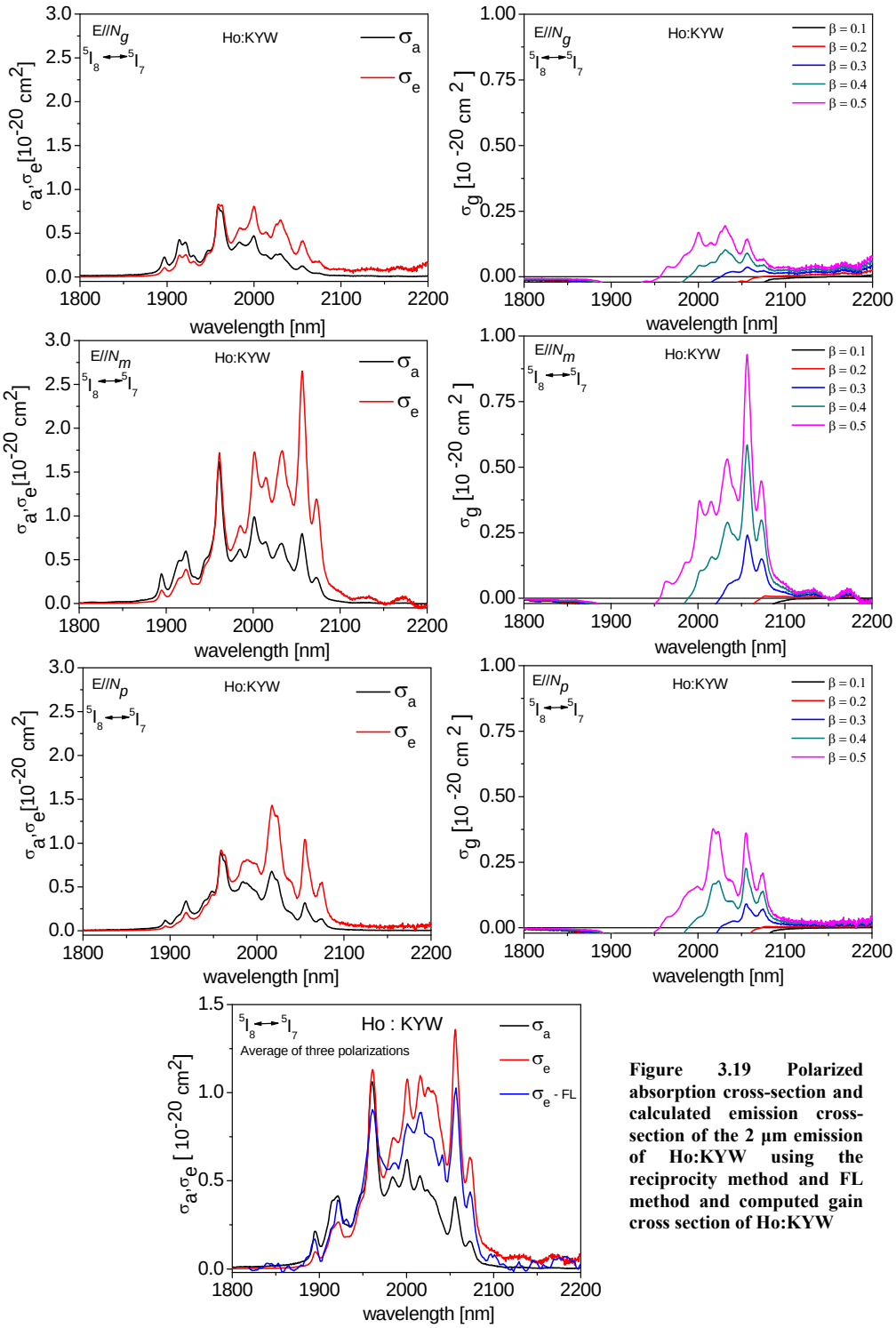

Figure 3.19 Polarized absorption cross-section and calculated emission cross-section of the 2 µm emission of Ho:KYW using the reciprocity method and FL method and computed gain cross section of Ho:KYW

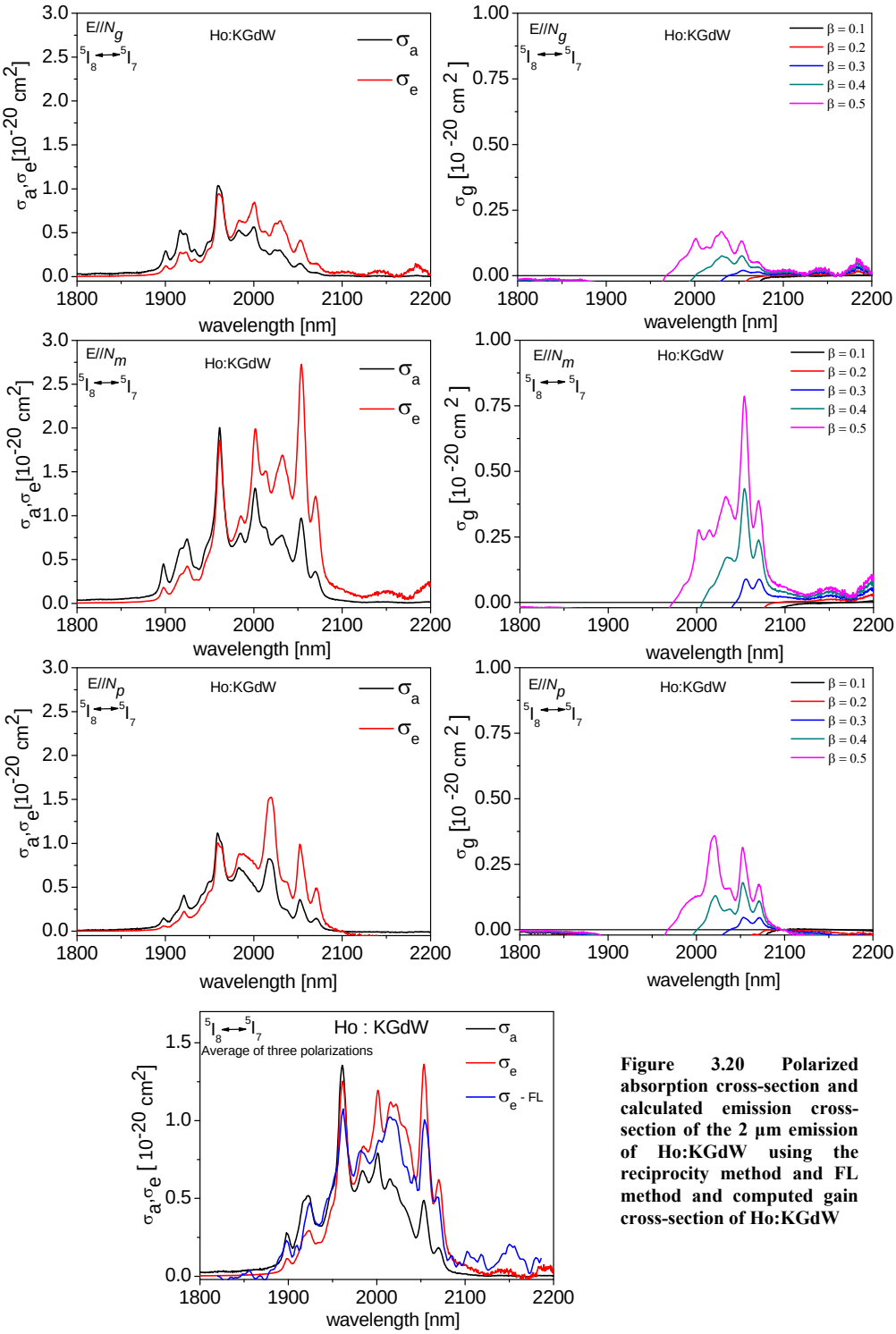

Figure 3.20 Polarized absorption cross-section and calculated emission cross-section of the 2 µm emission of Ho:KGdW using the reciprocity method and FL method and computed gain cross-section of Ho:KGdW

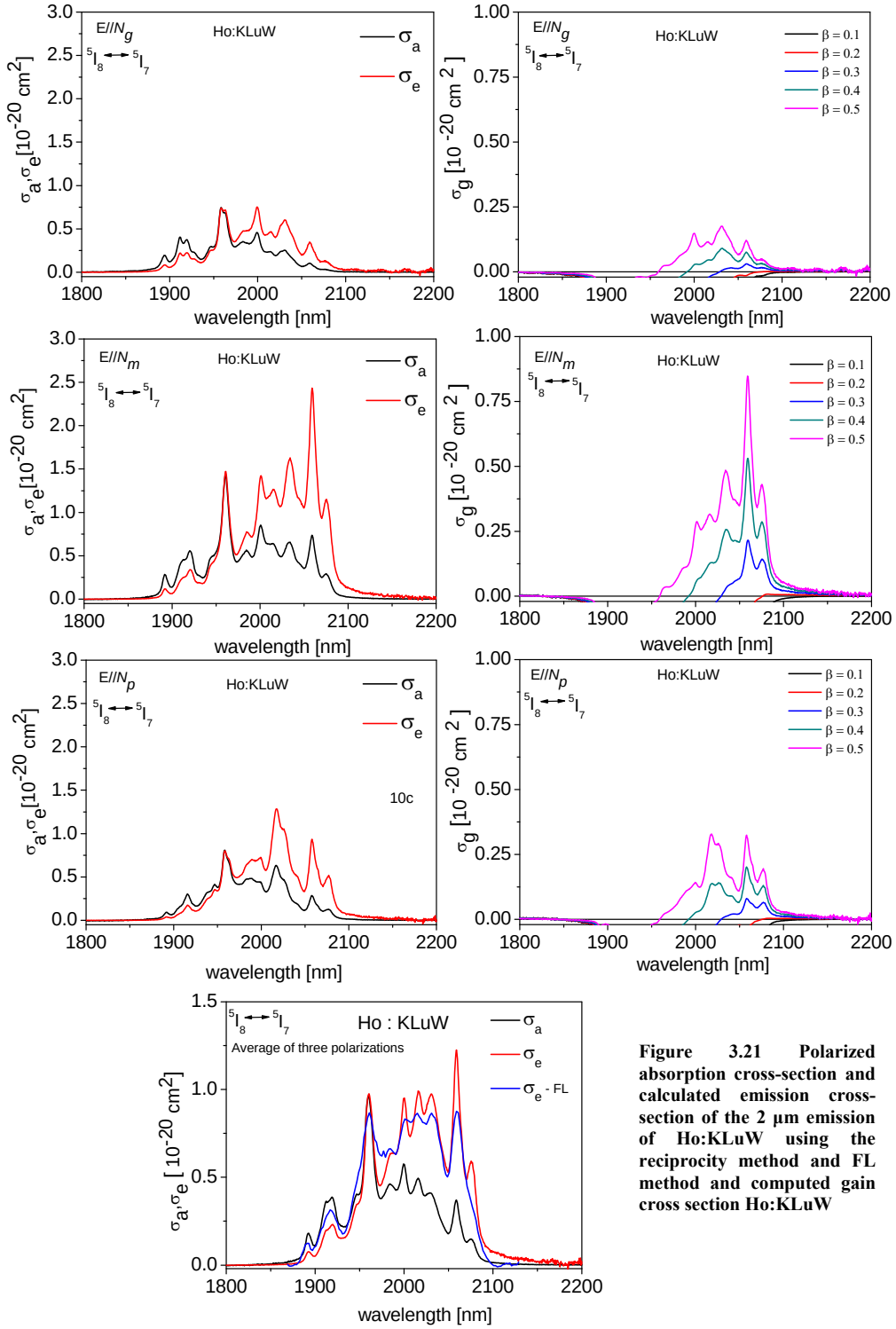

Figure 3.21 Polarized absorption cross-section and calculated emission cross-section of the 2 µm emission of Ho:KLuW using the reciprocity method and FL method and computed gain cross section Ho:KLuW

UNIVERSITAT ROVIRA I VIRGILI
INFRARED LASERS BASED ON HO3+:KRE(WO4)2 CRYSTALS WITH TM3+OR YB3+ AS SENSITIZERS
Venkatesan Jambunathan
ISBN:/DL: T.1243-2011

UNIVERSITAT ROVIRA I VIRGILI
INFRARED LASERS BASED ON HO3+:KRE(WO4)2 CRYSTALS WITH TM3+OR YB3+ AS SENSITIZERS
Venkatesan Jambunathan
ISBN:/DL: T.1243-2011

Chapter 4

Continuous-wave laser operation of Ho:KRE$(WO_4)_2$ crystals

This chapter gives a summary of the laser results obtained in this work. Laser operation was performed in continuous-wave regime for the co-doped (Ho,Tm):KLuW with Tm as sensitizer and a Ti:Sapphire laser as the pump source. For the single-doped Ho:KREW, RE=(Y, Gd, Lu) continuous-wave laser action was performed using in-band/resonant pumping with a diode-pumped Tm:KLuW laser emitting at 1946 nm and a fibre-coupled diode laser emitting at 1941 nm.

The following papers describe some of the results included in this chapter.

Paper II: V. Jambunathan, A. Schmidt, X. Mateos, M. C. Pujol, J. J. Carvajal, U. Griebner, V. Petrov, C. Zaldo, M. Aguiló and F. Díaz, "Crystal growth, optical spectroscopy and continuous-wave laser operation of co-doped (Ho,Tm):$KLu(WO_4)_2$ monoclinic crystals", submitted to J. Opt. Soc. Am. B.

Paper III: V. Jambunathan, X. Mateos, M. C. Pujol, J. J. Carvajal, C. Zaldo, M. Aguiló, F. Díaz, U. Griebner and V. Petrov, "Crystal growth, optical spectroscopy and continuous-wave laser operation of Ho:$KLu(WO_4)_2$ crystals", submitted to Appl. Phys. B.

Paper VI: V. Jambunathan, A. Schmidt, X. Mateos, M. C. Pujol, J. J. Carvajal, M. Aguiló, F. Díaz, U. Griebner and V. Petrov, "Continuous-wave co-lasing in a monoclinic co-doped (Ho,Tm):$KLu(WO_4)_2$ crystal", submitted to Laser Phys. Lett.

Paper VII: X. Mateos, V. Jambunathan, M. C. Pujol, J. J. Carvajal, F. Díaz, M. Aguiló, U. Griebner and V. Petrov, "CW lasing of Ho in $KLu(WO_4)_2$ in-band pumped by a diode-pumped Tm:$KLu(WO_4)_2$ laser", Opt. Express 18 (20), 20793 -20798 (2010).

Paper VIII: V. Jambunathan, X. Mateos, M. C. Pujol, J. J. Carvajal, M. Aguiló, F. Díaz, U. Griebner and V. Petrov, "Diode –Pumped Ho:$KLu(WO_4)_2$ laser at 2.08 μm", submitted to Appl. Phys. Express.

Paper IX: V. Jambunathan, X. Mateos, M. C. Pujol, J. J. Carvajal, F. Díaz, M. Aguiló, U. Griebner and V. Petrov, "Continuous-wave laser generation at ~2.1 μm in Ho:$KRE(WO_4)_2$ (RE= Y, Gd, Lu) crystals: a comparative study ", submitted to Opt. Express.

4.1 Continuous-wave laser operation of co-doped (Ho,Tm):KLuW

In the case of the (Ho,Tm):KLuW series, laser experiments were carried out for the first five samples described in chapter 3, with the laser setup described in chapter 2. Continuous-wave laser operation was realized for the first three samples, but not for the fifth sample because of the extremely high absorption in the crystal which led to a high temperature that prevented laser oscillation. For sample 4 only quasi-CW laser oscillation was achieved. Figure 10 in paper II shows the input-output characteristics of samples 1, 2 and 3 for all the transmission of output couplers used as mentioned in chapter 2. For sample 1, with 0.5at.%Ho and 2.5at.%Tm a maximum output power of 83 mW was reached with T_{oc} = 3% and a maximum slope efficiency of 10.8 % was calculated. The absorption of the crystal ranged from 81% to 94% depending on the incident power level.

When the Tm doping level was increased to 5at.% (sample 2), the absorption in the crystal and the interaction among ions also increased, so the output powers were higher. Again for T_{oc} = 3%, maximum power was measured to be 145 mW and slope efficiency was calculated to be 12.9 %. In this case, the absorption of the crystal ranged from 86% to 96%. In sample 3, when we increased the Ho doping level, the laser performances decreased (only 96 mW with a slope efficiency of 10.7%). Here the absorption of the crystal ranged from 79% to 87%. The increase in Ho content caused re-absorption of the laser due to the quasi-3 level nature of the Ho lasers.

Laser operated at 2061 nm in all cases independently of the doping level and as well as the transmission of the output coupler used. This is consistent with the maximum gain shown in figure 3.21 of chapter 3. Figure 11 in paper III shows the typical spectrum of the (Ho, Tm):KLuW laser. This emission corresponds to the $^5I_7 \rightarrow {}^5I_8$ transition of Ho. Thermal problems were also observed in all cases, because when we used a mechanical chopper with a duty cycle of 50%, a linear dependence of the output power versus the incident or absorbed power was observed. In all cases, oscillation of N_m polarization was selected since the crystals were positioned at Brewster's angle.

It is worth noting that for samples 1 and 2 dual wavelength operation was observed at 1937 nm or 1919 nm and 2061 nm. The new laser wavelengths corresponded to Tm and are studied in the section below together with the tuning of the laser. Sample 4 generated laser at 2061 nm only in the quasi-CW regime. Too much Tm doping caused extremely high absorption in the crystal leading to the sample cracking. We also tested sample 3, which emits only one wavelength for polarisation parallel to the N_p principal axis, by changing the orientation of the sample and propagation of light along the N_g axis. The experimental setup was the same and the

sample was again at Brewster's angle with the pump tuned to 793.5 nm the wavelength at which Tm absorbs most for the N_p principal axis (see figure 4 of paper II). Lasing was only possible in the quasi-CW regime. The maximum peak output power was 21 mW with T_{oc} =1.5%, 20 mW with T_{oc} = 3.0% and 14mW with T_{oc} =5.0% with an incident peak power of 1500 mW. The slope efficiency was as low as 2.7% and the laser wavelength was 2060 nm for all the T_{ocs}. Table 4.1 shows the maximum output power measured, the slope efficiencies and laser thresholds for every sample and every output coupler transmission in CW and quasi-CW regimes. It can be seen that the best sample had doping levels of 0.5at.%Ho and 5at.%Tm. Detailed experimental results can be found in paper II.

Table 4.1 Summary of the laser results from (Ho,Tm):KLuW crystals

Sample number	T_{oc} %	Output power [mW]		Slope efficiency [%]		Threshold [mW]		Laser wavelength [nm]
		Quasi-CW	CW	Quasi-CW	CW	Quasi-CW	CW	
1	1.5	92	70	10.7	8.7	82	77	2061
	3.0	104	83	12.6	10.8	88	83	
	5.0	93	62	12.3	7.9	97	90	
	9.0	65	50	9.6	8.0	154	149	
2	1.5	168	123	13.7	10.8	91	106	2061
	3.0	164	145	14.4	12.9	92	97	
	5.0	162	132	14.2	12.5	97	97	
	9.0	118	108	11.5	10.9	134	135	
3	1.5	140	88	11.8	8.3	152	171	2061
	3.0	151	96	15.5	10.7	164	177	
	5.0	182	93	15.3	9.3	208	260	
	9.0	140	70	14.5	7.9	232	269	
4	1.5	53	-	5.3	-	282	-	2061

4.2 Continuous-wave dual-wavelength lasing in co-doped (Ho,Tm):KLuW crystal

Dual wavelength laser action was achieved in sample 1 and 2 of the (Ho,Tm):KLuW series and since sample 2 (0.5%at.%Ho5at.%Tm:KLuW) shows better results than sample 1, it was chosen for antireflection coating and the CW laser experiment was repeated and reported. The experimental set up used is the same as shown in chapter 2 and some of the results can be found in paper VI. Figures 1 a) and b) in paper V show the calculated gain cross-section of Ho and Tm, respectively, and β is the inversion rate. This gain curve is sufficient to understand the dual-wavelength nature of the laser emission (see below).

Dual-wavelength laser oscillation was realized in CW regime for all the output couplers used. For each of them, we measured the output power as a function of the absorbed pump power. The laser threshold was reached in the 60 - 100 mW range of absorbed pump power and for all output couplers lasing started at 2061 nm, which corresponds to the $^5I_7 \rightarrow {}^5I_8$ transition of

Ho^{3+}. When the pump power was increased, a second wavelength appeared at 1937 nm in the output spectrum when output couplers of transmission, T_{oc} = 1.5%, 3% and 5% were used and even multiple wavelengths (1919 and 1928 nm in addition to 2061 nm) were observed for T_{oc} = 9%. These additional emissions are attributed to the $^3F_4 \rightarrow {}^3H_6$ transition of Tm^{3+}. Depending on the alignment of the cavity in the experiment with T_{oc} = 9%, the laser wavelengths shifted to multiple wavelength operation at 1931 nm, 1935 nm, 1937 nm and 1939 nm. This is due to the plateau found in the gain curves between ~1925 nm and ~1940 nm (see Fig. 1b of paper VI) which allows these wavelengths to be generated simultaneously. In fact, the dual-wavelength operation, the simultaneous generation in Ho and Tm ions in this crystal, occurs because the gain values of Ho and Tm are very similar at the laser wavelengths and several wavelengths can oscillate in a cavity with broad-band coated mirrors. The gain curves show that at low inversion levels, the gain cross-section of Ho at 2060 nm and that of Tm at 1937 nm are very similar, which leads to competition of these two wavelengths corresponding to different ions but oscillating simultaneously. If the output coupling losses are increased (T_{oc} = 9%), the Tm emission shifts to shorter wavelengths, typical of a three-level system, and operation in the next maximum of the gain curve takes place (1919 and 1928 nm) where the cross-section values are again closer to that of Ho at 2060 nm. We deduced that 1937 nm, 1928 nm and 1919 nm laser wavelengths are generated in Tm because there is no positive gain in this region for Ho. We carefully analyzed the difference in energy from each sublevel of the excited levels to each sublevel of the ground state in Tm and Ho and observed that, indeed, all these transitions are possible from the two ions. We only rejected the generation of the 1937 nm, 1928 nm and 1919 nm lasers from Ho because of the non-positive gain for wavelengths shorter than 1960 nm (Fig. 1a of paper 5) (even in the case of the maximum inversion rate of 0.5).

Figures 2 and 3 of paper VI and Figure 4.1 a) and b) show the input-output characteristics of the (Ho,Tm):KLuW laser for T_{oc} = 3%, 9%, 1.5% and 5%, respectively, and the corresponding output spectra as insets for T_{oc} = 3% and 9% , 4.1 a) and b) right for T_{oc} = 1.5% and 5% . From the figures and Table 1 of paper VI, it can be seen that the slope efficiency increases as the transmission of the output coupler increases. This is accompanied by an increase in the Tm laser part of the output power. For T_{oc} = 9% and maximum pump level, the output power is almost equally distributed between the two emissions and each ion produces slightly more than 100 mW (see Fig. 3 of paper V).

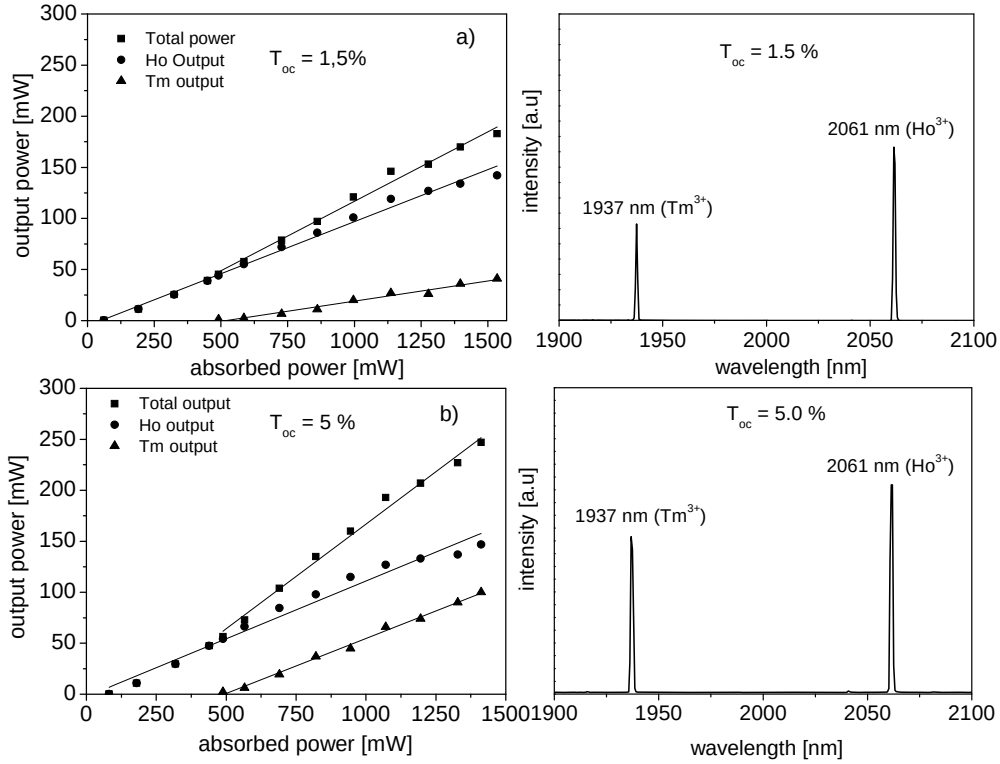

Figure 4.1 a) and b) Output power versus absorbed pump power for T_{oc} = 1.5 and 5 % (left) and the corresponding laser emission spectrum (right)

Finally tuning was performed with the help of the birefringent filter made of 1mm-thick quartz. The laser was continuously tuned from 1854 nm to 2063 nm with a T_{oc} = 3%. We used a dichroic mirror to separate the two lasers and measured the tuning range separately (see Figure 4.2).

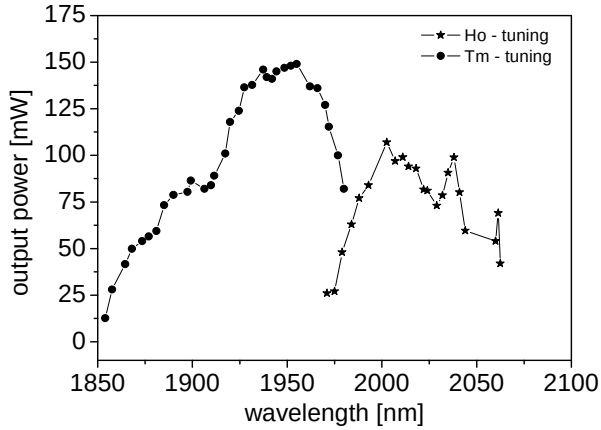

Figure 4.2 Tuning of the (Ho, Tm):KLuW laser

The Tm laser was tuned from 1854 nm to 1980 nm and the Ho laser from 1971 to 2063 nm. In general, we observed higher output power for the Ho laser (Figures 2 and 3 of paper VI and Figure 4.1 a) and b)). However, when we inserted the birefringent filter inside the cavity the Tm ion emission was more powerful. Table 4.2 shows the calculated slopes and measured laser thresholds and maximum output of the 0.5at %Ho 5at.%Tm.KLuW laser for different output couplers.

Table 4.2 Calculated slopes, measured laser thresholds and maximum output of the 0.5%Ho5%Tm:KLuW laser for different output couplers

T_{oc} %	Slope efficiency [%]			Threshold [mW]		Output power [mW]			Laser wavelength [nm]	
	Tm	Ho	Total	Ho	Tm	Ho	Tm	Total	Ho	Tm
1.5	3.9	10.2	13.6	62	490	142	41	183	2061	1937
3.0	9.2	12.7	21.1	58	395	156	88	244	2061	1937
5.0	10.8	11.3	20.6	80	488	147	100	247	2061	1937
9.0	12.8	10.2	24.8	97	361	109	115	224	2061	1919

4.3 Continuous-wave laser operation of in-band pumped Ho:KLuW

4.3.1 CW laser operation by in-band pumping using diode-pumped Tm:KLuW

Continuous wave laser action of the single-doped Ho:KLuW crystal was carried out by using a hemispherical cavity (see chapter 2). The pump source was a homemade diode pumped Tm:KLuW, which was scaled to 5.1W emitting at 1946 nm. A detailed report of the laser experiment performed can be found in paper VII. The sample was N_g cut and oriented for light propagation along the N_g principal optical direction and can be oriented for polarization parallel to the N_m or N_p principal optical directions. It was 3 mm thick and had an aperture of 3x3 mm^2. We tested 1.0, 3.0 and 5.0 at.% Ho:KLuW uncoated samples and we only managed to achieve laser action for the 3at.%Ho:KLuW sample. Here the pump is circularly polarized with the help of the quarter wave plate.

Figure 3 in paper VII compares the input output characteristics of the two pump lenses with focal lengths of f = 50 and f = 150 mm, a radius of curvature R_{OC}=25 mm with Toc = 1.8% and a cavity length of 26 mm. The figure shows that mode matching is better and laser efficiency higher when the focal length is 150 mm. Figure 4 in paper VII shows the dependence of the output power on the radius of curvature with Toc = 1.8%. The R_{OC} = 50 mm and 75 mm mirrors performed the same as and slightly better than R_{OC}=25mm. Figure 5 in paper VII compares the laser performance with two T_{ocs} =1.8 and 3.3 % and shows that the increase in the output coupler transmission had a very weak effect on the input-output characteristics, which was performed with R_{OC} = 50 mm and f =150 mm experimental condition. In all cases the pump

wavelength was 1946 nm and the emission wavelength 2078 nm and operated in the fundamental transversal mode. The quantum defect in this case was only 6%.

Finally, in order to estimate the slope efficiency with respect to the absorbed power, we assumed the single pass absorption of the 3at.%Ho:KLuW crystal to be 24% and 39% for f = 50 and 150 mm pump lenses, respectively. The input output characteristics with respect to the absorbed power are shown in figure 4.3.

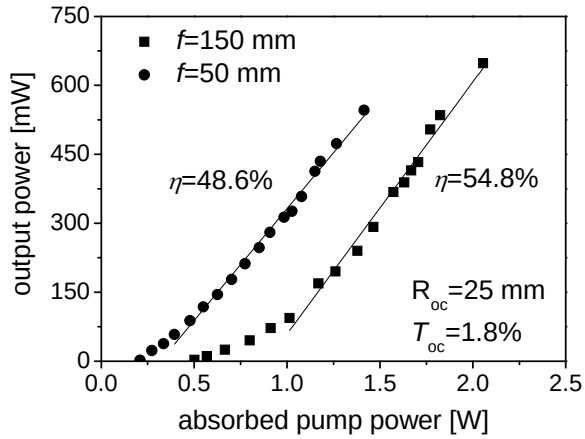

Figure 4.3 Estimated slope efficiencies versus absorbed power in the double pump pass Ho: KLuW laser

The figure shows that output is maximum (648 mW) for an absorbed pump power of 2.05 W in the double pass pumping for f = 150 mm. The slope efficiency is 54.8% with a laser threshold of 500 mW. For f = 50 mm the slope efficiency is 48% with a laser threshold of ~ 200 mW. To improve the efficiency it was decided to send this sample for antireflection coating along with the non lasing samples and to check if it is possible to lase or not.

4.3.2 In-band pumping of Ho:KLuW by fibre-coupled diode laser

Since only in 3at.% Ho:KLuW laser oscillation with Tm:KLuW pumping was achieved, this diode pumping on Ho:KLuW is confined only to this crystal but the crystal is antireflection coated for pump and laser wavelengths. The experimental setup used is the one described in chapter 2. Some of the results can also be found in paper VIII. Continuous-wave laser oscillation was realized for all the output couplers used with radii of curvature of 50mm. We measured the output power as a function of incident power for all the T_{oc} with a cavity length of 50mm. T_{oc} = 3% gives maximum power. The absorption in the crystal in the non lasing condition is 15.7 % and this constant value is used to calculate slope efficiency. A maximum output of 408 mW for an absorbed power of ~1500 mW and the laser threshold was 606 mW was acheived. For

purposes of calculation, we assumed single pass absorption because of the strong divergent non absorbed pump beam, which cannot be retro reflected back to the crystal by the output coupler. Figure 4.4 shows the input–output characteristics of the diode pumped Ho laser.

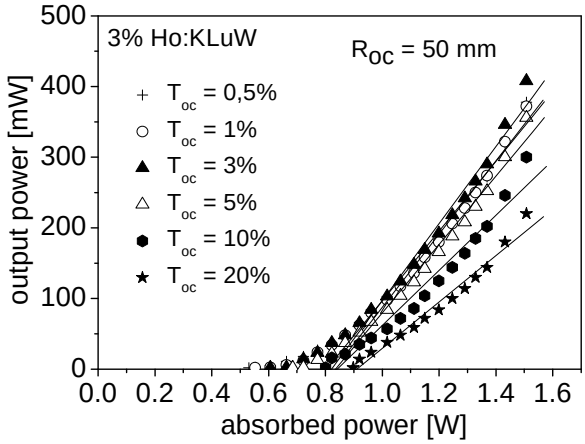

Figure 4.4 Output power versus absorbed power of the 3 at. % Ho:KLuW laser for several T_{OC} values with R_{OC} = 50 mm

The figure shows that the laser threshold increases and the laser wavelength shortens at higher output coupler transmissions (when the losses in the cavity are greater), which is typical for a quasi three level laser, and the laser wavelength follows the gain curves (see figure 3.21 of chapter 3). The laser results are summarised in table 4.3.

Table 4.3 Summary of laser results for 3%Ho: KLuW with diode laser as pump source

T_{oc} %	Output power [mW]	Slope efficiency [%]	Threshold [mW]	Laser wavelength [nm]
0.5	378	49.4	530	2080.4
1.5	372	51.8	552	2080.0
3.0	408	54.5	606	2078.5
5.0	356	48.4	684	2077.0
10.0	300	39.0	800	2076.0
20.0	220	32.8	898	2060.0

We also studied the influence of the radius of curvature of the output coupler with R_{oc} = 25, 50 and 75 mm and found that the effect was weak in terms of output power for a given pump spot size. We also estimated the beam quality parameter using the knife edge method [87] with R_{oc}=50 mm and calculated M^2 = 3.

4.3.3 In-band pumping of Ho:KREW by diode-pumped Tm:KLuW laser

For comparisons to be valid, experiments must be done under identical conditions. Hence, we decided to compare 3at.% Ho:KREW, RE=(Y, Gd, Lu) crystals under in-band pumping using diode-pumped Tm:KLuW laser to check which is a better host for Ho. Instead of using a homemade isolator in the experimental setup, we used a commercial isolator to avoid back coupling and made the pump polarization vertical using a half-wave plate. A detailed description of the experimental setup and results can be found in paper IX. The sample was N_g cut and oriented for light propagation along the N_g principal optical direction and for polarization parallel to the N_m principal optical direction. It was 3 mm thick, had an aperture of 3x3 mm^2 and was antireflection-coated for pump and laser wavelengths.

Continuous-wave laser operation was realized for all output couplers and for all three hosts. The physical cavity length in all cases was 50±1 mm. We measured the output power as a function of the incident power for all the output couplers. Figure 4.5 shows the input vs output characteristics of the Ho:KREW (Y, Gd, Lu) laser (left) and the corresponding laser spectra (right).

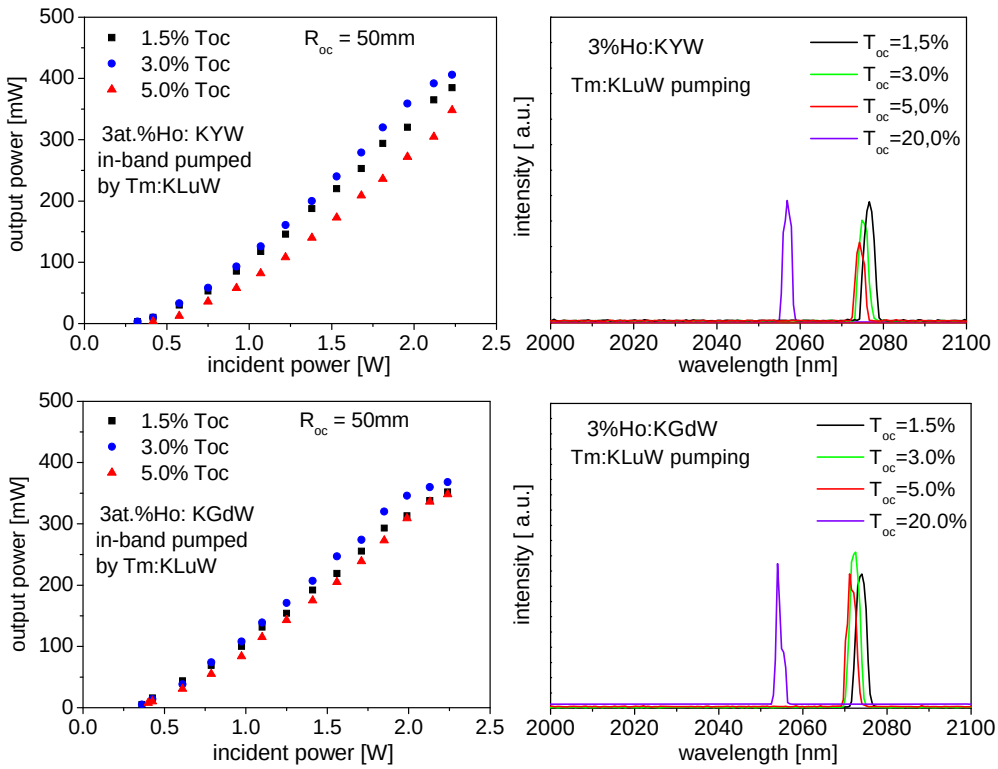

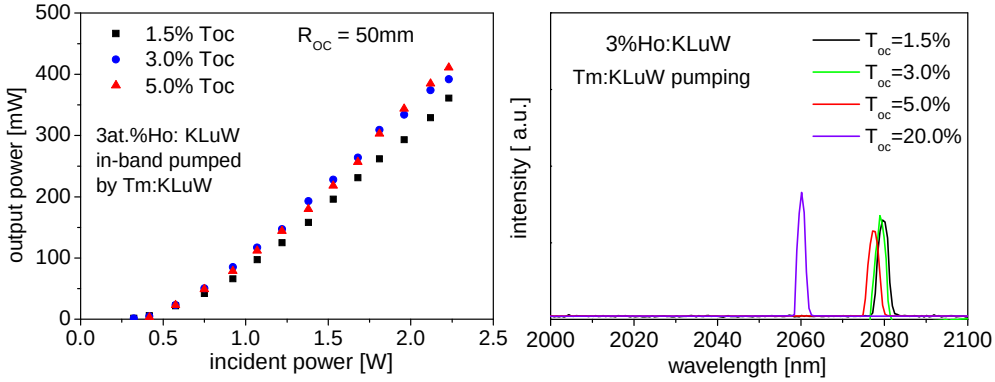

Figure 4.5 Output power versus incident pump power of the 3at.% Ho:KREW laser for several T_{ocs} with R_{OC} = 50 mm using Tm:KLuW laser as pump source (left) and corresponding laser spectra for several T_{ocs} (right)

The figures show that T_{oc} = 3% gives slightly better output than other T_{ocs} for Ho:KYW and Ho:KGdW, but in the case of Ho:KLuW T_{oc} = 3% and 5% perform equally and the laser threshold increases as the output coupler transmission increases. Here too the laser wavelength shortens at higher output coupler transmissions (when the losses in the cavity are greater). Table 4.4 summarizes the output power and observed wavelength with different T_{ocs}.

Table. 4.4 Summary of output power and observed wavelength for 3at.%Ho:KREW with different output couplers using Tm:KLuW laser as pump source

Sample (3at.%)	T_{OC} %	Output power [mW]	Laser wavelength [nm]
Ho:KYW	1.5	385	2076.5
	3.0	406	2075
	5.0	348	2074
	20.0	-	2057
Ho:KGdW	1.5	352	2073.5
	3.0	368	2072
	5.0	348	2071
	20.0	-	2054
Ho:KLuW	1.5	361	2080
	3.0	392	2079
	5.0	411	2077
	20.0	-	2060

In order to estimate the slope efficiency with respect to the absorbed power, we measured the absorption in the crystal in non-lasing conditions. We found 22.9% for Ho.KYW, 23.2% for Ho:KGdW and 21.5% for Ho:KLuW. In this case the non-absorbed power is retro-reflected back to the crystal and double pass pumping occurs so we decided to calculate slopes

for double pass absorption. Since in all cases T_{oc} = 3% gives higher output, the slopes with double pass configuration were estimated only with this value. Figure 4.6 shows the input-output characteristics of Ho:KREW with respect to absorbed power.

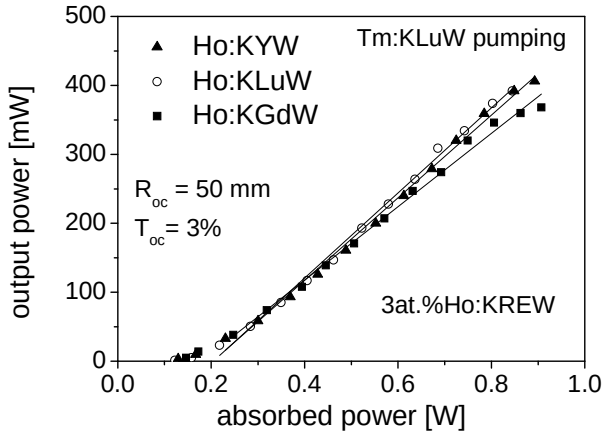

Figure 4.6 Input-output characteristics of 3at.%Ho:KREW using Tm:KLuW laser as pump source

The figure shows that all the hosts perform almost equally and table 4.5 shows that performance was best with Ho:KLuW although the difference from other hosts is not substantial. Output power was maximum (392 mW) for Ho:KLuW with a slope efficiency of 61.6% centered at 2079 nm, followed by Ho:KYW with a slope efficiency of 59.9% centered at 2075 nm, and finally Ho:KGdW with a slope efficiency of 53.2% centered at 2072 nm.

Table 4.5 Summary of estimated slopes for 3%Ho:KREW with Tm:KLuW pumping

Sample (3at.%)	Maximum output power [mW]	Slope efficiency [%]	Threshold [mW]	Laser wavelength [nm]
Ho:KYW	406	59.9	129	2075
Ho:KGdW	368	53.2	146	2072
Ho:KLuW	392	61.6	122	2079

With the same experimental configuration, antireflection coated 5at.%Ho:KLuW crystal was used in the laser experiment and continuous-wave laser action was achieved for all the output couplers used. It could not be achieved using an uncoated sample. We also measured the output power as a function of the incident power for all the output couplers used . Figure 4.7 shows the input vs output characteristics of 5at.% Ho: KLuW (left) and the corresponding laser spectra (right) respectively.

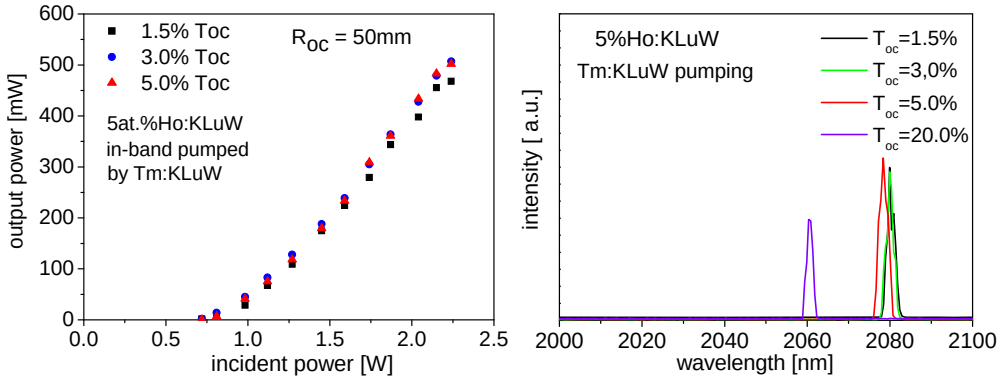

Figure 4.7 Output power versus incident pump power of the 5at.% Ho: KLuW laser for several T_{ocs} with R_{OC} = 50 mm using Tm: KLuW laser as pump source (left) and corresponding laser spectra for several T_{ocs} (right)

The figure shows that T_{oc} =3% and 5% perform to the same than T_{oc} =1.5%. Here too the laser wavelength shortens at higher output coupler transmissions (when the losses in the cavity are greater).

As before, in order to estimate the slope efficiency, we measured the absorption in the crystal in non-lasing conditions. It was found to be 34.2% and this is the value we used to calculate the slope efficiency under double pass configuration. Here also T_{oc} = 3% is used to estimate the slope, so that comparisons could be made with 3at.%Ho:KLuW. Figure 4.8 shows the input-output characteristics of the 5at.%Ho:KLuW laser with respect to absorbed power.

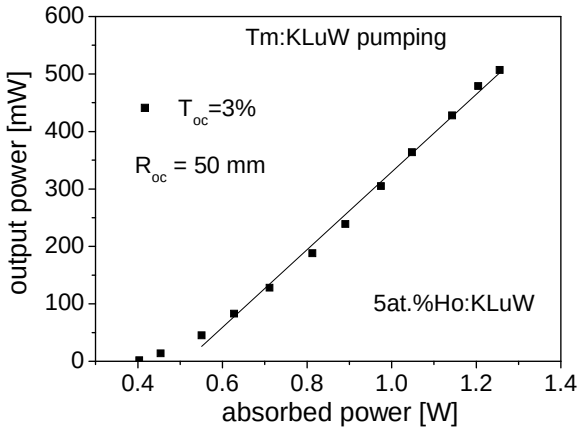

Figure 4.8 Input-output characteristics of 5at.%Ho:KLuW using Tm:KLuW laser as pump source

The figure shows that output is maximum (507 mW) with an absorbed power of 1255 mW and a corresponding slope efficiency of 67.6 % centred at 2080 nm. In comparison with 3at.%Ho:KLuW, this sample gives higher output and higher efficiency (see table 4.5) but the

laser threshold is 403 mW with respect to absorbed power. Table 4.6 shows the summary of the laser results.

Table 4.6 Summary of laser results for 5%Ho:KLuW with Tm:KLuW pumping

Sample	T_{OC} %	Output power [mW]	Slope efficiency [%]	Threshold [mW]	Laser wavelength [nm]
5 at.% Ho:KLuW	1.5	468	-	-	2080
	3.0	507	67.6	403	2080
	5.0	502	-	-	2077
	20.0	-	-	-	2060

4.3.4 In-band pumping of Ho:KREW by fibre-coupled diode laser

In this case, a comparison is made with 3at.% Ho:KREW, RE=(Y, Gd, Lu) crystals under in-band pumping using diode laser. The laser experiment was carried out using the setup described in chapter 2. Detailed information can also be found in paper IX. Continuous-wave laser operation was realized for all output couplers and for all three hosts. The physical cavity length in all cases was 50 mm. We measured the output power as a function of the incident power for all the output couplers. Figure 4.9 shows the input vs output characteristics of the Ho:KREW, RE = (Y, Gd, Lu) laser (left) and the corresponding laser spectra (right).

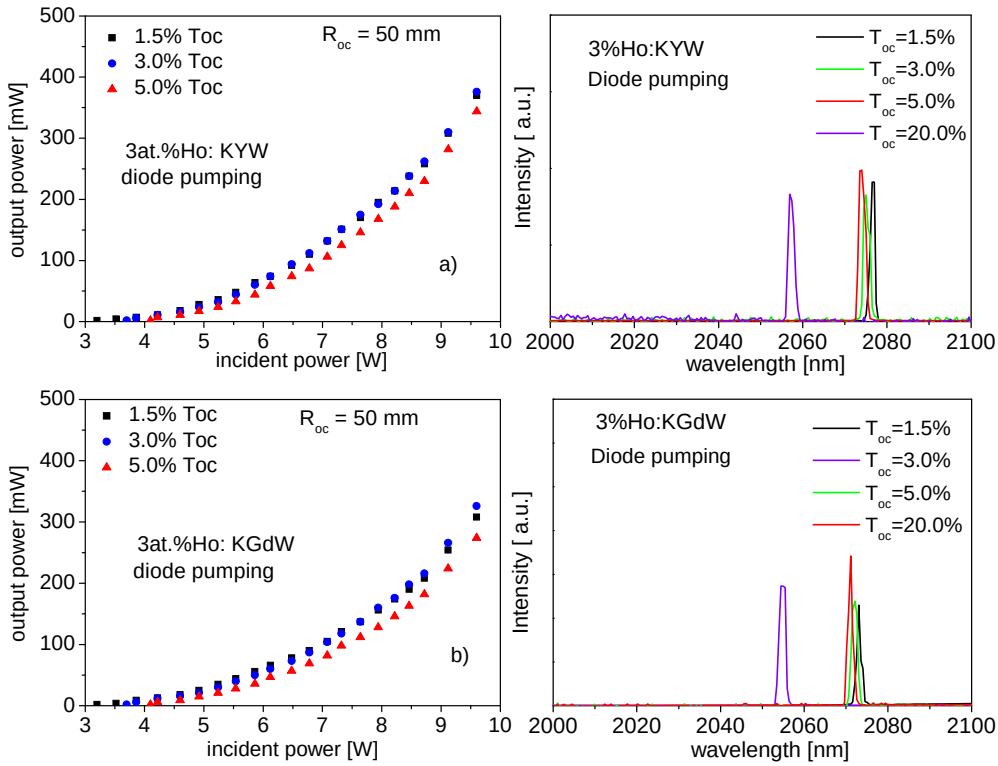

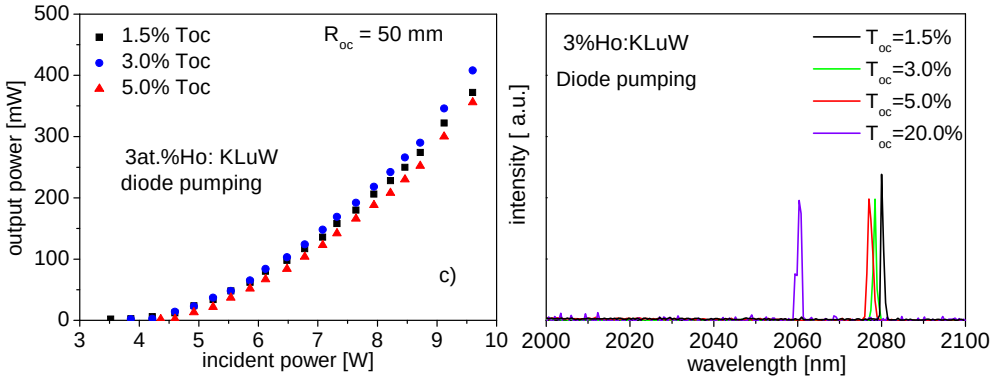

Figure 4.9 Output power versus incident pump power of the 3at.% Ho: KREW laser for several T_{ocs} with R_{OC} = 50 mm using diode laser as pump source (left) and corresponding laser spectra for several T_{ocs} (right)

The figures show that T_{oc} = 3% gives slightly better output than other T_{ocs} for all the hosts and the laser threshold increases at higher output coupler transmissions. The non linear behaviour of the curves is due to the fact that the wavelength at which the laser diode emits depends on the current level and the absorption is different at different wavelengths. Table 4.7 summarizes output power and observed wavelengths with different T_{ocs}.

Table. 4.7 Summary of output power and observed wavelength for 3at.%Ho:KREW with different output couplers using diode laser as pump source

Sample (3at.%)	T_{OC} %	Output power [mW]	Laser wavelength [nm]
Ho:KYW	1.5	426	2076
	3.0	438	2075
	5.0	404	2074
	20.0	-	2057
Ho:KGdW	1.5	366	2073
	3.0	390	2072
	5.0	326	2071
	20.0	-	2054.5
Ho:KLuW	1.5	372	2080
	3.0	408	2078.5
	5.0	356	2077
	20.0	220	2060

In order to estimate the slope efficiency with respect to the absorbed power, we measured the absorption in the crystal in non-lasing conditions to be 14.8% for Ho.KYW, 14.9% for Ho:KGdW and 15.7% for Ho:KLuW. In this case the non absorbed power is not retro-reflected back to the crystal (see above). Here too since T_{oc} = 3% gives higher output for all hosts, the slopes with single pass configuration were estimated only with this value. Figure 4.10 shows the input-output characteristics of Ho: KREW with respect to absorbed power.

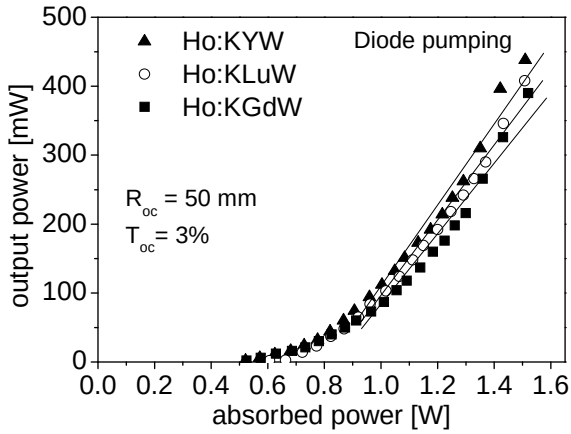

Figure 4.10 Input-output characteristics for 3at.%Ho:KREW using diode laser as pump source

The figure shows that all the hosts perform almost equally and as can be seen from table 4.8, performance was best with Ho:KYW, although the difference between other hosts is not substantial. Output power was maximum (438 mW) for Ho:KYW with a slope efficiency of 58.8% centered at 2075 nm, followed by Ho:KLuW with a slope efficiency of 54.5% centered at 2079 nm, and finally Ho:KGdW, with a slope efficiency of 51.2 % centered at 2072 nm.

Table 4.8 Summary of estimated slopes for 3%Ho:KREW with diode laser pumping

Sample (3at.%)	Maximum output power [mW]	Slope efficiency [%]	Threshold [mW]	Laser wavelength [nm]
Ho:KYW	438	58.8	129	2075
Ho:KGdW	390	51.2	146	2072
Ho:KLuW	408	54.5	122	2079

UNIVERSITAT ROVIRA I VIRGILI
INFRARED LASERS BASED ON HO3+:KRE(WO4)2 CRYSTALS WITH TM3+OR YB3+ AS SENSITIZERS
Venkatesan Jambunathan
ISBN:/DL: T.1243-2011

Conclusions

This section gives a summary of the conclusions based on the results obtained in this study.

Conclusions

In accordance with the general and specific objectives of the present study, the most significant results are: 1) the monoclinic phase of single doped Ho: KREW (RE=Y, Lu, Gd), and co-doped (Ho,Tm):KLuW and (Ho,Yb):KLuW was obtained at several doping concentrations; 2) these crystals were structurally, compositionally and spectroscopically characterized so that the material properties prior to laser experiments could be understood. Finally, the study of laser generation from Ho using in-band pumping and the sensitizer ion Tm showed that these materials are suitable candidates for the development of compact solid state infrared laser around ~2.1 μm for intermediate power levels.

Crack- and macro-defect-free single-doped Ho:KREW (RE=Y, Lu, Gd), co-doped (Ho,Tm):KLuW and (Ho,Yb):KLuW crystals were grown using the Top Seeded Solution Growth – Slow Cooling (TSSG-SC) method.

The variation of the unit cell parameters as a function of dopant concentration and temperature was investigated to determine how doping and temperature distort structure. The doping study shows that there is no significant change in the structure and the temperature study determines the linear thermal expansion coefficient of each host.

The compositional characterisation allowed us to know the exact concentration, the distribution coefficient and the stoichiometry of each crystal.

The spectroscopic characterisation of the active ion was carried out in terms of room temperature optical absorption to determine the energy levels and identify the exact excitation and laser wavelength region of interest. The low temperature (6K) made it possible to determine the energy positions of the Stark levels at each energy level. This study was carried out for all the single-doped, co-doped and triply doped systems. A photoluminescence study was also made of the active ions: the optical emission and life time of the laser wavelength region were measured around 2 μm for the single-doped and co-doped systems. Laser parameters such as emission cross-section and gain cross-section around the 2 μm region were determined and showed that these materials have great potential for generating this emission.

Finally, laser generation was achieved in the co-doped (Ho,Tm):KLuW crystals using a Ti:Sapphire laser as pump source. The optimum doping ratio for (Ho,Tm):KLuW was found to be (0.5at.%Ho5at.%Tm):KLuW. In addition, simultaneous laser generation at two different wavelengths was achieved with this crystal and the output power reaching the same for both wavelengths. For the single-doped Ho:KREW, laser oscillation was achieved with both the pump sources and for all three hosts. No significant difference in output and efficiency was

observed between these three hosts. Experimental work on laser generation around 2 μm is currently under way for the (Ho,Yb):KLuW crystals.

Future work needs to focus on the power scaling of such laser crystals using diode lasers as pump sources with optimized doping levels, thickness and pump wavelength. In addition new active medium architectures will be studied such as slab shaped and thin disk designed samples for power scaling. Laser pulse generation will be studied both in Q-switch (passive and active) regime to reach high energy pulses (mJ or μJ) and in mode-locked regime to achieve ultra-short laser pulses (picoseconds or femtoseconds).

UNIVERSITAT ROVIRA I VIRGILI
INFRARED LASERS BASED ON HO3+:KRE(WO4)2 CRYSTALS WITH TM3+OR YB3+ AS SENSITIZERS
Venkatesan Jambunathan
ISBN:/DL: T.1243-2011

References

1. M. Kohei, I. Toshilkazu, I. Shoken, S. Masahiko, A. Tetsuo, A. Kazuhiro and S. Atsushi, "Wind profile measurements by coherent Doppler lidar", J. National institute of information and communications technology **15**, 167–176 (2004).
2. K. Scholle, S. Lamrini, P. Koopmann and P. Fuhrberg, "2 μm laser sources and their possible applications", Frontiers in Guided Wave Optics and Optoelectronics, ISBN 978-953-7619-82-4, pp. 674, February 2010.
3. L.F. Johnson, J.E. Geusic and L.G. V. Uitert, " Cohernet oscillations from Tm^{3+}, Ho^{3+}, Yb^{3+} and Er^{3+} ions in yttrium aluminum garnet", Appl. Phys. Lett., **7,** 127–129 (1965).
4. J. A. Caird, L. G. Deshazer, and J. Nella, " Characteristics of room temperature 2.3 μm laser emission from Tm^{3+} in YAG and $YAlO_3$", IEEE J. Quantum Electron. **11**, 874 – 881 **(**1975).
5. V. Sudesh, J. A. Piper, E. M. Goldys, R.S. Seymour, "Growth, characterization, and laser potential of Tm:$La_2Be_2O_5$ ", J. Opt. Soc. Am. B, **15**, 239 – 246 **(**1998).
6. X. Han, J. M. C. Torres, M. Rico, C. Cascales, C. Zaldo, X. Matoes, S. River, U. Griebner and V. Petrov, "Spectroscopy and efficient laser operation near 1.95 μm of Tm^{3+} in disordered $NaLu(WO_4)_2$", J. Appl. Phys., **103**, 083110-1 – 083110-8 (2008).
7. Z.G. Wang, C.W. Song, Y.F. Li, Y.L. Ju and Y.Z. Wang, "CW and pulsed operation of a diode-end-pumped Tm:$GdVO_4$ laser at room temperature", Laser phys. Lett., **6**, 105 – 108 (2009).
8. M. Schellhorn, S. Ngcobo, C. Bollig, "High-power diode-pumped Tm:YLF slab laser", Appl. Phys. B, **94**, 195 – 198 (2009).
9. X. Cheng, F. Chen, G. Zhao, J. Xu, "High- efficiency, high -power, diode-pumped continuous-wave Tm:$YAlO_3$ slab lasers", Appl. Phys. B, **97**, 639 – 643 (2009).
10. S. Vatnik, I. Vedin, M.C. Pujol, X. Mateos, J.J. Carvajal, M. Aguiló, F. Díaz, U. Griebner, and V. Petrov, "Thin disk Tm-laser based on highly doped Tm:$KLu(WO_{4)2}$/$KLu(WO_4)_2$ epitaxy", Laser Phys. Lett., **7**, 435–439 (2010).
11. L.F. Johnson, J.E. Geusic and L.G. V. Uitert, "Efficient, high power coherent emission from Ho^{3+} ions in yttrium aluminum garnet, assisted by energy transfer", Appl. Phys. Lett., **8,** 200–202 (1966).
12. R. L. Remski, D. J. Smith, "Temperature dependence of pulsed laser threshold in YAG: Er^{3+}, Tm^{3+}, Ho^{3+} ", IEEE J. Quantum Electron. **6**, 750-751 **(**1970).
13. E. W. Duczunski, G. Huber, V.G. Ostroumov and I.A. Shcherbakov, "CW double cross pumping of the $^5I_7 - {}^5I_8$ laser transition in Ho^{3+}-doped garnets", Appl. Phys. Lett., **48,** 1562–1563 (1986).
14. T. Y. Fan, G.Huber, R L. BYER and P. Mitzscjerlich, "Continuous-wave operation of 2.1 μm of a diode-laser-pumped, Tm-sensitized Ho:$Y_3A_{l5}O_{12}$ laser at 300K ", Optics Lett., **12**, 678 – 679 (1987).
15. N. P. Barnes, W. J. Rodriguez and B. M. Walsh, "Ho:Tm:YLF laser amplifies", J. Opt. Soc. Am. B, **13**, 2872 – 2882 (1996).
16. F. Cornacchia, A. Di Lieto, P. Maroni, P. Minguzzi, A. Toncelli, M. Tonelli, E. Sorokin and I. Sorokina , "A cw room-temperture Ho,Tm:YLF laser pumped at 1.682 μm ", Appl. Phys. B, **73**, 191 – 194 (2001).
17. B. Baronti, F. Cornacchia, A. Di Lieto, P. Maroni, A. Toncelli and M. Tonelli, "Room temperature 2 μm Tm,Ho:YLF laser ", Optics and Lasers in Engineering, **39**, 277 – 282 (2003).

18. B.M. Walsh, N. P. Barnes, M. Petros, J. YU and U. N. Singh, "Spectroscopy and modeling of solid state lanthanide lasers: Application to trivalent Tm^{3+} and Ho^{3+} in $YLiF_4$ and $LuLiF_4$", J. Appl. Phys., **95**, 3255 –3271 (2004).

19. O. A. Louchev, Y. Urata, M. Yumoto, N. Saito and S. Wada, "Numerical simulation of high-power operation of 2 μm Co-doped Tm, Ho Solid-State Lasers", Advances in Solid-State Lasers: Development and Applications, Book edited by: Mikhail Grishin, ISBN 978-953-7619-80-0, pp. 630, February 2010.

20. L.J. Li, B. Q. Yao, C. W. Song, X. M. Duan, and T. H. Wang ," High efficiency 2.05-μm cw and AO Q-switched operation of diode end-pumped Tm, Ho:$GdVO_4$ laser", Laser Physics **18**,1512 – 1516 (2008).

21. A.A. Lagatsky , F. Fusari, S.V. Kurilchik , V.E. Kisel, A.S. Yasukevich , N.V. Kuleshov, A.A. Pavlyuk, C.T.A. Brown and W. Sibbett, "Optical spectroscopy and efficient continuous-wave operation near 2 μm for a Tm,Ho:KYW laser crystal", Appl. Phys. B **97**, 321 – 326 (2009).

22. X. Han, F. Fusari, M. D. Serrano, A. A. Lagatsky, J. M. C. Torres, C. T. A. Brown, C. Zaldo, and W. Sibbett, "Continuous-wave laser operation of Tm and Ho co-doped $NaY(WO_4)_2$ and $NaLu(WO_4)_2$ crystals", Opt. Express **18**, 5413 – 5149 (2009).

23. Th. Rothacher, W. Lüthy and H.P. Weber, "Diode pumping and laser properties of Yb:Ho:YAG", Optics Communications **155**, 68 – 72 (1998).

24. P.A. Budni, C. R. Ibach, S. D. Setzler, E. J. Gustafson, R. T. Castro, and E. P. Chicklis, "50-mJ, Q-switched, 2.09-μm holmium laser resonantly pumped by a diode-pumped 1.9-μm thulium laser", Opt. Lett., **28**,1016 – 1018 (2003).

25. B. Q. Yao, L. L. Zheng, R. L. Zhou, X. M. Duan, Y. J. Zhang, Y. L. Ju, Y. Z. Wang, G. J. Zhao and Q. Dong, "Holmium Laser In-Band Pumped by a Thulium Laser in the Same Host of $YAlO_3$", Laser Physics **18**,1501– 1504 (2008).

26. X.M. Duan, B.Q. Yao, C.W. Song, J. Gao, and Y.Z. Wang, "Room temperature efficient continuous wave and Q-switched Ho:YAG laser double-pass pumped by a diode-pumped Tm:YLF laser", Laser Phys. Lett. **5**, 800 – 803 (2008).

27. D.Y. Shen, A. Andolvand, L. J. Cooper, W.A. Clarkson, "Efficient Ho:YAG laser pumped by a cladding pumped tunable Tm:Silica-fibre laser", Appl. Phys. B **79**, 559 – 561 (2004).

28. B. Q. Yao, X. T. Yang, X. M. Duan, T. H. Wang, Y. L. Ju, and Y.Z. Wang, "Continuous-wave operation of a Ho:YAlO3 laser pumped by a Tm-doped silicon fiber laser", Laser Phys. Lett. **6**, 509 – 512 (2009).

29. J. Kwiatkowski, J.K. Jabczynski, L. Gorajek, W. Zendzian, H. Jelíınková, J. Sulc, M. Nemec, 2 and P. Koranda ," Resonantly pumped tunable Ho:YAG laser", Laser Phys. Lett. **6**, 531 – 534 (2009).

30. C. Bollig, R. A. Hayward, W. A. Clarkson, and D. C. Hanna," 2-W Ho:YAG laser intracavity pumped by a diode-pumped Tm:YAG laser", Opt. Lett., **23**,1757– 1759 (1998).

31. M. Schellhorn, A. Hirth, and C. Kieleck Ho:YAG laser intracavity pumped by a diode-pumped Tm:YLF laser Opt. Lett., **28**, 1933 – 1935 (2003).

32. S. So, J. I. Mackenzie, D. P. Shepherd, and W. A. Clarkson, J. G. Betterton, E. K. Gorton, and J. A. C. Terry ,"Intra-cavity side-pumped Ho:YAG laser",, Opt. Express **14**, 10481 – 10487 (2006).

33. C. D. Nabors, J. Ochoa, T. Y. Fan, A. Sanchez, H. K. Choi, and G. W. Turner, "Ho:YAG laser pumped by 1.9-μm diode lasers," IEEE J. Quantum Electron. **31**, 1603 – 1605 (1995).

34. K. Scholle, and P. Fuhrberg," In-band pumping of high-power Ho:YAG lasers by laser diodes at 1.9 μm," in Conference on Lasers and Electro-Optics/Quantum Electronics and Laser Science Conference, OSA Technical Digest (CD) (Optical Society of America, 2008), paper CTuAA1.

35. E. C. Honea, R. J. Beach, S. B. Sutton, J. A. Speth, S. C. Mitchell, J. A. Skidmore, M. A. Emanuel and S. A. Payne, "115-W Tm:YAG Diode-Pumped Solid-State Laser," IEEE J. Quantum Electron. **33**, 1592 –1600 (1997).

36. M. Schellhorn, "High-power diode-pumped Tm:YLF laser," Appl. Phys. B **91**, 71–74 (2008).

37. P. Koopmann, S. Lamrini, K. Scholle, P. Fuhrberg, K. Petermann, and G. Huber ," High Power Diode Pumped 2 μm Laser Operation of Tm:Lu_2O_3," in Conference on Lasers and Electro-Optics/Quantum Electronics and Laser Science Conference, OSA Technical Digest (CD) (Optical Society of America, 2010), paper CMDD1.

38. Z.G. Wang, C.W. Song, Y.F. Li, Y.L. Ju, and Y.Z. Wang, "CW and pulsed operation of a diode-end-pumped Tm:$GdVO_4$ laser at room temperature", Laser Phys. Lett. **6**, 105 –108 (2009).

39. B.Q. Yao, L.L. Zheng, X.M. Duan, Y.Z. Wang, G.J. Zhao, and Q. Dong ,"Diode-pumped room-temperature continuous wave Tm^{3+}doped Lu_2SiO_5 laser", Laser Phys. Lett. **5**, 714 – 718 (2008).

40. X. Mateos, V. Petrov, J. Liu, M.C. Pujol, U. Griebner, M.Aguiló, F. Díaz, M. Galan, and G. Viera, " Efficient 2- μm continuous-wave laser oscillation of Tm^{3+}:$KLu(WO_4)_2$", IEEE J. Quantum Electron. **42**, 1008 – 1015 (2006).

41. B.T. McGuckin and R.T. Menzies, "Efficient cw diode-pumped Tm,Ho:YLF laser with tunability near 2.067 μm ", IEEE J. Quantum Electron. **28**, 1025 – 1028 (1992).

42. W. J. He, B.Q. Yao, Y .L. Ju, and Y.Z. Wang," Diode-pumped efficient Tm,Ho:$GdVO_4$ laser with near-diffraction limited beam quality ", Opt. Express **14**, 11653 – 11659 (2006).

43. F. G. Yang, C. L. Sun, Z. Y. You, C. Y. Tu, G. Zhang, and H. Y. Zhu, "End pumped Tm, Ho:$NaY(WO_4)_2$ crystal laser at 2.07 μm", Laser Physics **20**, 1695 – 1697 (2010).

44. T. H. Maiman, "Stimulated optical radiation in Ruby", Nature **187**, 493 – 494 (1960).

45. M.J. Weber, "Handbook of optical materials", CRC press (2003).

46. P.V. Klevtsov and L.P. Koseeva, "Synthesis and X-ray and thermal studies of potassium rare-earth tungstates, $KLn(W0_4)_2$, Ln = Rare-earth element", Sov. Phys. Doklday **14**, 185 – 187 (1969) (transl. from Dokl. Akad. Nauk. SSSR, **185**, 571–574 (1969)).

47. P.V. Klevtsov, L.P. Kozeeva and L.Yu. Kharchenko," Study on the crystallization and polymorphism of double potassium and trivalent metal tungstates, $KR(WO_4)_2$ ", Sov. Phys. Crystallogr., **20**, 732 – 735 (1976) (transl. from Kristallografiya **20**, 1210 – 1215 (1975)) .

48. M.C. Pujol, R. Solé , J. Massons, Jna. Gavaldà, X. Solans, C. Zaldo, F. Diaz and M. Aguiló, "Structural study of monoclinic $KGd(WO_4)_2$ and effects of lanthanide substitution", J. Appl. Cryst., **34**, 1 – 6 (2004).

49. M.C. Pujol, X. Mateos, A. Aznar, X. Solans, S. Suriñac, J. Massons, F. Díaz, and M. Aguiló, "Structural redetermination, thermal expansion and refractive indices of $KLu(WO_4)_2$", J. Appl. Cryst., **39**, 230 – 236 (2006).

50. S.V. Borisov and R.F. Kletsova, "Crystal structure of $KY(WO_4)_2$", Sov. Phys. Crystallogr. **13**, 420 – 421 (1968). (transl. from Kristallografiya **13**, 517 -519 (1968)) .

51. P. Hartman and W. G. Pedrok, "On the relations between structure and morphology of crystals. I ", Acta Cryst., **8**, 49 – 52 (1955).

52. X. Mateos, R. Solé, Jna. Gavalda, M. Aguiló, J. Massons, F. Díaz,v"Crystal growth, optical and spectroscopic characterisation of monoclinic $KY(WO_4)_2$ co-doped with Er^{3+} and Yb^{3+}", Optical Materials, **28**, 423 – 431 (2006).

53. M.C. Pujol, M. Rico, C. Zaldo, R. Solé , V.Nikolov , X. Solans, M. Aguiló, F. Díaz, "Crystalline structure and optical spectroscopy of Er^{3+}-doped $KGd(WO_4)_2$ single crystals", Appl. Phys. B **68**, 187 – 197 (1999).

54. R. Solé, V. Nikolov, X. Ruiz, Jna. Gavaldà, X. Solans, M. Aguiló and F. Diaz "Growth of β-$KGd_{1-x}Nd_x(WO_4)_2$ single crystals in $K_2W_2O_7$ solvents", J. Cryst. Growth **169**, 600 – 603 (1996).

55. V. Petrov, M. C. Pujol , X. Mateos, Ó. Silvestre, S. Rivier, M. Aguiló, R. M. Solé, J. Liu, U. Griebner and F. Díaz, "Growth and properties of $KLu(WO_4)_2$, and novel ytterbium and thulium lasers based on this monoclinic crystalline host", Laser & Photon. Rev. **1**, 179 – 212 (2007).

56. M.C. Pujol, X. Mateos, R. Solé, J. Massons, Jna. Gavalda, F. Díaz and M. Aguiló, "Linear thermal expansion tensor in $KRE(WO_4)_2$ (RE = Gd, Y, Er and Yb) monoclinic crystals", Materials Science Forum **378-381**, 710 – 717 (2001).

57. Ó. Silvestre, J. Grau, M. C. Pujol, J. Massons, M. Aguiló, F. Díaz, M. T. Borowiec, A. Szewczyk, M. U. Gutowska, M. Massot, A. Salazar and V. Petrov "Thermal properties of monoclinic $KLu(WO_4)_2$ as a promising solid state laser host", Opt. Express **16**, 5022 – 5034 (2008).

58. S. Vatnik, M.C. Pujol, J.J. Carvajal, X. Mateos, M. Aguiló, F.Díaz and V. Petrov, "Thermo-optic coefficients of monoclinic $KLu(WO_4)_2$", Appl. Phys. B, **95**, 653 – 656 (2009).

59. M.T. Borowiec, T. Zayarnyuk, A. Pikul, M. Gotowska, M.C. Pujol, M. Aguiló, F. Díaz, A. Szewczyk, E.E. Zubov, V.P. Dyakonov, M. Baranski and H. Szymczak, "Specific heat of the monoclinic rare earth double tungstates", J. Low Temp. Phys., **160**, 119 – 130 (2010).

60. T.T. Basiev, A. A. Sobol, P. G. Zverev, L. I. Ivleva, V. V. Osiko, R. C. Powell " Raman spectroscopy of crystals for stimulated Raman scattering ", Opt. Materials, **11**, 307 - 314 (1999).

61. A. A. Kaminskii, K. Ueda, H. E. Eichler, J. Findeisen, S. N. Bagayev, F.A. Kuznetsov, Pavlyuk, G. Boulon and F. Bourgeois, "Monoclinic tungstates $KDy(Wo_4)_2$ and $KLu(Wo_4)_2$ – New $\chi(3)$– active crystals for laser Raman shifters", Jpn. J. Appl. Phys., **37**, L923 – L926 (1998).

62. R. D. Shannon, Acta Cryst. A, **32**, 751 – 767 (1976).

63. M.C. Pujol, M.A. Bursukova, F. Güell, X. Mateos, R. Solé, Jna. Gavaldà, M. Aguiló, J. Massons, F. Díaz, P. Klopp, U. Griebner, and V. Petrov, Growth, optical characterization, and laser operation of a stoichiometric crystal $KYb(WO_4)_2$, Phys. Rev. B **65**, 165121–1-165121–11 (2002).

64. J. Liu, V. Petrov, X. Mateos, H. Zhang, and J. Wang, "Efficient high-power laser operation of Yb : $KLu(WO_4)_2$ crystals cut along the principal optical axes," Opt. Letters **32**, 2016 – 2018 (2007).

65. G.H. Dieke, "Spectra and energy levels of rare earth ions in crystals", Interscience Publishers (1968).

66. A. Stingl, M. Lemzmer, Ch. Spielmann, F. Krausz and R. Szipöcs, "Sub-10-fs mirror-dispersion-controlled Ti: Sapphire laser", Opt. Letters, **20**, 602 – 604 (1995).

67. A. A. Kaminski, "Laser crystals and ceramics: recent advances", Laser & Photon. Rev. **1**, 93 – 177 (2007).

68. D.J.Dixon, L.F. Johnson, "Low-threshold 2-μm holmium laser excited by non radiative energy transfer from Fe^{3+} in YGG", Opt. Letters, **17**, 1782 – 1784 (1992).

69. S. R. Bowman, M. J. Winings, R. C. Y. Auyeung, J. E. Tucker, S .K. Searles, and B. J. Feldman, " Laser and spectral properties of Cr, Tm, Ho:YAG at 2.1 μm", IEEE J. Quantum Electron., **27**, 2142 – 2149 (1991).

70. H. Lotem, Y. Kalisky, J. Kagan and D. Sagie, " A 2 μm Holmium laser", IEEE J. Quantum Electron., **24**, 1193 – 1200 (1991).

71. D. Howse , M. Logie, A. G. Bluiett, S. O´Connor, N. J. Condon, J. Ganem and S.R. Bowman, " Optically-pumped mid-IR phosphor using Tm^{3+} - sensitized Pr^{3+}-doped KPb_2Cl_5," J. Opt. Soc. Am. B , **27**, 2384 –2392 (2010).

72. H. Gong , D.Yang, X. Zhao, E.Y. B. Punb, H. Lin, "Upconversion color tunability and white light generation in $Tm^{3+}/Ho^{3+}/Yb^{3+}$ doped aluminum germanate glasses," Opt. Materials, **32**, 554 – 559 (2010).

73. D. Hiyan, L. Yujing, X. Zhiguo, S. Jiayue, "Upconversion luminescence of $Yb^{3+}/Ho^{3+}/Er^{3+}/Tm^{3+}$ co-doped $KGd(WO_4)_2$ powders," J. Rare Earths , **28**, 697 – 700 (2010).

74. A. A. Kaminskii, A. G. Petrosyan, V. A. Fedorov, S. E. Sarkisov, V. V. Ryabchenkov, A. A. Pavlyuk, V. V. Lyubchenko, and I. V. Mochalov, "Two-micron stimulated emission by crystals with Ho^{3+} ions, based on the transition $^5I_7 \rightarrow {}^5I_8$," Sov. Phys. Dokl., **26**, 846 – 848 (1981) [Transl. from Dokl. Akad. Nauk SSSR, **260**, 64 – 67 (1981)].

75. A. A. Kaminskii, A. A. Pavlyuk, P. V. Klevtsov, I. F. Balashov, V. A. Berenberg, S. E. Sarkisov, V. A. Fedorov, M. V. Petrov, and V. V. Lyubchenko, "Stimulated radiation of monoclinic crystals of $KY(WO_4)_2$ and $KGd(WO_4)_2$ with Ln^{3+} ions," Inorg. Mater., **13**, 482 – 483 (1977) [transl. from Izv. Akad. Nauk. SSSR, Neorg. Mater., **13**, 582 – 583 (1977)].

76. J. J. Carvajal, M. C. Pujol, F. Diaz, "High-temperature solution growth: Application of laser and nonlinear optical crystals", Hand book of crystal growth, Springer, 725 – 759 (2010).

77. J. Rodriguez-Carvajal, "An introduction to the program", Full prof 2000 (Laboratorie Léon Brillouin, CEA-CNRS, Saclay), France (2001).

78. L. B. McCusker, R. B. Von Dreele, D. E. Cox, D. Louër and P. Scardi, "Rietveld refinement guidelines ", J. Appl. Cryst., **32,** 36 – 50 (1999).

79. R. Solé, O. Silvestre, J. Massons, Jna. Gavaldà, M. Aguiló, F. Díaz, "Physical properties of the 0.12 $KLu(WO_4)_2$ – 0.88 $K_2W_2O_7$ solution and single-crystal growth of $KLu(WO_4)_2$", J. Cryst. Growth, **310**, 1167 – 1173 (2008).

80. A. Majchrowski, M.T. Borowiec, E. Michalski, "Top seeded solution growth of $KHo(WO_4)_2$ single crystals ", J. Cryst. Growth, **264**, 201 – 207 (2004).

81. C. Görller-Walrand and K. Binnemans, "Rationalization of crystal – field parameterization," Hand book on the physics and chemistry of rare earths, Elsevier, 121- 283 (1996).

82. M. C. Pujol, C. Cascales, M. Rico, J. Massons, F. Diaz, P. Porcher, and C. Zaldo, "Measurement and crystal field analysis of energy levels of Ho^{3+} and Er^{3+} in $KGd(WO_4)_2$ single crystal," J. Alloys and Comp. **323-324**, 321 – 325 (2001).

83. M. C. Pujol, J. Massons, M. Aguilo, F. Diaz, M. Rico, and C. Zaldo, "Emission cross sections and spectroscopy of Ho^{3+} laser channels in $KGd(WO_4)_2$ single crystal," IEEE J. Quantum Electron. **38**, 93 –100 (2002).

84. O. Silvestre, M. C. Pujol, M. Rico, F. Güell, M. Aguiló, F. Díaz, "Thulium doped monoclinic, $KLu(WO_4)_2$ single crystals: growth and spectroscopy ", Appl. Phys. B, **87**, 707 – 716 (2007).

85. D. R. Gamelin and H . U. Güdel, "Upconversion process in transition metal and rare earth metal systems", Topics in current chemistry, **214**, 1- 56 (2001).

86. Stephen A. Payne, L.L. Chase, Larry K. Smith, Wayne L. Kway and William F. Kruple, "Infrared cross-section measurement for crystals doped with Er^{3+}, Tm^{3+}, Ho^{3+} ", IEEE J. Quantum Electron. **28**, 2619 – 2630 (1992).

87. T. F. Johnston Jr, "Beam propagation (M^2) measurement made easy as it gets : the four – cuts method ", Applied Opt. **37**, 4840- 4850 (1998).

UNIVERSITAT ROVIRA I VIRGILI
INFRARED LASERS BASED ON HO3+:KRE(WO4)2 CRYSTALS WITH TM3+OR YB3+ AS SENSITIZERS
Venkatesan Jambunathan
ISBN:/DL: T.1243-2011

Paper I

Near-infrared photoluminescence from Ho^{3+}–doped monoclinic $KLu(WO_4)_2$ crystal codoped with Tm^{3+}

V. Jambunathan, X. Mateos, M. C. Pujol, J. J. Carvajal, J. Massons, M. Aguiló and F. Díaz

Journal of Luminescence **129** (12), 1882-1885 (2009).

UNIVERSITAT ROVIRA I VIRGILI
INFRARED LASERS BASED ON HO3+:KRE(WO4)2 CRYSTALS WITH TM3+OR YB3+ AS SENSITIZERS
Venkatesan Jambunathan
ISBN:/DL: T.1243-2011

Journal of Luminescence 129 (2009) 1882–1885

Contents lists available at ScienceDirect

Journal of Luminescence

journal homepage: www.elsevier.com/locate/jlumin

Near-infrared photoluminescence from Ho^{3+}-doped monoclinic $KLu(WO_4)_2$ crystal codoped with Tm^{3+}

V. Jambunathan, X. Mateos *, M.C. Pujol, J.J. Carvajal, J. Massons, M. Aguiló, F. Díaz

Física i Cristal·lografia de Materials i Nanomaterials (FiCMA-FiCNA), Universitat Rovira i Virgili (URV), Campus Sescelades c/Marcel·lí Domingo, s/n, E-43007 Tarragona, Spain

ARTICLE INFO

Available online 10 May 2009

Keywords:
Photoluminescence
Ho^{3+}
Double tungstate crystals

ABSTRACT

The near-infrared 2.1 μm emission from Ho^{3+} in the monoclinic $KLu(WO_4)_2$ crystal codoped with Tm^{3+} has been studied. We grew the crystal by the Top-Seeded Solution Growth Slow-Cooling (TSSG-SC) method and characterize it in terms of optical absorption and luminescence. To quantify the emission cross-section we used the reciprocity method and calculated the gain cross-section to determine the possibility of further amplification and laser generation.

1. Introduction

A 2-μm laser has many applications in the areas of remote sensing [1] and medicine [2]. Especially interesting is the 2.1 μm emission from holmium (Ho) ions in medicine because of the relative maximum of absorption of water around this wavelength, so that it can be used in many different tissues of the human body. Ho:YAG lasers are commercially available and have many real applications in urology [3] and orthopaedics [4]. However, the main disadvantage of the Ho:YAG laser is that it needs to be pumped with flashlamps, reducing the whole efficiency.

Many studies focused on this emission from Ho-doped materials, both single-doped and codoped with thulium (Tm). The advantage of using single-doped Ho lasers with direct pumping of the $^5I_7$ level is that there is no dependence on energy transfer from other ions, which lends itself to various radiative and non-radiative losses. However, the technology of pump sources around 1.9 μm is not very mature, which is why some authors used the radiation coming from a Tm laser to pump a Ho crystal [5]. Parallel to this, many researchers have demonstrated laser operation in Ho–Tm-codoped crystals [6] making use of the fact that Tm ions transfer part of their energy to Ho ions, allowing for the generation of the 2.1 μm emission from Ho. This is especially interesting because Tm ions absorb very efficiently around 808 nm, which is the emitting wavelength of the commercially available AlGaAs laser diodes with very mature technology developed for the widely used Nd:YAG laser. Such diodes show very good beam profile and the possibility of delivering hundreds of watts. This seems very promising to overcome the disadvantage typical for Ho:YAG lasers. By exciting Tm ions (donor) to the $^3F_4$ level, they transfer part of their energy to the $^5I_7$ level of Ho (acceptor). Consequently, it turns out that the 2.1 μm emission from Ho is possible by this mechanism of energy transfer. This spectroscopic process is very important in solid-state systems because it enhances the luminescence emission from the acceptor ion. Such a phenomenon has been observed in many crystals doped even with other ions, for example Er–Yb, Pr–Yb, Tm–Yb, etc [7].

Our goal was to study the 2.1 μm infrared emission from Ho in an optical system codoped with Tm. Particularly, the host where the two ions are embedded is the monoclinic potassium lutetium double tungstate ((Ho,Tm):$KLu(WO_4)_2$ hereafter (Ho,Tm):KLuW). This crystal belongs to a family with general formula $KRE(WO_4)_2$ with RE = yttrium and rare earth. The monoclinic KREW crystals induce many advantages to the doping ion, among these the absorption and emission cross-sections are very high, partly due to the strong anisotropy of these biaxial crystals, and the possibility to dope them with high concentration of the active ions without substantial fluorescence quenching due to the relatively long distance between the ions in the structure. KLuW crystals crystallize in the monoclinic system with space group C2/c and point group 2/m. The cell parameters are $a = 10.576\ (7)$ Å, $b = 10.214\ (7)$ Å, $c = 7.487\ (2)$ Å and $\beta = 130.68\ (4)^\circ$ [8]. Many properties of KLuW have been previously studied [9] showing its suitability as a great host for solid-state lasers.

In the present work we focus on the crystal growth of (Ho,Tm):KLuW at 0.5% doping level of Ho and 2.5% of Tm. We analyse the optical absorption features of the $^3H_4$ pump level of Tm and the photoluminescence of the $^5I_7 \rightarrow {}^5I_8$ transition of Ho around 2.1 μm after energy transfer.

2. Experimental

In this study we grew the codoped (Ho,Tm):KLuW crystal by the Top-Seeded Solution Growth Slow-Cooling (TSSG-SC) method.

* Corresponding author.
E-mail address: xavier.mateos@urv.cat (X. Mateos).

0022-2313/$ - see front matter © 2009 Elsevier B.V. All rights reserved.
doi:10.1016/j.jlumin.2009.04.081

We used a home-made vertical tubular furnace with kanthal wire as heating element. To control the temperature we used a controller/programmer (Eurotherm 903P) and thermocouples. The mechanical design allowed for rotation of the crystal during the growth process to improve the mass and heat transfer.

The raw materials were K_2CO_3 (Fluka, 99.0%), WO_3 (Fluka, 99.9%), Lu_2O_3 (Metall rare earth limited, 99.999%), Ho_2O_3 (Fluka, 99.9%) and Tm_2O_3 (Metall rare earth limited, 99.999%) with a binary composition of 12 mol% solute ((Ho,Tm):KLuW)/88 mol% solvent ($K_2W_2O_7$). The solid-state mixture was introduced in a platinum crucible, 50 mm in diameter and 50 mm in length, and heated above the saturation temperature.

The concentration of the doping elements in the grown crystal was determined by an Electron Probe Micro analyser (EPMA) with Cameca sx50 equipment.

Due to the high physical anisotropy of KLuW, its optical study is necessary to be carried out according to the principal optical directions N_p, N_m and N_g. We then cut the crystal using a goniometer and a struers Accutom-50 diamond saw. Additionally, once the crystals were cut, we polished them with very high optical quality in terms of transparency, density of scratches and parallelism. This was done with the use of a Logytech PM5 polisher with an oscillatory arm with very precise control of rotation and pressure to the samples. This parameter depends on the hardness of the crystal. The final shape of the crystal, ready to use, was parallelepiped with faces parallel to the principal optical axes.

The polarized optical absorption spectra were recorded at room temperature with a Cary Varian 500 spectrophotometer, with a Glam-Thomson polarizer in front of the sample.

For the photoluminescence experiments we used a tunable Ti:sapphire laser in continuous-wave mode as pump source with a maximum of output power around 800 nm where the $^3H_4$ level of Tm absorbs. The collected infrared luminescence was focused on the slit of a 34 cm Jobin–Ybon monochromator and dispersed using a grating with 300 groves/mm blazed at 2 μm. For detection, a non-cooled extended InGaAs photodiode was used for the infrared emission from Ho centred around 2.1 μm. The signal from the lock-in amplifier was sent to a computer for storage and processing.

3. Results and discussion

The growth of the (0.5 at.% Ho, 2.5 at.% Tm):KLuW single crystal was achieved with super saturation by slow cooling in a *b*-oriented seed of an undoped KLuW crystal located at the centre of the surface of the solution, which was the coldest point of the system. The above orientation of the seed has been demonstrated to be the optimum one to grow the inclusion-free double tungstate crystals while keeping the highest growth rate [10]. The seed at the surface of the solution was constantly rotated at 40 rpm. The doping level was designed to have higher concentration of Tm, which is the sensitizer ion, than the Ho emitting ion to minimize the reabsorption of the 2.1 μm emission.

The cooling rate was 0.1 K/h for a cooling interval of 11.7 K. The crystal weighted 3.2 g and the growth rate was 273×10^{-4} g/h. The dimensions of the crystal were $11.06 \times 11.32 \times 8.92$ mm^3 along the *c*, a^* and *b* crystallographic directions, respectively.

Fig. 1 shows a photograph of the (0.5 at.% Ho, 2.5 at.% Tm):KLuW crystal without defects and good quality.

After growing the crystal, we prepared it as described in Section 2. We measured the real ion density in the crystal. These values are 5.534×10^{19} at/cm^3 for Ho and 2.057×10^{20} at/cm^3 for Tm. The distribution coefficient in the crystal was calculated

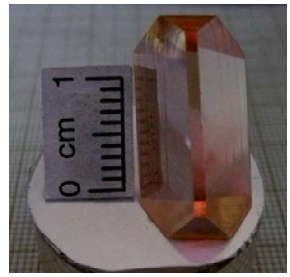

Fig. 1. Photography of the (0.5 at.% Ho, 2.5 at.% Tm):KLuW crystal grown and characterized in the present work.

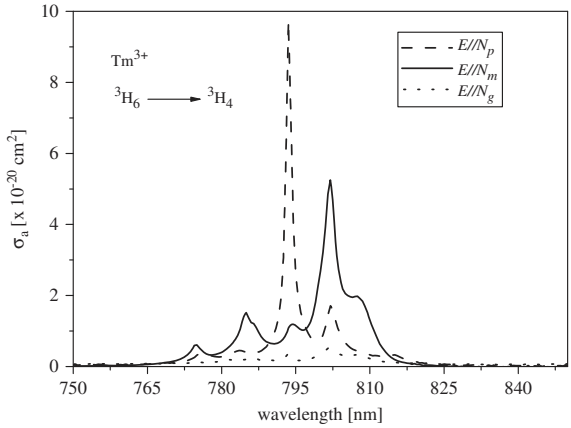

Fig. 2. Polarized optical absorption of the $^3H_4$ level of Tm in Ho,Tm:KLuW.

to be 1.7 for Ho and 1.26 for Tm. The stoichiometry of the crystal is then $KLu_{0.9600}Ho_{0.0085}Tm_{0.0315}(WO_4)_2$.

We measured the optical absorption of this crystal at room temperature in the 750–850 nm range to analyse the $^3H_4$ excited level of Tm (see Fig. 2). This level is excited by means of the Ti:sapphire laser in a different degree depending on the polarization. Thus, the maximum absorption is measured with polarization parallel to the N_p principal optical axis centred at 793.4 nm with an absorption cross-section of 9.7×10^{-20} cm^2. However, a band with maximum of absorption centred at 801.8 nm and absorption cross-section of 5.2×10^{-20} cm^2 was measured for polarization parallel to N_m. At the latter wavelength, the polarization parallel to N_p showed an absorption cross-section of 1.69×10^{-20} cm^2. The band centred at 801.8 nm (FWHM = 4 nm) for polarization parallel to N_m is suitable for diode pumping rather than the highest signal centred at 793.4 nm (FWHM = 1 nm) for polarization parallel to N_p for two reasons: (a) the former is broader than the latter. This means, that the requirements for the wavelength coming from a diode are not very crucial, so that a bandwidth of 3–4 nm is almost fully absorbed. This will not happen for the peak centred at 793.4 nm, which is very narrow and (b) the diodes centred at 808 nm are standard and very cheap in the market. On tuning the wavelength with temperature, one can reach ~802 nm very easily. To further shorten the wavelength to reach ~794 nm the diode should be customer-designed with the consequent increase of price and non-standard performance.

For the luminescence experiments, low power coming from the pump laser was sufficient to detect luminescence from Ho ions.

We optimized the pump wavelength with the tunable Ti:sapphire laser to 802 nm, recorded the emission spectrum around 2 μm and observed two different broad bands (see Fig. 3).

According to the spectrum shown in Fig. 8d of reference [11] there is no signal coming from Tm in KLuW at wavelengths longer than 1950 nm.

The second signal is then assigned to the $^5I_7 \rightarrow {}^5I_8$ transition of Ho^{3+}. The Ho emission is much less intense than that of Tm^{3+} in this crystal. We think that this is due to the fact that the ratio of Ho and Tm ions is not optimum in this crystal. According to the scheme in Fig. 4, the generation mechanism of the 1.9 μm emission in Tm ions is as follows: a photon pump of ~800 nm excites a Tm ion from the ground level to the $^3H_4$ level. From the latter, several radiative and non-radiative decays populate the $^3F_4$ level. From the $^3F_4$ level the ~2.1 μm emission is generated. In addition, it turns out there is a cross-relaxation mechanism with a second Tm ion so that the population in the ground is excited to the $^3F_4$ level originating a second excited Tm ion. This means that a photon pump could produce two Tm excited ($^3F_4$) ions, so that the quantum efficiency approaches 2. This has been reported in other materials doped with Tm [12]. Once Tm ions are excited in the $^3F_4$ level, part of their energy is transferred to Ho ions ($^5I_7$ level) almost resonantly. From this level of Ho, the 2.1 μm emission is generated. In this experiment we used a doping level of 0.5 at.% Ho and 2.5 at.% Tm. This means that other doping ratios could enhance the emission from Ho in detriment of the emission from Tm due to the increased energy transfer. This was the case previously observed in a similar host, (Ho,Tm):KGdW [13]; in this crystal the Ho concentration was more than two times higher than that of the crystal used in the present work. Also the Tm doping was higher.

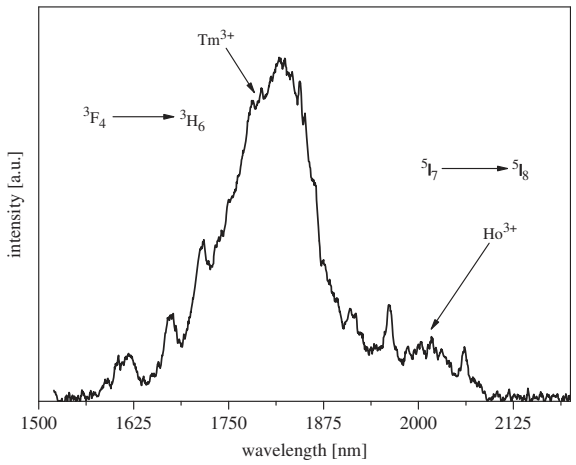

Fig. 3. Experimental emission observed in (0.5 at.% Ho, 2.5 at.% Tm):KLuW.

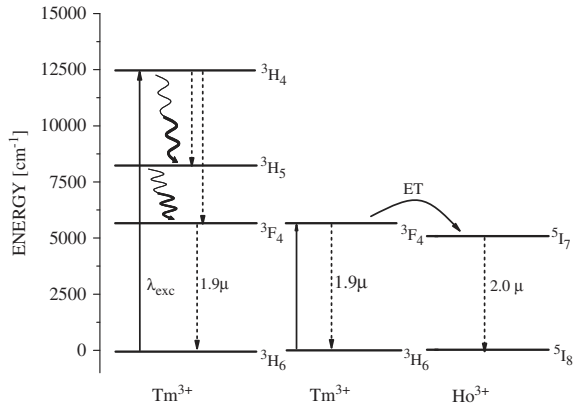

Fig. 4. Schematic of the pump-emission and energy transfer between Tm and Ho ions in KLuW.

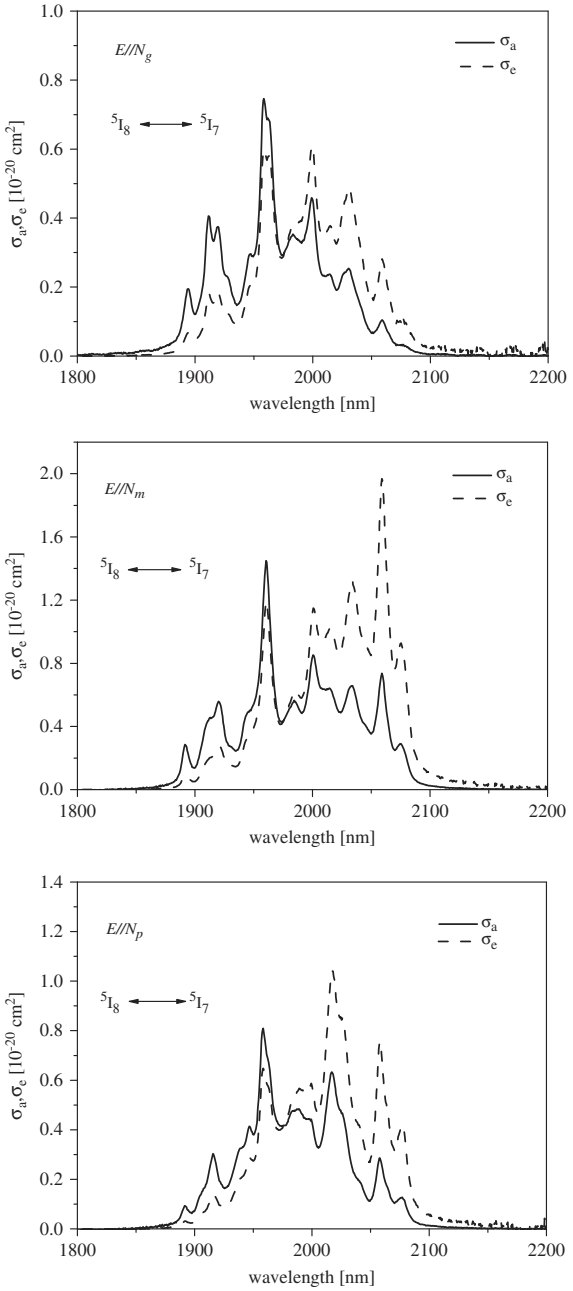

Fig. 5. Polarized absorption cross-section and calculated emission cross-section of the 2 μm emission of Ho^{3+} in KLuW.

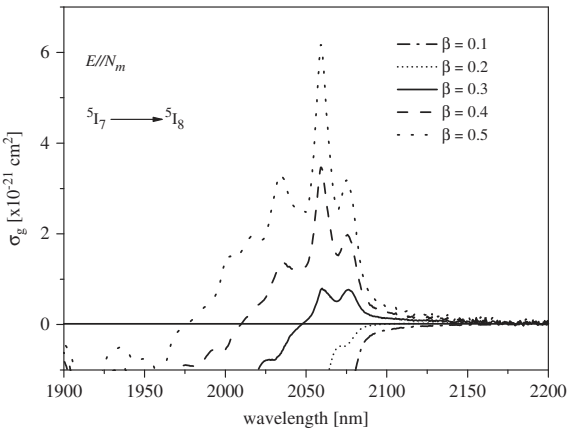

Fig. 6. Calculated gain cross-section of the $^5I_7 \rightarrow {}^5I_8$ transition of Ho^{3+} for polarization parallel to N_m.

To quantify the Ho emission around 2 μm, we used the reciprocity method to compute the polarized emission cross-section from the absorption cross-section spectra. For this, we first measured the optical absorption in the 1850–2150 nm range of a holmium single-doped 5 at.% Ho:KLuW crystal with light polarized parallel to the three principal optical directions, N_g, N_m and N_p.

From Fig. 5, one can observe that the maximum emission cross-section is accomplished for polarization parallel to N_m. Particularly, for this polarization a maximum of $\sim 2 \times 10^{-20}$ cm^2 was calculated at 2060 nm. Significantly lower emission cross-section was calculated for the other two polarizations. However, the maximum of emission for the other two polarizations occurred at a different wavelength, 2017 nm for N_p and 1998 nm for N_g. Larger emission cross-section than absorption cross-section gives an idea of the possibility for further amplification. This is observed for the three polarizations extending roughly 100 nm. The calculated emission cross-section of Ho^{3+} in the single-doped crystal is very similar to that of the codoped crystal. We show here the calculation for the single-doped one just to avoid any interference of the signal coming from the emission of thulium. To estimate this potential, we computed the gain cross-section with the following expression:

$$\sigma_g = \sigma_e \times \beta - (1 - \beta) \times \sigma_a \quad (1)$$

where σ_g is the gain cross-section, σ_a the absorption cross-section, σ_e the emission cross-section and β the inversion population level. Fig. 6 shows the calculated gain cross-section for N_m polarization indicating positive gain from 1975 nm for a maximum population inversion level of 0.5 of the $^5I_7 \rightarrow {}^5I_8$ transition of Ho^{3+}. More realistic inversion population with intermediate values would indicate a laser oscillation wavelength of 2060 nm where a rather sharp peak exists.

4. Conclusions

We have grown a (Ho,Tm):KLuW crystal with 0.5 at.% Ho, 2.5 at.% Tm doping ratio with very high optical quality by the Top-Seeded Solution Growth Slow-Cooling method. The preparation of the sample was done in terms of oriented cut and polishing along the three principal optical directions of this biaxial crystal. This allowed us to measure the polarized optical absorption of the $^3H_4$ pump level of Tm^{3+} and the infrared photoluminescence from the $^5I_7$ level of Ho^{3+} to its ground level, around 2 μm. From the calculation of the gain cross-section for the $^5I_7 \rightarrow {}^5I_8$ transition of Ho^{3+}, we expect positive gain with maximum at 2060 nm for polarization parallel to N_m. Additional advantage is the possibility of using diode pumping around 800 nm due to the codoping with Tm^{3+} because of its bandwidth of ~4 nm.

We further plan the growth of a complete set of crystals with several doping levels to achieve the most efficient ratio to improve the energy transfer and the first attempts to obtain continuous-wave lasing in this codoped system with Ti:sapphire laser and diode pumping.

Acknowledgements

This work was supported by the Spanish government under project MAT-05-06354-C03-02 and the Catalan government under project 2005SGR658. M.C. Pujol and J.J. Carvajal are supported by the Education and Science Ministry of Spain and European Social Fund under the Ramón y Cajal program, RYC2004-1453 and RYC2006-858, respectively.

References

[1] Jirong Yu, U. N. Singh, J. C. Barnes, N. P. Barnes, M. Petros, An efficient double-pulsed 2-micron laser for DIAL applications, In: A. Dabas, C. Loth, J. Pelon (Eds.), Advances in Laser Remote Sensing, 2000, pp. 53–55.
[2] Markolf H. Niemz, Laser–Tissue Interactions, Springer, Berlin, 2007.
[3] Futao Sun, Wentong Zhang, Yan Zhuang, Qingyu Dong, Aiwu Li, Pediatr. Surg. Int. 22 (2006) 514.
[4] O. Sahap Atik, Deniz Erdogan, Suna Omeroglu, Feza Korkusuz, M. Murad Uslu, Fatih Eksioglu, J. Clin. Laser Med. Surg. 1 (21) (2003) 3.
[5] D.Y. Shen, A. Abdolvand, L.J. Cooper, W.A. Clarkson, Appl. Phys. B 79 (2004) 559.
[6] E. Sani1, A. Toncelli, M. Tonelli, N. Coluccelli, G. Galzerano, P. Laporta, Appl. Phys. B 81 (2005) 847.
[7] X. Mateos, F. Güell, M.C. Pujol, M.A. Bursukova, R. Solé, Jna Gavaldà, M. Aguiló, F. Díaz, J. Massons, Appl. Phys. Lett. 80 (2002) 4510.
[8] M.C. Pujol, X. Mateos, A. Aznar, X. Solans, S. Suriñac, J. Massons, F. Díaz, M. Aguiló, J. Appl. Crystallogr. 39 (2006) 230.
[9] V. Petrov, M.C. Pujol, X. Mateos, Ò. Silvestre, S. Rivier, M. Aguiló, R. Solé, J. Liu, U. Griebner, F. Díaz, Laser Photon Rev. 1 (2007) 179.
[10] M.C. Pujol, M. Aguiló, F. Díaz, C. Zaldo, Opt. Mater. 13 (1999) 33.
[11] Ò. Silvestre, M.C. Pujol, M. Rico, F. Güell, M. Aguiló, F. Díaz, Appl. Phys. B 87 (2007) 707.
[12] Stuart D. Jackson, Opt. Commun. 230 (2004) 197.
[13] Ò. Silvestre, M.C. Pujol, F. Güell, M. Aguiló, F. Díaz, A. Brenier, G. Boulon, Appl. Phys. B 87 (2007) 111.

Paper II

Crystal growth, optical spectroscopy and continuous-wave laser operation of co-doped (Ho,Tm):$KLu(WO_4)_2$ monoclinic crystals

V. Jambunathan, A. Schmidt, X. Mateos, M. C. Pujol, J. J. Carvajal, U. Griebner, V. Petrov, C. Zaldo, M. Aguiló and F. Díaz

Submitted to Journal of Optical Society of America B.

UNIVERSITAT ROVIRA I VIRGILI
INFRARED LASERS BASED ON HO3+:KRE(WO4)2 CRYSTALS WITH TM3+OR YB3+ AS SENSITIZERS
Venkatesan Jambunathan
ISBN:/DL: T.1243-2011

UNIVERSITAT ROVIRA I VIRGILI
INFRARED LASERS BASED ON HO3+:KRE(WO4)2 CRYSTALS WITH TM3+OR YB3+ AS SENSITIZERS
Venkatesan Jambunathan
ISBN:/DL: T.1243-2011

Crystal growth, optical spectroscopy and continuous-wave laser operation of co-doped (Ho,Tm):$KLu(WO_4)_2$ monoclinic crystals

Venkatesan Jambunathan,[1] Andreas Schmidt,[2] Xavier Mateos,[1*] Maria Cinta Pujol,[1] Joan Josep Carvajal,[1] Uwe Griebner,[2] Valentin Petrov[2], Carlos Zaldo,[3] Magdalena Aguiló,[1] and Francesc Díaz [1]

[1]Física i Cristal·lografia de Materials i Nanomaterials (FiCMA-FiCNA-EMAS). Universitat Rovira i Virgili (URV), c/ Marcel·lí Domingo, s/n. E-43007 Tarragona, Spain
[2]Max Born Institute for Nonlinear Optics and short pulse Spectroscopy, Max-Born Strasse 2A, 12489 Berlin, Germany
[3] Instituto de Ciencia de Materiales de Madrid. Consejo Superior de Investigaciones Científicas. c/ Sor Juana Inés de la Cruz 3. E- 28049 Madrid, Spain
**Corresponding author: xavier.mateos@urv.cat*

We report on the crystal growth, optical spectroscopy and room-temperature continuous-wave laser generation at 2.06 µm in co-doped (Ho,Tm):$KLu(WO_4)_2$ monoclinic crystals. Co-doped crystals at different doping levels were grown by the Top-Seeded Solution Growth Slow-Cooling method (TSSG–SC). We characterized the spectroscopy of Ho and Tm ions in KLuW in terms of polarized optical absorption, photoluminescence and lifetime measurements. Continuous-wave laser operation at room-temperature at a wavelength of 2.06 µm was achieved in several crystals at different co-doping levels, establishing that the optimum doping ratio is 0.5at.%Ho-5.0at.%Tm:KLuW reaching a maximum output power of 145mW and a slope efficiency of 12.9%.

OCIS codes: (300.0300) Spectroscopy, (300.1030) Absorption, **(**250.5230) Photoluminescence, (140.5680) Rare earth and transition metal solid-state lasers, (140.3070) Infrared and far-infrared lasers

1. INTRODUCTION

Eye-safe solid-state lasers that operate in the 2 µm spectral range are the subject active research in recent years because of their potential applications in remote sensing, medical treatments and as a pump source for mid-IR Optical Parametric Oscillators (OPOs) [1]. Laser transitions around 2 µm exist in the trivalent lanthanide ions Tm^{3+} (Tm) (slightly below 2 µm) and Ho^{3+} (Ho) (slightly above 2 µm). The recent progress in power scaling of Tm-lasers is due to the possibility to pump them with commercially available GaAlAs laser diodes near 800 nm, however, Ho-lasers are usually excited by energy transfer through co-doping with Tm [2] or by direct in-band pumping with Tm fiber or bulk lasers [3]. Recently, GaSb diodes emitting around 1.9 µm also became available for in-band pumping of Ho-lasers [4] but certain properties, such as high brightness or powerful fiber coupling, are still a limitation.

Ho lasers differ only slightly in wavelength from Tm lasers but for medical applications this already translates into different penetration depth because water absorption shows pronounced wavelength dependence in the 2 µm spectral range. In the Q-switched mode for operation, for tissue application or as a pump source for mid-infrared optical parametric oscillators (OPO) and directed counter measures, Ho-lasers are definitely the preferable choice because the longer lifetime of the emitting level $^5I_7$ enables more energy to be stored.

The search for new crystalline hosts for solid-state lasers is the subject of study of many researchers. This work focuses on the development and investigation of the laser performance of a (Ho,Tm) co-doped potassium lutetium double tungstate crystal, shortly $KLu(WO_4)_2$ or KLuW, which belongs to the monoclinic family of potassium rare earth double tungstates, $KRE(WO_4)_2$ (RE = Lu, Gd and Y). This family of crystal hosts shows rather high anisotropy of the physical properties with very high transition cross-sections (absorption and emission) for selected polarizations. In addition, the monoclinic double tungstates allow for high degree of substitution of the RE ion by some active laser dopants approaching 100% doping levels [5] without substantial quenching of the fluorescence due to the relatively long ion-to-ion separation in the structure [6].

Among the KREW crystals, KLuW has been demonstrated to be very suitable for Yb- and Tm-doping to realize solid-state lasers operating in 1- and 2-µm ranges, respectively [7]. Concerning co-doping of such monoclinic crystalline hosts for 2-µm operation, CW laser action has been achieved only with the related (Ho,Tm):KYW [8].

In this work, we study KLuW crystals co-doped with Ho and Tm ions. We grew a series of co-doped crystals $Ho_xTm_y:KLu_{1-x-y}(WO_4)_2$ and analyzed their composition and variation of the cell parameters with the doping level. The spectroscopic characterisation at room-temperature includes optical absorption, emission and lifetimes is also presented. Finally, laser operation at 2.06 µm in the continuous-wave (CW) regime is demonstrated.

2. EXPERIMENTAL DETAILS

To grow the series of single crystals we used the Top-Seeded Solution Growth Slow-Cooling (TSSG-SC) method using a vertical tubular furnace with kanthal wire as heating element and a Eurotherm903P temperature controller/programmer with thermocouples to control the temperature. The powder precursors were K_2CO_3, WO_3, Lu_2O_3, Ho_2O_3 and Tm_2O_3 with analytical grade of purity. We mixed them so that the solution had a binary composition of 12 mol% (Ho,Tm):KLuW as solute and

Table 1. Summary of the growth features for the co-doped grown crystals.

Sample number	at.% of Ho^{3+} in solution	at.% of Tm^{3+} in solution	Cooling rate [K/h]	Cooling interval. [K].	Crystal weight [g]	Growth Rate ($x10^{-4}$) [g/h]	Crystal dimension along the crystallographic direction [mm]			Saturation Temp. [K]
							c	a*	b	
1	0.5	2.5	0.1	11.7	3.2	273	11.0	11.3	8.9	1164.8
2	0.5	5.0	0.1	21.2	6.5	311	15.2	15.6	9.9	1155.9
3	1.5	5.0	0.1	21.0	6.5	310	17.0	12.9	8.2	1157.0
4	2.5	5.0	0.1	20.0	7.3	363	15.7	14.3	10.6	1152.8
5	2.5	7.5	0.1	20.0	8.2	408	20.9	13.0	7.6	1161.6
6	2.5	10.0	0.1	20.0	6.7	336	19.9	12.3	7.3	1163.6

88 mol% $K_2W_2O_7$ as solvent, since with this composition the physical properties of the solution was well studied in previous works and prove to be the optimum for growing high quality crystals [9]. We used a crystalline seed of KLuW to favour the nucleation. The seed was rotated during the growth process to ensure the presence of a forced convective flow near the crystal in order to enhance mass and heat transport in the solution to avoid inclusions during the growth process. No pulling was applied. The concentration of the doping ions, Tm and Ho in the crystals was determined by Electron Probe Micro analysis (EPMA) technique with Cameca sx50 equipment. To evaluate the unit cell parameters for the grown crystals X-ray powder diffraction patterns were obtained using - AXS D8 - discover diffractometer. The diffraction patterns were recorded at $2\theta = 5 - 70°$ with step size = 0.02° and step time = 16 sec.

Due to the high anisotropy of the monoclinic KLuW crystals [6], the samples were cut and polished along the principal optical directions, namely N_g, N_m *and* N_p, associated to the three refractive indices n_g, n_m and n_p of this biaxial crystal. The samples were parallelepiped prisms with faces perpendicular to the principal optical axes. The anisotropy makes necessary to measure the optical absorption with polarized light. For this, we used a Glam Thomson polarizer located in front of the sample. To measure the optical absorption we used a Cary Varian 500 spectrophotometer. To decrease the temperature for low-temperature measurements we used a cryostat from Oerlikon Leybold Vacuum GmbH (coolpak 6000 model) with a closed cycle helium circuit. The emission spectra were recorded using a Ti:Sapphire laser as pump source. The luminescence was collected to a 34 cm Jobin –Yvon monochromator and dispersed using two kinds of diffraction gratings depending on the wavelength range to be detected. Thus, a diffraction grating with 300 grooves/mm was used for the emissions in the 2 µm range and the other with 1800 grooves/mm was used for the emissions in the visible. For detection of 2µm emissions we used a cooled InAs detector which was connected to a preamplifier and to a lock-in amplifier. For the measurement of visible emissions a PMTR928 photomultiplier tube was used. A computer stored the data for final processing. Lifetime measurements were carried out with a Quanta-Ray MOPO system pumping at 802 nm for the infrared emission and at 915 nm for the visible emissions. The luminescent signals were dispersed by a single grating SPEX spectrophotometer (f = 34 cm). For detecting the visible and the 2µm signals, a photomultiplier tube and a cooled InSb detector were used, respectively. The decay curves were collected using a Tektronix digital oscilloscope (TDS-520). The laser experiments were carried out by constructing a 3-mirrors V-type stigmatically compensated resonator, using a Ti:Sapphire laser as pump source tuned to 802 nm for all the crystals where they absorbs maximum. The resonator was formed by two curved mirrors with radii of curvature (Roc = -100 mm), which have high transmission > 98% at the pump wavelength and high reflection in the 1800-2100 nm range. Here one curved mirror acted as a pump mirror to the sample and also as folding mirror to the output coupler. The other curved mirror acts as a pump end mirror where leakage pump power from sample could be collected behind it. The uncoated (Ho,Tm):KLuW samples were mounted in a copper holder and inserted at Brewster's angle in between the two curved mirrors. The crystals were oriented for propagation of light along the N_g axis and polarization parallel to N_m axis. The thickness of the active elements was 3 mm and the aperture size was 3x3 mm^2. The cavity terminal was formed with a plane output coupler (OC) having the transmissions (T_{oc}) = 1.5 (±0.5), 3.0 (±0.5), 5.0 (±0.5), and 9.0 (±1.0) % in the 1820-2050 nm range. For focusing the pump beam to the crystal a lens with focal length of 75 mm and antireflection coated for 650-1100 nm range, was used. We used indium foil at the top and bottom surface of the crystals to have better contact with the copper holder which was actively water cooled to 16°C at the bottom part and passively cooled at the top part for dissipation of heat.

3. RESULTS AND DISCUSSION

A. Crystal growth

We introduced 200 g of solution mixture inside the furnace with the binary composition above mentioned in a platinum crucible of 50 mm in diameter and 50 mm in length. The mixture was homogenised by maintaining the solution at 50K above the saturation temperature for 5 to 6 hours. The thermal axial gradient of the furnace was ~1.5 K/cm. The seeding process was realized with a *b* crystallographic oriented seed located at the centre of the surface of the solution. After accurately determining the saturation temperature by observing the growth and dissolution of the seed in contact with the surface of the solution, the crystals grew by slow cooling at the rate of 0.1K/h for ~20K. After the crystals grew, they were slowly removed from the solution and kept above its surface being cooled to room temperature at a rate of 25K/h to avoid thermal shocks. The detailed growth methodology is described elsewhere [10]. We grew high quality (Ho,Tm):KLuW crystals at several doping levels. The crystals contained higher Tm concentration than Ho to have high absorption of the pump, optimum energy transfer from Tm to Ho ions and to minimize the re-absorption around 2.1 µm. Table 1 gives the summary of the grown crystals.

Table 2. Composition of the grown crystals.

at.% of Ho^{3+}	at.% of Tm^{3+}	Ho^{3+} in KLuW [at./cm^3]	Tm^{3+} in KLuW[at./cm^3]	Stoichiometric formula
0.5	2.5	$5.534x10^{19}$	$2.057\ x10^{20}$	$KLu_{0.960}Ho_{0.008}Tm_{0.032}(WO_4)_2$
0.5	5.0	$5.291x10^{19}$	$2.301\ x10^{20}$	$KLu_{0.957}Ho_{0.008}Tm_{0.035}(WO_4)_2$
1.5	5.0	$1.377x10^{20}$	$3.151\ x10^{20}$	$KLu_{0.931}Ho_{0.021}Tm_{0.048}(WO_4)_2$
2.5	5.0	$2.181x10^{20}$	$3.060\ x10^{20}$	$KLu_{0.920}Ho_{0.033}Tm_{0.047}(WO_4)_2$
2.5	7.5	$1.901x10^{20}$	$5.283\ x10^{20}$	$KLu_{0.890}Ho_{0.029}Tm_{0.081}(WO_4)_2$
2.5	10.0	$1.847x10^{20}$	$6.889\ x10^{20}$	$KLu_{0.866}Ho_{0.028}Tm_{0.106}(WO_4)_2$

The growth rate of the co-doped crystals was in the range of 273 – 408 x 10^{-4} g/h. In general, the growth rate increased with the increase of dopant levels. The weight of the crystal ranged from 3.2 – 8.1 g, depending on the cooling interval. The cooling rate was fixed at 0.1K/h for all the experiments because previous results showed that this rate was sufficient enough to ensure high quality crystals making the growth process faster [9]. The quality of the crystals was good. The dimensions of the crystals were typically 11 – 21 mm, 11 – 16 mm and 7 – 10 mm for the *c, a** and *b* crystallographic directions, respectively. Fig.1 shows the photograph of co-doped $KLu_{87.5}Ho_{2.5}Tm_{10.0}(WO_4)_2$ single crystal as an example. The actual concentration of the co-doped crystals was measured by EPMA and the summary of the concentration results are tabulated in Table 2 with stoichiometric formula.

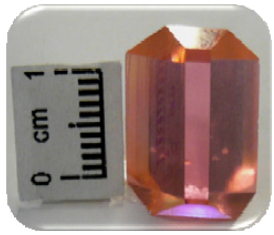

Fig.1. Photograph of $KLu_{87.5}Ho_{2.5}Tm_{10.0}(WO_4)_2$ single crystal.

B. Evolution of unit cell parameters

The study of evolution of unit cell parameters (*a*, *b* and *c*) as a function of the doping concentration is of great interest to know how the structure distorts when the doping concentration increases. The unit cell parameters of the grown crystals with different doping levels were calculated by fitting the X-ray patterns obtained with the FULLPROF software [11] using the rietveld method [12].

Fig. 2 shows the values of the *a,b,c,*and *V* (volume) parameters and their evolution, as well as the *β* angle (*β* is the angle between *a* and *c*) against the amount of Ho(X) and Tm(Y). Figure 2 shows that there is a small increase in unit cell parameters *a*, *b* and *c*, however, *β* remains basically constant with the increase of the dopant concentration. This increase is due to the fact that the dopant ions have bigger ionic radius than the Lu ions which are substituted for. Thus, Lu^{3+} is 0.977Å and the dopant ions Ho^{3+} and Tm^{3+}, are 1.015Å and 0.994Å, respectively. The ionic radius values were taken from the work reported in [13] for coordination number 8 according to the structure KLuW [6].

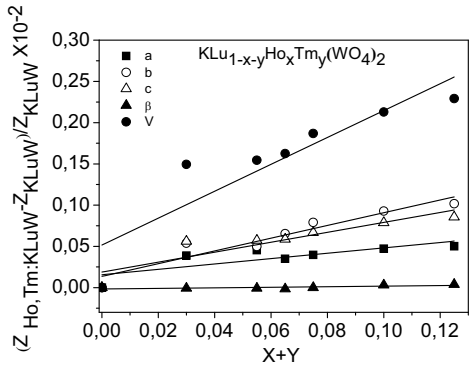

Fig. 2. Evolution of the unit cell parameters as a function of Ho and Tm concentrations in KLuW.

C. Optical absorption

We measured the room-temperature and low-temperature polarized optical absorption of the co-doped crystals. The absorption spectra were measured from 330 nm to 2200 nm range with the 0.5%at.%Ho2.5at.%Tm:KLuW crystal. The reason to consider this crystal was that the signal to noise ratio is good enough for optical absorption measurement. The thickness of the sample was 2.90 mm along N_g and 4.39 mm along N_p.

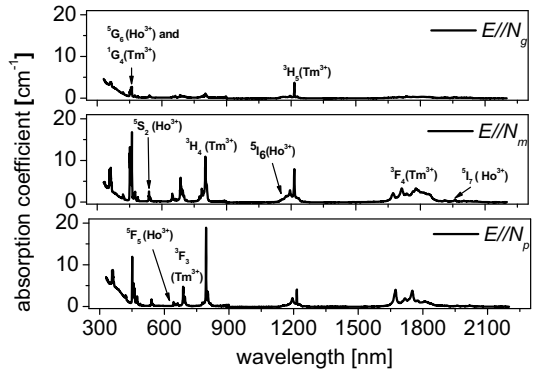

Fig. 3. Polarized room-temperature absorption of Ho,Tm:KLuW in the 330-2200 nm range.

Fig. 3 shows the room-temperature polarized optical absorption spectra of the co-doped system in the above range. Note the important anisotropy of this material for all the principal optical directions and notice the relatively high absorption around 800 nm, especially for N_m and N_p polarizations. This absorption band corresponds to the $^3H_6$ → $^3H_4$ transition of Tm and

shows a maximum absorption cross-section (σ_a) of $9.7x10^{-20}$ cm^2 for light polarized parallel to N_p centred at 793.4 nm and an absorption cross-section of $5.2x10^{-20}$ cm^2 for E//N_m centered at 802 nm. Fig. 4 shows detailed absorption spectra in the 750-850 nm range for the three polarizations. Note the relatively large broadness of the band for E//N_m around 800 nm, which is suitable for diode pump sources based on AlGaAs without special line width requirements.

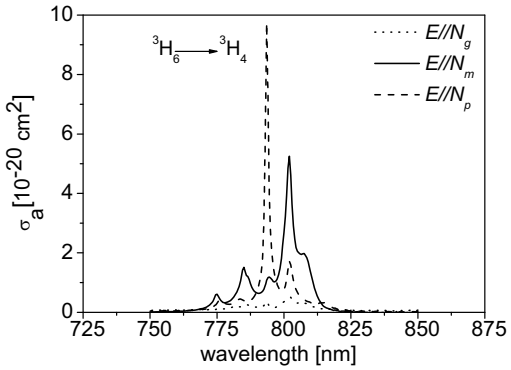

Fig. 4. Absorption cross-section of Tm in the 750- 850 nm range

To find the splitting of the different energy levels, we measured low-temperature optical absorption at 6K. When the temperature decreases, extra peaks caused by the thermal population of the various Stark levels of the ground state and possible vibronic (electron–phonon interaction) peaks are eliminated. The whole collection of spectra is not shown here for the sake of brevity. We observed that the energy level splitting of co-doped crystal exactly matches with the energy level splitting of single doped crystals (this is especially true for low doped samples). That's why in Table 3 we show the energy of Stark levels measured for single doped Tm:KLuW and single doped Ho:KLuW crystals [14,15]. The energy levels of the ground state were determined from the low-temperature photoluminescence experiments of the single doped crystals. In few energy levels, few of their Stark levels are missing according to the expected number of them.

.

D. Photoluminescence (Emission and lifetime)

The characterization of the luminescence of Ho in the co-doped (Ho,Tm):KLuW crystals is described in terms of room-temperature emission and lifetime measurements. Recording of the emission spectra of several crystals with different co-doped Ho,Tm ratios around 2µm and the measurement of their lifetime have been carried out. These valuable data give information to understand the dynamics of the electronic population among the excited energy levels during the excitation-deexcitation processes. The crystals studied in this work are 0.5/2.5, 0.5/5, 1.5/5, 2.5/5, 2.5/7.5, 2.5/10 at.%Ho/at.%Tm, respectively. For the emission spectra we pumped the crystals at a wavelength of 802 nm and collected the emissions in the 1600-2200 nm range. Figure 5 shows the emission spectra generated in Tm centred around 1840 nm and that in Ho centred around 2000 nm for all the series.

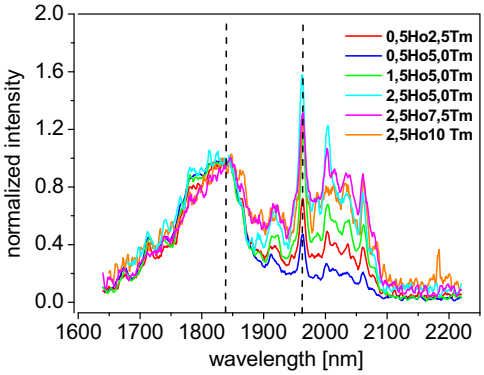

Fig. 5. Normalised emission spectra around 1.8 µm emission from Tm and 2.1 µm from Ho in (Ho,Tm):KLuW crystals after 802 nm excitation.

Table 3. Energy of Stark levels of each energy levels of Ho and Tm in KLuW.

$^{2S+1}L_J$	Energy of stark levels (cm^{-1}) from Ho^{3+}
$^5I_8$	0, 4, 6, 11, 21, 32, 43, 62, 106, 118, 144, 183, 209, 250, 292
$^5I_7$	5100, 5101, 5107, 5109, 5147, 5184, 5199, 5208, 5211, 5214, 5219, 5230, 5233, 5253,5288
$^5I_6$	8607, 8618, 8624, 8651, 8663, 8680, 8687, 8690, 8699, 8726, 8728, 8766, 8778
$^5I_5$	11173, 11180, 11193, 11196, 11225, 11238, 11259, 11272, 11317, 11319, 11321
$^5I_4$	13185, 13191, 13254, 13305, 13314, 13319, 13394, 13407
$^5F_5$	15349, 15364, 15367, 15400, 15403, 15430, 15442, 15456, 15552, 15556
$^5S_2$	18360, 18364, 18381, 18390,18393
$^5F_4$	18442, 18446, 18474, 18488, 18503, 18518, 18528, 18541, 18572
$^5F_3$	20471, 20495, 20520, 20593, 20595, 20620, 20631
$^5F_2$	21004, 21028, 21040, 21079, 21083
$^{2S+1}L_J$	Energy of Stark levels (cm^{-1}) from Tm^{3+}
$^3H_6$	0, 135, 155, 224, 247, 256, 279, 329, 346, 359, 513, 522, 530
$^3F_4$	5663, 5711, 5724, 5768, 5876, 5963, 5976, 5981, 6002
$^3H_5$	8231, 8369, 8379, 8389, 8441, 8452, 8481, 8500, 8599, 8612, 8654
$^3H_4$	12603, 12606, 12717, 12729, 12744, 12790, 12801, 12883, 12906
$^3F_3$	14493, 14511, 14529, 14561, 14564, 14617, 14625
$^3F_2$	15078, 15081, 15103, 15123
$^1G_4$	21092, 21121, 21128, 21233, 21353, 21361, 21535, 21581, 21613

These spectra are normalized with respect to the maximum of emission of Tm ion around 1940 nm to discuss about the influence of the doping ratio of Tm and Ho ions to understand how the energy transfer from the $^3F_4$ level of Tm to the $^5I_7$ level of Ho is favoured to generate the infrared emission from Ho with the highest possible intensity. To calculate the relative ratio of emission intensities of Ho and Tm we considered the maximum intensity and normalized the thulium intensity

to unity which is shown in Fig. 5 and Table 4. These are the following points inferred:

1) Considering sample 1 and 2 (case 1). Here we kept fixed the Ho concentration at a level of 0.5 at% and increased the thulium concentration from 2.5% in sample 1 to 5% in sample 2. From the spectra, we conclude that there is a drop of relative intensity of the Ho emission with the increase of Tm doping. This could be explained by higher interaction among Tm ions that results in lower emission from Ho. This dropping is not very pronounced because the real ion density in the crystals is not very different from sample 1 to sample 2 (see Table 2).

2) Now considering sample 2, 3 and 4 (case 2) we kept fixed the Tm concentration at 5% for all the three samples and we increased the holmium concentration being, 0.5% (sample 2), 1.5% (sample 3) and 2.5% (sample 4). From the relative ratio of the two emissions we conclude that when we increase the Ho doping there is an increase of the emission from Ho at 2 µm. This could be explained because of an improved energy transfer due to higher Ho doping.

3) If we consider sample 4, 5 and 6 (case 3), the Ho doping is again fixed as in case 1 and the Tm doping is increased. The observed tendency is the same than in case 1. The difference here is the doping levels, thus, Ho is kept fixed at 2.5 % and Tm doping ranges from 5 to 10%. What is clear is that higher doping levels (Ho+Tm), (case 3) show higher emission intensity from Ho than lower doping levels (case 1) giving evidence that reabsorption effects are not detrimental at the 2.5at.% doping level of Ho. Fig. 6a shows the evolution of the normalized relative intensity of Ho.

Table 4. Normalized relative ratio data and calculated energy transfer.

Sample number	Tm (normalized peak)	Ho (normalized peak)	% of Energy transfer
1	1	0.72	36.4
2	1	0.47	32.8
3	1	1.17	48.1
4	1	1.57	60.2
5	1	1.31	43.3
6	1	1.23	36.3

We also calculated the net energy transfer using the formula [16]

$$f_{Ho} = \frac{N_{Ho} \cdot \sum_i g_i \cdot e^{-\frac{E_i}{k \cdot T}}}{N_{Ho} \cdot \sum_i g_i \cdot e^{-\frac{E_i}{k \cdot T}} + N_{Tm} \cdot \sum_j g_j \cdot e^{-\frac{E_j}{k \cdot T}}}$$

Where f_{Ho} is the net energy transfer efficiency, N_{Ho} and N_{Tm} are the concentration of each ion, j are sums over the crystal filed splittings (i.e) $^5I_7$ of Ho and $^3F_4$ of Tm, E_i and E_j are the energy levels of the splittings, g_i and g_j are their degeneracies, k is the Boltzmann constant and T is the temperature. The calculated net energy transfer efficiency in percentage is tabulated in Table 4 and it follows the same tendency as the normalized experimental photoluminescence results obtained. Fig. 6b shows the evolution of the calculated net energy transfer.

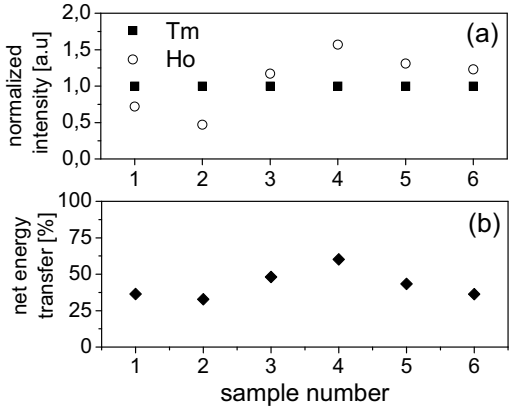

Fig. 6. a) Evolution of the normalized relative intensity of the 2µm emission from experimental values, and b) evolution of net energy transfer from calculated values.

To quantify the emission cross-section around 2 µm from Ho, we first measured the optical absorption in the 1800 – 2200 nm range of a single doped 5at.% Ho:KLuW crystal with light polarized parallel to the three principal optical directions. The reason to consider single doped crystal is just to avoid any interference of the signal coming from Tm. Later using the reciprocity method [17], we calculated the polarized emission-cross sections from the absorption cross-section spectra and averaged the three polarizations to compare with that computed by means of the Fücht-Ladenburg method [17], which makes use of the experimental photoluminescence spectrum and lifetime. We considered the photoluminescence spectra and lifetime of 1.5at.%Ho5at.%Tm:KLuW crystal for comparison. Fig. 7 shows the average of the polarised absorption cross section, calculated emission cross sections using Reciprocity method and the Fücht-Ladenburg method.

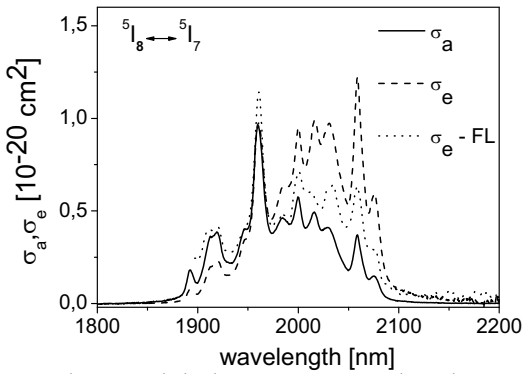

Fig. 7. Polarized room-temperature absorption cross-section and calculated emission cross-section by the reciprocity and the Füchtbauer-Ladenburg methods of Ho around 2µm.

The emission cross-sections at 2060 nm calculated by two methods have a maximum of 1.19x 10^{-20} cm^2 for reciprocity method and 0.65x10^{-20} cm^2 for Fücht-Ladenburg method. The values given by the former method are higher than those given by the latter due to

the fact that re-absorption is not taken into account in the calculation by the reciprocity method, so in the case of the value of latter case is more realistic although the life time is also affected by re-absorption.

Other emissions we observed were those generated from higher energy levels from both, Tm and Ho ions lying in the visible region (shown in Fig 8). Thus, we could measure the visible emissions, blue from Tm and Ho, green from Ho and red from Tm and Ho.

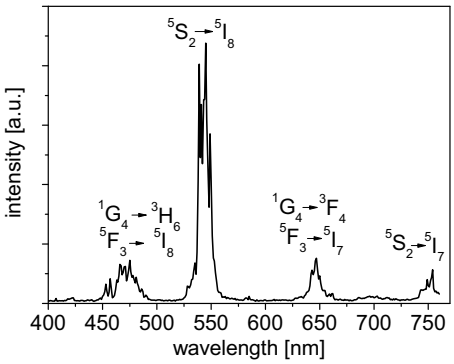

Fig. 8. Visible emissions observed in the (Ho,Tm):KluW crystal after 802 nm excitation.

The generation of all these emissions is explained with the help of the energy level scheme shown in Fig. 9 as follows. A pump photon excites a thulium ion at λ_{exc}= 802 nm (12469 cm^{-1}) to the $^3H_4$ level. At this wavelength Tm shows a peak with maximum absorption according with the optical absorption measurements shown previously for E//N_m. The pump laser was a Ti: Sapphire laser as explained before so that we could tune the pump wavelength for optimum emission signal. After excitation to the $^3H_4$ level, several radiative and non-radiative decays took place and populate the $^3F_4$ level of thulium.

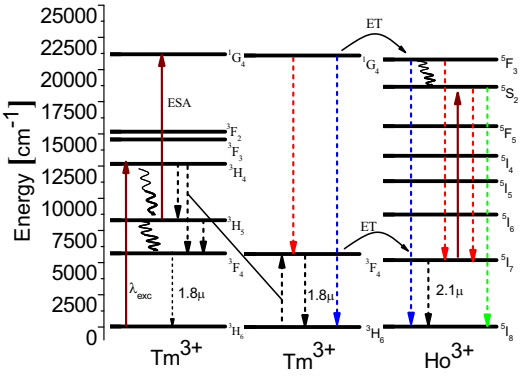

Fig. 9. Energy level scheme of Tm and Ho in KLuW with indication of the energy transfer mechanism and the generation of the observed emissions.

The latter level is also populated via cross-relaxation [18], so that a second ion is excited to that energy level leading to a quantum efficiency approaching 2. From the $^3F_4$ level of Tm two different ways of electronic depopulation occur, the first is the generation of the 1.8 emission from Tm and the second way is the energy transfer to the $^5I_7$ level of Ho, from where the 2.1 emission occurs. This transfer is rather efficient due to the small energy difference of the two involved levels, 5663 cm^{-1} for the $^3F_4$ of Tm and 5100 cm^{-1} for the $^5I_7$ of Ho. Other processes that take place are the up-conversion phenomena. These occur because additional pump photons are promoted from the $^3H_5$ level of Tm to $^1G_4$ level experiencing exited state absorption (ESA). From the $^1G_4$ level part of energy is transferred to $^5F_3$ of Ho and part of the electronic population is relaxed to the $^3F_4$ and $^3H_6$ levels of Tm generating the red (646 nm) and blue (475 nm) emissions respectively. From the $^5F_3$ level of Ho, part of the electrons depopulate non-radiatively to the $^5S_2$ level of Ho, from where the green (542 nm) and red (752 nm) emissions are generated to the $^5I_8$ and $^5I_7$ levels, respectively. Also from the $^5F_3$ level of Ho, blue (475 nm) and red (650 nm) emissions are generated to the to the $^5I_8$ and $^5I_7$ levels, respectively. These upconversion emissions are of course a source of losses for the 2μm emission, since these electrons will not contribute to the generation of any infrared emission. The reason to study several co-doping ratios is to know the optimum performance for the 2.1μm generation. The other possibility of electronic population in the $^5S_2$ level is the addition of more pump photons in the $^5I_7$ level of holmium with the help of a phonon of the lattice with maximum energy (~ 900 cm^{-1}). The mechanism of energy transfer from Tm to Ho has also been reported in other crystal hosts and glasses [16,19].

We measured the lifetime of the $^5S_2$ level around 540 nm (dominant green emission) by exciting the $^5I_5$ level of Ho at 915 nm and that of the $^5I_7$ level around 2μm by exciting the $^3H_4$ level of Tm around 802 nm. These measurements were realized for each combination of dopant ions. Table 5 shows the calculated lifetime from the experimental data.

Table 5. Life time measurement data

Sample number	τ (μs) for λ_{emi} = 540 nm	τ (ms) for λ_{emi} = 2.05 μm
1	4.0	3.7-4.1
2	4.0	3.8-4.0
3	3.8	5.3-5.6
4	3.9	5.1-5.6
5	3.4	4.1-4.3
6	3.1	3.0-3.3

The lifetime for the green emission is essentially the same that the lifetime for the single-doped Ho:KREW crystals [20]. Parallel to this, the lifetime of the green emission after excitation at 802 nm shows a rise time which corresponds to the energy transfer, however, it doesn't give any information about the realistic values since it is affected by the longer lifetime of the $^3H_4$ level (the values ranged from 69 to 6μs). From the measured values for 2 μm emission we deduced that at low Ho doping levels (0.5%, samples 1 and 2) the values are realistic, but the increase of Ho doping levels (samples 2, 3 and 4, keeping fixed the Tm doping level) give evidence of re-absorption phenomena lengthening considerably the lifetime. In samples 4, 5 and 6, we kept fixed the Ho doping level and increased that of Tm, having evidence of a strong interaction among the Tm ions that produced a shortening of the lifetime of the $^5I_7$ level of Ho.

The reabsorption effects observed in the lifetime measurements could be avoided by using crystal powder or the pinhole method.

E. Laser experiments

Laser experiments were carried out for the first five samples in CW regime, however we couldn't realize laser generation in the fifth sample, because of the extremely high absorption in the crystal leading to a high temperature that prevented laser oscillation. Only quasi-CW laser oscillation was achieved for sample 4. Figure 10 show the input-output characteristics of samples 1, 2 and 3 for all the transmission of output couplers above mentioned. For sample 1, with 0.5at.%Ho and 2.5at.%Tm a maximum output power of 83 mW was reached with Toc = 3% and a maximum slope efficiency of 10.8 mW was calculated. The absorption of the crystal ranged from 81% to 94% depending on the incident power level.

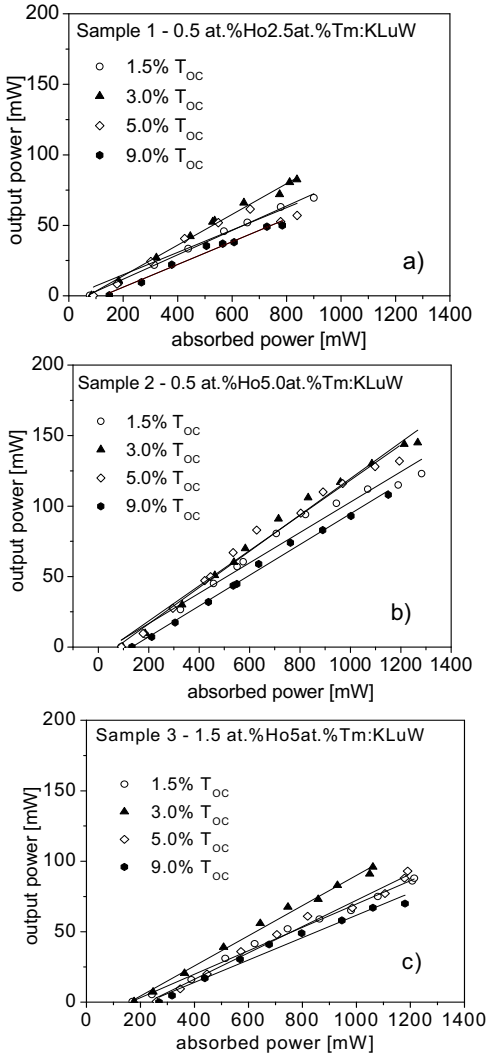

Fig. 10. Laser performance of the (Ho,Tm):KLuW laser for several co-doping ratio of crystals

In the case of increasing the Tm doping level up to 5at.%, the absorption in the crystal increased as well as the interaction among ions, so that higher output powers could be reached. Again for Toc=3%, a maximum power of 145 mW was measured and a slope efficiency of 12.9% was calculated. In this case, the absorption of the crystal ranged from 86% to 96%.

In the third case, we increased the Ho doping level, observing a drop in the laser performances. Only 96 mW were achieved with a slope efficiency of 10.7%. Here the absorption of the crystal ranged from 79% to 87%. The increase of Ho content provoked reabsorption of the laser due to the quasi-3 level nature of the Ho lasers.

Laser operating at 2061 nm was observed in all cases independently of the doping level used as well as the transmission n of the output coupler. Figure 11 shows the typical spectrum of the (Ho,Tm):KLuW laser. This emission corresponds to the $^5I_7 \rightarrow ^5I_8$ transition of Ho. Thermal problems were also observed in all cases, because when we used a mechanical chopper with a duty cycle of 50%, a linear dependence of the output power versus the incident or absorbed power was clearly observed.

It is worth to note that for sample 1 and 2 dual wavelength operation was observed at 1937 nm or 1919 nm and 2061 nm. The new laser wavelengths corresponded to Tm and were studied in a separated work [21] together with the tuning of the laser.

Sample 4 generated laser at 2061 nm only in quasi-CW regime. Too much Tm doping caused extremely high absorption in the crystal leading even to cracking of the sample.

Table 6 shows the maximum output power measured, the slope efficiencies and laser thresholds for every sample and every output coupler transmission in CW and quasi-CW regimes, showing that the best sample was that with 0.5at.%Ho and 5at.%Tm doping levels.

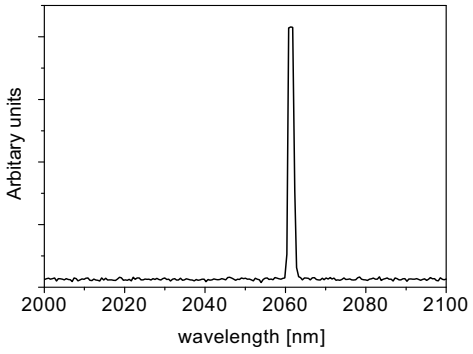

Fig. 11. Typical laser spectrum centered at 2061 nm generated in (Ho,Tm):KLuW.

Table 6. Summary of the laser results obtained in this work.

Sample number	T_{oc} %	Output power [mW]		Slope efficiency [%]		Threshold [mW]		λ_{laser} [nm]
		Quasi-CW	CW	Quasi-CW	CW	Quasi-CW	CW	
1	1.5	92	70	10.7	8.7	82	77	2061
	3.0	104	83	12.6	10.8	88	83	
	5.0	93	62	12.3	7.9	97	90	
	9.0	65	50	9.6	8.0	154	149	
2	1.5	168	123	13.7	10.8	91	106	2061
	3.0	164	145	14.4	12.9	92	97	
	5.0	162	132	14.2	12.5	97	97	
	9.0	118	108	11.5	10.9	134	135	
3	1.5	140	88	11.8	8.3	152	171	2061
	3.0	151	96	15.5	10.7	164	177	
	5.0	182	93	15.3	9.3	208	260	
	9.0	140	70	14.5	7.9	232	269	
4	1.5	53	-	5.3	-	282	-	2061

CONCLUSIONS

In conclusion, we have successfully grown a series of good quality (Ho,Tm):KLuW co-doped crystals by the Top- Seeded Solution Growth Slow-Cooling method (TSSG-SC) that allowed to determine an optimum dopant co-doping ratio for improved 2.0 μm laser generation. The spectroscopic characterization of this material was determined in terms of optical absorption, photoluminescence and lifetime of the 2μm and visible emissions, that allowed us to understand the electronic mechanism of the generation of these emissions. The laser experiments were realized for several crystal of different co-doping ratio levels and shown an optimum doping ratio of 0.5at.%Ho5at.%Tm:KLuW. Unfortunately we observed thermal problems in the laser operation of such crystals which limit the power scaling. Work is in progress to overcome this trouble, for example, different shape of the active medium (slabs and thin-disks) and optimized cooling holders are being studied.

ACKNOWLEDGMENTS

This work was supported by the Spanish Government under projects MAT2008-06729-C02-02/NAN, TEC2010-21574-C02-02, PI09/90527, HF2008-0045, DE2009-0002 and the Catalan Authority under project 2009SGR235. Joan Josep Carvajal is supported by the Education and Science Ministry of Spain and European Social Fund under the Ramon y Cajal program, RYC2006 – 858.

REFERENCES

1. Karsten Scholle, Samir Lamrini, Philipp Koopmann and Peter Fuhrberg, "2 μm Laser Sources and Their Possible Applications", book chapter form Frontiers in Guided Wave Optics and Optoelectronics, edited by Bishnu Pal and published by Intech, 471- 500 (2010).
2. V. Sudesh and K. Asai, "Spectroscopic and diode-pumped-laser properties of Tm,Ho:YLF; Tm,Ho:LuLF; and Tm,Ho:LuAG crystals: a comparative study", J. Opt. Soc. Am. B **20**, 1829-1837 (2003).
3. P. A. Budni, M. L. Lemons, J. R. Mosto, and E. P. Chicklis, "High-power/high-brightness diode-pumped 1.9-μm thulium and resonantly pumped 2.1-μm holmium lasers", IEEE J. Sel. Top. Quantum Electron. **6**, 629-635 (2000).
4. K. Scholle, and P. Fuhrberg, "In-band pumping of high-power Ho:YAG lasers by laser diodes at 1.9 μm," in Conference on Lasers and Electro-Optics/Quantum Electronics and Laser Science Conference, OSA Technical Digest (CD) (Optical Society of America, 2008), paper CTuAA1.
5. M.C. Pujol, M.A. Bursukova, F. Güell, X. Mateos, R. Solé, Jna. Gavaldà, M. Aguiló, J. Massons, F. Díaz, P. Klopp, U. Griebner, and V. Petrov, Growth, optical characterization, and laser operation of a stoichiometric crystal $KYb(WO_4)_2$, Phys. Rev. B **65**, 165121–1-165121–11 (2002).
6. M.C. Pujol, X. Mateos, A. Aznar, X. Solans, S. Suriñac, J. Massons, F. Díaz, and M. Aguiló, "Structural redetermination, thermal expansion and refractive indices of $KLu(WO_4)_2$", J. Appl. Cryst., **39**, 230-236 (2006).
7. V. Petrov, M. C. Pujol , X. Mateos, Ó. Silvestre, S. Rivier, M. Aguiló, R. M. Solé, J. Liu, U. Griebner and F. Díaz, "Growth and properties of $KLu(WO_4)_2$, and novel ytterbium and thulium lasers based on this monoclinic crystalline host", Laser & Photon. Rev. **1**, 179-212 (2007).
8. A. Lagatsky, F. Fusari, S. V. Kurilchik, V. E. Kisel, A. S. Yasukevich, N. V. Kuleshov, A. A. Pavlyuk, C. T. A. Brown, and W. Sibbett, "Optical spectroscopy and efficient continuous-wave operation near 2 μm for a Tm,Ho:KYW laser crystal", Appl. Phys. B **97**, 321-326 (2009).
9. R. Solé, O. Silvestre, J. Massons, Jna. Gavaldà, M. Aguiló, F. Díaz , "Physical properties of the 0.12 $KLu(WO_4)_2$–0.88 $K_2W_2O_7$ solution and single crystal growth of KLuW ", J. Cryst. Growth, **310,** 1167 - 1173 (2008).
10. R. Solé , V. Nikolov , X. Ruiz, Jna. Gavaldà, X. Solans, M. Aguiló and F. Diaz, "Growth of β-$KGd_{1-x}Nd_x(WO_4)_2$

single crystals in $K_2W_2O_7$ solvents", J. Cryst. Growth, **169,** 600 – 603 (1996).

11. J. Rodriguez-Carvajal, "An introduction to the program", Full prof 2000 " (Laboratorie Léon Brillouin, CEA-CNRS, Saclay), France, (2001).
12. L. B. McCusker, R. B. Von Dreele, D. E. Cox, D. Louër and P. Scardi, "Rietveld refinement guidelines ", J. Appl. Cryst. **32,** 36-50 (1999).
13. R. D. Shannon, Acta Cryst. A ,**32**, 751-767 (1976).
14. O. Silvestre, M.C. Pujol, M. Rico, F. Güell, M. Aguiló, F.Díaz, "Thulium doped monoclinic, $KLu(WO_4)_2$ single crystals: growth and spectroscopy ", Appl. Phys. B **87**, 707-716 (2007).
15. V. Jambunathan, X. Mateos, M.C. Pujol, J. J. Carvajal, M. Aguiló, F. Díaz, Física i Cristal·lografia de Materials i Nanomaterials (FiCMA-FICNA-EMAS), Universitat Rovira i Virgili, (URV), c/ Marcel·lí Domingo, s/n.E-43007 Tarragona, Spain, U. Griebner, V. Petrov, Max-Born Institute for Nonlinear Optics and short pulse Spectroscopy, Max-Born Strasse 2A, 12489 Berlin, Germany and C. Zaldo, Instituto de Ciencia de Materiales de Madrid. Consejo Superior de Investigaciones Científicas. c/ Sor Juana Inés de la Cruz 3. E- 28049 Madrid, Spain are preparing a manuscript to be called "Crystal growth, optical spectroscopy and continuous-wave laser operation of Ho:$KLu(WO_4)_2$ crystals".
16. T. Y. Fan, G.Huber, R L. BYER and P. Mitzscjerlich, "Spectroscopy and diode laser-pumped operation of Tm,Ho:YAG", IEEE J. Quantum Electron. **24**, 924 – 933 (1988).
17. Stephen A. Payne, L.L. Chase, Larry K. Smith, Wayne L.Kway and William F. Kruple, "Infrared cross-section measurement for crystals doped with Er^{3+}, Tm^{3+}, Ho^{3+}", IEEE J. Quantum Electron. **28**, 2619-2630 (1992).
18. Stuart D. Jackson, "Cross relaxation and energy transfer upconversion processes relevant to the functioning of 2μm Tm^{3+}-doped silica fibre lasers", Opt. Commun. **230**, 197 – 203 (2004).
19. L.D. da Vila, L. Gomes, L.V.G Tarelho, S.J.L. Riberio and Y. Messaddeq ," Dynamics of Tm-Ho energy transfer and deactivation of the 3F4 low level of thulium in fluorozirconate glasses", J. Appl. Phys. **95**, 5451- 5463 (2004).
20. M. C. Pujol, J. Massons, M. Aguilo, F. Diaz, M. Rico, and C. Zaldo, "Emission cross sections and spectroscopy of Ho^{3+} laser channels in $KGd(WO_4)_2$ single crystal," IEEE J. Quantum Electron. **38**, 93-100 (2002).
21. V. Jambunathan, A. Schmidt, X. Mateos, M. C. Pujol, J. J. Carvajal, M. Aguiló, F. Díaz, U. Griebner and V. Petrov, "Continuous-wave co-lasing in a monoclinic co-doped (Ho,Tm):$KLu(WO_4)_2$ crystal", Submitted to Laser Phys. Lett. (2011).

UNIVERSITAT ROVIRA I VIRGILI
INFRARED LASERS BASED ON HO3+:KRE(WO4)2 CRYSTALS WITH TM3+OR YB3+ AS SENSITIZERS
Venkatesan Jambunathan
ISBN:/DL: T.1243-2011

Paper III

Crystal growth, optical spectroscopy and continuous-wave laser operation of Ho:$KLu(WO_4)_2$ crystals

V. Jambunathan, X. Mateos, M. C. Pujol, J. J. Carvajal, C. Zaldo, U. Griebner, V. Petrov, M. Aguiló and F. Díaz

Submitted to Applied Physics B.

UNIVERSITAT ROVIRA I VIRGILI
INFRARED LASERS BASED ON HO3+:KRE(WO4)2 CRYSTALS WITH TM3+OR YB3+ AS SENSITIZERS
Venkatesan Jambunathan
ISBN:/DL: T.1243-2011

UNIVERSITAT ROVIRA I VIRGILI
INFRARED LASERS BASED ON HO3+:KRE(WO4)2 CRYSTALS WITH TM3+OR YB3+ AS SENSITIZERS
Venkatesan Jambunathan
ISBN:/DL: T.1243-2011

Crystal growth, optical spectroscopy and continuous-wave laser operation of Ho:KLu$(WO_4)_2$ crystals

V. Jambunathan[1], X. Mateos[1,2*], M. C. Pujol[1], J. J. Carvajal[1], C. Zaldo[3], U. Griebner[2], V. Petrov[2], M. Aguiló[1] and F. Díaz[1]

[1] *Física i Cristal·lografia de Materials i Nanomaterials(FiCMA-FiCNA). Universitat Rovira i Virgili (URV), Campus Sescelades c/ Marcel·lí Domingo, s/n. E-43007 Tarragona, Spain*
[2] *Max Born Institute for Nonlinear Optics and Short Pulse Spectroscopy, Max-Born Strasse 2A, D-12489 Berlin, Germany*
[3] *Instituto de Ciencia de Materiales de Madrid. Consejo Superior de Investigaciones Científicas. c/ Sor Juana Inés de la Cruz 3. E- 28049 Madrid, Spain*
** Corresponding author: xavier.mateos@urv.cat*

Abstract

We present the crystal growth, optical spectroscopy and room temperature continuous-wave laser operation of monoclinic Ho:KLu$(WO_4)_2$ crystals. Macro defect free crystals of several dopant concentrations were grown by Top Seeded Solution Growth - Slow Cooling method (TSSG–SC). The evolution of unit cell parameters depending on holmium doping level and temperature was studied using X-ray powder diffraction patterns. The spectroscopic properties were characterized in terms of room and low temperature optical absorption and photoluminescence. From the low temperature absorption measurement the energy Stark levels were determined. Calculation of the emission and gain cross-sections are presented. CW laser action was realized for a 3 and 5 at.Ho%:KLuW by in-band pumping using a Tm:KLuW laser of same host as pump source. A maximum output of 507 mW with a slope efficiency of 38 % with respect to the incident power was achieved in 5at.%Ho:KLuW. The laser operated at 2079 nm.

PACS: 81.10.Dn; 78.55.-m; 42.55.Rz

Keywords: KLu$(WO_4)_2$, Holmium (Ho^{3+}), Double tungstates, Photoluminescence, Solid state laser material.

1 Introduction

Infrared ~2 μm eye-safe lasers based on active lanthanide ions are of current interest because of their vast demand in scientific and technological applications, for example in medicine, remote sensing and as a pump source for OPO systems [1-4]. Efficient lanthanide-based ~2 μm infrared solid-state lasers can be accomplished by Ho ions due to large transition (absorption and emission) cross-sections and long lifetime of the $^5I_7$ manifold. The main drawback of the Ho lasers is to design a suitable and efficient pump source. For this, many authors used another lanthanide ion, thulium, to sensitize the Ho emission through energy transfer while pumping easily the Tm ions with commercial, powerful and compact diode lasers operating around 810 nm [5,6]. However, non-perfect energy resonance between energy levels and up-conversion processes provoked high losses reducing the laser efficiency in such laser systems. A second approach, in order to increase the laser efficiency and the output power, is to excite the Ho ions directly to the emitting level ($^5I_7$), the so-called in-band or resonant pumping using another ~2 μm laser operating at slightly shorter wavelength than that of Ho. Tm lasers are very suitable for this strategy, since their laser operation is in general at shorter wavelengths than those of Ho (depending on the host) but suitable to match the absorption curve of Ho in this spectral range. Solid-state and fiber lasers based on Tm served to pump Ho crystals with high efficiencies and output powers [7-12]. The great advantage of this strategy is the drastic reduction of the energy difference between the pump and laser energy, the so-called quantum defect, allowing the power scaling with lower risk of damaging of the active material.

Concerning the host for the active ion, the monoclinic double tungstate crystals, KRE$(WO_4)_2$ (RE = Y, Gd, Lu) are very suitable as solid-state lasers when doped with lanthanides as proved in the early years, specially for the Yb and Tm ions [13]. This crystalline material stands out because of the high transition cross-sections induced to the active ions and the possibility of a large range of doping levels, up to 100% as demonstrated previously [14]. Bearing all this in mind, our work focused on the crystal growth of a series of single-doped Ho:KLuW crystals, their spectroscopic characterization and their laser performance under resonant pumping using Tm:KLuW laser as pump source [15].

2 Experimental

Ho:KLuW crystals of several dopant concentrations of Ho were grown by the Top-Seeded-Solution Growth Slow-Cooling method (TSSG–SC) using $K_2W_2O_7$ as solvent. The detailed methodology of growth is described in reference [16]. The raw reagents were from Aldrich, Fluka and Metall rare-earth limited with analytical grade of purity. The chemical composition of the grown single crystals was measured using Electron Probe Micro analyzer (EPMA). X-ray powder diffraction was used to study the evolution of the unit cell parameters with the doping level (carried out with a Bruker-AXSD8-discover diffractometer) and the temperature (carried out with a Siemens D-5000 diffractometer).

For the spectroscopic characterization, taking into account the remarkable physical anisotropy of the KLuW crystal, these were cut and polished perpendicular to the principal optical directions, called as N_g, N_m and N_p (defined by the values of the refractive indexes, $n_g > n_m > n_p$) to study their behavior depending on the polarization of the incident light. The polarized room and low temperature optical absorption measurements were performed using a Glam-Thomson polarizer in front of the sample and were recorded in the 300 – 2400 nm range using a Cary Varian 500 spectrophotometer. To lower the temperature, a cryostat from Oerlikon Leybold Vacuum GmbH (coolpak 6000 model) with a liquid helium closed circuit was used. Room and low temperature photoluminescence of the Ho:KLuW crystal was performed by exciting the crystal using an optical parametric oscillator (OPO) system (Opotek, model Vibrant HE 355II+UV). The sample was placed behind the focusing

lens situated at an angle 90° with respect to the incident beam in order to avoid the influence of the pump. The emission signals were collected and dispersed through a 460 mm long Jobin-Yvon monocromator using a 300 groves/mm diffraction grating. For detection of the signal, we used a cooled InAs-based detector down to liquid nitrogen temperature (77K), connected to a preamplifier and to a lock-in amplifier for amplification of the signal. A personal computer was used for the processing of the data. The decay time measurement was carried out using a Quanta-Ray MOPO system and the signal was dispersed by a 340 mm long single grating SPEX spectrophotometer. For detection of the signal we used a cooled InSb detector and the decay curves were collected using a Tektronix digital oscilloscope (TDS-520).

Laser operation was carried out by a simple hemispherical resonator as shown in the figure 1. It comprises of a plane mirror (M5) which was antireflection coated for the pump wavelength in the 1900 – 1970 nm range and high reflection coated for laser wavelength in the 2000-2100nm range. The curved output coupler (M6) has a radii of curvature (RC) 50mm and has transmissions 1.5(±0.3)%, 3(±0.5)%, 5(±1.0)%, and 20(±4.0)% in the 1820 - 2050 nm range. For focusing the pump beam to the Ho:KLuW sample, we used a 50 mm focal length lens (L3). The active elements 3 and 5% Ho:KLuW were mounted in a Cu holder and was wrapped using indium foil for better contact and was cooled to 16°C at the top and bottom surface of the sample. The sample was antireflection coated for pump and a laser wavelength in a broad range from 1900 – 2200 nm and was placed as close to the pump mirror and was positioned for light parallel to N_m and for propagation of light along N_g. The thickness of the sample was 3mm and aperture 3 mm^2. The pump source was a Tm: KLuW laser described elsewhere [15]. It was centered at 1946nm with a maximum output power of 4.0 W using fibre coupled diode as pump source. The emission from the Tm:KLuW was linearly polarized along N_m principal axis. In order to avoid back coupling form Ho cavity we placed an optical isolator, For rotating the pump radiation a half wave plate is used to make it vertical.

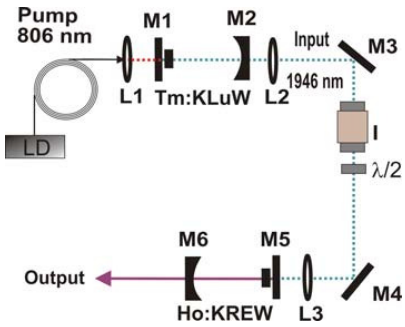

Figure 1 Laser setup of Ho:KLuW laser

3 Result and Discussion

3.1 Crystal growth

Defect-free Ho:KLuW single crystals with several Ho concentrations were grown by the TSSG-SC method. These were (in atomic percentage in the solution), 0.5at.%, 1.0at.%, 3at.%, 5at.% and 7.5at.%, where the active Ho ions substitute for the Lu ions in the structure. To grow the single crystals, 200 g of the solution mixture were inserted in a platinum crucible of 50 cm in diameter and 50 cm in height. The mixture was composed of proper amounts of K_2CO_3, Ho_2O_3, WO_3 and Lu_2O_3 reagents. The solution composition was 12 mol.% KLuW as solute – 88.0 mol.% $K_2W_2O_7$ as solvent because previous studies of the solubility curves [17] confirmed that this ratio with low solute content is optimum to produce sharp changes in the saturation temperature with small changes in the composition as well as to allow for the growing of high quality crystals.

The filled crucible was introduced in a home-made vertical tubular furnace so that the mixture was homogenized 50 K above the saturation temperature for about 7-8 hours. The thermal axial gradient measured in the solution was maintained around ~1.5 K/cm. To favor nucleation, a crystallographic *b*-oriented KLuW seed was used and located at the center of the surface of the homogeneous solution. The saturation temperature was determined by accurate growth and/or dissolution of the seed. The solution temperature was then decreased by about 20 K at a rate of 0.1 - 0.15 K/h while the seed was rotated at 40 rpm in order to enhance the mass and heat transfer to the growing crystal. After approximately 8 to 10 days of growth, the crystals were slowly removed from the solution at the rate of 1mm/10min and after loosing contact with the solution, the furnace was cooled to room temperature at a rate of 25 K/h to room temperature to avoid cracking of the crystals due to sudden change in temperature. The dimensions of the grown crystals ranged typically from 17.13 to 20.84 mm, from 9.85 to 10.16 mm, and from 6.87 to 7.71 mm for *c, a** and *b* crystallographic directions, respectively. Figure 2 shows a photography of 1at.% Ho:KLuW crystal as an example. The weight of the crystals was in the range of 4.5 – 5.5 g. The growth rate of the crystal varied from 231 to $243x10^{-4}$ g/h. The saturation temperature of the crystals was between 1158 and 1168 K. Table 1 summarizes all these parameters for each grown crystals, as well as the ion density measured in the crystal, thus giving the stoichiometric formula.

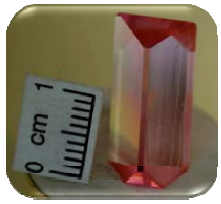

Figure 2 Photograph of 1at.% Ho:KLuW crystal

3.2 Evolution of unit cell parameters with the doping level and temperature

The Ho:KLuW crystal shows similar morphology to that of un-doped KLuW [18]. The study of the evolution of the unit cell parameters as a function of the doping concentration is of great interest to know how the structure modifies when the doping concentration increases, since a priori, we don't know which, is the optimum doping level for infrared laser operation. Furthermore, when laser active media are under high pump power conditions, heat is generated in them producing mechanical stress due to thermal expansion. Thus being it is necessary to be characterized.

UNIVERSITAT ROVIRA I VIRGILI
INFRARED LASERS BASED ON HO3+:KRE(WO4)2 CRYSTALS WITH TM3+OR YB3+ AS SENSITIZERS
Venkatesan Jambunathan
ISBN:/DL: T.1243-2011

at.% of Ho^{3+}	Cooling rate [K/h]	Cooling interval [K]	Crystal weight [g]	Growth Rate ($x10^{-4}$) [g/h]	Crystal dimension along the crystallographic direction [mm]			Saturation Temp. [K]	Ho^{3+} in KLuW [at./cm^3]	Stoichiometric formula
					c	a*	b			
0.5	0.10	24.0	5.5	231	18.43	9.85	7.71	1158.3	5.456×10^{19}	$KLu_{0.992}Ho_{0.008}(WO_4)_2$
1.0	0.10	20.0	4.8	242	19.13	10.16	6.87	1157.9	9.307×10^{19}	$KLu_{0.986}Ho_{0.014}(WO_4)_2$
3.0	0.10	21.2	4.9	230	20.84	10.07	6.90	1166.5	2.543×10^{20}	$KLu_{0.961}Ho_{0.039}(WO_4)_2$
5.0	0.10/0.15	17.0/3.0	4.5	238	17.13	10.03	7.30	1167.8	4.119×10^{20}	$KLu_{0.937}Ho_{0.063}(WO_4)_2$
7.5	0.10/0.15	16.5/3.5	4.6	243	17.64	9.96	7.26	1164.9	5.246×10^{20}	$KLu_{0.920}Ho_{0.080}(WO_4)_2$

Table 1 Summary of the crystal grown experiments, their concentration by EPMA and stoichiometric formula

For this, we first studied the evolution of the unit cell parameters with the following doping levels: 1at.%, 5at.%, 10at.%, 15at.%, 25at.%, 35at.%, 50at.% and 100at.%). These were calculated by fitting the X-ray powder diffraction patterns obtained with 2θ = 5-70° with step size 0.02° and step time 16s and by using the FULLPROF software [19]. Figure 3 shows the evolution of unit cell parameters with the increase of the doping level of Ho in the structure. We conclude that there is an increase in the unit cell parameters *a, b* and *c,* however β (angle between *a* and *c* remains basically constant. The reason of this expansion is that the ionic radius of Ho^{3+} (1.015Å) is slightly longer than that of Lu^{3+} (0.977Å) (values taken from [20] for coordination number 8), so that, the higher amount of Ho substituting for Lu, the longer are the cell parameters.

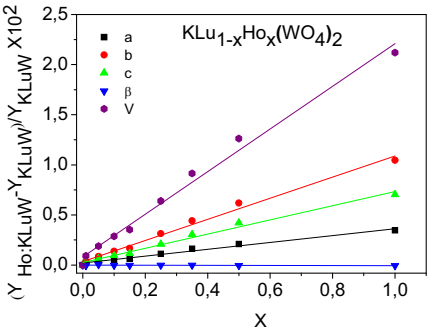

Figure 3 Evolution of unit cell parameters of Ho:KLuW with doping concentration

The second part of this study was to know how the unit cell parameters evolve with the increase of temperature. For determining the linear thermal expansion tensor, the unit cell parameters of 3%Ho: KLuW crystal powder was taken and measured as a function of temperature (303, 323, 373, 473, 573, 673, 773, 873 K) and were calculated by fitting the X-ray power diffraction patterns obtained with 2θ = 10-70° with step size 0.03° and step time 5s and by using fullprof software. Figure 4 shows the evolution of unit cell parameters with respect to temperature and it is inferred from the figure the unit cell parameters increase with increase in temperature and β remains basically constant. This means the crystal is expanding because of temperature in all directions.

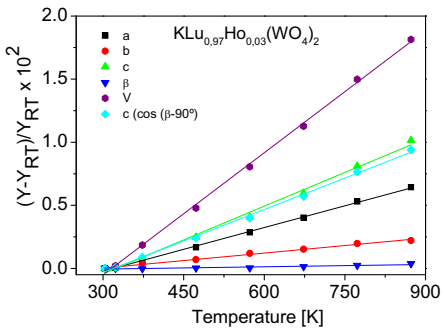

Figure 4 Evolution of unit cell parameters and volume with temperature

The values of the linear thermal expansion coefficients are the slopes of the linear relationship between the change in the (ΔL/L) and the temperature with respect to the crystallographic directions. The values of the monoclinic 3at.%Ho:KLuW are α_a=11.5X10^{-6} K^{-1}, α_b=3.98X10^{-6} K^{-1}, α_c=17.8X10^{-6} K^{-1}, α_{c*}=16.6X10^{-6} K^{-1}, α_v=32.2X10^{-6} K^{-1}.

The linear thermal expansion tensor at room temperature (RT) in the crystallographic system X_1//a, X_2//b, X_3// c* was given by

$$\alpha_{ij} = \begin{pmatrix} 11.5 & 0 & -3.41 \\ 0 & 3.98 & 0 \\ -3.41 & 0 & 16.6 \end{pmatrix} \times 10^{-6}\, K^{-1}$$

and the linear thermal expansion tensor in the principal systems X'_1//a, X'_2//b, X'_3// c is the following.

$$\alpha'_{ij} = \begin{pmatrix} 9.79 & 0 & 0 \\ 0 & 3.98 & 0 \\ 0 & 0 & 18.31 \end{pmatrix} \times 10^{-6}\, K^{-1}$$

The principal axis with maximum thermal expansion , X'_3 can be found 14.1° anticlockwise rotation from the *c* crystallographic axis with the positive *b* axis pointing towards the observer and the principal axis with medium thermal expansion X'_1 can be found at 26.6° clockwise from the *a* crystallographic axis. The thermal expansion ellipsoid for a 3at.%Ho:KLuW is shown in the figure 5. The thermal expansion is in accordance with un-doped KLuW [18].

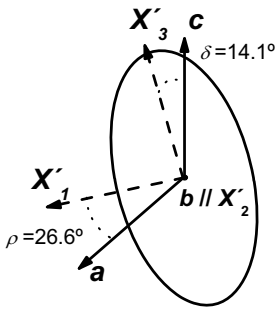

Figure 5 Thermal expansion ellipsoid of 3at.%Ho:KLuW

3.3 Optical absorption

Polarized optical absorption at room temperature of holmium in KLuW host was performed using the cut and polished crystal as mentioned earlier. We considered 1at.%Ho sample with concentration (9.307 x10^{19} at./cm^3) and thickness 2.91mm along N_p and 2.71mm along N_g. This concentration and thickness were sufficient enough to get a noise free signal and also to avoid saturation of the detectors. Figure 6 shows the polarized room temperature absorption cross section spectra of 1at.% Ho:KLuW crystal in the 300-2200 nm range where the reader could easily observe the anisotropy of this material. Polarization parallel to N_m shows in general the highest values of absorption cross section. Around 450 – 460 nm the $^5G_6$ level has the highest absorption cross section with a value of 25.86 x 10^{-20} cm^2.

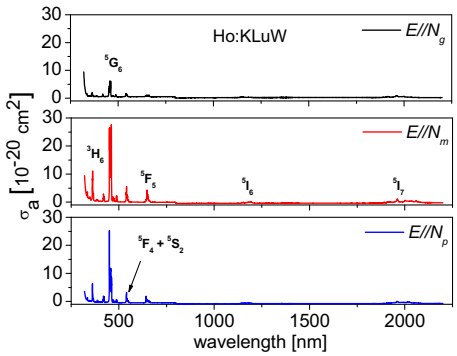

Figure 6 Polarised room temperature absorption cross-section of 1at.%Ho:KLuW crystal in the 300-2200 nm range

The splitting of different manifolds is in agreement with its multiplicity. In low temperature, the extra peaks caused by thermal population of various sublevels of ground state and possible vibronic peaks were eliminated. Figure (7a-7q) shows the polarized low temperature absorption spectra of each excited state from ground state of each manifolds and * indicates the electronic transitions of each sublevels. These experimentally determined sublevels are in agreement with the splitting expected by the crystalline field of similar host Ho:KGdW [21]. Table 2 shows 171 stark levels of Ho^{3+} in KLuW. The peaks are assigned by comparing the intensity of each of the polarizations N_g, N_m and N_p. Also it is worth mentioning in table 2, the label which were not in parentheses indicates the polarization character of every peak and the one in parenthesis indicates the contribution of the other polarization is also present in that peak.

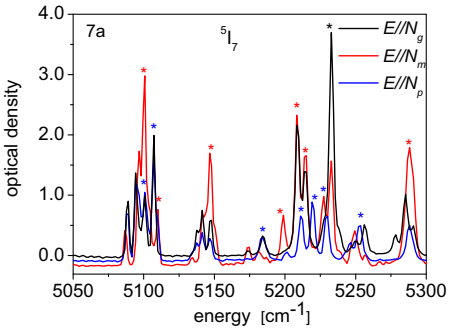

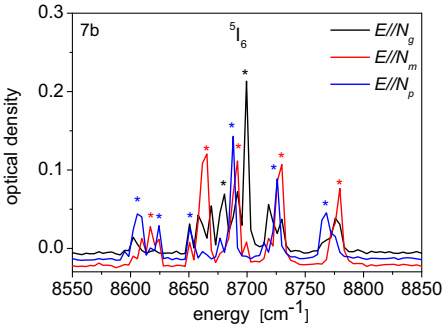

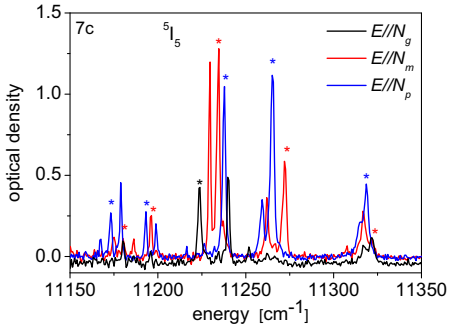

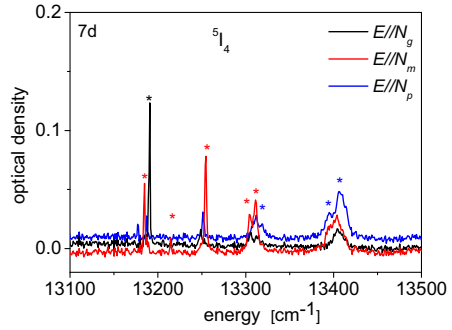

UNIVERSITAT ROVIRA I VIRGILI
INFRARED LASERS BASED ON HO3+:KRE(WO4)2 CRYSTALS WITH TM3+OR YB3+ AS SENSITIZERS
Venkatesan Jambunathan
ISBN:/DL: T.1243-2011

in

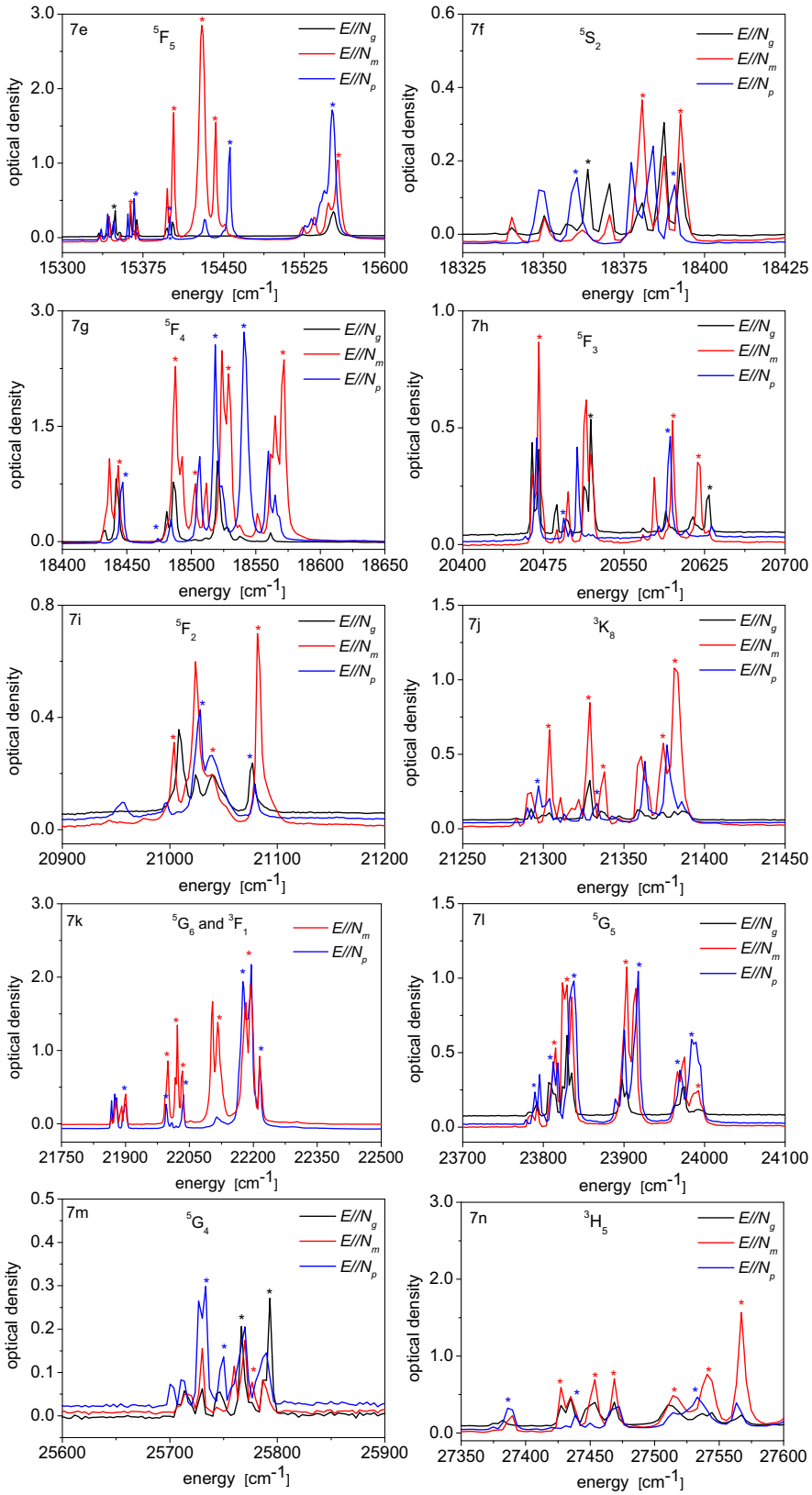

UNIVERSITAT ROVIRA I VIRGILI
INFRARED LASERS BASED ON HO3+:KRE(WO4)2 CRYSTALS WITH TM3+OR YB3+ AS SENSITIZERS
Venkatesan Jambunathan
ISBN:/DL: T.1243-2011

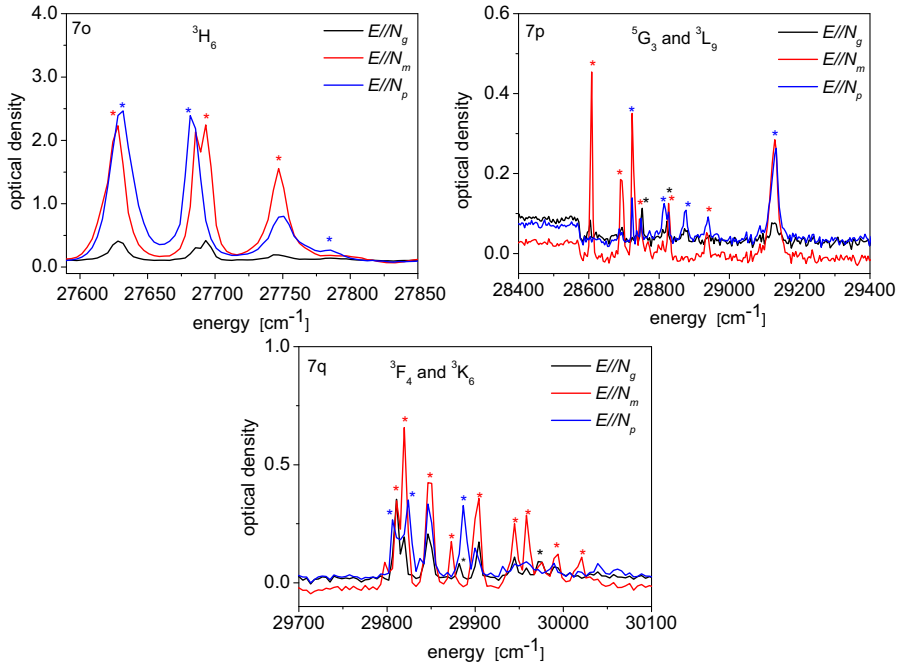

Figure7(a-q) Low temperature (6K) optical absorption of KLuW single crystal doped with holmium and recorded with polarized light parallel to the three principal optical directions N_g, N_m and N_p

$^{2s+1}L_J$	E //$N_{g,m,p}$	E_{exp} (cm^{-1})
$^5I_7$	m	5100
	p(g)	5101
	p(g)	5107
	mg(p)	5109
	mg(p)	5147
	p(g)	5184
	m	5199
	mg	5208
	p	5211
	mg	5214
	p	5219
	p	5230
	g(m)	5233
	p	5253
	m(p)	5288
$^5I_6$	p(mg)	8607
	m(p)	8618
	p(m)	8624
	p(g)	8651
	mg	8663
	g	8680
	p	8687
	mg	8690
	gm	8699
	p	8726
	mg	8728
	p	8766
	mg	8778
$^5I_5$	p	11173
	mg(p)	11180
	p	11193
	mg	11196
	g	11225
	m	11235
	p(g)	11238
	p	11259
	m	11272
	p(mg)	11319
	mg	11321
$^5I_4$	m	13185
	g	13191
	m	13214
	mg(p)	13254
	m	13305
	mg(p)	13314
	p	13319
	p(mg)	13394
	p(mg)	13407
$^5F_5$	g(p)	15349
	mg	15364
	p	15367
1 peak missing	p	15400
	mg	15403
	m	15430
	m	15442
	p	15456
	p(g)	15552
	m	15556
$^5S_2$	p	18360
	g	18364
	mg	18381
	p	18390
	mg	18393
$^5F_4$	mg	18442
	p	18446
	p	18474
	mg	18488
	m	18503
	p	18518
	m	18528
	p	18541
	m	18572
$^5F_3$	mg	20471
	p	20495
	g(m)	20520
	p(g)	20593
	m	20595
	m	20620
	g(p)	20629
$^5F_2$	m	21004
	p	21028
	gm(p)	21040
	p	21079
	m	21083
$^3K_8$	p	21297
	mg(p)	21304
	mg	21329
10 peaks missing	p	21333
	mg	21338
	m	21374
	m	21382
$^5G_6$ and $^5F_1$	p(m)	21900
	p	21966
	m	21999
	m	22022
	m	22032
6 peaks missing	p	22035
	m	22115
	p(m)	22177
	m(p)	22194
	p(m)	22218
$^5G_5$	p	23789
	p(g)	23812
1 peak missing	mg	23815
	mg	23830
	p	23837
	mgp	23903
	p(m)	23918
	p(mg)	23967
	p	23984
	m(p)	23994
$^5G_4$	p(mg	25734
	p(g)	25747
4 peaks missing	g(mp)	25767
	mg	25776
	g(mp)	25794
$^3H_5$	p(m)	27387
	mg	27427
	p(mg)	27439
2 peaks missing	mg	27453
	mg(p)	27469
	mg(p)	27515
	p(g)	27533
	mg	27541
	mg(p)	27567
$^3H_6$	m	27627
	p(g)	27631
7 peaks	p	27681

missing	mg	27694
	mg(p)	27747
	p	27783
G_3 and $^3L_9$	mg	28607
	mg(p)	28693
	p(m)	28725
	m(p)	28746
	g	28751
15 peaks missing	p	28816
	g	28822
	m	28828
	p(g)	28875

	m(p)	28937
	p(mg)	29129
$^3F_4$ and $^3K_6$	p	29807
	mg	29811
	mg	29821
	p	29823
8 peaks missing	mg(p)	29848
	m	29873
	g	29881
	p	29887
	mg(p)	29902
	mg(p)	29944

	m(p)	29959
	g(m)	29975
	mg(p)	29991
	m	30020
$^5I_8$		0
2 peaks missing	*	4
	*	6
	*	11
	*	21
	*	32
		43
		62

106
118
144
183
209
250
292

* were the extra peaks observed from the low temperature absorption measurement.

.

TABLE 2 Experimental energy levels, E_{exp}, (in cm^{-1}) and polarization label, $E//N_{g,p,m}$, of Ho^{3+} ions observed in the KLuW single crystal. The energy values of the Stark levels have experimentally been obtained by optical absorption and for the ground state ($^5I_8$), by photoluminescence at 6 K.

3.4 Photoluminescence

The objective of the photoluminescence experiment was to determine the emission properties of holmium ion at room temperature around 2.1 µm and also to determine the energy sublevels of the ground state ($^5I_8$ level) by low temperature emission experiments. The photoluminescence were carried out in the 5at.%Ho:KLuW crystal with concentration (4.119 x10^{20} at./cm^3) and was excited at 454 nm (22000cm^{-1}). This level was chosen for exciting the crystal for luminescence experiments because the absorption cross-section was maximum when compared to the other levels as mentioned earlier. After excitation, several de-excitation processes took place radiatively and non-radiatively as shown in the energy level diagram (Figure 8). We observed several emission channels like blue, green, red and infrared 2 µm emissions. We mainly focused on 2 µm emission which is of our interest to amplify it in a resonator. Figure 9a shows the un-polarized 2 µm emission spectrum measured and as can be seen it comprises of a broad emission band which extends from 1850 – 2100 nm. From the low temperature emission around 2 µm ($^5I_7 \rightarrow {}^5I_8$) and low temperature emission around 550 nm ($^5S_2 \rightarrow {}^5I_8$) we could determine the energy sublevels of the ground level $^5I_8$ (see table 2).

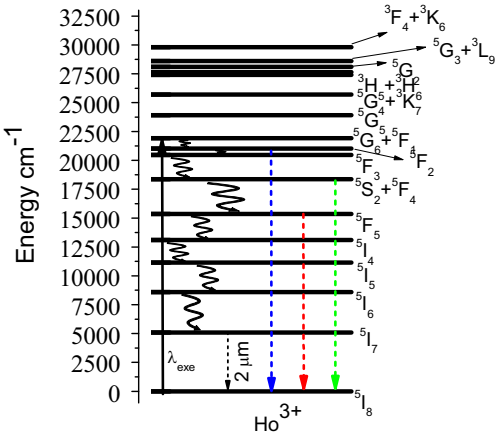

Figure 8 Energy level diagram of Ho^{3+} in KLuW

The important parameter which defines the laser performance of a material is the emission cross-section which can be calculated by reciprocity method (RM) [22] which makes use of the experimental absorption cross section and Füchtbauer-Ladenburg (FL) [22] method which makes use of the experimental emission and lifetime. To quantify and to compare the shape of the experimental photoluminescence obtained around 2 µm from Ho^{3+}, we first measured the optical absorption in the 1800 – 2200 nm range of single doped 5at.% Ho:KLuW crystal with light polarized parallel to the three principal optical directions, N_g, N_m *and* N_p. Later using RM method, we calculated the polarized emission-cross section and made the average of three polarizations since we use this to compare with the un-polarized experimental photoluminescence. With the FL method we also calculated emission cross-section. Figure 9b shows the average of absorption and the calculated emission cross sections using RM and FL methods.

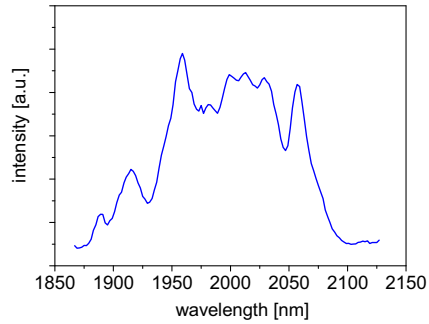

Figure 9a Un-polarized emission spectra of 5%Ho:KLuW in the 2 micron region.

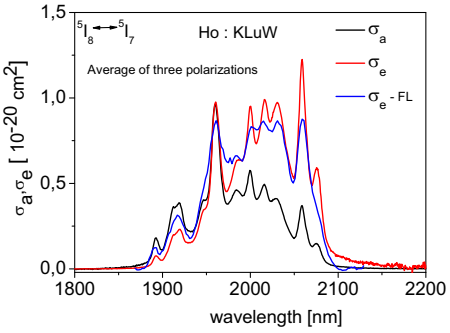

Figure 9b Calculated emission cross section using Reciprocity method and Fücht-Ladenburg method

It is inferred from figure 9b, the average emission cross-section at 2060 nm was ~1.22x 10^{-20} cm^2 with the RM method and ~0.87x 10^{-20} cm^2 with the FL

method and the shape of the spectra is quite similar in both cases.

It is worth knowing about the emission and gain-cross section for each of the principal optical directions because during laser experiments the sample will be oriented in any one of the principal optical directions. Figure 10 a, b, c shows the polarized absorption cross-section and calculated emission cross section using reciprocity method for $E//N_g,N_m$ and N_p principal optical directions respectively for Ho:KLuW. From the figures, we could estimate a maximum emission-cross section of ~0.76×10^{-20} cm^2 for $E//N_g$ at 2000 nm, ~2.42×10^{-20} cm^2 for $E//N_m$ at 2060 nm and ~1.29×10^{-20} cm^2 for $E//N_p$ at 2017 nm.

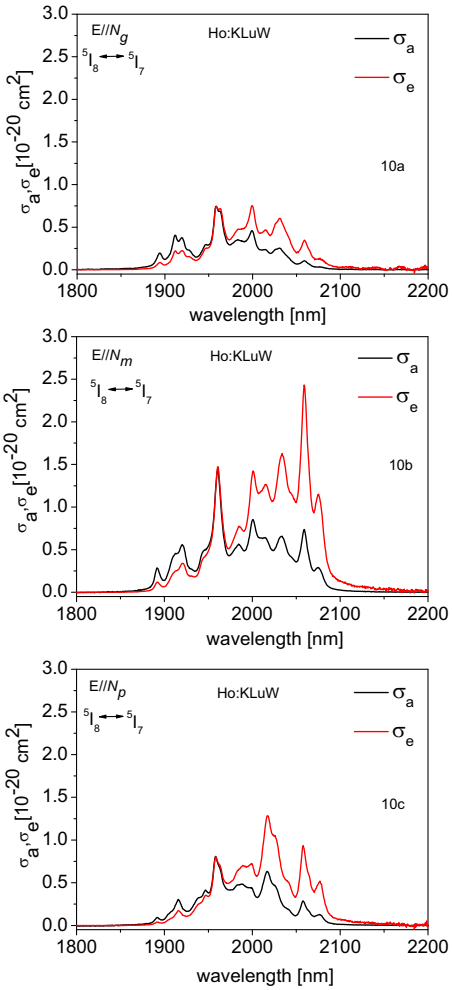

Figure 10 a,b,c Polarized absorption cross-section and calculated emission cross section for $E//N_g,N_m$ *and* N_p principal optical directions respectively for Ho:KLuW

We also computed the gain cross-section with the following expression:

$$\sigma_g = \sigma_e \times \beta - (1-\beta) \times \sigma_a$$

where σ_g is the gain cross-section, σ_a is the absorption cross-section, σ_e is the emission cross-section and β is the inversion population level.

Figure 11 a, b, c shows the calculated gain cross-section for $E//N_g,N_m$ *and* N_p principal optical directions respectively. From the figures it is inferred that for a maximum population inversion level of 0.5, positive gain is calculated for wavelength greater than 1960 nm and one could expect laser oscillation presumably at the maximum of the curve depending on how the losses are in the cavity.

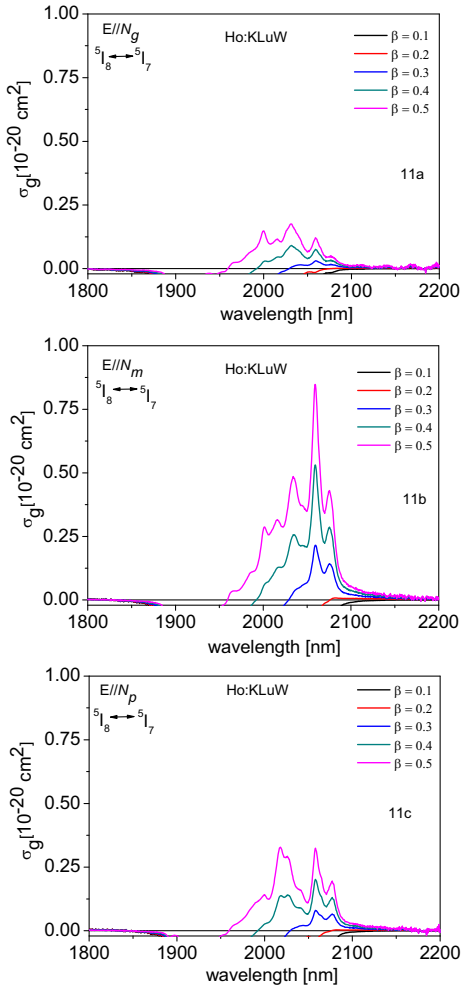

Figure 11 a,b,c Calculated gain cross section $E//N_g,N_m$ and N_p principal optical directions respectively

3.5 Decay time measurements

The decay time was measured by exciting the sample with wavelengths one at 1175 nm and the other at 914 nm. The monochromator was fixed at 2050 nm for both the exciting wavelengths and the decay curves were observed in a digital oscilloscope. We measured the life times for different concentrations and as example, figure 12 shows the light intensity decays of the $^5I_7$ level emission of 3at.% Ho:KLuW at different wavelengths

excitations. In all the cases the obtained decay curves were found to single exponential and the computed life time for various concentrations are tabulated in table 3.

at.% Ho	λ_{exe} [nm]	τ [ms]	λ_{exe} [nm]	τ [ms]
1at.%	1175	5.5	914	5.8
3at.%	1175	8.4	914	8.4
5at.%	1175	7.8	914	9.2

TABLE 3 Decay time measurement at different excitation wavelength in Ho^{3+}:KLuW crystals

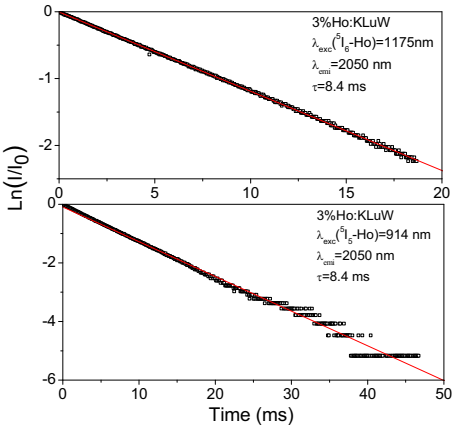

Figure 12 Light intensity decays of the $^5I_7$ level emission of 3at.%Ho: KLuW at different wavelength excitations

From table 3 we can infer the measurement of the life time was affected by re-absorption in the case of 3 and 5at.% crystals because it is longer than the radiative life time calculated using the Judd-Ofelt approach (5.863 ms for the $^5I_7$ level of Ho:KGdW) [21] and there is no significant change in the measured life time by exciting the crystals at different wavelengths. In order to avoid the re-absorption we plan to measure dacay time using powder or thinner samples.

3.6 Laser experiments

Laser experiments were carried out with the setup described in the experimental section. CW laser action was realized for 3at.%Ho:KLuW and for 5at.%Ho:KLuW. In all cases the incident power was limited to 2.3 W in order to avoid damage of the active media since the pump spot was of the order of 30 µm. Figure 13 and 14 show the input-output characteristics of the 3at.% and 5at.% Ho:KLuW lasers, respectively with RC=50mm, f=50mm and T_{oc}=1.5, 3 and 5% with physical cavity length 50±1 mm.

From the figures it is inferred that 5 at.% Ho:KLuW crystal gives higher output power when compared to 3at.% Ho:KLuW. Note that in the previous work laser operation was achieved in only 3at.% Ho:KLuW uncoated crystal [23], however in this work the output power is improved with the coating of the crystals and even laser action is achieved with higher doping level (5at.%). A summary of the laser results is shown in table 4.

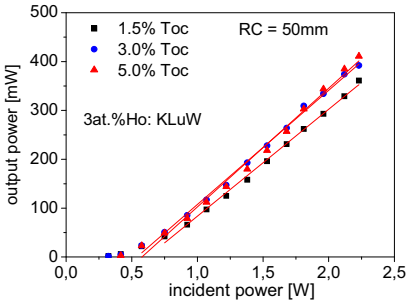

Figure 13 Output power vs. incident power of 3at.%Ho:KLuW laser

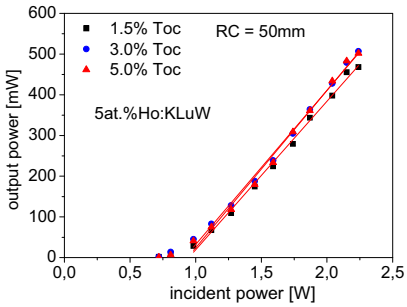

Figure 14 Output power vs. incident power of 5at.%Ho:KLuW laser

Sample	T_{oc} %	P_{out} [mW]	η [%]	P_{th} [mW]	λ [nm]
3%Ho: KLuW	1.5	361	21.9	323	2080
	3.0	392	23.4	323	2079
	5.0	411	24.3	417	2077
	20.0	-	-	-	2060
5%Ho: KLuW	1.5	468	36.4	720	2080
	3.0	507	37.9	720	2080
	5.0	502	38.6	720	2078
	20.0	-	-	-	2060

Table 4 Summary of laser results with R_{OC} = 50 mm, η: slope efficiency, P_{th}: laser threshold, λ: laser wavelength

It can be observed in both curves, power scaling could be realized since we didn't observe any limitation due to thermal loading during laser operation. Also one could observe a shift towards shorter laser wavelengths in both cases with the increase of the transmission of the output coupler (see table 4). This is typical for quasi-three level laser systems and is clearly observed when we used an output coupler with T_{OC}=20%. The shift in wavelength is in accordance with the gain curve (see figure 11 b). The explanation to this fact is due to the effect of the crystal field on the Stark level components. Thus, with T_{OCS} ranging from 1.5% to 5%, the emission is attributed to the first three lowest Stark levels of the $^5I_7$ multiplet to the highest Stark level of the ground state, $^5I_8$ and for T_{OC}=20%, the emission is attributed to a transition from the fifth Stark level of $^5I_7$ to the highest Stark level of the ground state.

4 Conclusions

In conclusion, we have grown macro defect free Ho:KLuW crystals of different doping concentrations by the Top Seeded Solution Growth - Slow Cooling (TSSG-SC) method. These crystals were structurally, compositionally and spectroscopically characterized so that the material properties prior to laser experiments were understood. Finally, the laser was generated in 3 and 5at.% Ho:KLuW crystals in-band pumped using a Tm:KLuW laser. The latter crystal delivered maximum output power of 507 mW and the corresponding slope efficiency amounted to 38% centered at 2079 nm. Future work focuses on the power scaling of these infrared lasers using diode lasers as pump sources with optimized doping levels, thickness and pump wavelength.

Acknowledgements

This work was supported by the Spanish Government under projects MAT2008-06729-C02-02/NAN, MAT2008-04046-E/MAT, TEC2010-21574-C02-02, PI09/90527, HF2008-0045, DE2009-0002 and the Catalan Authority under project 2009SGR235. J. J. Carvajal is supported by the Education and Science Ministry of Spain and European Social Fund under the Ramon y Cajal program, RYC2006–858. V. Jambunathan would like to thank the Spanish ministry of education through the student mobility program, TME2009-00417. We also acknowledge support from the EC's Seventh Framework program (LASERLAB-EUROPE, grant agreement nº 228334) and the German-Spanish bilateral program Acciones Integradas (DAAD ID 50279160).

References

1 S. Pierre, G. M. Preminger, World J. urology 25, 235 (2007).
2 R. Targ, M. J. Kavaya, R. M. Huffaker, and R. L. Bowles, Appl. Opt. **30**, 2013 (1991).
3 S. W. Henderson, C. P. Hale, J. R. Magee, M. J. Kavaya, and A. V. Huffaker, Opt. Lett. **16** , 773 (1991).
4 P. A. Budni, L.A. Pomeranz, M.L. Lemons, C.A. Miller, J.RMosto, and E.P. Chicklis, J. Opt. Soc. Am. B, **17**, 723 (2000).
5 V. Sudesh and K. Asai, J. Opt. Soc. Am. B **20**, 1829 (2003).
6 Atsushi Sato, Kazuhiro Asai, Kohei Mizutani, Opt. Lett. **29**, 836 (2004).
7 R. C. Stoneman and L. Esterowitz, Opt. Lett. **17**, 736 (1992).
8 S. So, J. I. Mackenzie, D. P. Shepherd, W. A. Clarkson, J. G. Betterton, E. K. Gorton, and J. A. C. Terry, Opt. Express **14**, 0481 (2006).
9 D. Xiao-Ming, Y. Bao-Quan , Z. Yun-Jun, S. Cheng-Wei, G. Jing, J. You-Lun, W. Yue-Zhu, Chin. Phys. Lett. **25**, 1693 (2008).
10 B. Q. Yao, L. L. Zheng, R. L. Zhou, X. M. Duan, Y. J. Zhang, Y. L. Ju, Z. Wang ,G. J. Zhao, and Q. Dong, Laser Physics, **18**, 1501 (2008).
11 B.Q. Yao, X. M. Duan, L. L. Zheng, Y. L. Ju, Y.Z. Wang, G. J. Zhao and Q. Dong, Opt. Express **16**, 14668 (2008).
12 D.Y. Shen, A. Abdolvand , L. J. Cooper, W.A. Clarkson, Appl. Phys. B **79**, 559 (2004).
13 V. Petrov, M. C. Pujol , X. Mateos, Ó. Silvestre , S. Rivier, M. Aguiló, R. M. Solé, J. Liu, U. Griebner and F. Díaz, Laser & Photon. Rev. **1**, 179 (2007).
14 M. C. Pujol, M.A. Bursukova, F. Güell, X. Mateos, R. Solé, Jna. Gavaldà, M. Aguiló, J. Massons, F. Díaz, P. Klopp, U. Griebner, and V. Petrov, Phys. Rev. B **65**, 165121–1 (2002).
15 X. Mateos, V. Petrov, J. Liu, M.C. Pujol, U. Griebner, M.Aguiló, F. Díaz, M. Galan, and G. Viera, IEEE J. Quantum Electron. **42**, 1008 (2006).
16 R. Solé, V. Nikolov , X. Ruiz , Jna. Gavaldà, X. Solans , M.Aguiló, F. Diaz , J. Cryst. Growth **169,** 600 (1996).
17 R. Solé, O. Silvestre, J. Massons, Jna. Gavaldà, M.Aguiló,F. Díaz , J. Cryst. Growth **310**, 1167 (2008).
18 M.C. Pujol, X. Mateos, A. Aznar, X. Solans, S. Suriñac, J. Massons, F. Díaz, and M. Aguiló, J. Appl. Cryst. **39**, 230 (2006).
19 J. Rodriguez-Carvajal, "An introduction to the program Full prof 2000", Laboratorie Léon Brillouin, CEA-CNRS, Saclay, France, 2001.
20 R. D. Shannon, Acta Cryst. A **32**, 751 (1976).
21 M. C. Pujol, J. Massons, M. Aguilo, F. Diaz, M. Rico and C. Zaldo, IEEE J. Quantum Electron. **38**, 93 (2002).
22 S. A. Payne, L. L. Chase, L. K. Smith, W. L. Kway and W. F. Kruple, IEEE J. Quantum Electron **28**, 2619 (1992).
23 X. Mateos, V. Jambunathan, M. C. Pujol, J. J.Carvajal, F. Díaz, M. Aguiló, U. Griebner and V. Petrov, Opt. Express **18**, 20793 (2010).

Paper IV

Growth and spectroscopy of (Ho,Yb):KLu(WO_4)$_2$ crystals

V. Jambunathan, X. Mateos, M. C. Pujol, J. J. Carvajal, M. Aguiló and F. Díaz

Physics Procedia 8 ,162–167 (2010).

UNIVERSITAT ROVIRA I VIRGILI
INFRARED LASERS BASED ON HO3+:KRE(WO4)2 CRYSTALS WITH TM3+OR YB3+ AS SENSITIZERS
Venkatesan Jambunathan
ISBN:/DL: T.1243-2011

Available online at www.sciencedirect.com
ScienceDirect
Physics Procedia 8 (2010) 162–167
Physics Procedia
www.elsevier.com/locate/procedia

VI Encuentro Franco-Español de Química y Física del Estado Sólido
VI[ème] Rencontre Franco-Espagnole sur la Chimie et la Physique de l'État Solide

Growth and spectroscopy of (Ho,Yb):$KLu(WO_4)_2$ crystals

Venkatesan Jambunathan, Xavier Mateos*, Maria Cinta Pujol, Joan Josep Carvajal, Magdalena Aguiló and Francesc Díaz

Física i Cristal·lografia de Materials i Nanomaterials (FiCMA-FiCNA), Universitat Rovira i Virgili (URV), Campus Sescelades c/Marcel·lí Domingo, s/n, E-43007 Tarragona, spain.

Abstract

We report the crystal growth and optical spectroscopy of co-doped monoclinic (Ho,Yb):$KLu(WO_4)_2$ single crystals. Macro-defect free single crystals with different co-doping ratios were grown by using Top Seeded Solution Growth -Slow Cooling method (TSSG –SC). The spectroscopic characterization at room temperature of this material in terms of polarized optical absorption and photoluminescence was performed showing that this compound is a potential solid state laser material for the generation of 2 μm laser emission.

Keywords: Optical absorption; Photoluminescence; Ho^{3+}, Yb^{3+}, Double tungstate crystals.

1. Introduction

The development of eye-safe solid-state lasers in the near infrared range is of special interest due to their potential scientific and technological applications. Intense research is devoted to generate laser emission around 2 μm from Tm^{3+} and Ho^{3+} ions because of their eye safe nature and practical applications in the field of medicine and remote sensing [1]. In particular, the emission from Ho^{3+} is slightly above the 2 μm but the technological problem of efficient pumping of Ho^{3+} is the reason why many authors used Tm^{3+} as sensitizer of the Ho^{3+} [2,3]. On the other hand, the use of Yb^{3+} [4,5] as sensitizer of Ho^{3+} is also an option due to efficient energy transfer between Yb^{3+} and Ho^{3+} and also the existence of commercially available high-power diode lasers operating around 980 nm suitable for pumping Yb^{3+} ions.

The monoclinic double tungstate crystals, $KRE(WO_4)_2$ (RE = Y,Gd and Lu), shortly KREW, have demonstrated to be excellent laser hosts for several laser active ions. For example, efficient laser action of Yb^{3+} around 1μm and Tm^{3+} around 2μm has been reported [6]. These materials stand out because of the large absorption and emission cross-section and the long ion-to-ion separation that makes the doping at high levels feasible with reduced

* Corresponding author. Tel.: +34 - 977558790.
E-mail address: xavier.mateos@urv.cat

1875-3892 © 2010 Published by Elsevier Ltd.
doi:10.1016/j.phpro.2010.10.028

concentration quenching of the fluorescence. These features made us confident that the Ho-doped KREW crystals could be used for IR laser generation well above 2 μm.

In this context, our goal was to study the 2.1 μm infrared emission from Ho^{3+} in an optical system co-doped with Yb^{3+}. The host where the two ions are embedded is the monoclinic potassium lutetium double tungstate ((Ho,Yb):$KLu(WO_4)_2$ here after (Ho,Yb):KLuW)). KLuW crystals crystallize in the monoclinic system with space group *C2/c* and point group 2/m. The cell parameters are a = 10.576 (7) Å, b = 10.214 (7) Å, c = 7.487 (2) Å and β= 130.68 (4)° [7].

In this work, we present the growth and spectroscopy of (Ho,Yb):KLuW crystals showing their potential as a solid state laser material around 2μm.

2. Experimental details

To grow the single crystals we used the Top Seeded Solution Growth Slow Cooling (TSSG-SC) method using a vertical tubular furnace with kanthal wire as heating element and an Eurotherm903P temperature controller/programmer with thermocouples to control the temperature. The powder precursors were K_2CO_3, WO_3, Lu_2O_3, Ho_2O_3 and Yb_2O_3 with analytical grade of purity. We mixed them stoichiometrically, so that the solution had a binary composition of 12mol% (Ho,Yb):KLuW as solute and 88 mol% $K_2W_2O_7$ as solvent. The seed was rotated during the growth process to ensure the presence of a forced convective flow near the crystal in order to enhance mass and heat transport conditions in the solution to avoid inclusions during the growth process and no pulling was applied.

Taking into account the high anisotropy of the monoclinic KLuW crystals [6], the samples were cut and polished along the principal optical directions, namely $\boldsymbol{N_g}$, $\boldsymbol{N_m}$ and $\boldsymbol{N_p}$ as parallelepipedic prisms with faces perpendicular to the principal optical axes. A Cary Varian 500 spectrophotometer was used to measure the optical absorption and emission spectra were recorded using a Ti:Sapphire laser as pump source and the luminescence was collected to a 34 cm Jobin –Yvon monocromator. Three kind of diffraction grating elements namely 300 groves/mm , 600 groves/mm and 1200 groves/mm were used for dispersion of the fluorescence depending on the wavelength range to be detected. For detection of 2 μm emission we used a cooled InAs detector which was connected to a preamplifier and to a lock-in amplifier. For visible measurement a PMTR928 photomultiplier tube was used and for near infrared emission a cooled R5509-72 photomultiplier was used. A computer was used to store the data for final processing.

3. Result and discussion

Macro-defect free single crystals with different co-doping ratios were grown by the TSSG- SC method as mentioned earlier.To obtain the single crystals, 200 g of the power mixture were introduced in a platinum crucible of 50 mm in diameter and 50 mm in height, that was inserted in the vertical tubular furnace. The axial temperature gradient in the solution was ~1.5 – 2 K/cm. The seeding process was realized with a ***b*** crystallographic oriented seed located at the centre of the surface of the solution. After accurately determining the saturation temperature by observing the growth and dissolution of the seed in contact with the surface of the solution, the crystals grew without pulling due to the super-saturation created by slow cooling at the rate of 0.1K/h for ~20K. After the crystals grew, they were removed slowly from the solution and kept above its surface while the furnace was cooled to room temperature at a rate of 25K/h to avoid thermal shock of the crystals. The growth methodology is described in a more detailed way in a previous work [8].

Table 1 gives the summary of the grown crystals. The saturation temperature is in the range of 1168 – 1182 K. The cooling rate was fixed at 0.1K/h because this rate was sufficient enough to ensure high quality crystals. The weight of the crystals ranges from 4.40– 8.44g The growth rate of the co-doped (Ho,Yb):KLuW crystals was in the range of 226 – 356 x 10^{-4} g/h and it is inferred that the growth rate increases with increasing the dopant concentration except the first crystal. The dimension of the crystals were typically 17 – 19 mm, 9 – 15 mm and 5 – 8 mm along the *c, a** and *b* crystallographic directions, respectively. The quality of the grown crystals was good.

Figure.1(left) shows the photograph of co-doped 0.5 at. %Ho 0.5 at. % Yb:KLuW single crystal as an example and Figure.1(right) shows the morphological scheme of the grown crystals. From the morpholical scheme it is also inferred that the (Ho,Yb):KLuW crystals follows the same morphology as that of undoped KLuW[7] crystal which is formed by the {110}, {-111}, {010}, and {310} faces.

Table 1: Summary of crystals grown in this work

at. % Ho	at. % Yb	Saturation temp. [K]	Cooling interval [K]	Crystal weight[g]	Growth rate x 10^{-4} [g/h]	Crystal dimension [mm] c	a*	b
0.5	0.5	1168.05	23.6	5.85	248	17.87	10.18	7.80
0.5	2.5	1164.55	19.5	4.40	226	18.21	9.75	6.77
1.5	2.5	1182.65	23.8	5.61	236	17.34	9.55	6.89
2.5	2.5	1177.25	17.0	5.27	310	18.61	10.90	5.10
3.5	2.5	1173.30	19.5	6.58	338	15.77	13.51	6.62
3.5	3.5	1174.10	21.0	7.45	355	19.08	12.03	6.09
3.5	5.0	1178.75	23.7	8.44	356	17.21	14.84	7.08

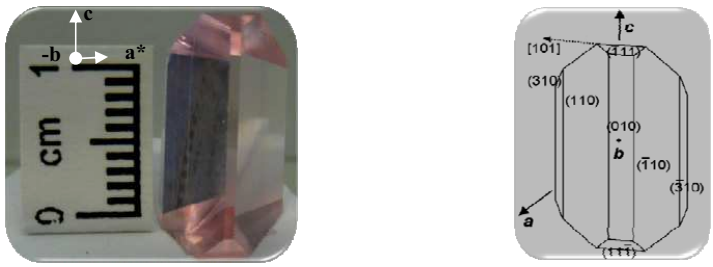

Figure 1: Left: Photograph of (Ho,Yb):KLuW crystal; right: Morphological scheme of the grown crystal.

Figure 2 shows the room temperature absorption coefficient in the 300 –2400 nm range, with polarized light parallel to the N_m principal optical axis for the 1.5at.%Ho2.5at.%Yb:KLuW crystal. Only one polarization is shown for the sake of clarity. The labelled manifolds were associated with the transition from ground state to the higher excited states of Ho^{3+} and Yb^{3+}, respectively.

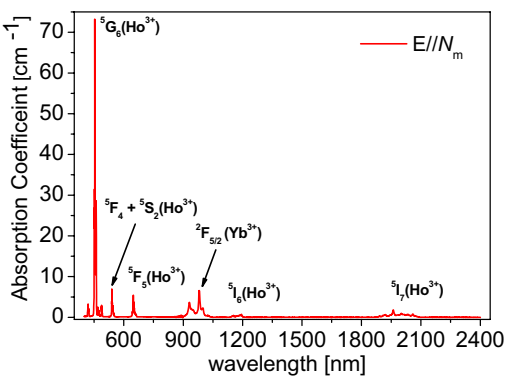

Figure 2 : Polarised optical absorption spectra of the (Ho,Yb):KLuW in the 300 – 2200 nm range for E//N_m.

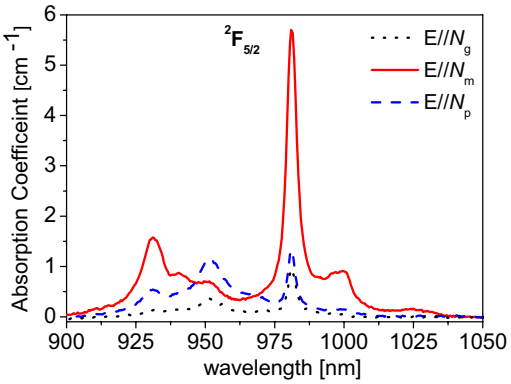

Figure 3: Polarised optical absorption (Ho,Yb):KLuW in the 900– 1050 nm range.

Figure 3 shows the absorption coefficient in the 900- 1050 nm range. It shows that the absorption of Yb^{3+} is rather broad and this makes the requirement for the pump source to be less strict in terms of line-width, so that diode pump could be perfectly used for laser action.

Absorption, emission and gain cross section calculations were carried out for single doped 5at.% Ho:KLuW and the relevant details can be found in a previous work [9]. Net gain indicates that laser oscillation is possible and is especially high for 2060 nm for N_m polarization, where we found a sharp maximum in the gain curves. The difficulties to achieve laser emission in these crystals will be: firstly, the high threshold due to the energy transfer process and the quasi-three level nature of this IR transition in Ho^{3+} ions; and secondly the losses due to upconversion processes.

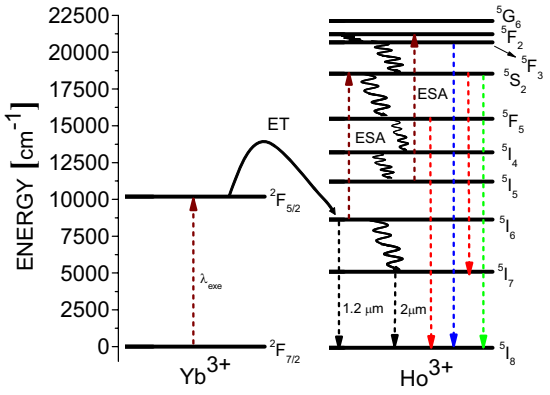

Figure 4 : Energy level scheme of the codoped (Ho^{3+},Yb^{3+}) system

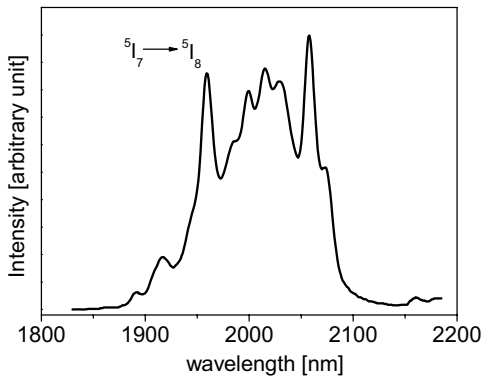

Figure 5 : 2 μm emission from Ho^{3+} after excitation of Yb^{3+} at 980nm.

The generation of the emission channels from the (Ho,Yb):KLuW system is well explained with the help of the energy level scheme shown in Figure 4. After excitation of ytterbium at $^2F_{5/2}$ level, part of the energy is transferred to populate the holmium $^5I_6$ level. As soon as this $^5I_6$ level gets populated, two different ways of electronic depopulation occur. The first way is the population (up-conversion) of the $^5S_2$ level by excited state absorption (ESA) process and the second way is the depopulation (down-conversion), which is the generation of 1.2 micron emission and also, the population of lower $^5I_7$ level via non-radiative mechanism. This $^5I_7$ is the emission level from where the 2μm emission occurs. A second excited state absorption also occurs from $^5I_5$ level (populated via multiple non-radiative multiphonon decay processes from $^5S_2$ level), since the energy difference between $^5I_5$ and $^5F_2$ level is almost resonant to the pump, which makes the $^5F_2$ level populated. Both up-converting processes lead to populate the $^5S_2$ level, from where a very high green fluorescence is emitted. The blue fluorescence emission is from the $^5F_3$ level. The red fluorescence emissions are from the $^5S_2$ and $^5F_5$ levels. The mechanism of energy transfer from Yb^{3+} to Ho^{3+} has been also reported in other hosts [10,11].

The photoluminescence was done out by exciting the crystals at 980 nm using a Ti:Sapphire laser as pump source for the 1.5at.%Ho2.5at.%Yb:KLuW crystal and the emission channels were detected as mentioned earlier. Figure 5 shows the 2 μm emission which is of our interest and the transition is from $^5I_7$ to $^5I_8$ level of Ho^{3+}. Figure 6 shows the ~1.2 μm which is the transition from $^5I_6$ to $^5I_8$ level of Ho^{3+}. Figure 7 shows the visible emissions from $Ho3^+$ with a clear domain of the green emission.

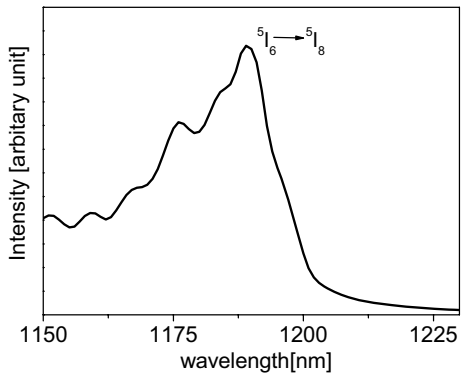

Figure 6 : 1.2 μm emission from Ho^{3+} after excitation of Yb^{3+} at 980nm.

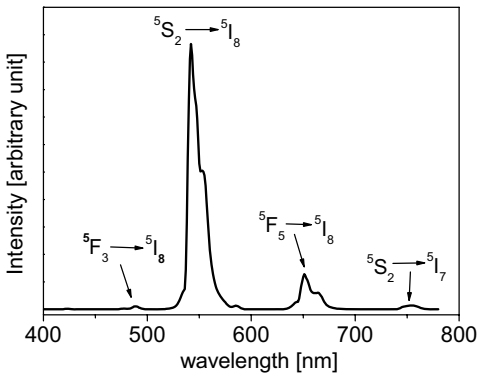

Figure 7 : Visible emissions from Ho^{3+} after excitation of Yb^{3+} at 980nm.

5. Conclusions

In summary, we have successfully grown macro-defect free (Ho,Yb):KLuW single crystals at several co-doping ratios by the TSSG–SC method. The spectroscopic characterisation of this material in terms of polarized optical absorption and photoluminescence was performed showing that it is a potential solid state laser material for the generation of 2 μm emission. Our future work is devoted to laser generation at 2μm wavelength with diode or Ti: Sapphire laser pumping.

Acknowledgements

This work was supported by the Spanish Government under projects MAT2008-06729-C02-02/NAN, MAT2008-04046-E/MAT, TEC2010-21574-C02-02, PI09/90527, HF2008-0045, DE2009-0002 and the Catalan Authority under project 2009SGR235. Joan Josep Carvajal is supported by the Education and Science Ministry of Spain and European Social Fund under the Ramon y Cajal program, RYC2006 – 858.

References

[1] K. Scholle, S. Lamrini, P. Koopmann and P. *Fuhrberg 2 μm Laser Sources and Their Possible Applications* book chapter form Frontiers in Guided Wave Optics and Optoelectronics, edited by Bishnu Pal and published by Intech, 471- 500 (2010).

[2] H. Hemmati, 2*.07–μm CW diode laser pumped Tm,Ho:YLiF$_4$ room temperature laser* Optics Letters, 14, 435-437(1989).

[3] V. Sudesh and K. Asai *Spectroscopic and diode pumped laser properties of Tm,Ho:YLF; Tm,Ho:LuLF; and Tm,Ho:LuAG crystals : a comparative study*" Journal of the Optical Society of America. B, 20, 1829- 1837(2003).

[4] A. Diening and S. Kück, *Spectroscopy and diode-pumped laser oscillation of Yb^{3+}, Ho^{3+}-doped yttrium scandium gallium garnet* Journal of Applied Physics, 87, 4063– 4068(2000).

[5] Th. Rothacher, W. Lüthy, H.P. Weber, *Diode pumping and laser properties of Yb:Ho:YAG* Optics Communications, 155, 68–72(1998).

[6] V. Petrov, M.C. Pujol , X. Mateos, Ó. Silvestre ,S. Rivier, M. Aguiló, R . M. Solé, J . Liu ,U. Griebner and F. Díaz, *Growth and properties of KLu(WO$_4$)$_2$, and novel ytterbium and thulium lasers based on this monoclinic crystalline host* Laser & Photon. Rev.1,2, 179-212(2007).

[7] M.C. Pujol, X. Mateos, A. Aznar, X. Solans, S. Suriñac, J. Massons, F. Díaz, and M. Aguiló, *Structural redetermination, thermal expansion and refrective indices of* $KLu(WO_4)_2$ J. Appl. Cryst., 39, 230-236 (2006).

[8] R. Solé, V. Nikolov , X. Ruiz , Jna. Gavaldà, X. Solans , M. Aguiló, F. Diaz , *Growth of* β *-*$KGd_{1-x}Nd_x(WO_4)_2$ *single crystals in* $K_2W_2O_7$ *solvents* Journal of crystal growth, 169, 600-603(1996).

[9] V. Jambunathan, X. Mateos, M.C. Pujol, J.J. Carvajal, J. Massons, M. Aguilo, and F. Diaz, *Near - infrared photoluminescence from* Ho^{3+}*-doped monoclinic* $KLu(WO_4)_2$ *crystal codoped with* Tm^{3+} J. Lum., 129, 1882-1885 (2009).

[10] R. Wälti, W. Lüthy, H.P. Weber, S.YA. Rusanow, A.A. Yakpvñev, A.I. Zagumenyi, I. Shcherbakov and A.F. Umyskov, Yb^{3+}/Ho^{3+} *energy exchange mechanisms in Yb:Ho:YAG crystals for 2μm or 540nm lasing* J.Quant. Specrosc. Radiat. Transfer, 4, 671- 681(1995).

[11] H. Wang, C. Tu, Z. You, F. Yang, Y. Wei, Y. Wang, J. Li, Z. Zhu, G. Jia, X. Lu, *Conversion of infrared radiation into visible emission in* $NaGd(WO_4)_2$*:*Yb^{3+}*,* Ho^{3+} *crystals* Appl. Phys. B, 88, 57–60 (2007)

UNIVERSITAT ROVIRA I VIRGILI
INFRARED LASERS BASED ON HO3+:KRE(WO4)2 CRYSTALS WITH TM3+OR YB3+ AS SENSITIZERS
Venkatesan Jambunathan
ISBN:/DL: T.1243-2011

Paper V

Control of the cool/warm white light generation from lanthanide ions in monoclinic double tungstate crystals

V. Jambunathan, X. Mateos, M. C. Pujol, J. J. Carvajal, M. Aguiló and F. Díaz

Journal of Luminescence (Accepted).

UNIVERSITAT ROVIRA I VIRGILI
INFRARED LASERS BASED ON HO3+:KRE(WO4)2 CRYSTALS WITH TM3+OR YB3+ AS SENSITIZERS
Venkatesan Jambunathan
ISBN:/DL: T.1243-2011

UNIVERSITAT ROVIRA I VIRGILI
INFRARED LASERS BASED ON HO3+:KRE(WO4)2 CRYSTALS WITH TM3+OR YB3+ AS SENSITIZERS
Venkatesan Jambunathan
ISBN:/DL: T.1243-2011

Control of the cool/warm white light generation from lanthanide ions in monoclinic double tungstate crystals

V. Jambunathan, X. Mateos*, M. C. Pujol, J. J. Carvajal, F. Díaz and M. Aguiló
Física i Cristal·lografia de Materials i Nanomaterials(FiCMA-FiCNA). Universitat Rovira i Virgili (URV), c/ Marcel·lí Domingo, s/n. E-43007 Tarragona, Spain
** Corresponding author: xavier.mateos@urv.cat*

We studied the physical effects arising from the combination of several concentrations of luminescent ions, Ho, Tm and Yb in a biaxial crystal to achieve the optimum multicolour emission for cool or warm white light generation. White light is generated by the simultaneous emission and combination of three photons at wavelengths, 475 nm (blue), 542 nm (green) and 651 nm (red) with associated energies, 21053 cm^{-1}, 18450 cm^{-1} and 15361 cm^{-1}, respectively. The physical mechanism that generated the white light involved the absorption of infrared photons and after partial energy transfer to neighboring ions, excited state absorption and upconversion phenomena took place to combine the emerging photons at the above wavelengths. White light is generated with rather high efficiency and very low excitation threshold. The control of simultaneous light generation is accomplished with the amount of dopant ions in the crystal.

1. Introduction

Solid-state lighting is one of the most promising areas for energy saving that Governments, companies and scientists pursued for several years. It is, and will be, an important research target for the next decade. Among all solid-state light emitters, light emitting diodes (LEDs) are, by far, the most studied systems as sources of illumination as well as organic light emitting diodes (OLEDs) and polymer light emitting diodes (PLEDs) [1].

Many works have been devoted to the generation of visible light produced in luminescent ions embedded in solid-state materials, glasses and crystals. Such a visible light usually makes reference either to the blue, green or red colours, which are the fundamental components or primary colours of white light, but that are in general independently generated. With the advent of efficient and relatively cheap laser diodes, the physical phenomenon of up-conversion in such luminescent ions enables the generation of visible light from infrared radiation by suitable lanthanide (Ln^{3+}) combinations [2, 3]. Up to now, only few works are devoted to this multicolour generation using the singular combination of Ho, Tm and Yb as multicolour emitters, see for example [4]. The Yb ion acts as absorbing ion of the infrared pump wavelength due to its advantages: (i) It has a broad absorption band which means that the requirements to the linewidth of the pump sources are not crucial making them cheaper, and (ii) it only shows an excited energy level in its electronic structure, so that the absorbed energy will be almost completely transferred to the visible emitter ions with minimum losses. The neighbours, Ho and Tm ions stand out because they show intense green, blue and red luminescence simultaneously.

Apart from the exotic combination of luminescent ions, the host in which they are embedded plays also a very important role. We choose a monoclinic (biaxial) crystal, with complex optics because the luminescent ions show in this crystal a very large transition (absorption and emission) cross-sections, which means high efficiency in the absorption-emission process due, in part, by the biaxial nature of the crystal. This host is the monoclinic phase of the potassium lutetium double tungstate ($KLu(WO_4)_2$), shortly KLuW. In addition, the Lu ion, accepts to be substituted for Yb, Tm and Ho with very low crystalline lattice distortion, ensuring very high crystalline quality.

In this work, we studied the white light generation in (Ho,Tm,Yb):KLuW crystals. For this, we first grew several doping combinations of crystals and studied the optical absorption and visible photoluminescence of these materials.

2. Experimental

To investigate the physical background of the white light generation and control the increase of red photons (warm white light), we grew codoped (Ho,Yb):KLuW and (Tm,Yb):KLuW crystals and triply doped (Ho,Tm,Yb):KLuW crystals at different doping levels by the Top Seeded Solution Growth Slow-Cooling method (TSSG-SC). The methodology of growth was described elsewhere [5]. The chemical composition of the grown single crystals was measured using Elecron Probe Micro Analyser (EPMA) with Cameca sx50 equipment. Due to the high anisotropy of KLuW crystals, those were cut and polished with faces perpendicular to the principal optical directions N_g, N_m and N_p (they are defined by $n_p<n_m<n_g$ which are related to the principal refractive indices). The room- and low-temperature absorption spectra were measured with a Glam Thomson polarizer in front of the sample and were recorded using a Cary Varian 500 spectrophotometer. For low-temperature measurements we used a cryostat from Oerlikon Leybold Vacuum GmbH (coolpak 6000 model) with liquid helium to cool the samples. Room and low temperature photoluminescence was performed by exciting the crystal using a Ti:Sapphire laser and the signal was collimated on a 460 mm Jobin-YVon monocromator and then dispersed using a grating with 1800 groves/mm. For detecting the signal a PMTR928 photomultiplier tube was used and was amplified using lockin amplifier. A computer was used to store the data for final processing.

3. Result and discussions

3.1. Crystal growth

The crystals studied in this work were grown in a platinum crucible of 50 cm in diameter and 50 cm in height, 200 g of the solution mixture (12 mol.% KLuW as solute – 88.0 mol.% $K_2W_2O_7$ as solvent). Raw materials were K_2CO_3, Ho_2O_3, Tm_2O_3, Yb_2O_3, Lu_2O_3 and WO_3 from Aldrich, Fluka and Metall rare earth limited (with analytical grade of purity). The thermal axial gradient in the solution was maintained at around ~1.5 K/cm for all the crystal

growth experiments. A crystallographic ***b*** oriented KLuW seed was used at the center of the surface of the homogeneous solution to grow the single crystals. The saturation temperature, required for growing the crystals was determined by the growth and dissolution of the seed in contact with the surface of the solution. The solution temperature was decreased by about 20 K at the rate of 0.1 Kh^{-1}. The crystal was rotated at 40 rpm. After 8 – 10 days of growth, the crystals were slowly removed from the solution to room temperature at 25 Kh^{-1} to avoid thermal shock. The doping ratios of the crystals were planned to have a fixed value of Yb^{3+} and vary the composition by varying the doping level of Ho^{3+} and Tm^{3+}.

3.2. Optical absorption

Further characterization, prior to the examination of the photoluminescence, was devoted to the knowledge of the polarized optical absorption features of these biaxial crystals to know exactly the energy of each level for all three ions to understand the energy transfer among them for the simultaneous generation of the blue, green and red colours. For this measurement, we considered the 1.0at.%Ho 0.5at.%Tm 1.0at.%Yb:KLuW sample. It was 2.85 mm thick along N_p and 2.93 mm along N_g and N_m principal optical directions to measure the polarized room- and low-temperature optical absorption. From these measurements, not shown here for the sake of brevity, we could determine the energy position of the energy levels of the three ions.

3.3. Photoluminescence

The photoluminescence measurements were carried out by optical excitation at the maximum of the optical absorption of ytterbium ions at 980 nm (with an associated energy of 10204 cm^{-1}) using a Ti:Sapphire laser. This wavelength matches the commercially available InGaAs diodes, which can be used as a pump source for real application. We examined several doping combinations based on (Tm,Yb):KLuW and (Ho,Yb):KLuW crystals before the study of the triply doped (Ho, Tm, Yb):KLuW crystals. Fig. 1(a) shows the signals belonging to the Tm emissions in the 400 – 800 nm range for (Tm,Yb):KLuW. Photons with a wavelength of 475 nm in the blue (with associated energy of 21092 cm^{-1}) were generated as follows: First, excited Yb ions transferred part of their energy from the $^2F_{5/2}$ level of Yb to the $^3H_5$ level of Tm (see the energy diagram in Fig. 2) although these two energy levels are not exactly resonant. The difference in energy (~1973 cm^{-1}) is coupled to the lattice of the crystal with the participation of 2 phonons of ~908 cm^{-1} in energy (maximum phonon energy in monoclinic KLuW measured with Raman spectroscopy [5]). Once the electrons are in the $^3H_5$ excited energy level of Tm, they relax very fast to the $^3F_4$ energy level (energy difference of ~2568 cm^{-1}) which experiences upconversion energy-transfer (ETU) from Yb ions so that these electrons are promoted to the $^3F_2$ level. Part of the electronic population of the $^3F_4$ level generates the 1950 nm (not shown here) emission decaying to the ground state, $^3H_6$. From the $^3F_2$ level photons with associated wavelength of 663 nm (corresponding to the red) are emitted with energy ~15078 cm^{-1} also to the ground state with low probability [6]. In addition, from the $^3F_2$ level, energy relaxation takes place populating the $^3H_4$ level and a second ETU process increase their energy to the $^1G_4$ level from where the photons with energy of 21053 cm^{-1} are generated (475 nm in the blue spectral range). From the $^1G_4$ level, a red emission, centered at 648 nm (15429 cm^{-1}) is also generated with higher probability than the red photons generated from the $^3F_2$ level. The process of generation of blue photons is here more efficient than the generation of red photons in Tm-doped crystals (see Fig. 1(a)). The low intensity of the red emission is also explained by the reabsorption of the photons from the $^3F_4$ to the $^1G_4$ levels and from the $^3H_6$ to the $^3F_2$ levels, which are resonant in energy. The inset in Fig. 1(a) shows a photograph of the illuminated crystal with a clear blue emission under infrared pumping. All these electronic transitions taking place in Tm end in the ground state. An additional peak is observed associated to a photon with energy 22026 cm^{-1} (454 nm) from the highest Stark level of the $^1G_4$ level of Tm.

Fig. 1(b) shows the photoluminescence generated in (Ho,Yb):KLuW crystals after Yb excitation. In this case, part of the energy of excited Yb ions is transferred to the $^5I_6$ level of Ho, which experiences excited-state absorption (ESA) with the energy of a pump photon to the $^5S_2$ + $^5F_4$ levels (close in energy) from where photons at 542 nm (with associated energy of 18416 cm^{-1}) are emitted with very high intensity. It is even possible to observe a shoulder in the spectrum with two wavelengths very close to each other corresponding to the electronic transition of $^5S_2$ + $^5F_4$ levels to the ground state. The energy corresponding to the $^5F_4$ level corresponds to the highest peak with a wavelength of 542 nm (18450 cm^{-1}). The shoulder corresponds to a wavelength of 552 nm (18116 cm^{-1}), transition which takes place from the $^5S_2$ level (18360 cm^{-1}) to the higher lying Stark levels of the ground state. Only, very little part of electrons excited in the $^5S_2$ level is relaxed to the $^5F_5$ level where photons at 651 nm (red emission – 15349 cm^{-1}) are generated. Part of the electronic population decays non-radiatively to the $^5I_5$ level where a pump photon is absorbed promoting electrons to the $^5F_3$ level (energy 20471 cm^{-1}). The photons generated from this level have an associated wavelength of 488 nm, with weak intensity in Fig. 1(b). The red photons coming from the $^5F_3$ level to the upper Stark level of the $^5I_7$ level with associated wavelength of 660 nm (see Fig. 1(b)) show a rather low intensity as in the case of Tm because after careful analysis of the energy distribution of the levels, a resonant transition may occur and consequently, these are reabsorbed from the $^5I_7$ level of Ho (with energy 5100 cm^{-1}) to the $^5F_3$ level of Ho (20449 cm^{-1}). From the latter level non-radiative relaxations take place with a certain probability also populating the $^5S_2$ level of Ho allowing the generation of the green emission. The intra-ion reabsorbed red photons with energies 15078 cm^{-1} for Tm and 15349 cm^{-1} for Ho explains why the blue emission in the Tm,Yb system and the green emission in the Ho,Yb system are so strong while the red emission in both systems (separately) is so weak (see Figs. 1(a) and 1(b)).

Once we doped the crystals with the three ions, Yb served again as ion for excitation and now the energy transfer processes occur from Yb to Tm and Ho simultaneously populating the $^3H_5$ level of Tm and the $^5I_6$ level of Ho that experienced a relaxation to the $^3F_4$ level of Tm and to the $^5I_7$ level of Ho, respectively. In this new scenario, between the levels $^3F_4$ of Tm and $^5I_7$ of Ho a strong energy transfer exists due to their energy resonance which allows these levels to be greatly populated. This modifies the electron dynamics in the ions. In these energy levels, a second pump photon with energy 10204 cm^{-1} is absorbed very efficiently (more than with only two doping

ions in the crystal due to the higher amount of electrons excited in the $^3F_4$ and $^5I_7$ levels) allowing the population of the $^3F_2$ level of Tm and the $^5F_5$ level of Ho from where the red photons are generated. Thus, more intense red emission is expected and observed in relation to the blue and green emissions (Fig. 1(c)).

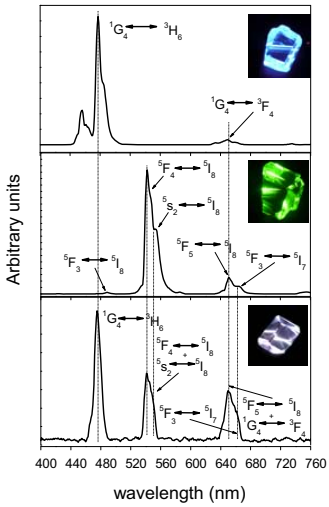

Fig. 1. Visible photoluminescence under infrared excitation. a) 4%Tm,5%Yb:KLuW, b) 1.5%Ho,2.5%Yb:KLuW and c) 1.0%Ho,0.5%Tm,1.0Yb:KLuW.

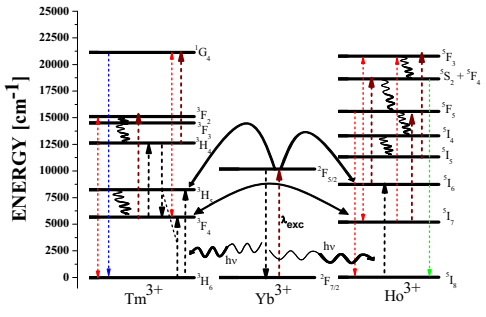

Fig. 2. Energy level diagram of Ho, Tm and Yb ions in KLuW.

The intensity of the red emission balances the generation of white light being the key parameter for it and approaching it to warm white light. Depending on the composition of the crystal, essentially, the content in Tm and Ho ions, one can control the intensity of blue, green and specially red light necessary to balance the energy of these three photons to reach the proper intensity ratio for the white light generation. Fig. 1(c) shows the photoluminescence of a (Ho, Tm, Yb):KLuW crystal with a combination of the three ions generating the three photons simultaneously with the blue, green and red signals providing clear white light observed in its inset when the crystal was illuminated with the infrared light.

To control the white light generation towards warmer white light with the amount of dopants in the crystal, we studied the generation of the three photons for several crystals by fixing the amount of exciting ion (Yb) and modifying properly the other Tm and Ho ions. The composition of the crystals is summarized in Table 1 and Fig. 3 shows the evolution of the generation (integrated area) of photons in the visible at several wavelengths depending on the composition of the crystals. Crystal 1 and crystal 2 show a clear dominant blue colour because the amount of Tm and Ho ions is not high enough to interact among them enhancing the generation of photons associated to the green and specially the red colours. In crystal 3, the higher doping of Ho ions makes the transfer from Tm to be more efficient, thus enhancing the green and red photons compared to samples 1 and 2. Sample 4 is very interesting because the higher doping of Tm provoked even a further increase of the Ho visible emissions due the stronger interaction with Ho making the difference of intensities very small. Not only the visible emissions from Ho increased but also the 2,06 µm of Ho (not shown here) dropped in sample 4 considerably, indicating that the electronic population of the $^5I_7$ level of Ho is basically intended for the population of the $^5S_2$ + $^5F_4$ and $^5F_5$ levels. In sample 5, with the increase of Ho, the energy transfer from Ho to Tm becomes more important being the 2,06 µm of Ho even less intense than in crystal 4, as well as its (from Ho) visible emissions (see Fig. 3) but increasing importantly the blue emission from Tm, thus balancing the combinations of colours and providing a close ideal coordinates for the white colour. To increase the proximity to the ideal white light we considered that increasing the emissions from Ho, this could help. In fact, in crystal 6 with an increase of Ho doping we could observe this phenomenon, although the content in Tm also increased without intention providing even higher blue emission. The final increase in Tm content, sample 7, and slight decrease in Ho content provided an almost perfect warm white coordinates with an almost perfect balance in the generation of the three photons. For crystals 2 to 7 we consider that the content of Yb in the crystals remains unchanged, see Table 1. The white light generation threshold was reached when the pump power amounted only to 75 mW for sample 7.

In order to understand the perception of colour obtained in the crystals, we made use of the CIE 1931 XYZ colour space and calculated the CIE chromaticity coordinates of all the studied crystals with the help of colour matching functions and the photoluminescence spectra obtained. The CIE 1931 colour coordinates, x, y and z can be calculated integrating the area of the signals for each colour and normalising them. We plotted the colour coordinates in Fig. 4. Note that all triply doped crystals with doping levels of Ho higher than 1at.% are in the region considered as white colour, while the coordinates of sample 7 gives the warmest white colour.

TABLE 1. List of compositions of the grown crystals

Sample	at.% in the solution	Stoichiometric formula in the crystal
1	0.2Ho0.2Tm1.0Yb	$KLu_{0.9766}Ho_{0.0047}Tm_{0.0036}Yb_{0.0151}(WO_4)_2$
2	0.5Ho0.5Tm1.0Yb	$KLu_{0.9718}Ho_{0.0084}Tm_{0.0064}Yb_{0.0134}(WO_4)_2$
3	1.0Ho0.5Tm1.0Yb	$KLu_{0.9675}Ho_{0.0127}Tm_{0.0062}Yb_{0.0136}(WO_4)_2$
4	1.0Ho0.8Tm1.0Yb	$KLu_{0.966}Ho_{0.0121}Tm_{0.0090}Yb_{0.0123}(WO_4)_2$
5	1.2Ho0.8Tm1.0Yb	$KLu_{0.9638}Ho_{0.0148}Tm_{0.0090}Yb_{0.0124}(WO_4)_2$
6	1.5Ho0.8Tm1.0Yb	$KLu_{0.9552}Ho_{0.0223}Tm_{0.0106}Yb_{0.0119}(WO_4)_2$
7	1.5Ho1.0Tm1.0Yb	$KLu_{0.9577}Ho_{0.0186}Tm_{0.0121}Yb_{0.0116}(WO_4)_2$

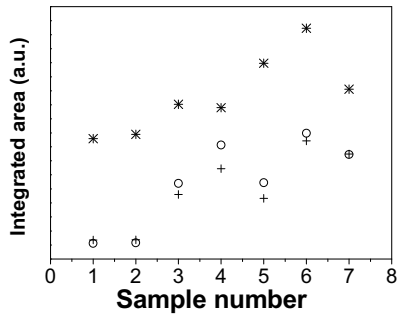

Fig. 3. Evolution of the blue (astherisks), green (dots) and red (cross) emissions in the Tm, Ho, Yb system after infrared excitation.

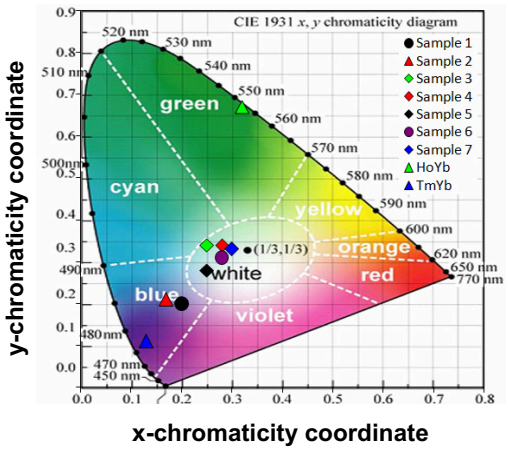

Fig. 4. CIE (x,y) chromaticity diagram indicating the colour coordinates.

4. Conclusions

In summary, we could generate simultaneously three photons with energies corresponding to the blue, green and red in the visible spectral range, which in a suitable ratio, are perceived as white light. This was accomplished after careful study of the photoluminescence and understanding of the complex mechanism of energy transfer among ions. The control of the energy transfer allowed us to reach the optimum composition for warmer white light generation in the monoclinic double tungstates. The perception of colour is quantified by the CIE chromaticity diagram.

ACKNOWLEDGMENTS

This work was supported by the Spanish Government under projects MAT2008-06729-C02-02/NAN, MAT2008-04046-E/MAT, TEC2010-21574-C02-02, PI09/90527, HF2008-0045, DE2009-0002 and the Catalan Authority under project 2009SGR235. Joan Josep Carvajal is supported by the Education and Science Ministry of Spain and European Social Fund under the Ramon y Cajal program, RYC2006 – 858.

References

[1]M. H. Crawford, IEEE J. Sel. Top. Quant. Electron. **15**, 1028 (2009).
[2]J. Wang and P. A. Tanner, J. Amer. Chem. Soc., **132**, 947 (2010).
[3]S. Heer, K. Kömpe, H. U. Güdel and M. Haase, Adv. Mat., **16**, 23 (2004).
[4]H. Gong, D. Yang, X. Zhao, E. Yun Bun Pun, H. Lin, Opt. Mat. **32**, 554 (2010).
[5]V. Petrov, M. C. Pujol, X. Mateos, Ò. Silvestre, S. Rivier, M. Aguiló, R. M. Solé, J. Liu, U. Griebner and F. Díaz, Laser & Photon. Rev. **1**, 179 (2007).
[6]O. Silvestre, M.C. Pujol, M. Rico, F. Güell, M. Aguiló and F. Díaz , Appl. Phys. B, **87**, 707 (2007).

UNIVERSITAT ROVIRA I VIRGILI
INFRARED LASERS BASED ON HO3+:KRE(WO4)2 CRYSTALS WITH TM3+OR YB3+ AS SENSITIZERS
Venkatesan Jambunathan
ISBN:/DL: T.1243-2011

Paper VI

Continuous-wave co-lasing in a monoclinic co-doped (Ho,Tm):$KLu(WO_4)_2$ crystal

V. Jambunathan, A. Schmidt, X. Mateos, M. C. Pujol, J. J. Carvajal, M. Aguiló, F. Díaz, U. Griebner and V. Petrov

Submitted to Laser Physics Letters.

UNIVERSITAT ROVIRA I VIRGILI
INFRARED LASERS BASED ON HO3+:KRE(WO4)2 CRYSTALS WITH TM3+OR YB3+ AS SENSITIZERS
Venkatesan Jambunathan
ISBN:/DL: T.1243-2011

UNIVERSITAT ROVIRA I VIRGILI
INFRARED LASERS BASED ON HO3+:KRE(WO4)2 CRYSTALS WITH TM3+OR YB3+ AS SENSITIZERS
Venkatesan Jambunathan
ISBN:/DL: T.1243-2011

Continuous-wave co-lasing in a monoclinic co-doped (Ho,Tm):KLu$(WO_4)_2$ crystal

V. Jambunathan,[1] A. Schmidt,[2] X. Mateos,[1,2*] M. C. Pujol,[1] J. J. Carvajal,[1] M. Aguiló,[1] F. Díaz,[1] U. Griebner,[2] and V. Petrov[2]

[1]Física i Cristal·lografía de Materials i Nanomaterials (FiCMA-FiCNA), Universitat Rovira i Virgili (URV), Campus Sescelades c/Marcel·lí Domingo, s/n, E - 43007 Tarragona, Spain,

[2]Max-Born-Institute for Nonlinear Optics and Short Pulse Spectroscopy, Max-Born-Strasse 2A, D -12489 Berlin, Germany

*Corresponding author: xavier.mateos@urv.cat

Abstract: We present continuous-wave laser operation at two wavelengths oscillating simultaneously and originating from two different active ions in a monoclinic co-doped (Ho,Tm):KLu$(WO_4)_2$ crystal. Dual-wavelength lasing is accomplished at room temperature using Ti:sapphire laser pumping. The Ho-ion, lasing at 2061 nm and the Tm-ion, lasing at 1937 nm or 1919 nm, generate together a maximum output power of 244 mW with a maximum slope efficiency of 24.8%. Tuning with a birefringent filter is possible from 1854 to 2063 nm, with individual tuning ranges of 1854 to 1980 nm for Tm and 1971 to 2063 nm for Ho.

Key words: co-lasing, dual-wavelength, double tungstates, KREW

PACS: 42.70.Hj, 42.55.Px, 42.55.Rz, 07.57.Hm

1. Introduction

Co-lasing of two different wavelengths has been demonstrated in few solid-state laser materials doped with different rare earth ions. These include co-doped systems and lasing of two different ions such as (Er,Nd):YAG (2.9 μm from Er and 1.06 μm from Nd) [1], (Ho,Nd):YAG (3.0 μm from Ho and 1.06 μm from Nd) [2], (Cr,Er,Tm,Ho):YAG (2.1 μm from Ho and 2.9 μm from Er) [3] or singly doped crystals operating on different transitions of the same ion such as Nd:YVO_4 (1064 and 1342 nm) [4]. An interesting work on dual-wavelength lasers is found in [5]. Little attention has been paid, however, to dual-wavelength operation of the (Ho,Tm) co-doped system (1.9 μm from Tm and 2.1 μm from Ho) although Tm has often been used as sensitizer for Ho-doped materials [6-8]. This combination is interesting for potential applications in the field of medicine and remote sensing because water absorption is quite different in these two spectral ranges. Additional advantage of the (Ho,Tm) system is that the sensitizer ion (Tm) can be directly pumped by readily available AlGaAs diodes. We demonstrated previously continuous-wave (CW) laser operation of Tm in KLu$(WO_4)_2$ (shortly, KLuW) with diode pumping [9] and of Ho in KLuW with Tm-laser in-band pumping [10]. The host (KLuW) belongs to the monoclinic KRE$(WO_4)_2$ (RE = Y, Gd and Lu), shortly KREW, family. The KREW family of crystals stands out for their high absorption and emission cross-sections when doped with active rare-earth ions, partly due to the strong anisotropy of these monoclinic crystals. Many properties of KLuW indicate its high potential as a host for solid-state lasers [11-14].

2. Results and discussion

2.1. Crystal growth and spectroscopy

High quality single-crystals with different co-doping ratio were grown by the Top Seeded Solution Growth Slow-Cooling method (TSSG-SC) using $K_2W_2O_7$ as solvent. The optimized methodology of growth for KREW crystals can be found elsewhere [11]. Spectroscopy of co-doped (Ho,Tm):KLuW was characterized in terms of polarized optical absorption and photoluminescence, and the relevant information can be found in a previous work [15]. Detailed and extended data related with the crystal growth and optical spectroscopy of a whole series of (Ho,Tm):KLuW co-doping ratios will be published elsewhere. From the optical absorption spectra,

we found that Tm shows a maximum absorption cross-section of 5.2×10^{-20}cm^2 at 802 nm for E//$\boldsymbol{N_m}$. Emission cross-sections were calculated by the reciprocity method and used to obtain the gain cross-section curves for Ho and Tm ions. For the sake of brevity only gain curves for E//$\boldsymbol{N_m}$ are presented in Fig. l which is sufficient to understand the dual-wavelength nature of the laser emission reported below. Gain curves of Ho for several inversion levels (β) in the 1900-2100 nm range (Fig. 1a) show an absolute maximum centered at 2060 nm. Gain curves of Tm (Fig. 1b) show positive gain for wavelengths greater than 1775 nm with local maxima at ~1850 nm, ~1920 nm and ~1950 nm. It is worth mentioning that around 1950 nm there is an overlap in the absorption curves of Ho and Tm which is not taken into account in the reciprocity method used for the calculation of the emission cross-section, and consequently in the calculation of the gain cross-section.

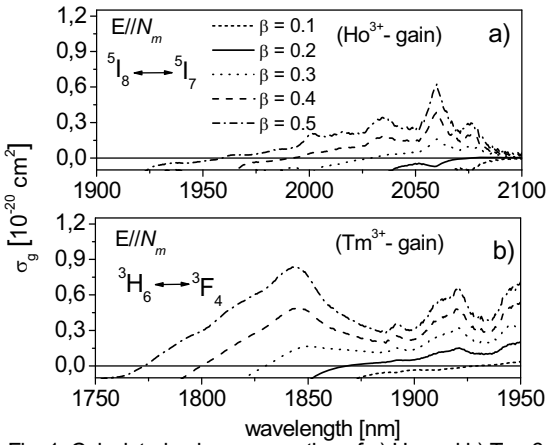

Fig. 1. Calculated gain cross-section of a) Ho and b) Tm. β is the inversion rate.

2.2. Laser experiments

Laser operation was studied with a V-type astigmatically compensated resonator as shown in Fig. 2. It comprises two curved mirrors, with radii of curvature ROC = -100 mm, which are highly transmitting (>98%) at the pump wavelength and highly reflecting in the 1800-2100 nm range, and a plane output coupler (OC) for which mirrors of transmission T_{oc} = 1.5(±0.5)%, 3.0(±0.5)%, 5.0(±0.5)% and 9.0(±1.0)% in the 1820-2050 nm range were used. The active medium, a (0.5at.% Ho, 5.0at.% Tm):KLuW crystal, anti-reflection coated around 800 nm for pump and 1900-2200 nm range for laser wavelengths, was positioned at Brewster angle between the two curved mirrors and oriented for light propagation along $\boldsymbol{N_g}$ principal optical direction and polarization parallel to $\boldsymbol{N_m}$ principal optical direction. The thickness of the sample was 3 mm and the aperture 3×3 mm^2. The ion density in this crystal was 5.291×10^{19} cm^{-3} (Ho^{3+}) and 2.301×10^{20} cm^{-3} (Tm^{3+}). The pump source used was a Ti:sapphire laser tuned to 802 nm to excite the Tm ions. To focus the pump light onto the crystal we used an anti-reflection coated lens with focal length of 75 mm. The crystal was actively cooled from the bottom part by water running through the crystal holder (temperature: 16°C) and passively cooled from the top part by the Cu-holder. Indium foil was used on both contact surfaces.

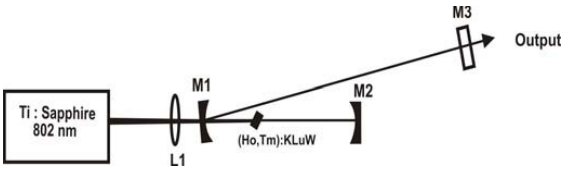

Fig. 2. Laser set-up constructed to carry out the laser experiments. Total cavity length = 70 cm.

Dual-wavelength laser oscillation was realized in CW regime for all the output couplers used. For each of them, we measured the output power as a function of absorbed pump power. The laser threshold was reached at 60-100 mW of absorbed pump power and for all output couplers, lasing started at 2061 nm which corresponds to the $^5I_7 \rightarrow {}^5I_8$ transition of Ho^{3+}. Increasing the pump power, a second wavelength at 1937 nm appeared in the output spectrum when output couplers of transmission, T_{oc} = 1.5%, 3% and 5% were used and even multiple wavelengths (1919 and 1928 nm in addition to 2061 nm) were observed for T_{oc} = 9%. These additional emissions are attributed to the $^3F_4 \rightarrow {}^3H_6$ transition of Tm. Depending on the alignment of the cavity with the T_{oc} = 9% output coupler, multiple wavelength operation at 1931, 1935, 1937 and 1939 nm, was also observed. The reason for this can be explained by the plateau found in the gain curves between ~1925 nm and ~1940 nm (see Fig. 1b). In fact, the dual-wavelength operation, i.e. simultaneous generation of Ho and Tm ions in this crystal, occurs because the gain values of Ho and Tm are very similar at the laser wavelengths and several wavelengths can oscillate in a cavity with broad-band coated mirrors. The gain curves show that at low inversion levels, the gain cross-section of Ho at 2060 nm and that of Tm at 1937 nm are very similar which leads to competition of these two wavelengths corresponding to different ions but oscillating simultaneously. Increasing the output coupling losses (T_{oc} = 9%), the Tm emission shifts to shorter wavelengths, as typical for a three-level system, and operation in the next maximum of the gain curve takes place (1919 and 1928 nm) where the cross-section values are again closer to that of Ho at 2060 nm. We concluded that the 1937, 1928 and 1919 nm laser wavelengths originate from Tm because there is no positive gain in this region for Ho. We carefully analyzed the difference in energy from each sublevel of the excited state to each sublevel of the ground state in Tm and Ho and although such wavelengths could be assigned to transitions in either of the dopants, Ho-lasing was

rejected because the gain in Ho is negative below 1960 nm (Fig. 1a) even for inversion rates as high as 0.5. In a recent report on the same co-doping but in a different host [16], the authors observed net gain of Ho in this spectral region but this seems not to be the case for the KLuW host.

Figures 3 and 4 show the input-output characteristics of the (Ho,Tm):KLuW laser for T_{oc} = 3% and 9%, respectively, and the corresponding output spectra (as inset). From these figures and Table 1, it can be seen that the slope efficiency increases with the transmission of the output coupler. This is accompanied by an increase of the Tm laser part in the output power. For T_{oc} = 9% and maximum pump level, the output power is almost equally distributed among the two emissions and each ion produces slightly more than 100 mW (see Fig. 4).

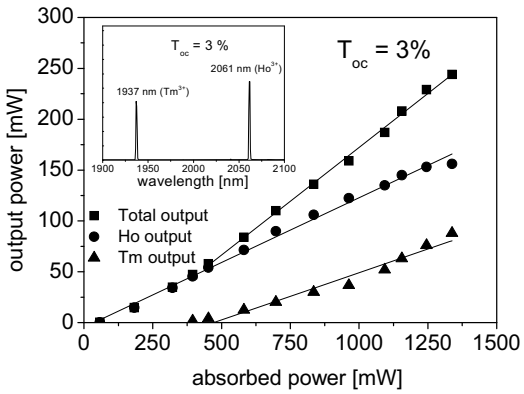

Fig. 3. Output power versus absorbed pump power for T_{oc}=3 % and the corresponding laser emission spectrum (inset).

With the help of a 1 mm thick birefringent filter made of quartz, the laser could be continuously tuned from 1854 to 2063 nm with a T_{oc} = 3%. The Tm emission was tunable from 1854 to 1980 nm and the Ho emission was tunable from 1971 to 2063 nm Fig. 5). In general, we observed higher output power for the Ho laser (see Fig 3 and 4), however, in the case of independent lasing of the two ions with the birefringent filter inside the cavity the Tm ion emission was more powerful. Note that the narrow region of overlap in Fig. 5 corresponds to wavelengths which substantially differ from the wavelengths characteristic for the co-lasing regime (Figs. 3 and 4).

Table. 1 Calculated slopes and measured laser thresholds of the (Ho,Tm):KLuW laser for different output couplers.

T_{oc} %	slope %			threshold (mW)	
	Tm	Ho	total	Ho	Tm
1.5	3.9	10.2	13.6	62	490
3.0	9.2	12.7	21.1	58	395
5.0	10.8	11.3	20.6	80	488
9.0	12.8	10.2	24.8	97	361

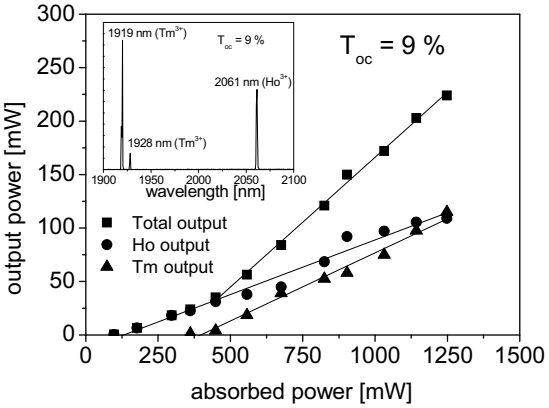

Fig.4. Output power vs. absorbed pump power for T_{oc}=9 % and the corresponding laser emission spectrum (inset).

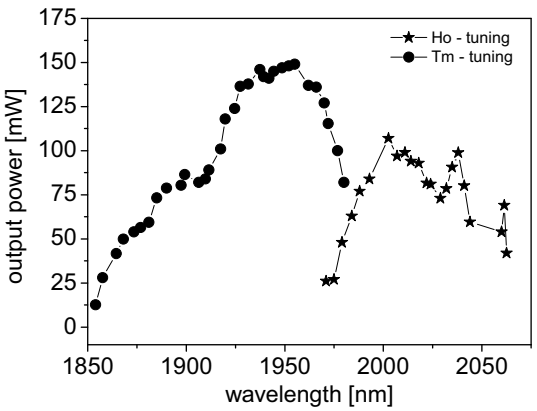

Fig.5. Tuning of the (Ho,Tm):KLuW laser.

3. Conclusion

In conclusion, we demonstrated simultaneous dual-wavelength CW laser action in a monoclinic co-doped (Ho,Tm):KLuW crystal at room-temperature. The laser wavelengths are attributed to Ho at 2061 nm and Tm at 1937 or 1919 nm. The maximum total laser output power reached 244 mW and the maximum slope efficiency was 24.8%. In the latter case, using T_{oc} = 9%, the output power was equally distributed between two discrete lines, at 2061 and 1919 nm. Continuous laser tuning was possible in a more than 200 nm broad wavelength range, from 1854 to 2063 nm. Higher output powers are expected at optimized doping ratios for better energy transfer from Tm to Ho. Future power scaling will also rely on diode pumping.

Acknowledgements: This work was supported by the Spanish Government under projects MAT2008-06729-C02-02/NAN, TEC2010-21574-C02-02, PI09/90527, DE2009-

0002 and the Catalan Authority under project 2009SGR235. J. J. Carvajal is supported by the Education and Science Ministry of Spain and European Social Fund under the Ramon y Cajal program, RYC2006 – 858.

References

[1] W. Q. Shi, R. Kurtz, J. Machan, M. Bass, M. Birnbaum, and M. Kokta, Appl. Phys. Lett. **51**, 1218-1120 (1987).
[2] J. Machan, R. Kurtz, M. Bass, M. Birnbaum, and M. Kokta, Appl. Phys. Lett. **51**, 1313-1315 (1987).
[3] B. M. Walsh, K. E. Murray and N. P. Barnes, J. Appl. Phys. **91**, 11-17 (2002).
[4] X. H. Fu, H. H. Tan, Y. M. Li, E. J. Hao, G. Shen, and L. S. Qian, Laser. Phys. **17**, 1345-1348 (2007).
[5] B.M. Walsh, Laser Phys. 20, 622-634 (2010).
[6] B.Q. Yao, G. Li, P.B. Meng, G.L. Zhu, Y.L. Ju and Y. Z. Wang, Laser Phys. Lett. **7**, 857–861 (2010).
[7] X. L. Zhang, L. Li, J. H, Cui, Y.L. Ju and Y.Z. Wang, Laser. Phys. Lett., 7, 194-197 (2010).
[8] R. L. Zhou, Y. L. Ju, C.T. Wu, Z. G. Wand and Y. Z. Wang, Laser Phys, 20, 1320-1323 (2010).
[9] X. Mateos, V. Petrov, J. Liu, M.C. Pujol, U. Griebner, M. Aguiló, F. Díaz, M. Galan, and G. Viera, IEEE J. Quantum Electron. **42**, 1008-1015 (2006).
[10] X. Mateos, V. Jambunathan, M. C. Pujol, J. J. Carvajal, F. Díaz, M. Aguiló, U. Griebner and V. Petrov, Opt. Express, **18**, 20793-20978 (2010).
[11] V. Petrov, M. C. Pujol , X. Mateos, Ó. Silvestre, S. Rivier, M. Aguiló, R. M. Solé, J. Liu, U. Griebner, and F. Díaz, Laser & Photon. Rev. **1**, 179-212 (2007).
[12] J. Liu, H. Zhang, W. Han, V. Petrov and J. Wang, Opt. Express 16, 4960-4964 (2008).
[13] J. Liu, V. Petrov, X. Mateos, H. Zhan and J. Wang, Opt. Lett, 32, 2016-2018 (2007).
[14] X. Mateos, V. Petrov, M. Aguiló, R.M. Solé, Jna. Gavaldà, J. Massons, F. Díaz and U. Griebner, IEEE J. Quant. Electron, 40, 1056-1059 (2004).
[15] V. Jambunathan, X. Mateos, M. C. Pujol, J. J. Carvajal, J. Massons, M. Aguiló, and F. Díaz, J. Lum. **129**, 1882-1885 (2009).
[16] X. Han, F. Fusari, M. D. Serrano, A. A. Lagatsky, J. M. Cano-Torres, C. T. A. Brown, C. Zaldo and W. Sibbett, Opt. Express **18**, 5413-5419 (2010).

Paper VII

CW lasing of Ho in $KLu(WO_4)_2$ in-band pumped by a diode-pumped $Tm:KLu(WO_4)_2$ laser

X. Mateos, V. Jambunathan, M. C. Pujol, J. J. Carvajal, F. Díaz, M. Aguiló,
U. Griebner and V. Petrov

Optics Express 18 (20), 20793 -20798 (2010).

UNIVERSITAT ROVIRA I VIRGILI
INFRARED LASERS BASED ON HO3+:KRE(WO4)2 CRYSTALS WITH TM3+OR YB3+ AS SENSITIZERS
Venkatesan Jambunathan
ISBN:/DL: T.1243-2011

CW lasing of Ho in $KLu(WO_4)_2$ in-band pumped by a diode-pumped Tm:$KLu(WO_4)_2$ laser

Xavier Mateos,[1,2*] Venkatesan Jambunathan,[1] Maria Cinta Pujol,[1] Joan Josep Carvajal,[1] Francesc Díaz,[1] Magdalena Aguiló,[1] Uwe Griebner,[2] and Valentin Petrov[2]

[1]*Física i Cristal·lografia de Materials i Nanomaterials (FiCMA-FiCNA). Universitat Rovira i Virgili (URV), c/ Marcel·lí Domingo, s/n..E-43007 Tarragona, Spain*

[2]*Max Born Institute for Nonlinear Optics and Ultrafast Spectroscopy, Max-Born Strasse 2A, 12489 Berlin, Germany*

**xavier.mateos@urv.cat*

Abstract: We demonstrate continuous wave (CW) room temperature laser operation of the monoclinic Ho^{3+}-doped $KLu(WO_4)_2$ crystal using a diode-pumped Tm^{3+}:$KLu(WO_4)_2$ laser for in-band pumping. The slope efficiency achieved amounts to ~55% with respect to the absorbed power and the maximum output power of 648 mW is generated at 2078 nm.

OCIS codes: (140.5680) Rare earth and transition metal solid-state lasers; (140.3070) Infrared and far-infrared lasers; (140.3480) Lasers, diode-pumped

References and links

1. G. J. Koch, J. Y. Beyon, F. Gibert, B. W. Barnes, S. Ismail, M. Petros, P. J. Petzar, J. Yu, E. A. Modlin, K. J. Davis, and U. N. Singh, "Side-line tunable laser transmitter for differential absorption lidar measurements of CO_2: design and application to atmospheric measurements," Appl. Opt. **47**(7), 944–956 (2008).
2. S. A. Pierre, and D. M. Albala, "The future of lasers in urology," World J. Urol. **25**(3), 275–283 (2007).
3. P. A. Budni, L. A. Pomeranz, M. L. Lemons, C. A. Miller, J. R. Mosto, and E. P. Chicklis, "Efficient mid-infrared lasing using 1.9-μm-pumped Ho:YAG and $ZnGeP_2$ optical parametric oscillators," J. Opt. Soc. Am. B **17**(5), 723–728 (2000).
4. V. Sudesh, and K. Asai, "Spectroscopic and diode-pumped-laser properties of Tm,Ho:YLF; Tm,Ho:LuLF; and Tm,Ho:LuAG crystals: a comparative study," J. Opt. Soc. Am. B **20**(9), 1829–1837 (2003).
5. E. Sani, A. Toncelli, M. Tonelli, N. Coluccelli, G. Galzerano, and P. Laporta, "Comparative analysis of Tm-Ho:KYF_4 laser crystals," Appl. Phys. B **81**(6), 847–851 (2005).
6. K. Scholle, and P. Fuhrberg, "In-band pumping of high-power Ho:YAG lasers by laser diodes at 1.9 μm," in Conference on Lasers and Electro-Optics CLEO'08, Technical Digest (CD) (Optical Society of America, 2008), paper CTuAA1.
7. M. Eichhorn, "Quasi-three-level solid-state lasers in the near and mid infrared based on trivalent rare earth ions," Appl. Phys. B **93**(2-3), 269–316 (2008).
8. D. Y. Shen, A. Abdolvand, L. J. Cooper, and W. A. Clarkson, "Efficient Ho:YAG laser pumped by a cladding-pumped tunable Tm:silica-fibre laser," Appl. Phys. B **79**(5), 559–561 (2004).
9. S. So, J. I. Mackenzie, D. P. Shepherd, W. A. Clarkson, J. G. Betterton, E. K. Gorton, and J. A. C. Terry, "Intra-cavity side-pumped Ho:YAG laser," Opt. Express **14**(22), 10481–10487 (2006).
10. B. M. Walsh, "Review of Tm and Ho materials: spectroscopy and lasers," Laser Phys. **19**(4), 855–866 (2009).
11. V. Petrov, M. C. Pujol, X. Mateos, Ó. Silvestre, S. Rivier, M. Aguiló, R. M. Solé, J. Liu, U. Griebner, and F. Díaz, "Growth and properties of $KLu(WO_4)_2$, and novel ytterbium and thulium lasers based on this monoclinic crystalline host," Laser & Photon. Rev. **1**(2), 179–212 (2007).
12. J. Liu, V. Petrov, X. Mateos, H. Zhang, and J. Wang, "Efficient high-power laser operation of Yb:$KLu(WO_4)_2$ crystals cut along the principal optical axes," Opt. Lett. **32**(14), 2016–2018 (2007).
13. X. Mateos, V. Petrov, J. Liu, M. C. Pujol, U. Griebner, M. Aguiló, F. Díaz, M. Galan, and G. Viera, "Efficient 2 μm continuous-wave laser oscillation of Tm^{3+}:$KLu(WO_4)_2$," IEEE J. Quantum Electron. **42**, 1008–1015 (2006).
14. A. A. Kaminskii, A. G. Petrosyan, V. A. Fedorov, S. E. Sarkisov, V. V. Ryabchenkov, A. A. Pavlyuk, V. V. Lyubchenko, and I. V. Mochalov, "Two-micron stimulated emission by crystals with Ho^{3+} ions, based on the transition $^5I_7 \rightarrow {}^5I_8$," Sov. Phys. Dokl. **26**, 846–848 (1981) (Transl. from Dokl. Akad. Nauk SSSR **260**, 64–67 (1981)).
15. A. A. Kaminskii, A. A. Pavlyuk, P. V. Klevtsov, I. F. Balashov, V. A. Berenberg, S. E. Sarkisov, V. A. Fedorov, M. V. Petrov, and V. V. Lyubchenko, "Stimulated radiation of monoclinic crystals of $KY(WO_4)_2$ and $KGd(WO_4)_2$ with Ln^{3+} ions," Inorg. Mater. **13**, 482–483 (1977) (transl. from Izv. Akad. Nauk. SSSR, Neorg. Mater. **13**, 582–583 (1977)).
16. A. A. Lagatsky, F. Fusari, S. V. Kurilchik, V. E. Kisel, A. S. Yasukevich, N. V. Kuleshov, A. A. Pavlyuk, C. T. A. Brown, and W. Sibbett, "Optical spectroscopy and efficient continuous-wave operation near 2 μm for a Tm, Ho:KYW laser crystal," Appl. Phys. B **97**(2), 321–326 (2009).

#127838 - $15.00 USD Received 30 Apr 2010; revised 5 Jul 2010; accepted 11 Aug 2010; published 16 Sep 2010

17. M. C. Pujol, C. Cascales, M. Rico, J. Massons, F. Diaz, P. Porcher, and C. Zaldo, "Measurement and crystal field analysis of energy levels of Ho^{3+} and Er^{3+} in $KGd(WO_4)_2$ single crystal," J. Alloy. Comp. **323–324**(1-2), 321–325 (2001).
18. M. C. Pujol, J. Massons, M. Aguilo, F. Diaz, M. Rico, and C. Zaldo, "Emission cross sections and spectroscopy of Ho^{3+} laser channels in $KGd(WO_4)_2$ single crystal," IEEE J. Quantum Electron. **38**(1), 93–100 (2002).
19. V. Jambunathan, X. Mateos, M. C. Pujol, J. J. Carvajal, J. Massons, M. Aguilo, and F. Diaz, "Near-infrared photoluminescence from Ho^{3+}-doped monoclinic $KLu(WO_4)_2$ crystal codoped with Tm^{3+}," J. Lumin. **129**(12), 1882–1885 (2009).

1. Introduction

Ho^{3+} (Ho) lasers operating at wavelengths slightly above 2 μm find applications in remote sensing, medical treatments and as pump sources for mid-IR OPOs [1–3]. Diode-pumping of such lasers can be realized by co-doping the active material with Tm^{3+} (Tm) ions making profit from the well established AlGaAs laser diodes emitting around 800 nm and the energy transfer to Ho^{3+} ions [4,5]. Such energy transfer, however, ultimately limits the overall pump efficiency while up-conversion mechanisms result in excitation of higher energy levels of Tm whose population is no longer involved in the transfer of energy to Ho. Thus, direct excitation of the upper emitting level of Ho ($^5I_7$) with a laser pump source, also known as in-band pumping or resonant pumping, remains the most promising approach for up-scaling the output power and increasing the efficiency of all-solid-state Ho-lasers emitting on the $^5I_7 \rightarrow {}^5I_8$ transition. It ensures minimum thermal load which is essential for the quasi-three level operation scheme in order to avoid re-absorption. Although direct in-band diode-pumping of a Ho:YAG laser has been already demonstrated with (AlGaIn)(AsSb) laser diodes [6], very efficient and powerful diode-pumped Tm lasers [7], including Tm-fiber lasers, offer more flexibility with respect to the spectral and spatial characteristics and are widely used for pumping Ho-lasers, e.g [3,8], including intracavity pumping, e.g [9].

Many oxide and fluoride type crystals were shown to be suitable host materials for the Ho^{3+} ion and laser operation with high output power and efficiency has been demonstrated with quite few of them [7,10]. However, little attention has been paid to the monoclinic potassium double tungstates with the general formula $KRE(WO_4)_2$ (KREW) where RE is a passive trivalent ion (Y, Gd, or Lu). KYW and KGdW were known as very efficient and promising hosts for the Nd^{3+} ion at intermediate power levels for long time and more recently they showed similar nice potential for Yb^{3+} doping (near 1 μm) and Tm^{3+} doping (slightly below 2 μm). The doped KREW crystals stand out because of their very high transition cross sections (absorption and emission) and weak concentration quenching of the fluorescence which is related to the relatively large dopant-to-dopant separation. The less known KLuW was recently shown to be especially suited for Yb and Tm doping due to the matching of the ionic radii of the passive and active rare earths [11]. Thus, the maximum laser slope efficiency for a diode-pumped Yb:KLuW laser reached 80% and the output power 11 W [12]. In the case of Tm doped KLuW, these values were 69% and 4 W, respectively [13].

In this work we demonstrate, for the first time to our knowledge, continuous-wave (CW) room temperature lasing of Ho^{3+} in a singly-doped monoclinic crystalline host belonging to the KREW family (KLuW) under in-band pumping. Stimulated emission on the $^5I_7 \rightarrow {}^5I_8$ transition of Ho in KLuW at 2079 nm was achieved before only by flash-lamp pumping at ~110 K [14], similar to the first demonstrations of Ho lasing on this transition in the other two isostructural hosts, KYW and KGdW [14,15]. Note that recently the co-doped Tm,Ho:KYW laser crystal has been investigated with indirect Ti:sapphire laser pumping at 802 nm [16]. In the present work, the pump source for the Ho:KLuW laser is a diode-pumped home-made Tm-laser based on the same host material, KLuW, and described in detail elsewhere [13]. Slope efficiency of ~55% is achieved in this initial experiment with Ho:KLuW.

2. Experiment

A series of Ho-doped KLuW crystals have been grown with doping concentration ranging from 0.5 to 7.5 at. % by the Top Seeded Solution Growth method with Slow Cooling of the solution (TSSG-SC). For the growth, a platinum crucible with a diameter 50 mm and a height

#127838 - $15.00 USD Received 30 Apr 2010; revised 5 Jul 2010; accepted 11 Aug 2010; published 16 Sep 2010

of 50 mm was used. The composition of the solution was 12 mol. % KLuW as solute and 88 mol. % $K_2W_2O_7$ as solvent. The raw materials were K_2CO_3, Ho_2O_3, WO_3 and Lu_2O_3 reagents from Aldrich, Fluka and Metall (with analytical grade of purity). A ***b***-oriented KLuW was used as a seed positioned perpendicularly with respect to the solution surface.

Spectroscopic characterization of Ho:KLuW in terms of polarized optical absorption and luminescence at room temperature is a subject of current investigations which will be published elsewhere. However, related data on Ho:KGdW can be found in [17,18] while relevant data on Tm-Ho co-doped KYW [16] and KLuW [19] also exist. Concerning the in-band laser pumping employed in the present work, it can be seen from Fig. 1, which shows the absorption cross section (σ_a) in the 1800-2200 nm spectral range, corresponding to the $^5I_8 \rightarrow {}^5I_7$ transition of Ho in KLuW, that at a pump wavelength of 1946 nm the absorption for the two polarizations, $E//N_m$ and $E//N_p$ is practically the same: $\sigma_a(E//N_m)=0.49\times10^{-20}$ cm^2 and $\sigma_a(E//N_p)=0.42\times10^{-20}$ cm^2. The principal optical axes of monoclinic crystals, N_p, N_m and N_g, are defined by $n_p<n_m<n_g$ relating to the principal refractive indices. Note that, as with other dopants, Ho-doped KLuW exhibits anisotropic absorption and emission with higher cross sections for light polarized parallel to the N_m and N_p dielectric axes in comparison to $E//N_g$.

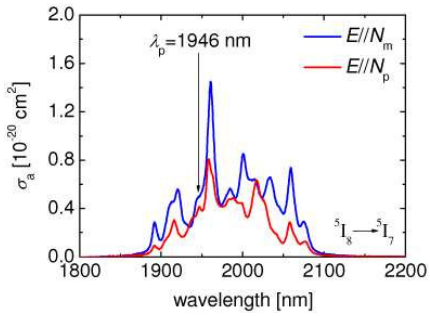

Fig. 1. Absorption cross-section of the $^5I_8 \rightarrow {}^5I_7$ transition of Ho in KLuW for $E//N_m$ and $E//N_p$.

The active elements were oriented along the three orthogonal principal optical directions as parallelepipedic samples with their faces parallel to the N_m and N_p directions allowing light propagation along the N_g direction. Typically, we cut and polished the active elements to a thickness of 3 mm and an aperture of 3×3 mm^2. They remained uncoated.

CW laser operation was studied in a near-hemispherical resonator formed by a plane pump mirror (M5 in Fig. 2), antireflection (AR) coated for the pump wavelength and high-reflection (HR) coated for the laser wavelength. The output coupler series (M6) comprised several curved mirrors with 25, 50 and 75 mm radius of curvature (RC). The transmission of the output couplers used (T_{OC}) was 1.5% and 3% in the range from 1900 to 2050 nm. This contributed to an almost double pass pumping of the Ho:KLuW crystal since 98.5% and 97% of the non-absorbed pump radiation, respectively, was retroreflected by the output coupler. Two lenses (L2) were used to pump the Ho crystals with 50 and 150 mm focal length. The active elements were mounted in a Cu holder that served as a heat sink but no active cooling was applied. They were positioned under normal incidence to the pump beam as close as possible to the plane mirror M5.

#127838 - $15.00 USD Received 30 Apr 2010; revised 5 Jul 2010; accepted 11 Aug 2010; published 16 Sep 2010

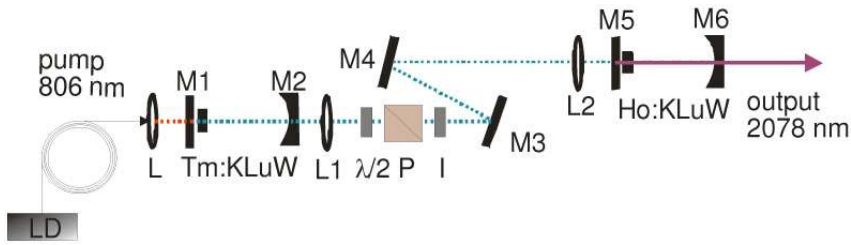

Fig. 2. Laser setup: λ/2 and P (half-wave plate and polarizer acting as attenuator), L (AR-coated lens assembly for collimation and focusing of the fiber output with f=30 mm), L1 (AR-coated collimating lens with f=150 mm), I (isolator: quarter-wave plate), L2 (AR-coated focusing lens), M3, M4 (plane bending mirrors), M1, M5 (plane pump mirrors), M2 (Tm-laser output coupler with RC=75 mm), and M6 (Ho-laser output coupler).

The pump source was a Tm:KLuW laser described elsewhere [13]. Its output was up-scaled to 5.1 W at 1946 nm using a fiber coupled and unpolarized diode-based pump source (Lumics) whose emission at high currents was centered at 806 nm. The radiation from the Tm:KLuW laser was linearly polarized along its N_m principal optical axis. After the attenuator we placed an optical isolator (I) to avoid any back coupling from the Ho-laser set-up. Since we used for this a quarter-wave plate the pump beam to the Ho-laser was circularly polarized.

3. Results and discussion

The fact that the pump beam incident onto the Ho crystal exhibited circular polarization was unimportant in our case since, as already mentioned, the absorption of the Ho:KLuW crystal at the wavelength of 1946 nm is not substantially different for the two polarizations involved. Note that according to Fig. 1, the pump absorption is quite different at the maximum near 1960 nm but the pump wavelength of 1946 nm was fixed in our case by the optimum output coupling (5%) and the natural polarization selection of the Tm:KLuW laser [13]. In any case, the Ho:KLuW laser output was always linearly polarized with E//N_m although the pump was not linearly polarized. This can be explained by the higher gain cross-section for this polarization as previously observed for Yb and Tm doping of the same host [11].

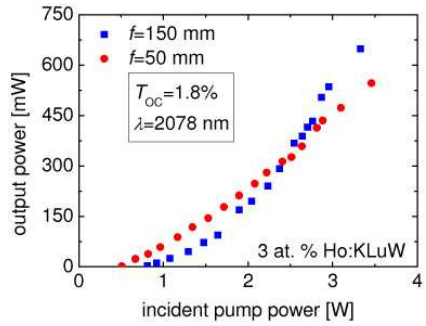

Fig. 3. Output power vs. incident pump power of the Ho:KLuW laser: comparison of the two pump lenses with focal lengths of f=50 mm and f=150 mm with an RC=25 mm output coupler (T_{OC}=1.8% @ 2078 nm).

Doping concentrations of 1, 3 and 5 at. % were tested but CW laser oscillation was possible only with the 3 at. % Ho-doped KLuW sample. Too low absorption or insufficient absorption bleaching in the three-level system are thought to be the reasons for the critical concentration dependence. The Ho:KLuW laser performance with the two pump lenses available is compared in Fig. 3 for an output coupler with RC=25 mm and physical cavity

#127838 - $15.00 USD Received 30 Apr 2010; revised 5 Jul 2010; accepted 11 Aug 2010; published 16 Sep 2010

length of 26 mm. Better mode matching at high powers and higher laser efficiency is observed for a focal length of f=150 mm. Note that for this measurement the Tm:KLuW pump laser was operated at maximum output power and the attenuator (Fig. 2) was applied to vary the pump level for the Ho:KLuW laser without affecting the pump beam characteristics. With T_{OC}=1.8% (at the laser wavelength), the maximum output power from the Ho:KLuW laser was 648 mW at an incident pump power of 3.3 W. It should be noted that the single pass absorption of the crystal at high incident powers was only 24% and 39% for the f=50 mm and f=150 mm lenses, respectively, and slightly higher, 28% and 42%, respectively, at low incident powers. The variation of these values is indicative of absorption bleaching effects.

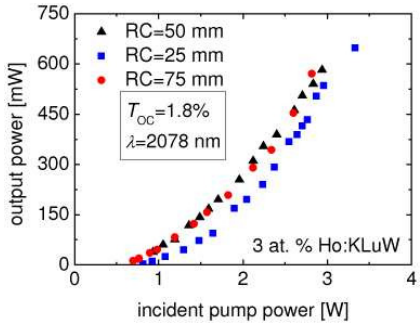

Fig. 4. Dependence of the output power of the Ho:KLuW laser on the radius of curvature (RC) of its output mirror. The pump lens is f=150 mm.

We also studied the influence of the radius of curvature of the output coupler of the Ho:KLuW laser and Fig. 4 shows the input-output characteristics obtained with the f=150 mm pump lens and T_{OC}=1.8% output coupling. Note that the values for RC=25 mm (squares in Fig. 4) are the same as those shown in Fig. 3. The RC=50 and 75 mm mirrors performed equally well and slightly better than the RC=25 mm output coupler.

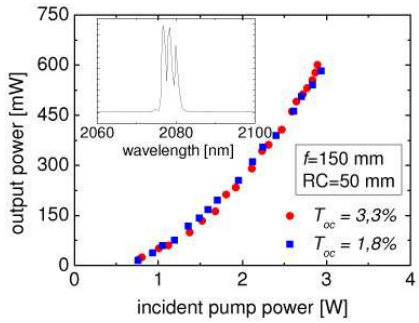

Fig. 5. Comparison of the Ho:KLuW laser performance for T_{OC}=1.8% and T_{OC}=3.3%. Inset: laser spectrum centered at 2078 nm.

In all cases shown above (Figs. 3 to 5) the pump wavelength of the Tm laser was 1946 nm and the Ho:KLuW laser oscillated at 2078 nm. This gives a quantum defect of only ~6%. The increase of the output coupler transmission had a very weak effect on the input – output characteristics of the Ho:KLuW laser. This is illustrated in Fig. 5 where an f=150 mm pump lens is employed and two RC=50 mm output couplers are compared. The laser wavelength remained also unchanged (2078 nm). In the whole power range, the Ho:KLuW laser operated in the fundamental transversal mode due to the relatively small pump waist diameter (e.g. of

#127838 - $15.00 USD Received 30 Apr 2010; revised 5 Jul 2010; accepted 11 Aug 2010; published 16 Sep 2010

the order of 30 µm as measured with the *f*=50 mm pump lens), which could be easily seen on an IR visualization card.

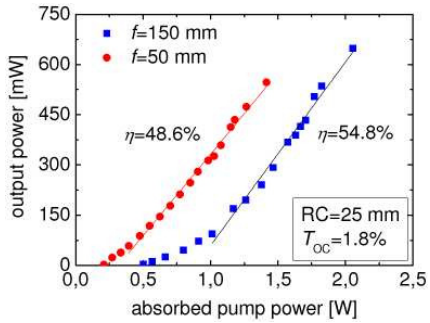

Fig. 6. Estimated slope efficiencies against absorbed power in the double pump pass Ho:KLuW laser using an output coupler with RC=25 mm and T_{OC}=1.8%.

If we assume the single pass absorption of the Ho:KLuW crystal to be 24% and 39% for the *f*=50 and 150 mm pump lenses, respectively, the input-output characteristics with respect to the absorbed pump power are shown in Fig. 6. The maximum output power of 648 mW corresponds to an absorbed pump power of 2.05 W for the *f*=150 mm pump lens while the laser threshold is at ~0.5 W of absorbed power. The slope efficiency in this case amounts to 54.8%. The mode matching is better with this lens. Using a pump lens with a shorter focal length (50 mm) results in lower pump threshold (~200 mW) but reduced slope efficiency. These slope efficiencies seem not limited by up-conversion losses. Note that both the slope efficiency and the output power achieved in this initial experiment exceed those recently reported with co-doped Tm,Ho:KYW although the latter were obtained with Ti:sapphire laser pumping [16]. It should be also noted that the slope efficiency values in our case can be regarded as a lower limit since the second pump pass may have different spatial distribution.

4. Conclusion

In conclusion, the first results obtained with in-band pumping of a CW Ho:KLuW laser reveal promising potential of this new laser material operating at 2078 nm at room temperature. No thermal roll-off in the power dependence and no damage to the uncoated active element have been observed for the available pump power. Further work will be devoted to optimization of the crystal parameters (length and doping level), improvement of the overlap between the laser and pump modes using longer samples, AR-coating of the Ho:KLuW active elements, study of the tuning potential and the use of fiber-coupled diodes for in-band pumping.

Acknowledgments

The research leading to these results has received funding from the EC's Seventh Framework Programme (LASERLAB-EUROPE, grant agreement n° 228334). This work was supported by the Spanish Government under projects MAT 2008-06729-C02-02/NAN and PI09/90527 and by the Catalan Authority under project 2009SGR235. J. J. Carvajal acknowledges support by the Education and Science Ministry of Spain and European Social Fund under the Ramon y Cajal program, RYC2006 – 858.

#127838 - $15.00 USD Received 30 Apr 2010; revised 5 Jul 2010; accepted 11 Aug 2010; published 16 Sep 2010

UNIVERSITAT ROVIRA I VIRGILI
INFRARED LASERS BASED ON HO3+:KRE(WO4)2 CRYSTALS WITH TM3+OR YB3+ AS SENSITIZERS
Venkatesan Jambunathan
ISBN:/DL: T.1243-2011

Paper VIII

Diode –Pumped Ho:KLu$(WO_4)_2$ laser at 2.08 µm

V. Jambunathan, X. Mateos, M. C. Pujol, J. J. Carvajal, M. Aguiló, F. Díaz,
U. Griebner and V. Petrov

Submitted to Applied Physics Express.

UNIVERSITAT ROVIRA I VIRGILI
INFRARED LASERS BASED ON HO3+:KRE(WO4)2 CRYSTALS WITH TM3+OR YB3+ AS SENSITIZERS
Venkatesan Jambunathan
ISBN:/DL: T.1243-2011

UNIVERSITAT ROVIRA I VIRGILI
INFRARED LASERS BASED ON HO3+:KRE(WO4)2 CRYSTALS WITH TM3+OR YB3+ AS SENSITIZERS
Venkatesan Jambunathan
ISBN:/DL: T.1243-2011

Diode-pumped Ho:KLu$(WO_4)_2$ laser at 2.08 μm

Venkatesan Jambunathan [1], Xavier Mateos [1,2*], Maria Cinta Pujol [1], Joan Josep Carvajal [1], Magdalena Aguiló [1], Francesc Díaz [1], Uwe Griebner [2], and Valentin Petrov[2]

[1]*Física i Cristal·lografia de Materials i Nanomaterials (FiCMA-FiCNA-EMAS), Universitat Rovira i Virgili (URV), Campus Sescelades c/Marcel·lí Domingo, s/n, E - 43007 Tarragona, Spain,*
[2]*Max-Born-Institute for Nonlinear Optics and Short Pulse Spectroscopy,* Max-Born-Strasse 2A, *D -12489 Berlin, Germany*
**Corresponding author: xavier.mateos@urv.cat*

We report on efficient continuous-wave diode-pumped laser operation of Ho in the monoclinic KLu$(WO_4)_2$ crystal at ~2080 nm, resonantly pumped at a wavelength of ~1941 nm by a fiber coupled GaSb diode stack. A maximum output power of 408 mW and a slope efficiency of 54.5% with respect to the absorbed pump power were achieved. A comparison of the laser performance within the Ho-doped KRE$(WO_4)_2$ family of monoclinic crystals showed a slightly superior performance of Ho:KY$(WO_4)_2$, achieving a maximum output power of 438 mW and a slope efficiency of 58.8% under identical conditions.

In recent years, infrared solid-state lasers based on Ho^{3+} ions (Ho) operating slightly above 2 μm have been the subject of intensive research due to a number of possible applications [1]. Ho-doped crystals tend to have larger cross sections in comparison to other eye-safe rare-earth (RE) ions but unfortunately the Ho ion doesn't exhibit suitable absorption features matching the range of available laser diodes. Hence, Tm^{3+} (Tm) was used mainly in the past as a sensitizer in diode-pumped systems, but up-conversion losses in this co-doped system are a serious limitation which can be only avoided by physical separation of the two lasers. Direct excitation using resonant or in-band pumping of the $^5I_7$ excited level of Ho at ~1.9 μm offers the advantages of high quantum efficiency for the ~2.1 μm laser transition and minimal heat load to the active element, both important prerequisites for power scaling in this spectral range. Resonant pumping of Ho lasers by separate Tm lasers in continuous-wave (CW) or Q-switched regimes has been extensively studied, including several Tm crystal and fiber lasers, e.g. [2-4]. However, these Tm lasers, being diode-pumped near 800 nm, lead to low overall efficiency of such cascaded pump schemes.

It is clear that direct in-band pumping by 1.9 μm laser diodes will be the ultimate solution for high power scaling of Ho lasers. The first such experiment was carried out in 1995 using mixed GaInAsSb-InGaAsP diodes and the Ho:YAG laser generated an output power of 0.7 W at -53°C [5]. More recently, using a 150 W diode stack of (AlGaIn)(AsSb) laser diodes at 1.91 μm, an output power of 40 W with a slope efficiency of 57% were obtained with Ho:YAG [6], subsequent improvement led to 55 W and 62% at 2.122 μm, respectively [7]. Fiber-coupled InGaAs-diodes with volume Bragg gratings (VBG) for locking to 1.86 μm were also applied for pumping Ho:YAG, but the slope efficiency achieved, even with quasi-CW pumping at 2 Hz, was 24% at maximum [8].

The optically inert monoclinic potassium RE double tungstate crystals with general formula KRE$(WO_4)_2$ (hereafter KREW, with RE=Lu, Gd and Y) stand out for the high absorption and emission cross-sections when doped with active lanthanide ions. Thus, they are especially attractive for compact and highly efficient laser sources at intermediate power levels. In particular, KLuW was shown to be especially suited for Yb and Tm doping [9]. Related to Ho:KLuW, lasing on the $^5I_7 \rightarrow {}^5I_8$ transition at 2078 nm has just been achieved with a slope efficiency of ~55% using in-band pumping with a diode-pumped Tm:KLuW laser [10].

Here we report on similar efficiencies achieved at room-temperature with a diode-pumped CW Ho:KLuW laser using fiber coupled GaSb pump diodes. In addition, we compare the laser performance with the isostructural monoclinic crystals Ho:KYW and Ho:KGdW.

Several Ho-doped single crystals were grown with doping levels of 0.5 at.%, 1 at.%, 3 at.% and 5 at.% in the solution by the Top-Seeded Solution Growth Slow-Cooling (TSSG-SC) method, but since only the 3%-doped Ho:KLuW sample showed lasing under Tm-laser pumping [10], the present study was confined to this doping level. The Ho-ion density measured in this crystal was 2.54×10^{20} cm^{-3}, corresponding in fact to 3.9 at.%. The active element was prepared in such a way that the beam propagation was along the Ng principal optical direction. The two faces which contain the other two principal optical axes, Nm and Np, were polished and antireflection (AR) coated for the pump and laser wavelengths in a broad 1900-2200 nm range. From optical absorption measurements we deduced very similar absorption cross-section for the two polarizations (E//N_m and E//N_p) at the pump wavelength (~1941 nm), with values of 0.4×10^{-20} cm^2 and 0.35×10^{-20} cm^2, respectively (see Fig. 1a). Emission cross-sections were calculated by the reciprocity method and were used to calculate the gain cross-section curves for Ho in the 2000-2150 nm range. For the sake of brevity only gain curves for E//N_m are presented in Fig. lb.

The laser experiments were performed in a hemispherical two mirror cavity. The pump source was a fiber-coupled GaSb laser diode module (DILAS) which had a maximum output power of 16 W and wavelength varying from 1932 to 1941 nm depending on the current level. The core diameter of the fiber was 400 μm (NA=0.22). The cavity was formed by a plane mirror which served as pump mirror, AR coated for the pump wavelength and high-reflection (HR) coated for the laser wavelength (2000-2100 nm). The thickness of the pump mirror was 2 mm. The lens assembly at the end of the fiber comprised a collimator and an aspherical lens with a working distance of 3 mm resulting in a pump spot size of about 220μm.

As output couplers we used several curved mirrors with radius of curvature, R_{OC}=25, 50 and 75 mm. The transmission of the output couplers was T_{OC}=0.5(±0.2)%, 1.5%(±0.3)%, 3.0(±0.5)%, 5.0(±1.0)%, 10.0(±2.0)% and 20.0(±4.0)% in the range from 1820 to 2050 nm. The active element, a cube with dimensions 3×3×3 mm^3, was mounted in a Cu holder using indium foil for better contact at the top and bottom surfaces and the holder temperature

ISBN:/DL: T.1243-2011

was maintained at 16°C. The sample was located as close as possible to the pump mirror.

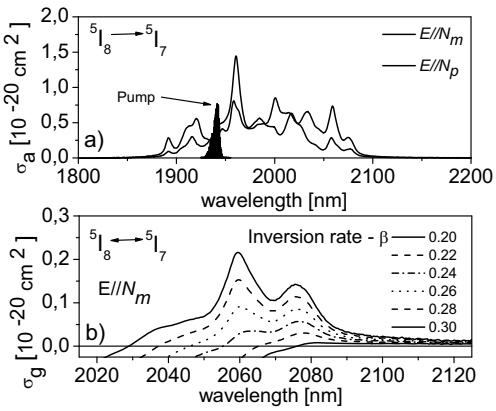

Fig. 1. a) Absorption cross-section of Ho:KLuW for E//N_m and E//N_p and b) calculated gain cross-sections for E//N_m.

CW laser oscillation was realized for all the output couplers. With R_{OC}=50 mm output couplers, we measured the output power as a function of the incident power for an optimized cavity length of 50 mm. The measured crystal absorption in non-lasing conditions amounted to 15.7% and this constant value was used for calculation of the efficiency. A maximum output power of 408 mW was achieved for a maximum absorbed power of ~1500 mW using T_{OC}=3%, Fig. 2. The Ho-laser operated at 2078.5 nm with a threshold of 606 mW (with respect to the absorbed power). This gives a slope efficiency of 54.5% assuming single-pass absorption which is justified because the strongly divergent non-absorbed pump beam cannot be retroreflected by the output coupler.

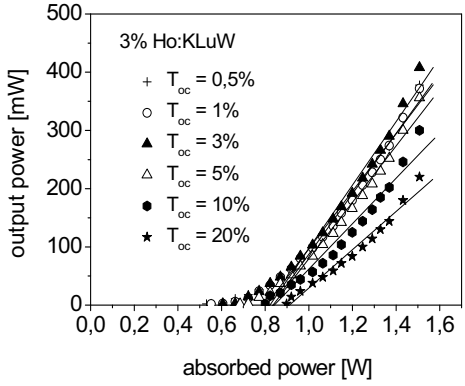

Fig. 2. Output power P_{out} versus absorbed power of the 3 at. % Ho:KLuW laser for several T_{OC} values (R_{OC} = 50 mm).

The laser threshold increases and the laser wavelength shortens when increasing the losses in the cavity (higher transmission of the output coupler), as typical for a quasi-three level laser. All these results are summarized in Fig. 2 and Table 1. The laser wavelength behavior follows the gain curves presented in Fig. 1b in an inversion rate range of β=0.2-0.3. Only for T_{OC}=20%, where the losses are very high, there is a jump to shorter wavelengths at 2060 nm, which correspond to a different electronic transition from the Stark levels of the excited $^5I_7$ multiplet. Thus, for output couplers with transmission ranging from 0.5% to 10%, the four lowest Stark levels of the $^5I_7$ multiplet emit to the highest Stark level of the ground state, $^5I_8$. For T_{OC}=20%, the emission is attributed to a transition from the fifth Stark level of $^5I_7$ to the highest Stark level of the ground state, $^5I_8$. This is consistent with the energy differences of the involved Stark levels estimated from low-temperature optical absorption and emission studies; these results will be published in a separate publication.

Table 1. Summary of laser results with R_{OC} = 50 mm, η: slope efficiency, P_{th}: laser threshold, λ: laser wavelength.

Toc %	P_{out} [mW]	η [%]	P_{th} [mW]	λ [nm]
0.5	378	49.4	530	2080.4
1.5	372	51.8	552	2080.0
3.0	408	54.5	606	2078.5
5.0	356	48.4	684	2077.0
10.0	300	39.0	800	2076.0
20.0	220	32.8	898	2060.0

The influence of the radius of curvature of the output coupler of the Ho:KLuW laser, studied using R_{OC}=25, 50 and 75 mm, was weakly pronounced in terms of output power for the given pump spot size. The beam quality parameter measured with R_{OC}=50 mm gave M^2=3.

Finally, we compared the three monoclinic hosts of the KREW family doped with Ho, namely, KLuW, KYW and KGdW. To this aim, we used 3 at. % doped samples with equal dimensions and orientations, and the same type of AR coating and cooling. With an output coupler of 3% transmission (R_{OC}=50 mm), the three hosts performed almost identically. The actual ion density was 2.15×10^{20} cm^{-3} for Ho:KYW or 3.4 at. % and 1.71×10^{20} cm^{-3} for Ho:KGdW or 2.7 at. %, but the small differences observed in the performance cannot be attributed to this effect because the results were normalized to the actual absorbed power. They are rather related to the difference in ionic radius between the dopant (Ho, ionic radius = 1.015Å) and the passive ions being substituted, Lu for KLuW (ionic radius = 0.977 Å), Y for KYW (ionic radius = 1.019 Å) and Gd for KGdW (ionic radius = 1.053 Å). As can be seen in Fig. 3, the best performance was achieved with Ho:KYW although the difference is not substantial. The maximum output power obtained with Ho:KYW reached 438 mW and the corresponding slope efficiency was 58.8% with the laser operating at 2075 nm. Then, Ho:KLuW followed with 54.5% efficiency, operating at 2078.5 nm (Table 1), and finally Ho:KGdW, operating at 2072 nm, showed a slope efficiency of 51.2% with respect the absorbed power. In fact, the actual absorption of the three crystals was very similar at 1941 nm pump wavelength: 14.8% for KYW, 15.7% for KLuW and 14.9% for KGdW. According to the optical absorption of the three crystals, not shown here, for a pump wavelength of 1960 nm, at the maximum of absorption, substantial increase of the absorbed power and an improvement of the laser performance can be expected for all three of them.

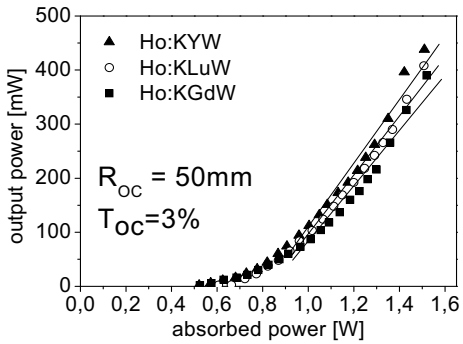

Fig. 3. Comparison of the laser performance for the three hosts, Ho:KYW, Ho:KLuW and Ho:KGdW.

In conclusion, we demonstrated CW laser operation in resonantly diode-pumped Ho:KLuW, Ho:KYW, and Ho:KGdW lasers. We studied the influence of the output coupler transmission and radius of curvature in a simple two-mirror cavity. The three Ho-doped monoclinic crystals performed almost equally well and very promising slope efficiencies were achieved with all of them in this initial experiment: 54.5% with Ho:KLuW and 58.8% with Ho:KYW. Further work will focus on improved cavity and pump geometries for better mode-matching and single transverse mode operation as well as new and more powerful fiber-coupled laser-diode pump sources operating at slightly longer wavelengths, near 1960 nm.

This work was supported by the Spanish Government under projects MAT2008-06729-C02-02/NAN, TEC2010-21574-C02-02, PI09/90527, DE2009-0002 and the Catalan Authority under project 2009SGR235. J. J. Carvajal is supported by the Education and Science Ministry of Spain and European Social Fund under the Ramon y Cajal program, RYC2006 – 858. V. Jambunathan would like to thank the spanish ministry of education through the student mobility program, TME2009-00417. We also acknowledge support from the EC's Seventh Framework program (LASERLAB-EUROPE, grant agreement nº 228334) and the German-Spanish bilateral program Acciones Integradas (DAAD ID 50279160).

References

1. M. Eichhorn, Appl. Phys. B **93**, 269 (2008).
2. P. A. Budni, M. L. Lemons, J. R. Mosto and E. P. Chicklis, IEEE J. Sel. Top. Quantum Electron. **6**, 629 (2000).
3. P. A. Budni, C. R. Ibach, S. D. Setzler, E. J. Gustafson, R. T. Castro and E. P. Chicklis, Opt. Lett. **28**, 1016-1018 (2003).
4. M. Schellhorn, Opt. Lett. **35**, 2609 (2010).
5. C. D. Nabors, J. Ochoa, T. Y. Fan, A. Sanchez, H. K. Choi, and G. W. Turner, IEEE J. Quantum Electron. **31**, 1603 (1995).
6. K. Scholle, and P. Fuhrberg, in Conference on Lasers and Electro-Optics/Quantum Electronics and Laser Science Conference, OSA Technical Digest (CD) (Optical Society of America, 2008), paper CTuAA1.
7. S. Lamrini, Ph. Koopmann, K. Scholle, and P. Fuhrberg, private communication.
8. N. P. Barnes, F. Amzajerdian, D. J. Reichle, W. A. Carrion, G. E. Busch, and P. Leisher, Appl. Phys. B, doc. DOI 10.1007/s00340-010-4195-3 (in press).
9. V. Petrov, M. C. Pujol, X. Mateos, Ó. Silvestre, S. Rivier, M. Aguiló, R. M. Solé, J. Liu, U. Griebner, and F. Díaz, Laser & Photon. Rev. **1**, 179 (2007).
10. X. Mateos, V. Jambunathan, M. C. Pujol, J. J. Carvajal, F. Díaz, M. Aguiló, U. Griebner and V. Petrov, Opt. Express **18**, 20793-20798 (2010).

UNIVERSITAT ROVIRA I VIRGILI
INFRARED LASERS BASED ON HO3+:KRE(WO4)2 CRYSTALS WITH TM3+OR YB3+ AS SENSITIZERS
Venkatesan Jambunathan
ISBN:/DL: T.1243-2011

UNIVERSITAT ROVIRA I VIRGILI
INFRARED LASERS BASED ON HO3+:KRE(WO4)2 CRYSTALS WITH TM3+OR YB3+ AS SENSITIZERS
Venkatesan Jambunathan
ISBN:/DL: T.1243-2011

Paper IX

Continuous-wave laser generation at ~2.1 μm in Ho:KRE$(WO_4)_2$ (RE= Y, Gd, Lu) crystals: a comparative study

V. Jambunathan, X. Mateos, M. C. Pujol, J. J. Carvajal, F. Díaz, M. Aguiló, U. Griebner and V. Petrov

Submitted to Optics Express.

UNIVERSITAT ROVIRA I VIRGILI
INFRARED LASERS BASED ON HO3+:KRE(WO4)2 CRYSTALS WITH TM3+OR YB3+ AS SENSITIZERS
Venkatesan Jambunathan
ISBN:/DL: T.1243-2011

Continuous-wave laser generation at ~2.1 μm in Ho:KRE$(WO_4)_2$ (RE= Y, Gd, Lu) crystals: a comparative study

Venkatesan Jambunathan,[1] Xavier Mateos,[1,2*] Maria Cinta Pujol,[1] Joan Josep Carvajal,[1] Francesc Díaz,[1] Magdalena Aguiló,[1] Uwe Griebner,[2] and Valentin Petrov[2]

[1] *Física i Cristal·lografía de Materials i Nanomaterials (FiCMA-FiCNA-EMAS), Universitat Rovira i Virgili (URV), Campus Sescelades c/Marcel·lí Domingo, s/n, E - 43007 Tarragona, Spain,*
[2]*Max Born Institute for Nonlinear Optics and Ultrafast Spectroscopy, Max-Born Strasse 2A, 12489 Berlin, Germany*
[*]*xavier.mateos@urv.cat*

Abstract: A comparison of the laser performance of the monoclinic Ho:RE$(WO_4)_2$ (RE = Y, Gd, Lu) crystals under identical experimental conditions was performed. The comparison deals with the laser generation in Holmium ions at ~2.1μm by using two different pump sources, a diode laser operating at 1942 nm and a diode-pumped Tm:KLu$(WO_4)_2$ laser operating at 1946 nm. The results show laser slope efficiencies higher than 60% with respect to the absorbed power and output powers higher than 400 mW. The laser performances of Ho:KY$(WO_4)_2$ and Ho:KLu$(WO_4)_2$ are very similar and slightly superior to those of Ho:KGd$(WO_4)_2$.

OCIS codes: (140.5680) Rare earth and transition metal solid-state lasers; (140.3070) Infrared and far-infrared lasers; (140.3480) Lasers, diode-pumped

References and links

1. K. Scholle, S. Lamrini, P. Koopmann and P. Fuhrberg, "2 μm Laser Sources and Their Possible Applications", Frontiers in Guided Wave Optics and Optoelectronics, ISBN 978-953-7619-82-4, pp. 674, February 2010.
2. V. Sudesh and K. Asai, "Spectroscopic and diode-pumped-laser properties of Tm,Ho:YLF; Tm,Ho:LuLF; and Tm,Ho:LuAG crystals: a comparative study," J. Opt. Soc. Am. B **20**, 1829-1837 (2003).
3. E. Sani, A. Toncelli, M. Tonelli, N. Coluccelli, G. Galzerano, and P. Laporta, "Comparative analysis of Tm-Ho:KYF_4 laser crystals," Appl. Phys.B **81**, 847-851 (2005).
4. P.A. Budni, C.R. Ibach, S.D. Setzler, E.J. Gustafson, R.T. Castro and E.P. Chicklis "50-mJ, Q-switched, 2.09-μm holmium laser resonantly pumped by a diode-pumped 1.9-μm thulium laser", Opt. Lett. **28**, 1016-1018 (2003).
5. B. Q. Yao, L. L. Zheng, R. L. Zhou, X. M. Duan, Y. J. Zhang, Y. L. Ju, Z. Wang ,G. J. Zhao, and Q. Dong, "Holmium Laser In-Band Pumped by a Thulium Laser in the same host of $YAlO_3$," Laser Physics **18,** 1501-1504 (2008).
6. D. Y. Shen, A. Abdolvand, L. J. Cooper, and W. A. Clarkson, "Efficient Ho:YAG laser pumped by a cladding-pumped tunable Tm:silica-fibre laser," Appl. Phys. B **79**, 559-561 (2004).
7. K. Scholle, and P. Fuhrberg, "In-band pumping of high-power Ho:YAG lasers by laser diodes at 1.9 μm," in Conference on Lasers and Electro-Optics/Quantum Electronics and Laser Science Conference, OSA Technical Digest (CD) (Optical Society of America, 2008), paper CTuAA1.
8. J. Liu, V. Petrov, X. Mateos, H. Zhang, and J. Wang, "Efficient high-power laser operation of Yb:KLu$(WO_4)_2$ crystals cut along the principal optical axes," Opt. Lett. **32**, 2016 – 2018 (2007).
9. X. Mateos, V. Petrov, J. Liu, M.C. Pujol, U. Griebner, M. Aguiló, F. Díaz, M. Galan, and G. Viera, "Efficient 2 μm continuous-wave laser oscillation of Tm^{3+}:KLu$(WO_4)_2$," IEEE J. Quantum Electron. **42**, 1008-1015 **(**2006).
10. S. Rivier, X. Mateos, Ò. Silvestre, V. Petrov, U. Griebner, M. C. Pujol, M. Aguiló, F. Díaz, S. Vernay, and D. Rytz , " Thin-disk Yb:KLu$(WO_4)_2$ laser with single-pass pumping," Opt. Lett. **33**, 735 – 737 (2008).
11. V. Petrov, M. C. Pujol, X. Mateos, Ó. Silvestre, S. Rivier, M. Aguiló, R. M. Solé, J. Liu, U. Griebner, and F. Díaz, "Growth and properties of KLu(WO4)2, and novel ytterbium and thulium lasers based on this monoclinic crystalline host," Laser & Photon. Rev. **1**, 179–212 (2007).

UNIVERSITAT ROVIRA I VIRGILI
INFRARED LASERS BASED ON HO3+:KRE(WO4)2 CRYSTALS WITH TM3+OR YB3+ AS SENSITIZERS
Venkatesan Jambunathan
ISBN:/DL: T.1243-2011

12. X. Mateos, V. Jambunathan, M. C. Pujol, J. J.Carvajal, F. Díaz, M. Aguiló, U. Griebner and V. Petrov, "CW lasing of Ho in KLu(WO4)2 in-band pumped by a diode-pumped Tm:KLu(WO4)2 laser", Opt. Express **18**, 20793-20798 (2010).
13. S. A. Payne, L.L. Chase, L. K. Smith, W. L.Kway and W. F. Kruple, "Infrared cross-section measurement for crystals doped with Er^{3+}, Tm^{3+}, Ho^{3+}", IEEE J. Quantum Electron. **28**, 2619-2630 (1992).
14. R. Solé, V. Nikolov, X. Ruiz, Jna. Gavaldà, X. Solans, M. Aguiló and F. Diaz "Growth of β-$KGd_{1-x}Nd_x(WO_4)_2$ single crystals in $K_2W_2O_7$ solvents", J. Cryst. Growth, **169,** 600 – 603 (1996).

1. Introduction

Currently, there is an increasing interest in infrared solid-state lasers based on Ho^{3+} ions (Ho) operating slightly above 2 μm due to the potential applications in the fields of medicine, remote sensing and as a pump source for OPO´s [1]. Interesting advantages of the Ho doped crystals is that such laser crystals offer high gain cross-section and long lifetime of the emitting $^5I_7 \rightarrow {}^5I_8$ transition. The only drawback of the Ho ion is that it doesn't exhibit any suitable absorption band for usual laser diodes. In order to overcome this drawback many researchers used Tm as sensitizer in diode pumped systems around 800 nm [2,3]. However, this co-doped system leads to up-conversion losses which in turn, lead to poor efficiency. More efficient is the alternative pump scheme using direct pumping of the emitting level through Tm lasers operating near 1.9 μm, including Tm crystals and Tm fibers [4-6]. More recently, efficient diode lasers operating also around 1.9 μm have demonstrated to be promising for power scaling of Ho –based laser crystals [7]. The great advantage of direct excitation of the Ho emitting level (the so called, in-band pumping) is the minimum heat generated in the crystals due to the small quantum defect between the pump and laser wavelengths which allows for power scaling of the 2.1 μm laser.
The well known laser hosts, the monoclinic $KRE(WO_4)_2$ (RE=Y, Gd, Lu) crystals (hereafter KREW) have demonstrated to be very suitable for Yb and Tm ions in different active media configurations such as slabs and thin disk [8-11]. Such family of crystals stands out because of the large transition cross-sections induced to the lanthanide ions due to the monoclinic nature. This spectroscopic feature is especially true for some polarizations. Apart from Yb and Tm, we recently demonstrated laser generation in Ho:KLuW laser using a diode-pumped Tm:KLuW laser [12]. In this work, we compare the laser performance of in-band pumped Ho –doped KREW crystals (three hosts of the same family) under two different pump sources, a diode-pumped Tm:KLuW laser operating at 1946 nm and a diode laser operating at 1942 nm.

2. Experiment

A series of Ho-doped KREW crystals have been grown at several doping concentration ranging from 0.5 to 7.5 at.% by the Top Seeded Solution Growth Slow Cooling method (TSSG-SC). The concentration of the crystals was measured using Electron probe micro analysis (EPMA) technique. Due to the strong anisotropy of the monoclinic KREW crystals [11], the samples were cut and polished along the principal optical directions, namely N_g, N_m and N_p, associated to the three refractive indices n_g, n_m *and* n_p of this biaxial crystal. The samples were parallelepipedic prisms with faces perpendicular to the principal optical directions. Spectroscopic characterization of Ho:KREW crystals was in terms of polarized room and low temperatures optical absorption measured using a Cary Varian 500 spectrophotometer. The emission cross-section of the transition near 2.1 μm was computed by means of the reciprocity method [13] from the absorption cross-section spectra.

Concerning the laser experiment, two types of pump sources were used. One is a fiber-coupled GaSb laser diode module which had a maximum output power of 16 W and wavelength varying from 1932 to 1942 nm depending on the current level. The core diameter of the fiber was 400 μm. Attached to the end of the fiber a special lens assembly was used to collimate and focus the pump beam to a 2:1 imaging ratio. The second pump source is a diode –pumped Tm:KLuW laser described in a previous work [9], and comprises of a diode laser

operating at 806 nm and a 3%Tm –doped KLuW crystal delivering a maximum of 4 W centred at 1946 nm. The laser radiation from the Tm:KLuW laser was linearly polarized parallel to its N_m principal optical axis. Both the experiments were performed in a hemispherical two mirror linear cavity (see Figure 1a and 1b). It was formed by a plane pump mirror (M5), antireflection (AR) coated for the pump wavelengths and high-reflection (HR) coated for the laser wavelength (2000-2100 nm). The output coupler (M6) has a radius of curvature RC = 50 mm. The transmission of the output couplers used (T_{OC}) was 1.5%(±0.3)%, 3 (±0.5)%, 5(±1.0)%, and 20(±4.0)% in the 1820 - 2050 nm range. In the case of diode pumping setup, the resulting pump spot size was 220 µm in diameter. In the case of Tm:KLuW laser pumping setup, the output was collimated to an isolator (I) which helped us to avoid any back coupling from the Ho cavity to the Tm laser. To rotate the polarization a half-wave plate was used, so that the pump beam to the Ho-laser was vertically polarized. The resulting pump spot size in this configuration was measured to be 30 µm. Schematics of the two laser arrangements are shown in Figure 1.

The dimensions of the coated active elements (N_g-cut) were 3×3×3 mm^3. We mounted them in a Cu-holder for cooling and used indium foil for better contact at the top and bottom surfaces. The cooling temperature was 16°C. The samples were located as close as possible to the pump mirror and were positioned under normal incidence to the pump beam.

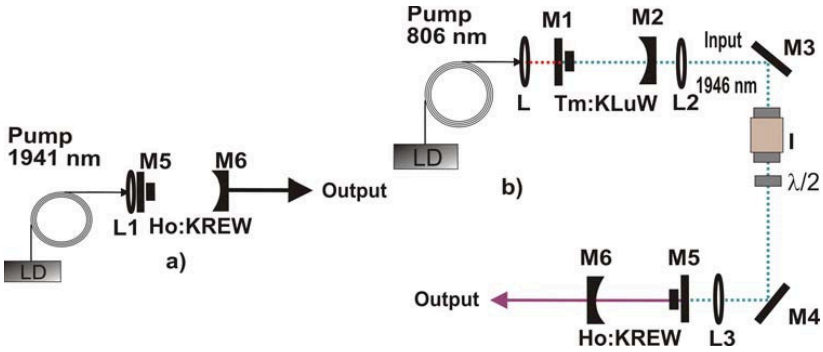

Fig. 1 Laser setup: a) Diode pumped Ho:KREW laser (L1 (special imaging 2:1 lens assembly which comprises of a collimator and aspherical lens with f = 6 mm), M5 (plane pump mirror), M6(Ho –laser output coupler). b) Tm:KLuW pumped Ho:KREW laser (λ/2 - half-wave, I – Isolator, L (AR-coated lens assembly for collimation and focusing of the fiber output with f=30 mm), L2 (AR-coated collimating lens with f=50mm), L3 (AR-coated focusing lens), M3, M4 (45° bending mirrors), M1 (plane pump mirror , AR @ 800 nm and HR for laser wavelength), M2 (Tm-laser output coupler with RC=25 mm and Toc=3%), and M6 (Ho-laser output coupler).

3. Results and discussion

Crystals of several doping concentrations were grown by TSSG-SC method as mentioned previously. For growing the single crystals, we introduced 200 g of solution mixture inside the furnace with the binary composition of 12mol% Ho:KREW as solute and 88 mol% $K_2W_2O_7$ as solvent in a platinum crucible of 50 mm diameter and 50 mm in length using K_2CO_3, WO_3, RE_2O_3 (RE = Y, Gd, Lu), and Ho_2O_3 with analytical grade of purity. The mixture was homogenized by maintaining the solution at 50K above the saturation temperature for 5 to 6 hours. The thermal axial gradient of the furnace was ~1.5 K/cm. The seeding process was realized with a *b* crystallographic oriented seed (e.g. for growing Ho:KYW crystals, a KYW seed was used) located at the centre of the surface of the solution. After accurately determining the saturation temperature by observing the growth and dissolution of the seed in

contact with the surface of the solution, the crystals grew by slow cooling at the rate of 0.1K/h for ~20K. After the crystals grew, they were slowly removed from the solution and kept above its surface being cooled to room-temperature at a rate of 25K/h to avoid thermal shock of the crystals. The detailed growth methodology is described elsewhere [14]. During the growth process the seed was rotated at 40 rpm for KYW and KLuW and 60 rpm for KGdW, in order to enhance mass and heat transport in the solution and to avoid inclusions during the growth processes. Since only 3at.% Ho.KLuW showed laser operation [12], for a comparative study in this work among the whole family and the two pump sources, we considered only 3at.% Ho:KREW crystals. Table 1 gives the summary of the crystal growth details and Table 2 summarizes the dopant content in the crystals as well as the real chemical stoichiometric formula.

Spectroscopy of Ho in KREW crystals has been studied in terms of polarized room and low temperatures optical absorption. From the optical absorption measurements, we analyzed the absorption features of the $^5I_7$ level because this is the pump region. Figure 2 (a, b, c) shows the absorption cross-section for all the three hosts in the 1800 – 2200 nm range for $E//N_m$ and N_p. Note the high degree of anisotropy where N_m absorbs almost two times more than N_p and the broadness of the spectra. The maximum of absorption is centered near 1960 nm with a Full-Width at Half Maximum (FWHM) of ~10 nm which make these crystals ideal for diode pumping. For the two pump wavelengths used in the laser experiments, the absorption cross-sections are reported in Table 3. Note that at 1941 nm for $E//N_m$ and N_p the absorption is very similar so that in the case of diode pumping (un-polarized pump beam) the two polarizations absorb 50%.

Table 1: Summary of the Ho:KREW crystal growth experiments

Host	*Saturation temp. [K]*	*Cooling rate [K/h]*	*Cooling interval [K]*	*Crystal weight [g]*	*Growth rate x 10^{-4} [g/h]*	*Crystal dimension [mm] along crystallographic direction.*		
						c	*a**	*b*
3at.%Ho:KYW	1168.2	0.1	21.4	4.13	193	15.86	8.42	8.70
3at.%Ho:KGdW	1179.5	0.05	22.0	3,47	158	12.80	9.60	5.86
3at.%Ho:KLuW	1166.5	0.1	21.2	4.88	230	20.84	10.07	6.90

Table 2: Summary of the EPMA results for the grown Ho:KREW crystals

Host	*Ho^{3+} [at./cm^3]*	*Stoichiometric formula*
3at.%Ho:KYW	2.15 x10^{20}	$KY_{0.966}Ho_{0.034}(WO_4)_2$
3at.%Ho:KGdW	1.71x10^{20}	$KGd_{0.973}Ho_{0.027}(WO_4)_2$
3at.%Ho:KLuW	2.54 x10^{20}	$KLu_{0.961}Ho_{0.039}(WO_4)_2$

UNIVERSITAT ROVIRA I VIRGILI
INFRARED LASERS BASED ON HO3+:KRE(WO4)2 CRYSTALS WITH TM3+OR YB3+ AS SENSITIZERS
Venkatesan Jambunathan
ISBN:/DL: T.1243-2011

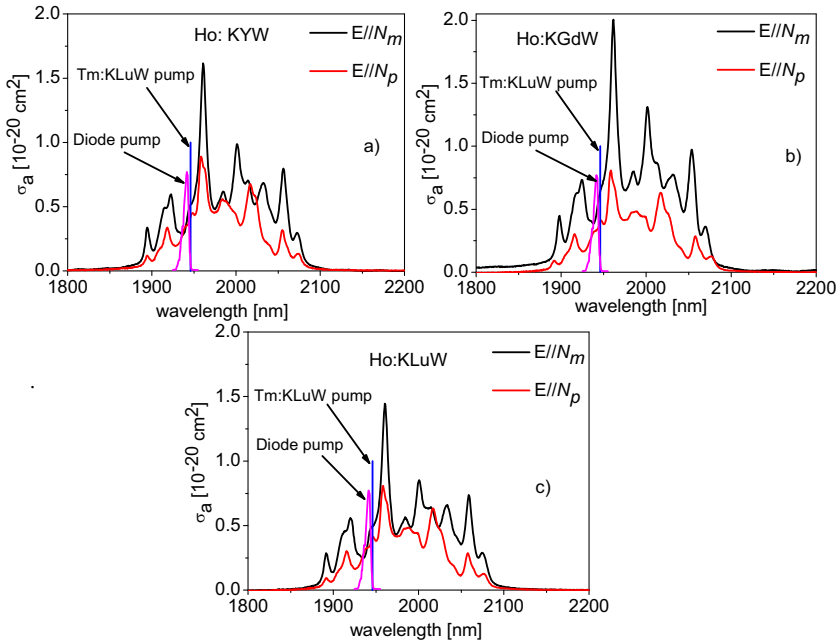

Fig. 2 : Absorption cross-section of the $^5I_8 \leftrightarrow {}^5I_7$ transition of Ho in KREW (a) KYW , b) KGdW, c) KLuW) for E//N_m and E//N_p.

Table 3 Absorption cross- section of Ho for different pump wavelengths for E//N_m and E//N_p

Crystal	*E//$N_{m,p}$*	*λ [nm]*	*σ_a [10^{-20}cm^2]*
Ho:KYW	N_m	1941	0.38
	N_p	1941	0.32
	N_m	1946	0.52
Ho:KGdW	N_m	1941	0.47
	N_p	1941	0.34
	N_m	1946	0.65
Ho:KLuW	N_m	1941	0.40
	N_p	1941	0.32
	N_m	1946	0.49

In order to compute the emission cross-section we used the reciprocity method as mentioned earlier and for the calculation of the gain cross-section we used the following expression (1)

$$\sigma_g = \sigma_e \times \beta - (1-\beta) \times \sigma_a \qquad (1)$$

(Where σ_g is the gain cross-section, σ_a is the absorption cross-section, σ_e is the emission cross-section and β is the inversion rate). Figure 3 shows the calculated emission cross-section for E//N_m in the 1800-2200 nm range , because this polarization shows the highest values. We calculated a maximum emission cross-section of ~2.65x10^{-20} cm^2 at 2056 nm for Ho:KYW, ~2.70x10^{-20} cm^2 at 2054 nm for Ho:KGdW and ~2.45x10^{-20} cm^2 at 2059 nm for Ho:KLuW for

E//N_m. For the other two polarizations N_g and N_p the emission cross-sections are smaller. From figure 3 (d, e, f), positive gain in the $^5I_7 \leftrightarrow {}^5I_8$ transition is achieved from 2020 nm or 2040 nm depending on the host to 2100 nm. Two local maxima of gain are located at 2056 and 2073 nm for Ho:KYW, 2054 and 2071 nm for Ho:KGdW and 2059 and 2078 nm for Ho:KLuW respectively for the inversion rates used in the calculations. In this figures we plotted inversion ratios from 0.2 to 0.3 as more realistic ones because these describe perfectly the laser results of this work, later presented. More detailed results of the growth and spectroscopy of Ho:KREW will be published elsewhere.

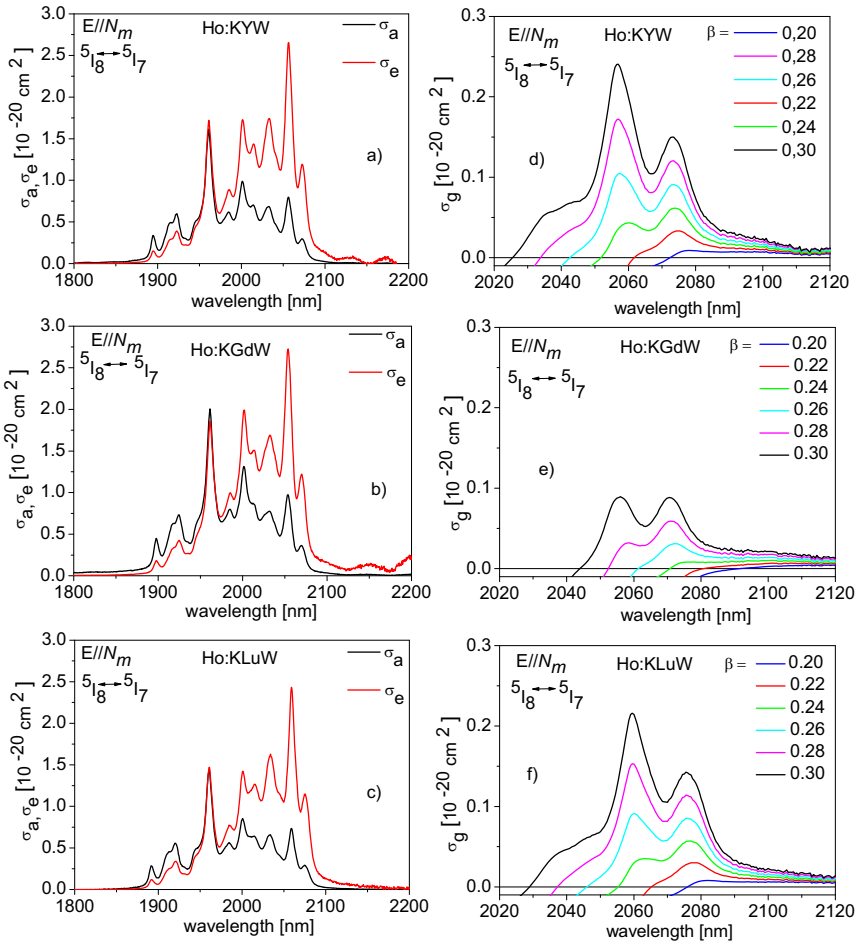

Fig. 3: Absorption, emission and gain cross-sections of the $^5I_8 \leftrightarrow {}^5I_7$ transition of Ho in KREW for E//N_m.

CW laser action was realised for all output couplers used and for all the three hosts using both the pump sources. In all cases, we measured the output power as a function of the incident power and estimated the slope efficiencies with respect to the incident pump power (See table 4). Figure 4 (a, b, c) shows the output-input characteristics of the Ho:KREW lasers

UNIVERSITAT ROVIRA I VIRGILI
INFRARED LASERS BASED ON HO3+:KRE(WO4)2 CRYSTALS WITH TM3+OR YB3+ AS SENSITIZERS
Venkatesan Jambunathan
ISBN:/DL: T.1243-2011

under in-band pumping by the diode laser while figure 4 (d ,e, f) shows those characteristics in the case of in-band pumping by a diode pumped Tm:KLuW laser.

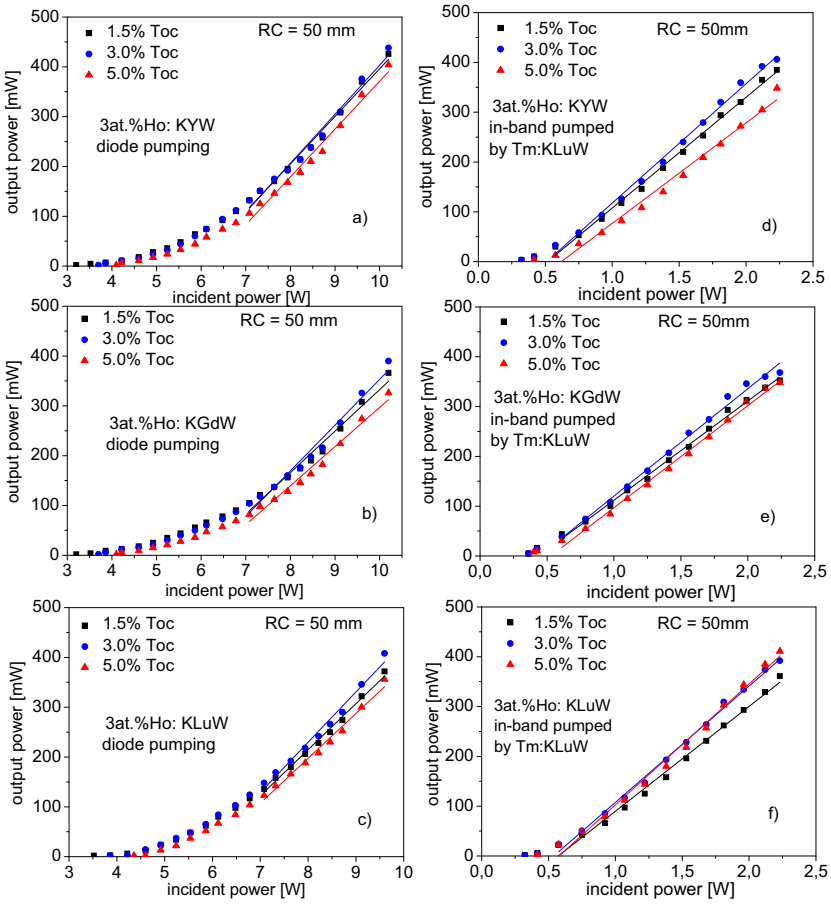

Fig. 4. Output power vs. incident pump power of the Ho:KREW laser (Diode pump and Tm:KLuW as pump source) for various Tocs and RC=50mm

In the case of diode pumping, T_{OC} = 3% gave slightly better output power for all the three hosts when compared to other T_{OCS}. The non-linear behavior of these curves is because the diode laser wavelength shifts with the increase of the current (pump power level) so that at higher pump powers the longer wavelengths are better absorbed according to the optical absorption spectra (see figure 2). In the case of diode pumping, from P_{in} = 7W we assumed a linear behavior of the output power against the incident power and calculated the slope efficiencies from this value (see table 4). During the laser experiments with Tm:KLuW pumping the incident power was limited to ~ 2.3W in order to avoid any risk of damage in the crystal because the spot size was only 30 μm.

ISBN:/DL: T.1243-2011

The same study was performed in the case of Tm laser pumping. The results are shown in figure 4 (d, e, f). Again, in almost all cases, T_{OC} = 3% gave slightly better output when compared to other T_{OCS} for Ho:KYW and Ho:KGdW, but in the case of Ho:KLuW T_{OC} = 3% and 5% performed similarly. As can be observed in all curves, power scaling would be feasible because we didn't observe any limitation due to thermal reasons during laser operation and the only limitation was the pump power available.

A shifting towards shorter laser wavelengths was observed with the increase of the transmission of the output coupler as typical for three level laser systems (see table 4). This is clearly observed when we used an output coupler with T_{OC}=20% (not shown in figure 4) because the laser wavelength shifted considerably according with the gain curves for each host (see figure 3 d, e, f). The explanation to this fact could be found in the effect of the crystal field on the Stark components of the energy level (such a detailed spectroscopic analysis will be published elsewhere). Thus, for KYW and KLuW with T_{OCS} ranging from 1.5% to 5%, the emission is attributed to the first three lowest Stark levels of the $^5I_7$ multiplet to the highest Stark level of the ground state, $^5I_8$ and for T_{OC}=20%, the emission is attributed to a transition from the fifth Stark level of $^5I_7$ to the highest Stark level of the ground state. For KGdW with T_{OCS} ranging from 1.5% to 5%, the emission is attributed to the first two lowest Stark levels of the $^5I_7$ multiplet to the highest Stark level of the ground state and for T_{OC}=20%, the emission is attributed to a transition from the third Stark level of $^5I_7$ to the highest Stark level of the ground state. A summary of the maximum output power achieved and laser wavelengths as a function of the T_{OC} in the case of the two pump sources for each crystal is reported in table 4.

Table 4 Summary of laser results for the two pump sources

Pump source	*Sample (3at.%)*	*T_{OC}%*	*Maximum Output power [mW]*	*Slope efficiency [%]*	*Wavelength* [nm]
Diode pump	Ho:KYW	1.5	426	9.54	2076
		3.0	438	9.85	2075
		5.0	404	9.60	2074
		20.0	-	-	2057
Tm:KLuW	Ho:KYW	1.5	385	22.26	2076.5
		3.0	406	23.98	2075
		5.0	348	20.19	2074
		20.0	-	-	2057
Diode pump	Ho:KGdW	1.5	366	8.33	2073
		3.0	390	9.18	2072
		5.0	326	7.85	2071
		20.0	-	-	2054.5
Tm:KLuW	Ho:KGdW	1.5	352	19.90	2073.5
		3.0	368	21.55	2072
		5.0	348	20.49	2071
		20.0	-	-	2054
Diode pump	Ho:KLuW	1.5	372	9.24	2080
		3.0	408	10.09	2078.5
		5.0	356	9.06	2077
		20.0	220	-	2060
Tm:KLuW	Ho:KLuW	1.5	361	21.06	2080
		3.0	392	23.35	2079
		5.0	411	24.30	2077
		20.0	-	-	2060

We also studied the influence of the radius of curvature of the output coupler of the Ho:KLuW laser, using RC = 25, 50 and 75 mm and T_{OC}=1.5% in the case of diode pumping.

The results are shown in figure 5. From the figure, the effect of mode matching is found to be weakly pronounced. The slope efficiency with respect to incident power was in the range of 8.1 – 9.5 %.

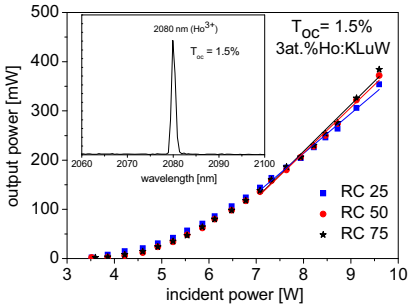

Fig. 5 Output-input characteristics of the 3at.%Ho:KLuW crystal with different R_{OC}s and T_{OC}=1.5% (Inset: typical laser spectrum centred at 2080 nm)

Since T_{OC} =3% gives higher output power in both cases of the pump sources, only T_{OC} =3% is considered for estimating the slope efficiencies with respect the absorbed power. For diode pumping it is justified to have single pass absorption because the pump beam is much divergent and the non-absorbed pump beam cannot be retro-reflected by the output coupler to the crystal, but in case of Tm:KLuW laser pumping, the pump beam is retro-reflected and double pass absorption occurs because the output coupler show nearly 97% reflection of the pump wavelength. We measured the single pass absorption of the crystal in each host using the diode laser and these were found to be 14.8% for Ho:KYW, 15.7% for Ho:KLuW and 14.9% for Ho:KGdW. Concerning the absorption with Tm:KLuW pumping of each host, the single pass absorption amounted to 22.9% for KYW, 21.5% for KLuW and 23.2% for KGdW. Using these values the absorbed power was calculated so that figure 3 was re-plotted in figure 6 only for T_{OC} = 3% and the slopes were estimated. Table 5 shows the summary of estimated slopes and laser thresholds.

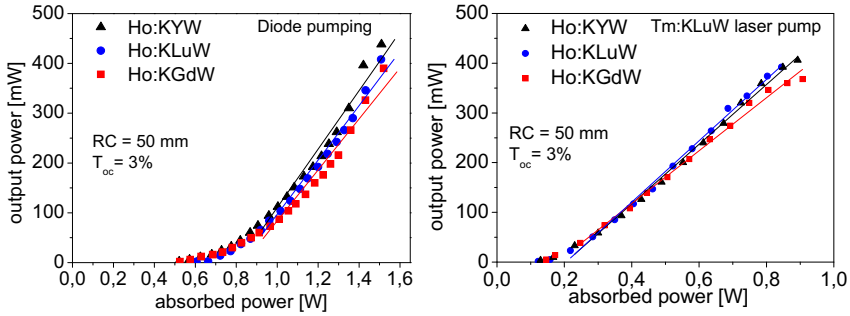

Fig. 6 Estimated slope efficiencies for 3at.%Ho:KREW crystals with respect to the absorbed power using the two pump sources

From figure 6 and table 5, it is inferred that all the three hosts perform almost equally. As can be seen from table 5, the best performance was achieved with Ho:KYW in the case of diode pumping and Ho:KLuW with Tm:KLuW laser pumping, although the difference is not substantial. In terms of diode pumping, the maximum output power obtained with Ho:KYW reached 438 mW and the corresponding slope efficiency was 58.8% centered at 2075 nm, then

followed by Ho:KLuW with 54.5% efficiency, centered at 2078.5 nm, and finally Ho:KGdW, centered at 2072 nm with slope efficiency of 51.2% with respect to the absorbed power. In terms of Tm:KLuW laser pumping, the maximum output power obtained with Ho:KYW reached 406 mW and the corresponding slope efficiency was 59.9% centered at 2075 nm, then followed by Ho:KLuW with 61.6% efficiency, centered at 2079 nm, and finally Ho:KGdW, centered at 2072 nm with slope efficiency of 53.2% with respect to the absorbed power.

Table 5 Summary of estimated slopes for the two pump sources

Pump source	*Sample (3at.%)*	*Maximum Outut power* [mW]	*Slope efficiency* [%]	*Threshold* [mW]	*Wavelength* [nm]
Diode pump	Ho:KYW	438	58.8	521	2075
Tm:KLuW	Ho:KYW	406	59.9	129	2075
Diode pump	Ho:KGdW	390	51.2	525	2072
Tm:KLuW	Ho:KGdW	368	53.2	146	2072
Diode pump	Ho:KLuW	408	54.5	606	2078.5
Tm:KLuW	Ho:KLuW	392	61.6	122	2079

4. Conclusion

In conclusion, a comparison of the laser properties of the Ho:KYW, Ho:KGdW, and Ho:KLuW crystals under identical experimental conditions were made by using two different pump sources, a diode laser operating at 1942 nm and a Tm:KLuW laser operating at 1946 nm. We establish that all hosts perform similarly. The best performance achieved a slope efficiency as high as ~62%. Further power scaling to reach the Watt level is planned by optimization of the thickness of the active medium, the more optimum pump laser wavelength according to the optical absorption spectrum of Ho in KREW and a more powerful laser diode.

Acknowledgments

This work was supported by the Spanish Government under projects MAT2008-06729-C02-02/NAN, TEC2010-21574-C02-02, PI09/90527, DE2009-0002 and the Catalan Authority under project 2009SGR235. J. J. Carvajal is supported by the Education and Science Ministry of Spain and European Social Fund under the Ramon y Cajal program, RYC2006 – 858. V. Jambunathan would like to thank the spanish ministry of education through the student mobility program, TME2009-00417. We also acknowledge support from the EC's Seventh Framework program (LASERLAB-EUROPE, grant agreement nº 228334) and the German-Spanish bilateral program Acciones Integradas (DAAD ID 50279160).